Aircraft Observations of Tropical Cyclones
Past, Present, and Future

Michael M. Bell

University of Hawai'i Mānoa

Colorado State University
Starting Fall 2016

Acknowledgements: NSF & ONR for funding support
NRL, NCAR/EOL, NASA, and NOAA/HRD for data and field support

Hurricane Patricia from the NASA WB-57 (Joe Gerky, WB-57 Cockpit)

Hurricane Patricia from the NASA WB-57 (Joe Gerky, WB-57 Cockpit)

Tropical Storm Oho
Saturday October 3, 2015
5 AM HST Advisory 2
NWS Central Pacific Hurricane Center

Current Information:
Center Location 14.2 N 154.6 W
Max Sustained Wind 40 mph
Movement N at 6 mph

Forecast Positions:
● Tropical Cyclone ○ Post-Tropical
Sustained Winds: D < 39 mph
S 39-73 mph H 74-110 mph M > 110mph

Potential Track Area: Day 1-3 Day 4-5

Watches: Hurricane Trop.Storm

Warnings: Hurricane Trop.Storm

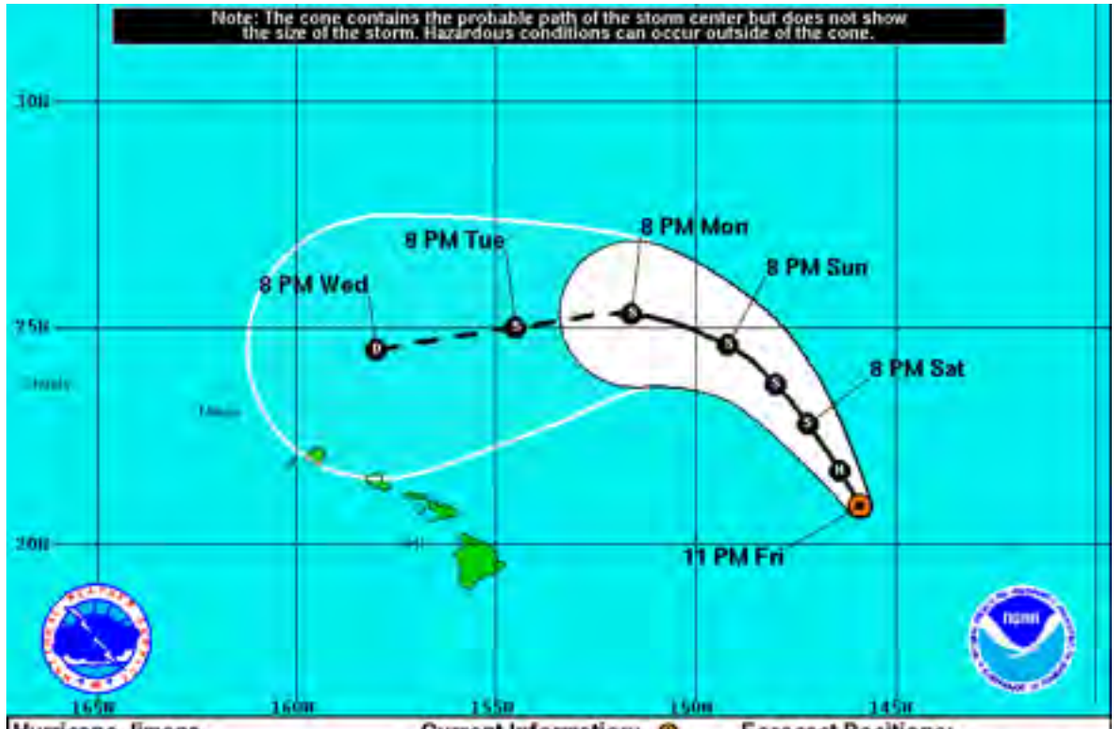

Hurricane Jimena
Friday September 4, 2015
11 PM HST Advisory 39
NWS Central Pacific Hurricane Center

Current Information:
Center Location 20.9 N 145.9 W
Max Sustained Wind 85 mph
Movement NNW at 7 mph

Forecast Positions:
● Tropical Cyclone ○ Post-Tropical
Sustained Winds: D < 39 mph
S 39-73 mph H 74-110 mph M > 110mph

Potential Track Area: Day 1-3 Day 4-5

Watches: Hurricane Trop.Storm

Warnings: Hurricane Trop.Storm

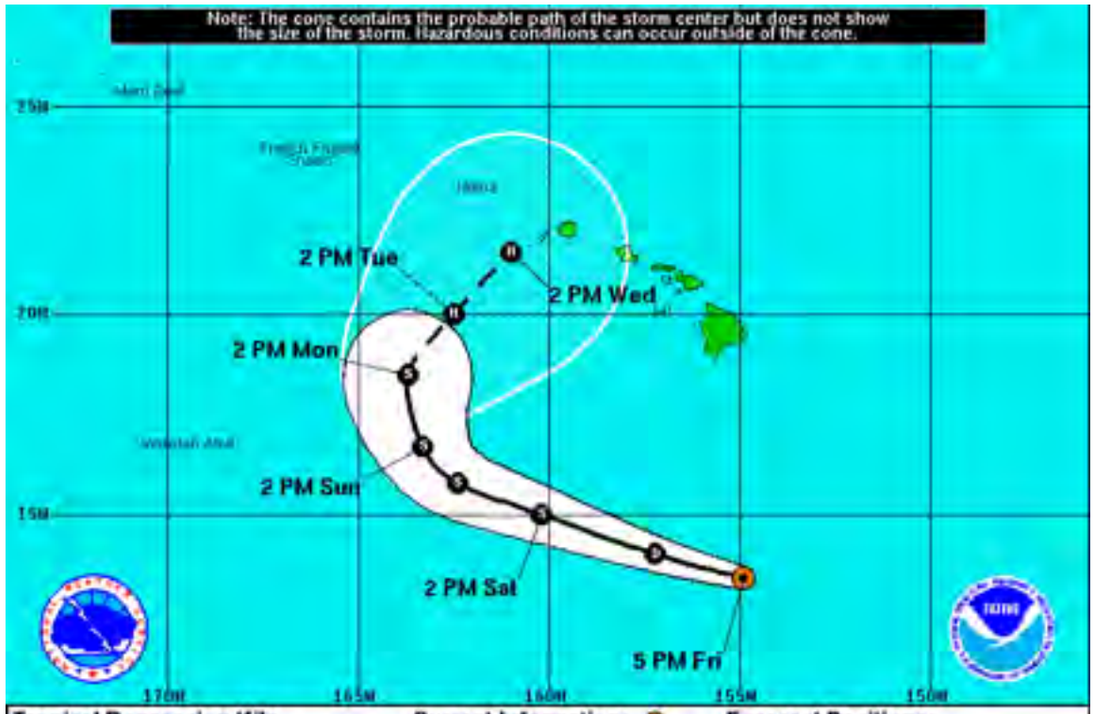

Tropical Depression Kilo
Friday August 21, 2015
5 PM HST Advisory 6
NWS Central Pacific Hurricane Center

Current Information:
Center Location 13.4 N 154.9 W
Max Sustained Wind 35 mph
Movement WNW at 14 mph

Forecast Positions:
● Tropical Cyclone ○ Post-Tropical
Sustained Winds: D < 39 mph
S 39-73 mph H 74-110 mph M > 110mph

Potential Track Area: Day 1-3 Day 4-5

Watches: Hurricane Trop.Storm

Warnings: Hurricane Trop.Storm

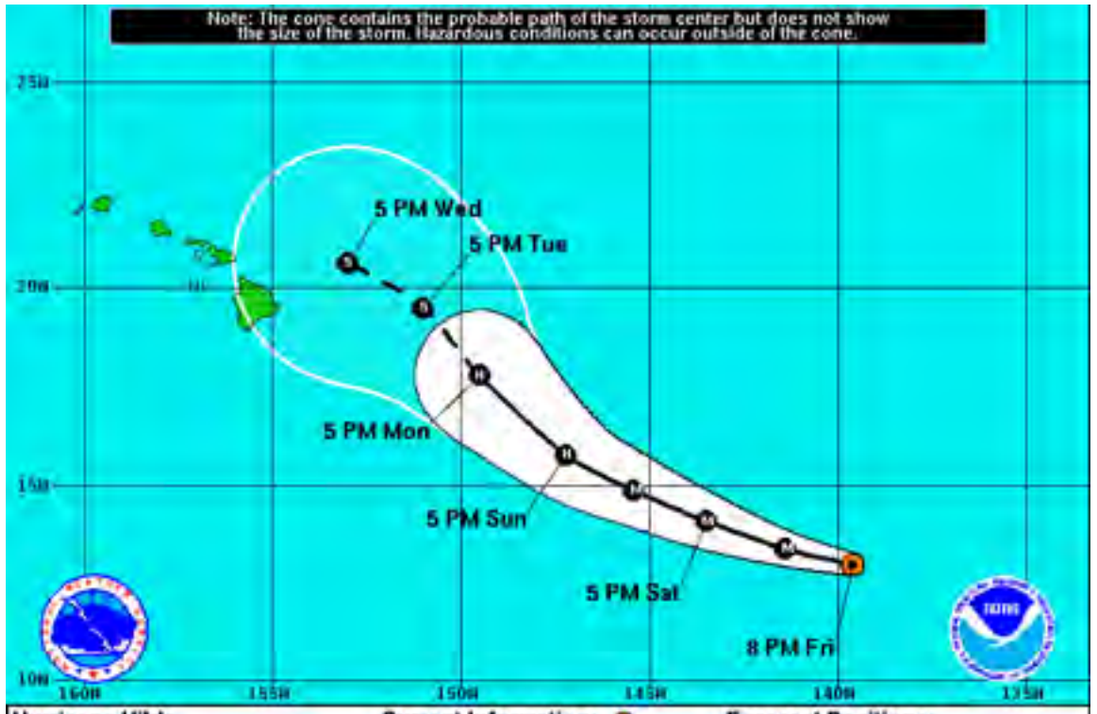

Hurricane Hilda
Friday August 7, 2015
8 PM PDT Advisory 9
NWS National Hurricane Center

Current Information:
Center Location 13.0 N 139.6 W
Max Sustained Wind 105 mph
Movement W at 15 mph

Forecast Positions:
● Tropical Cyclone ○ Post-Tropical
Sustained Winds: D < 39 mph
S 39-73 mph H 74-110 mph M > 110mph

Potential Track Area: Day 1-3 Day 4-5

Watches: Hurricane Trop.Storm

Warnings: Hurricane Trop.Storm

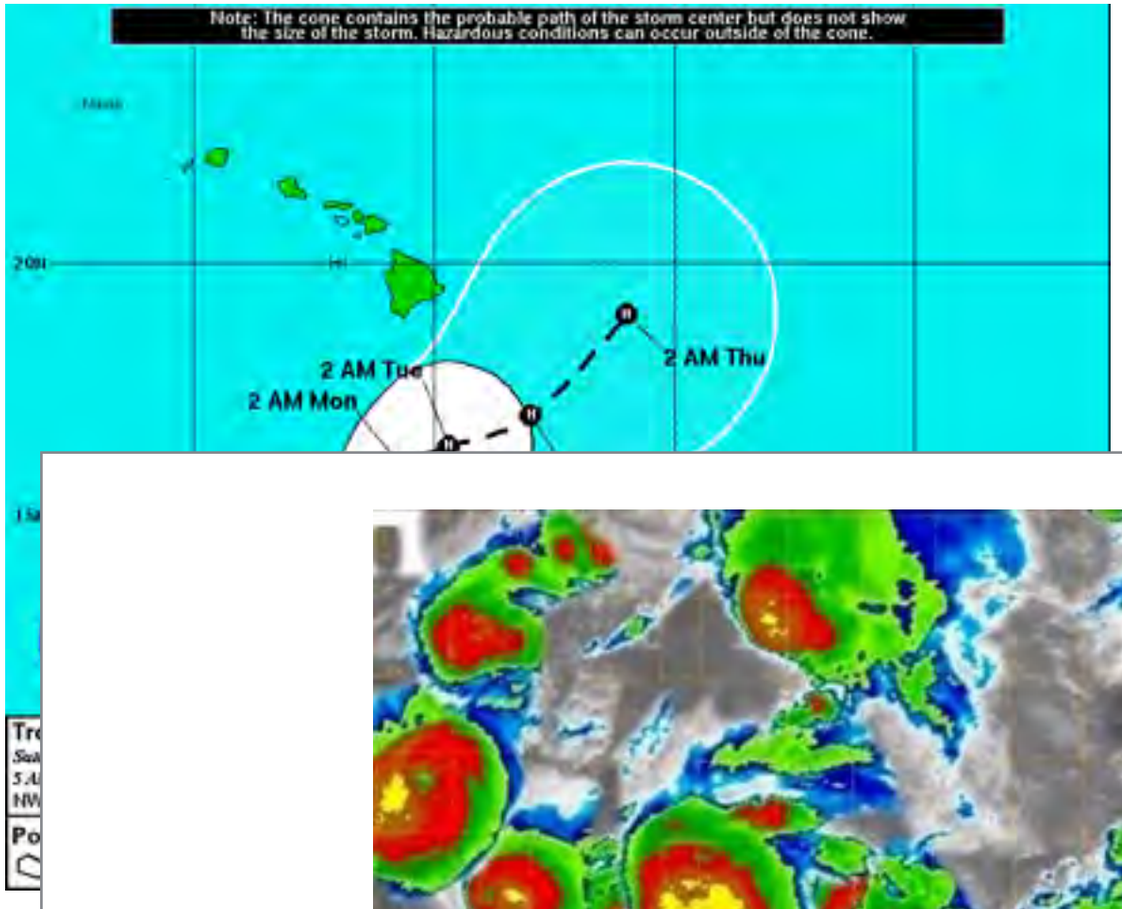

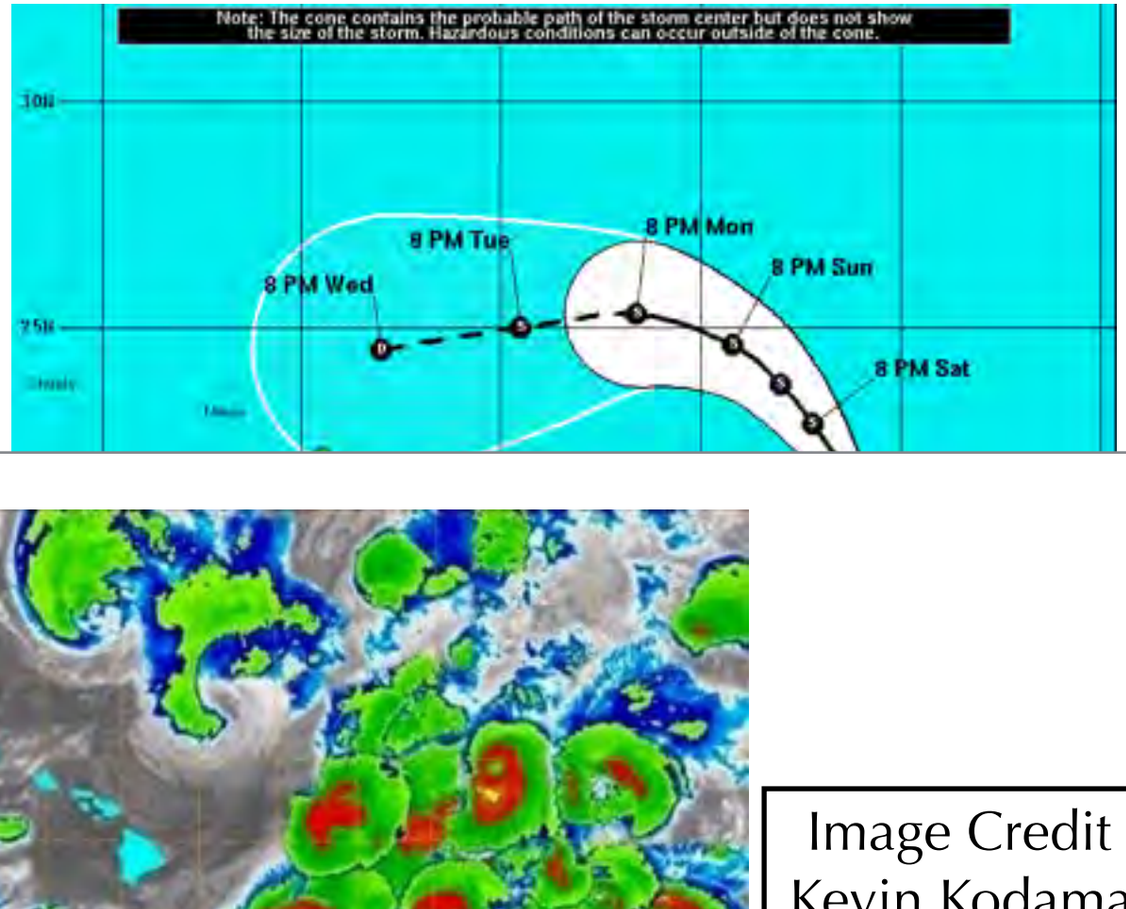

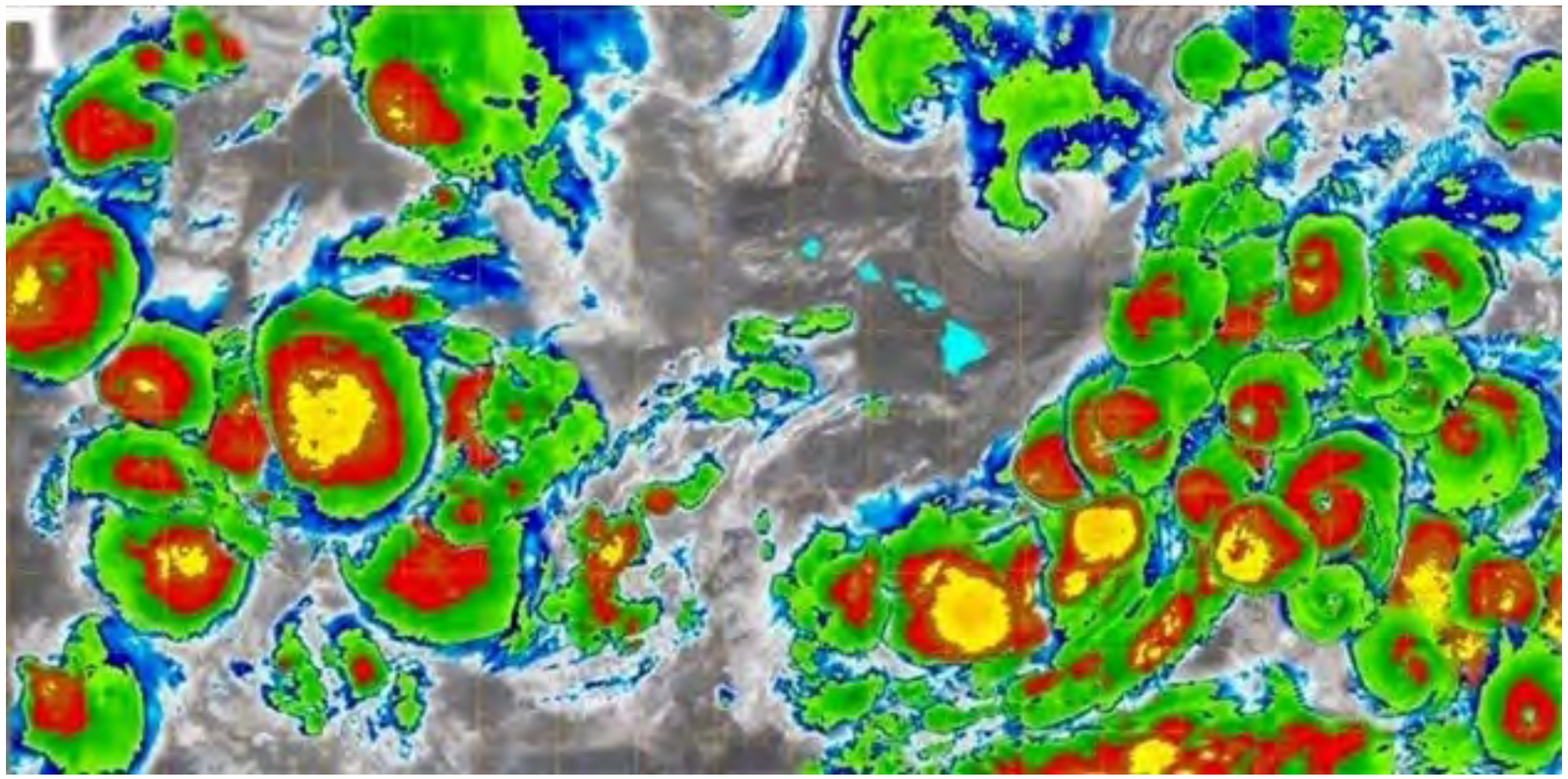

Image Credit
Kevin Kodama
NWS Honolulu

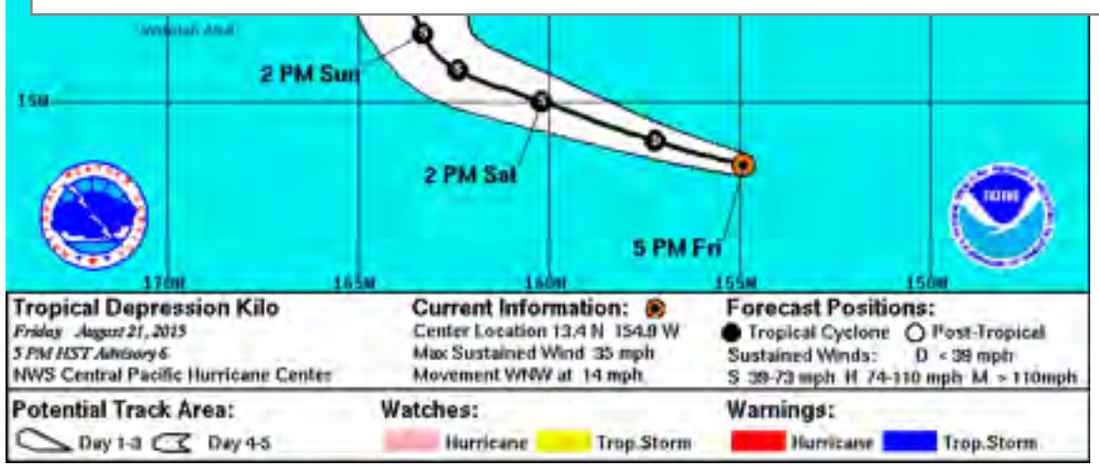

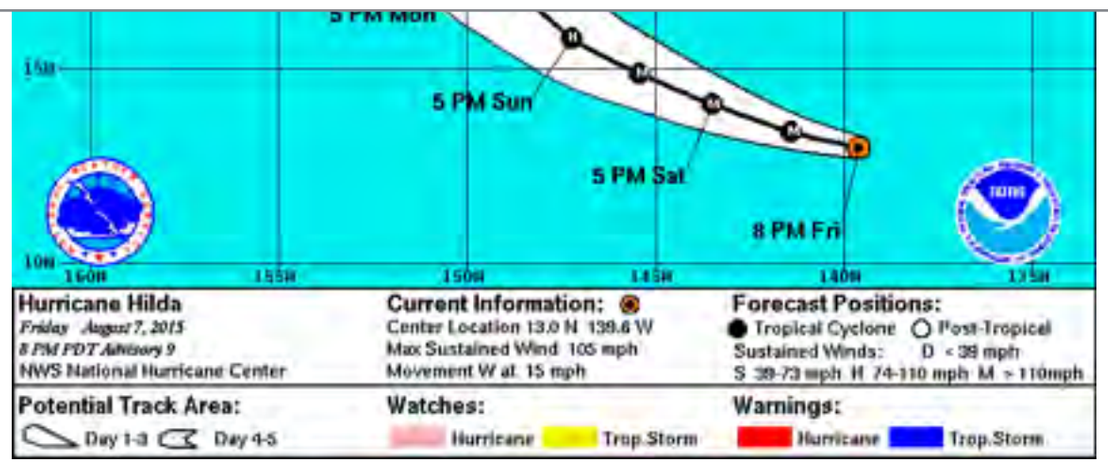

Tropical Storm Darby (2016)

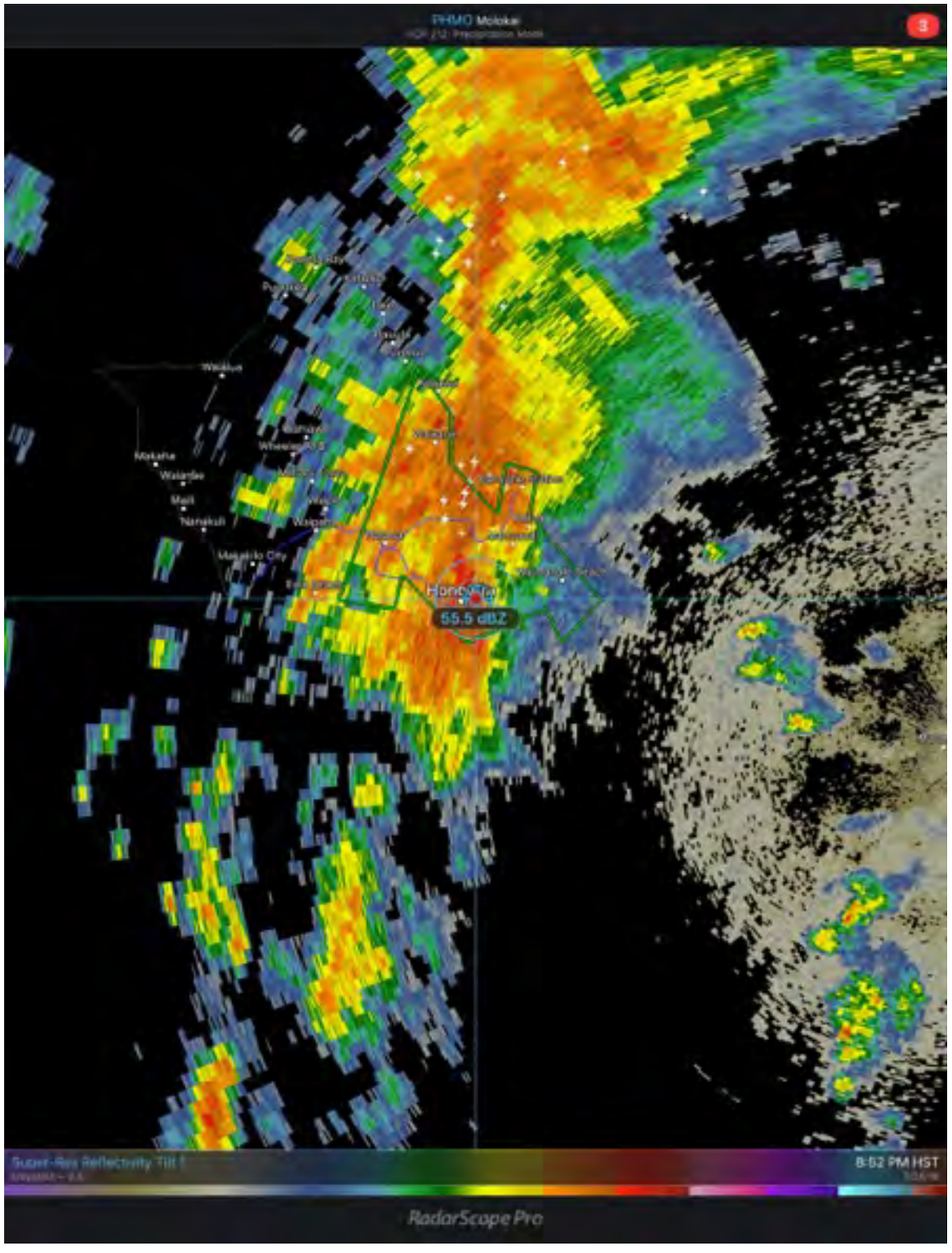

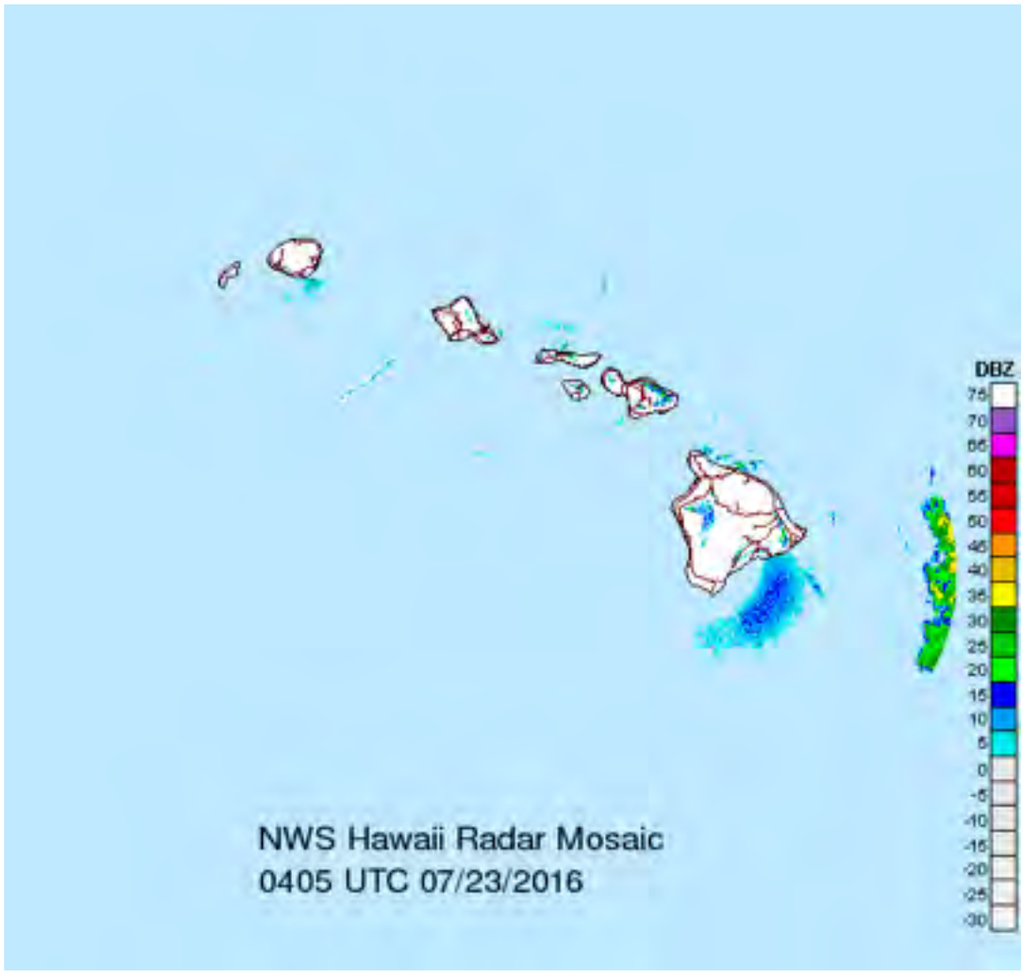

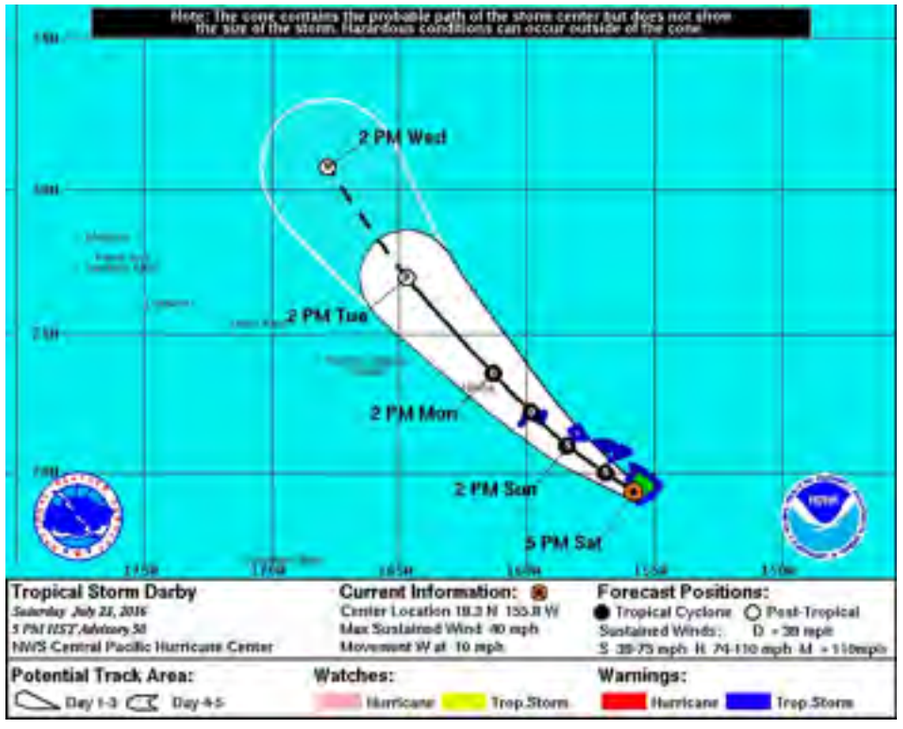

Outline

- **Part I 08/04: Introduction and TC Formation**
  - Background and Technological History
  - Results from THORPEX-Pacific Area Regional Campaign (TPARC)/Tropical Cyclone Structure (2008)
  - Results from PREDICT (2010)
- **Part II 08/05: Structure and Intensity Change**
  - Background and Theory
  - Results from RAINEX (2005), TPARC/TCS08, and TCI2015
  - Recent research results on composite structure of TCs from aircraft reconnaissance

TC formation and intensification involves multi-scale interactions

ln E

Downscale Enstrophy Cascade

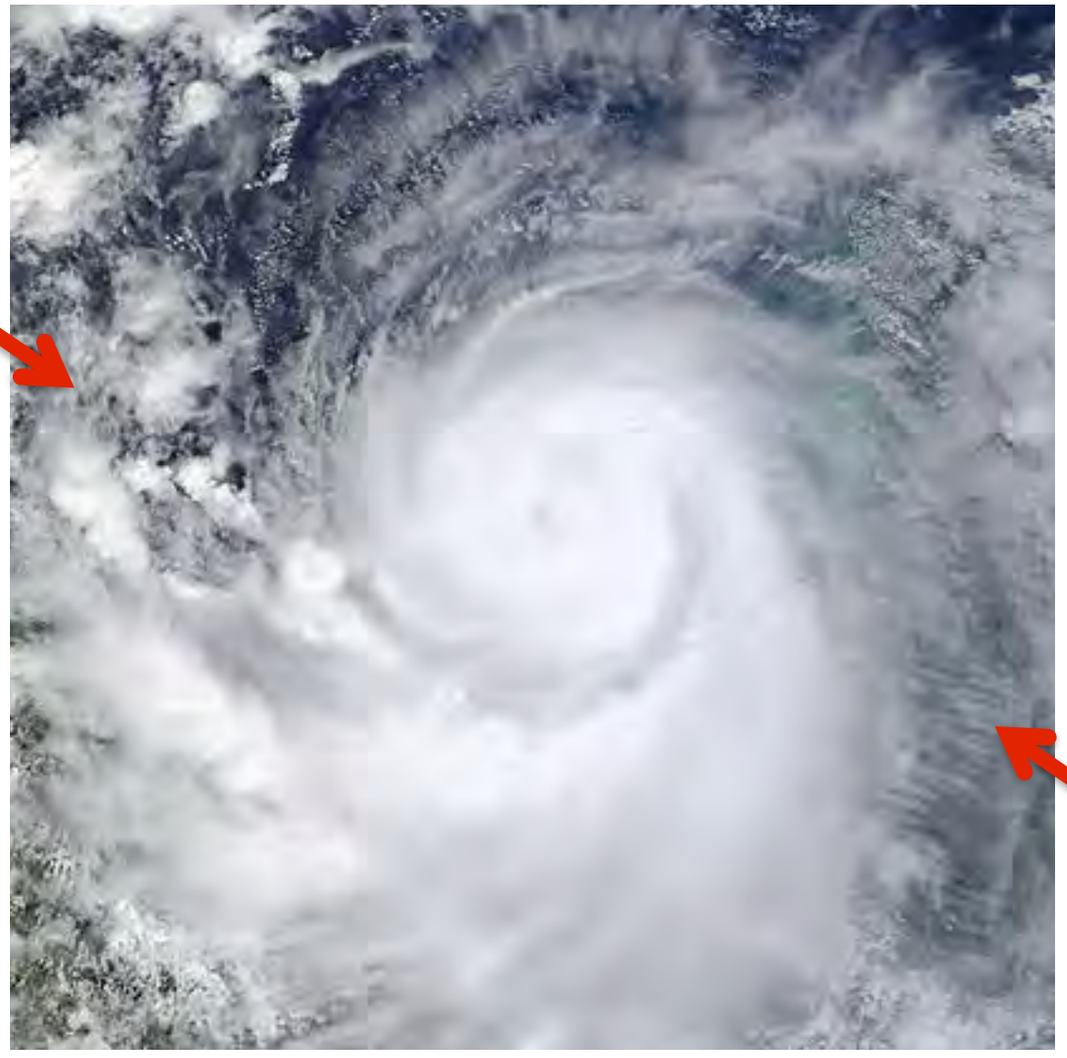

Upscale Energy Cascade

ln k

Intra-seasonal
MJO
>8,000 km

Synoptic
Easterly Waves
2,000 – 8,000 km

Meso-α:
Easterly wave critical layer
200 – 2,000 km

Meso-β:
TC, MCS, gravity waves
20 – 200 km

Meso-γ:
Rotating convection
Downdrafts, Gust fronts
2 – 20 km

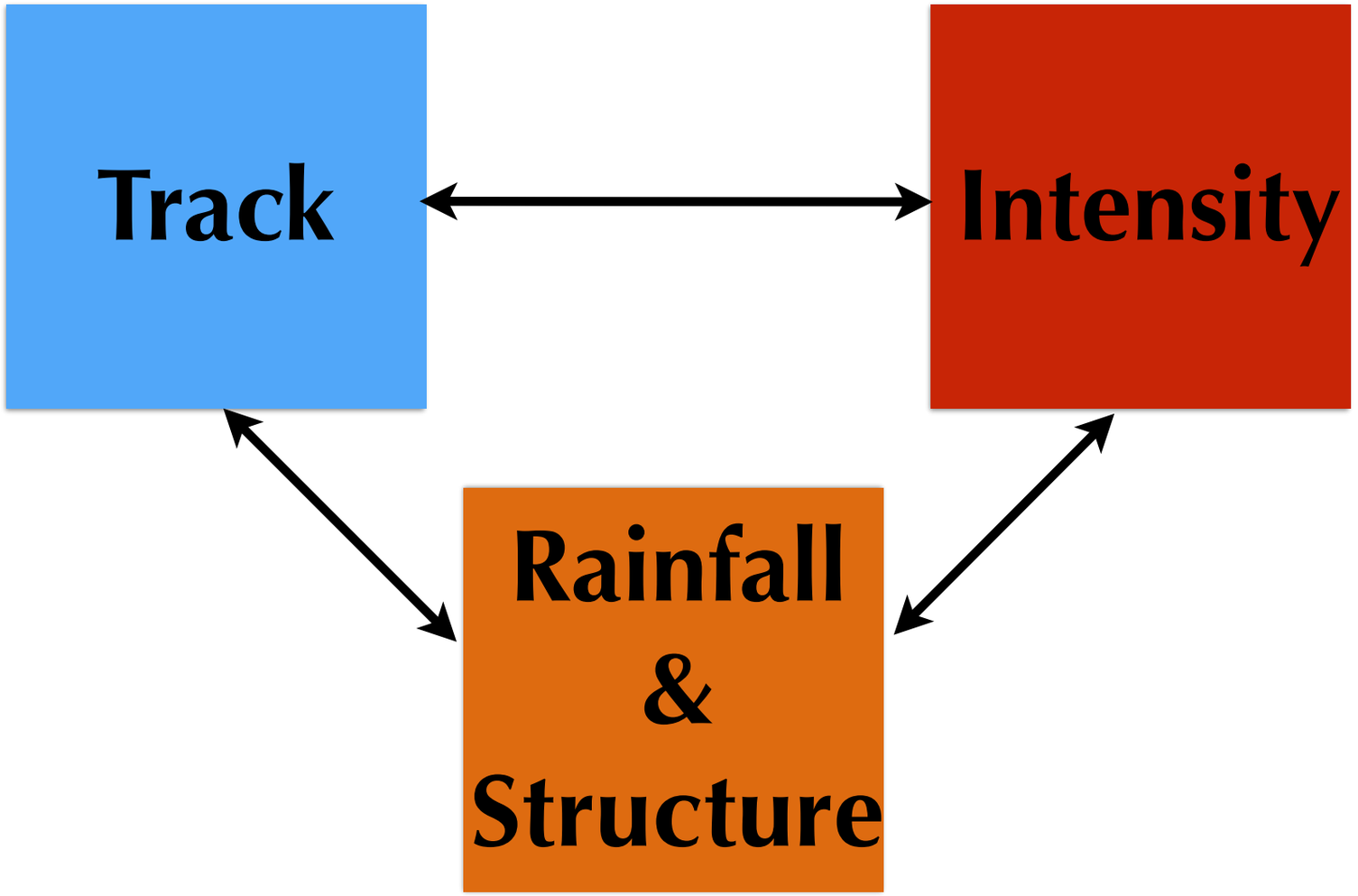
Track
Intensity
Rainfall
&
Structure

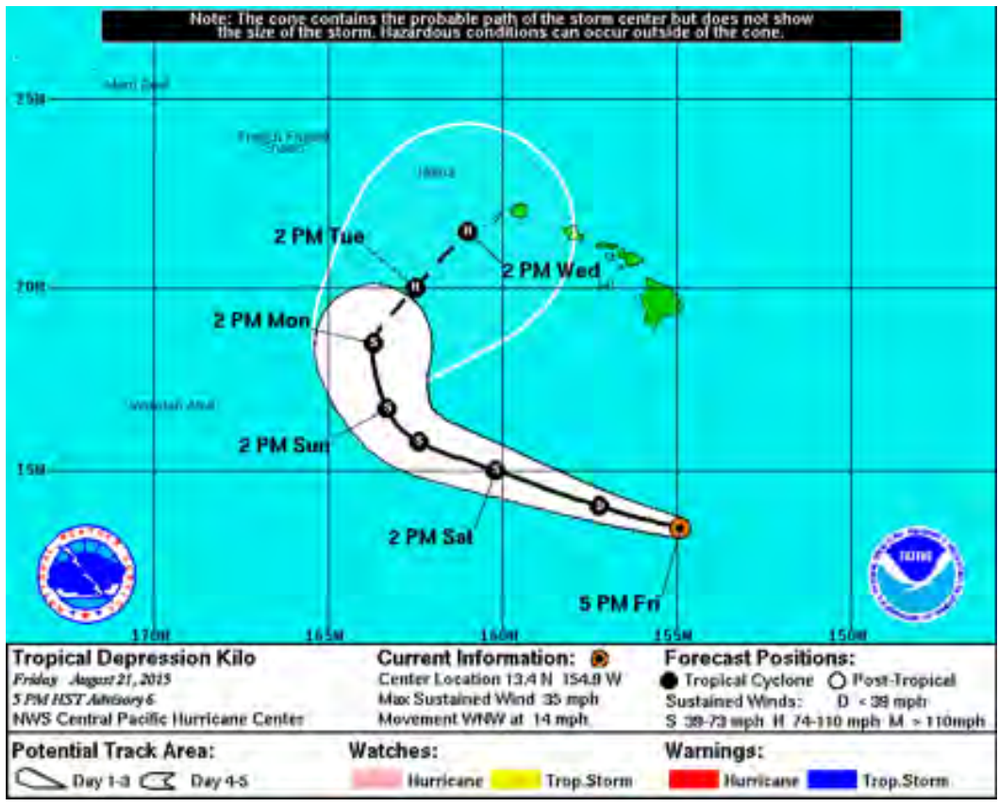
Note: The cone contains the probable path of the storm center but does not show the size of the storm. Hazardous conditions can occur outside of the cone.
2 PM Tue
2 PM Wed
2 PM Mon
2 PM Sun
2 PM Sat
5 PM Fri
Tropical Depression Kilo
Friday August 21, 2015
5 PM HST Advisory 6
NWS Central Pacific Hurricane Center
Current Information:
Center Location 13.4 N 154.9 W
Max Sustained Wind 35 mph
Movement WNW at 14 mph
Forecast Positions:
Tropical Cyclone
Post-Tropical
Sustained Winds: D < 39 mph
S 39-73 mph H 74-110 mph M > 110mph
Potential Track Area:
Day 1-3
Day 4-5
Watches:
Hurricane
Trop.Storm
Warnings:
Hurricane
Trop.Storm

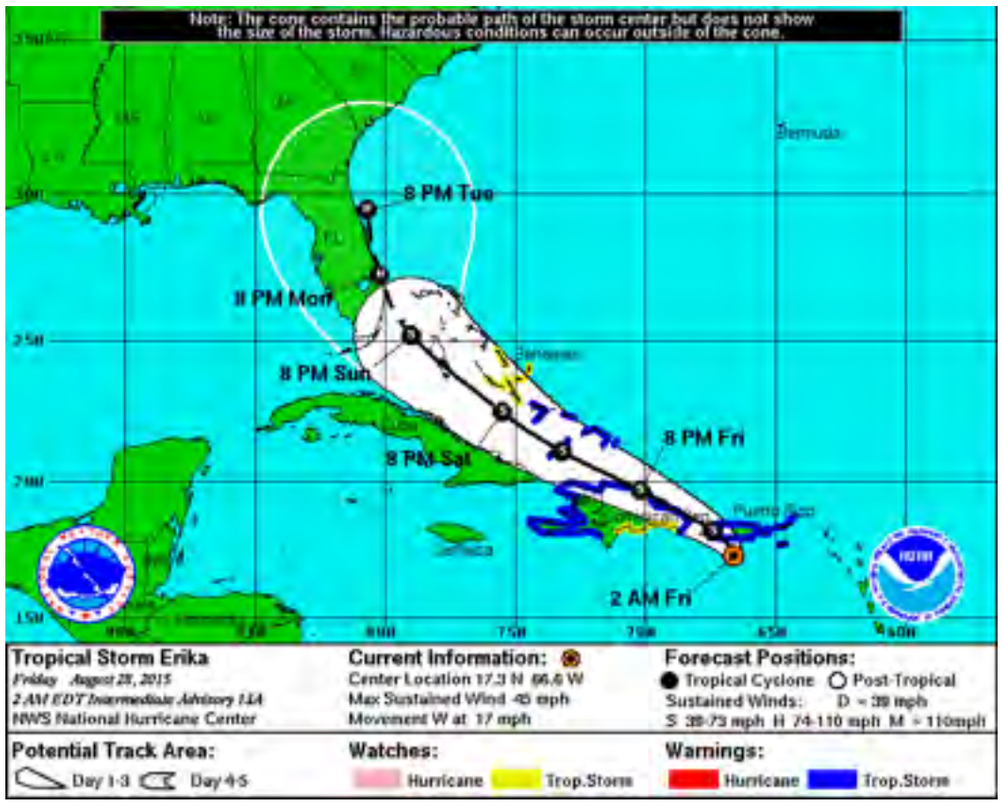
Note: The cone contains the probable path of the storm center but does not show the size of the storm. Hazardous conditions can occur outside of the cone.
8 PM Tue
8 PM Mon
8 PM Sun
8 PM Sat
8 PM Fri
2 AM Fri
Tropical Storm Erika
Friday August 28, 2015
2 AM EDT Intermediate Advisory 11A
NWS National Hurricane Center
Current Information:
Center Location 17.3 N 66.6 W
Max Sustained Wind 45 mph
Movement W at 17 mph
Forecast Positions:
Tropical Cyclone
Post-Tropical
Sustained Winds: D < 39 mph
S 39-73 mph H 74-110 mph M > 110mph
Potential Track Area:
Day 1-3
Day 4-5
Watches:
Hurricane
Trop.Storm
Warnings:
Hurricane
Trop.Storm

Aircraft Advantages

- Take measurements where you want them
- 3-D spatial variations from a mobile platform
  - Examples: 2-D horizontal mapping, 2-D vertical cross-section, vertical stack of line measurements
  - Remote sensing at close range allows for 1, 2 or 3-D measurements
- Possibly large payload for concurrent measurements of multiple variables with high accuracy and precision
  - Examples: wind, turbulence, cloud microphysics, radiation, aerosol, chemistry, radar, dropsonde ….

Aircraft Disadvantages

- Can’t stand still (Limited temporal resolution)
- Mobile platform adds uncertainty to measurements
  - Need to measure aircraft motion very accurately
  - Corrections needed for compressibility, adiabatic heating, flow distortion induced by aircraft, hydrometeor impacts
- Cost

Operational limitations

- Altitude limitations (minimum and maximum altitude)
- Protected air space
- Safety related requirements (hard down time, maintenance)
- Not feasible for continuous measurements

Basic Instrumentation on NOAA P3

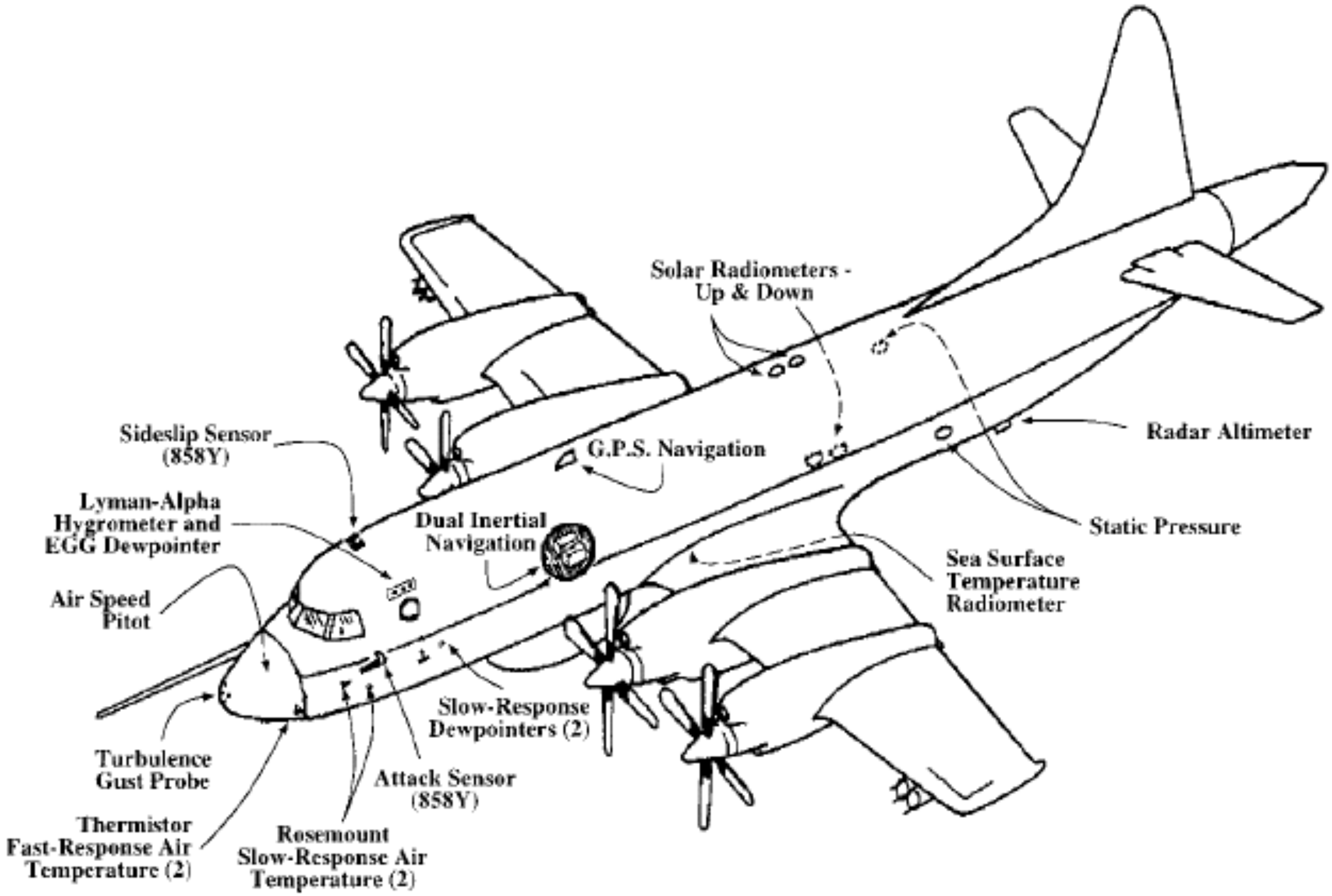

FIG. 1. Sketch of NOAA WP-3D instrumentation.

Jet (non-penetrating) vs Turboprop (penetrating)

- G-V Jet: better range & altitude, but cannot penetrate heavy precipitation

Length: 96 ft 5 in (29.4 m)
Wingspan: 93 ft 4 in (28.5 m)
Payload: 6,500 lb (2,948 kg) (Research Payload 3,500 lbs)
Maximum speed: 510 kts (Mach 0.885)
Cruise speed: 488 knots, 904 km/h
Range: 5,800 nautical miles (10,742 km)
Service ceiling: 51,000 ft (15,545 m)
Powerplant: 2 × Rolls-Royce BR710A1-10 turbofan, 14,750 lbf (65 kN) each

- C-130 Turboprop: less range & altitude, but can penetrate eyeball

Payload: 45,000 lb (20,000 kg)
Length: 97 ft 9 in (29.8 m)
Wingspan: 132 ft 7 in (40.4 m)
Maximum speed: 320 knots (366 mph, 592 km/h) at 20,000 ft (6,060 m)
Cruise speed: 292 knots (336 mph, 540 km/h)
Range: 2,050 nmi (2,360 mi, 3,800 km)
Service ceiling: 33,000 ft (10,060 m) empty;[56] 23,000 ft (7,077 m) with 42,000 pounds
Powerplant: 4 × Allison T56-A-15 turboprops, 4,590 shp (3,430 kW) each

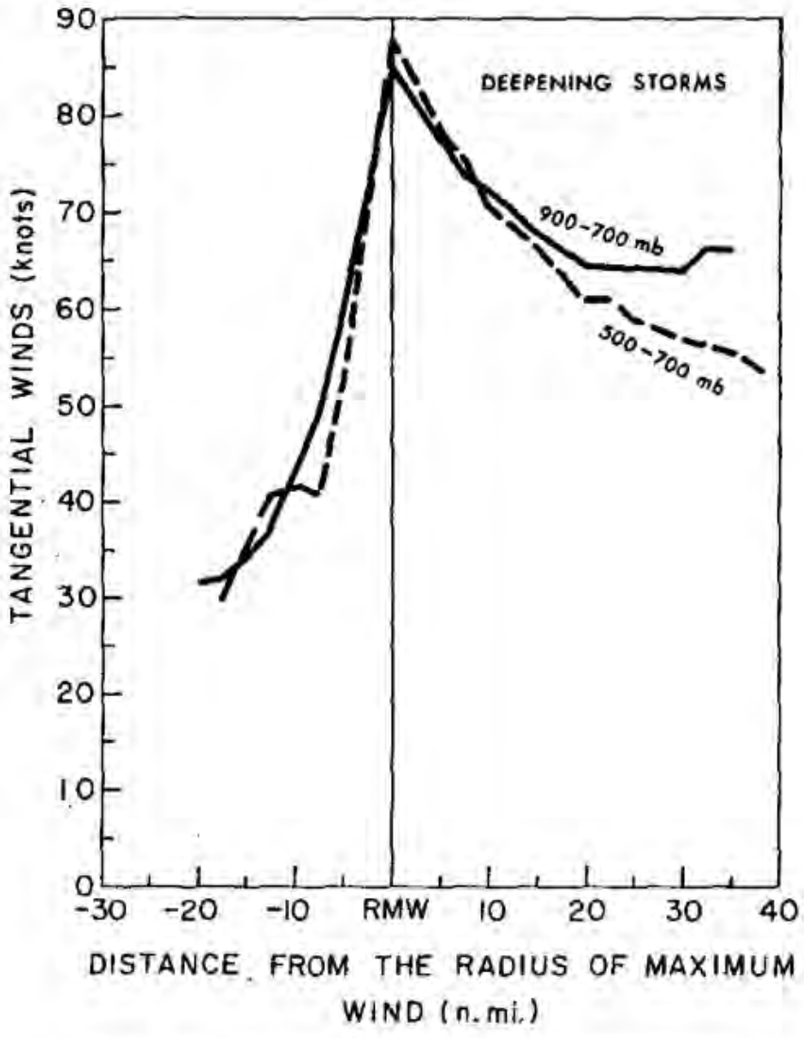

FIG. 42. Tangential wind profiles for deepening storms (Method I).

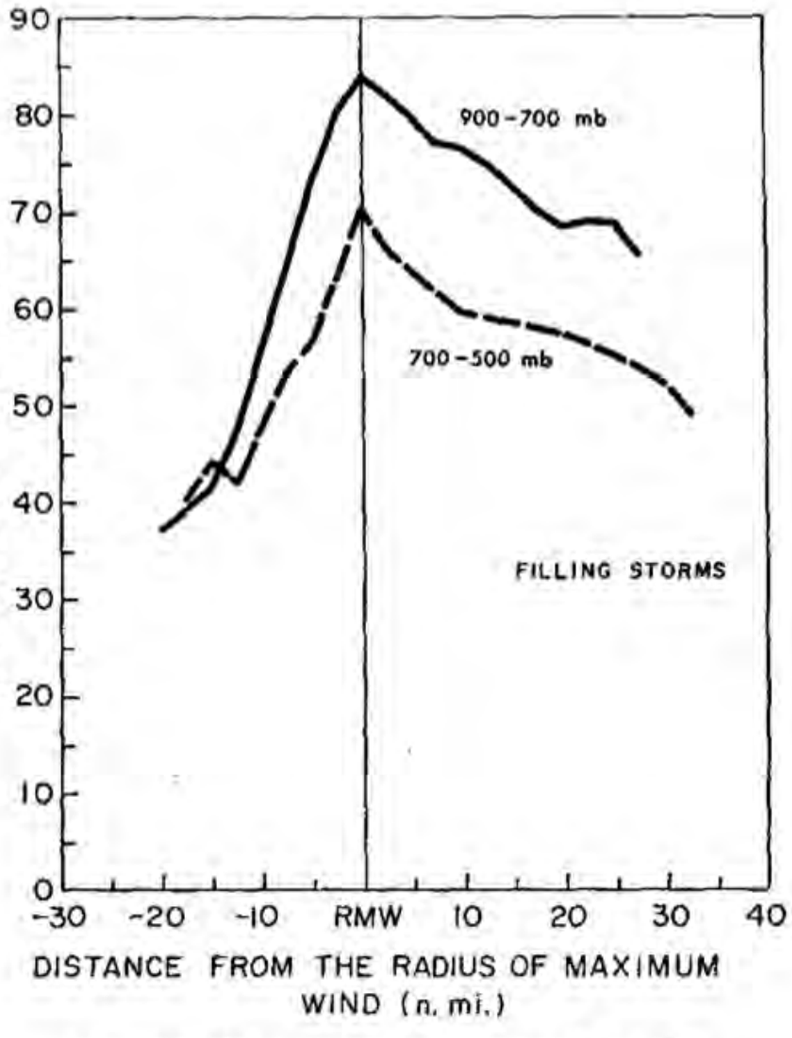

FIG. 43. Tangential wind profiles for filling storms (Method I).

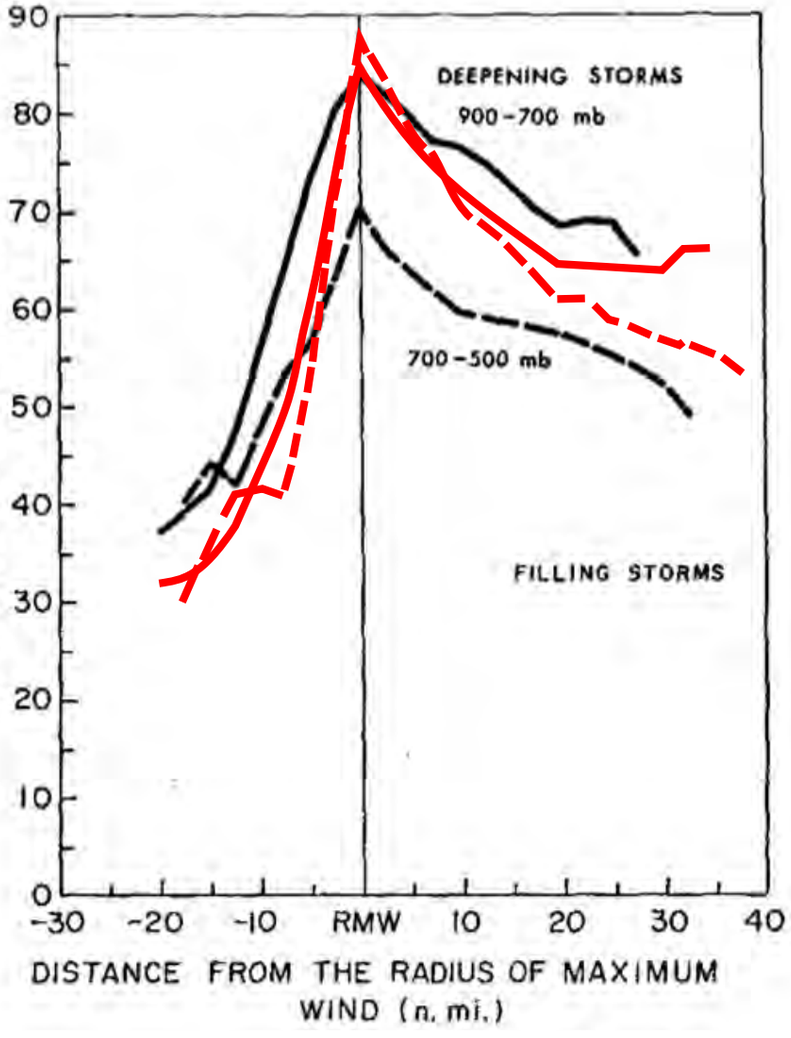

The Hurricane's Inner Core Region. I. Symmetric and Asymmetric Structure

DENNIS J. SHEA[1] AND WILLIAM M. GRAY

Dept. of Atmospheric Science, Colorado State University, Fort Collins 80521

(Manuscript received 14 July 1972, in revised form 1 August 1973)

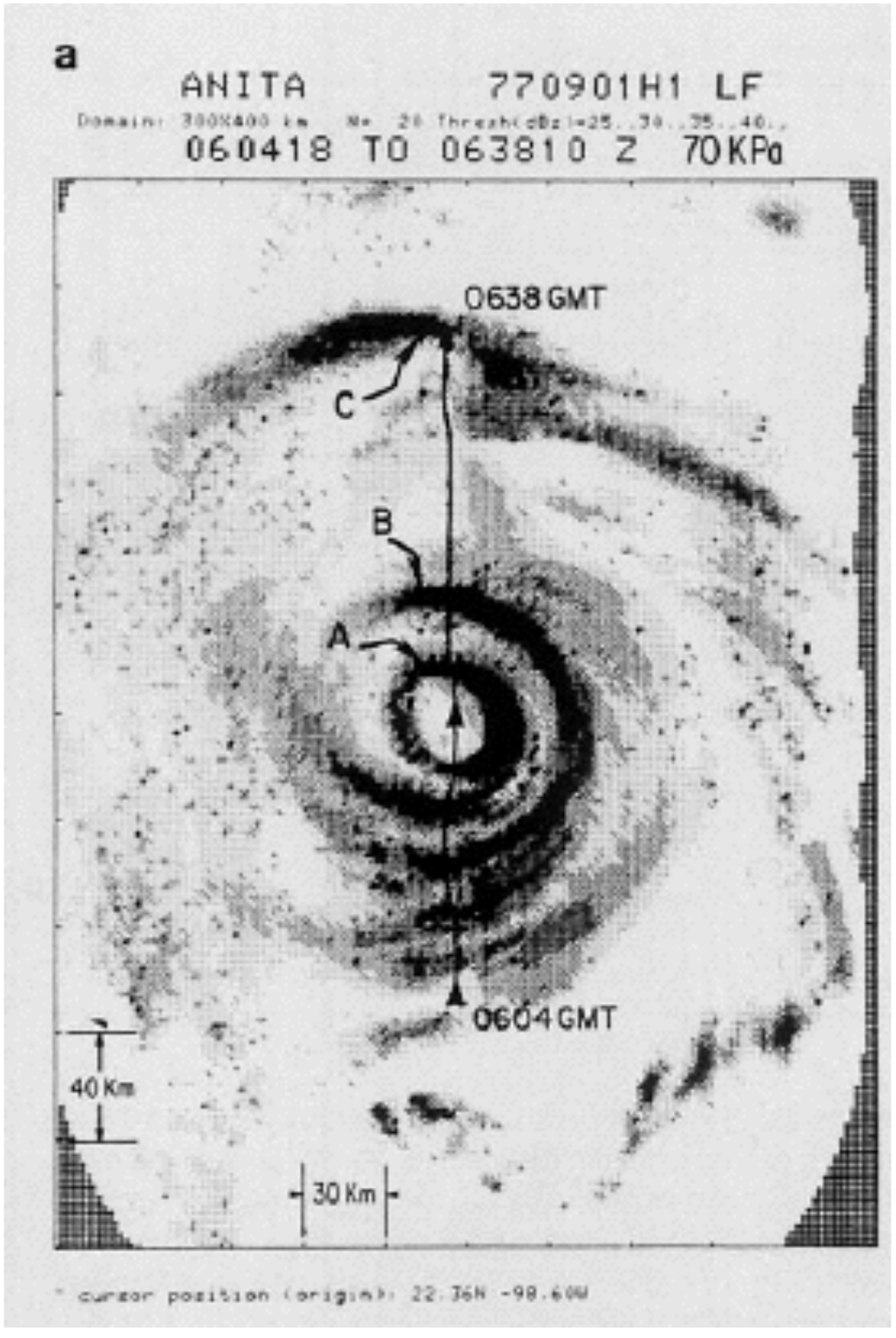

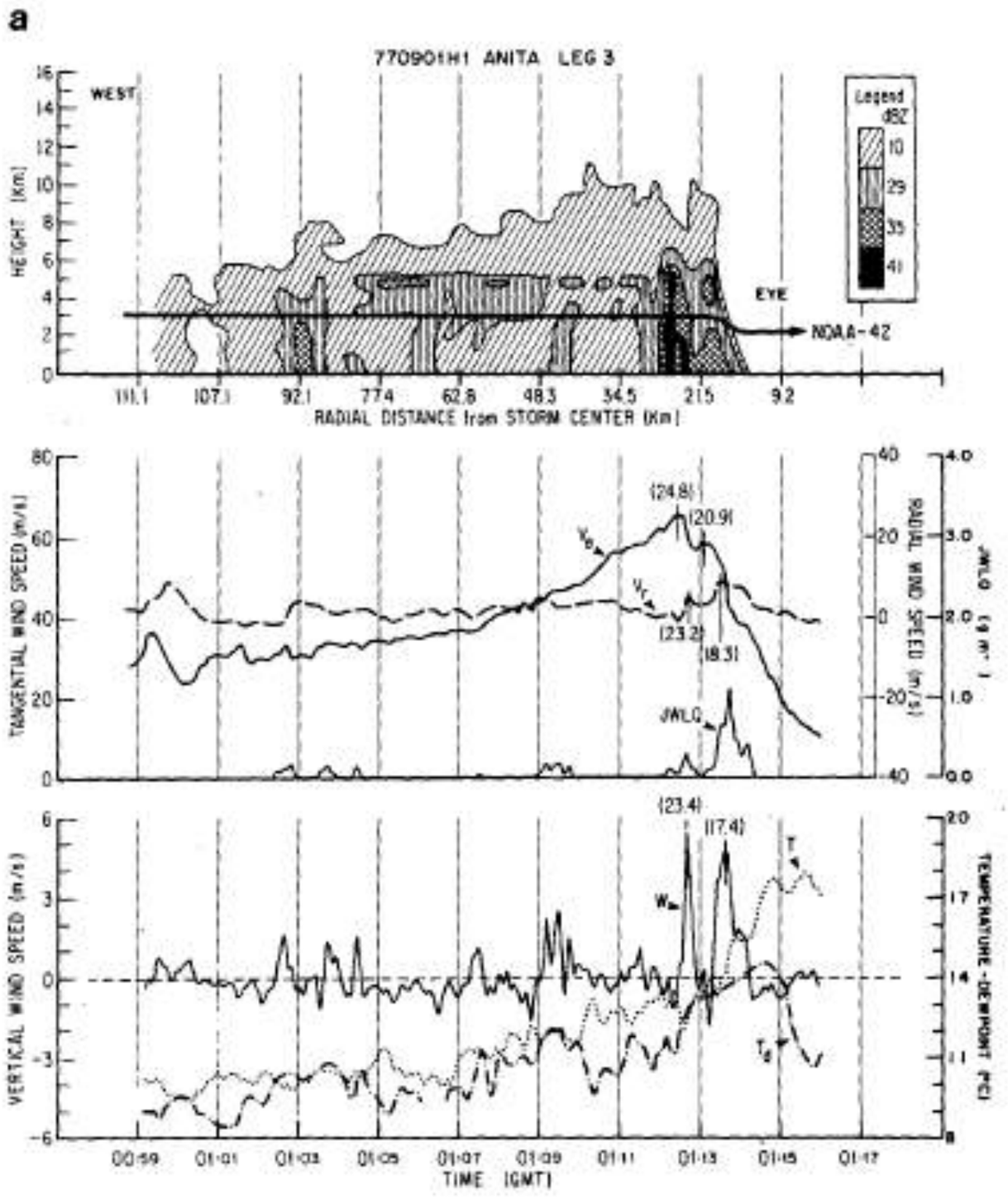

FIG. 4. Profiles of radar reflectivity, tangential wind V_t, radial wind V_r, cloud water content JWLQ, vertical wind W, temperature T, and dew point T_d, from (a) Hurricane Anita, (b) Hurricane Frederic, (c) Hurricane Allen on 5 August, and (d) Hurricane Allen on 8 August. All wind data are relative to the moving storms. The radar reflectivity cross section was generated by compositing vertical rays from the tail radar at four samples per min. Locations of the peaks of the horizontal and vertical wind are indicated in parentheses. The aircraft flew from west of the centers inward to the eyes.

Mesoscale and Convective-Scale Characteristics of Mature Hurricanes. Part I: General Observations by Research Aircraft

DAVID P. JORGENSEN

NOAA, Atlantic Oceanographic and Meteorological Laboratory, Hurricane Research Division, Miami, FL 33149

(Manuscript received 7 February 1983, in final form 27 December 1983)

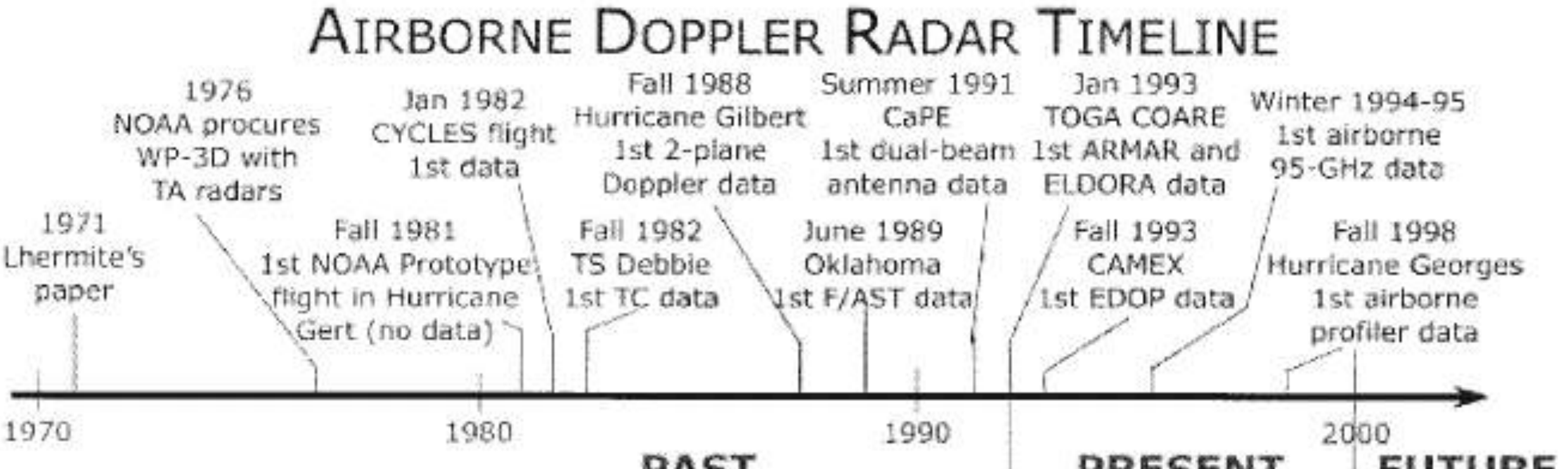

FIG. 1. Airborne Doppler radar time line, representative as of Mar 2000.

From Lee et al. (2003)

- First proposed by Lhermite (1971)
- Data collected in tropical cyclones, squall lines, thunderstorms, boundary layer, tropical and marine clouds, orographic, north Atlantic, and more

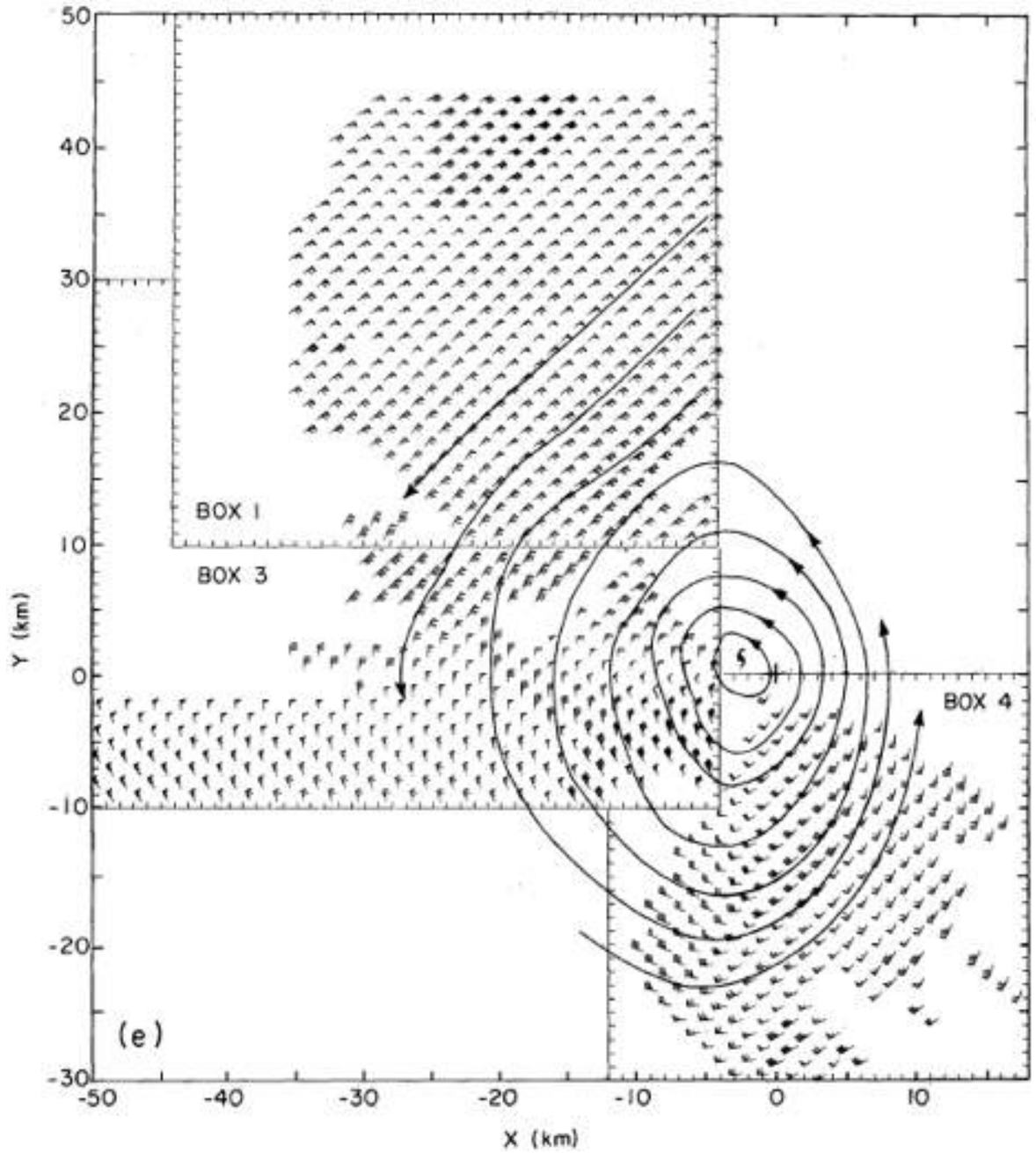

FIG. 2e. Mosaic of Doppler-derived winds in Boxes 1, 3, and 4, with streamlines and storm-center location implied by the streamlines of the Doppler winds also indicated.

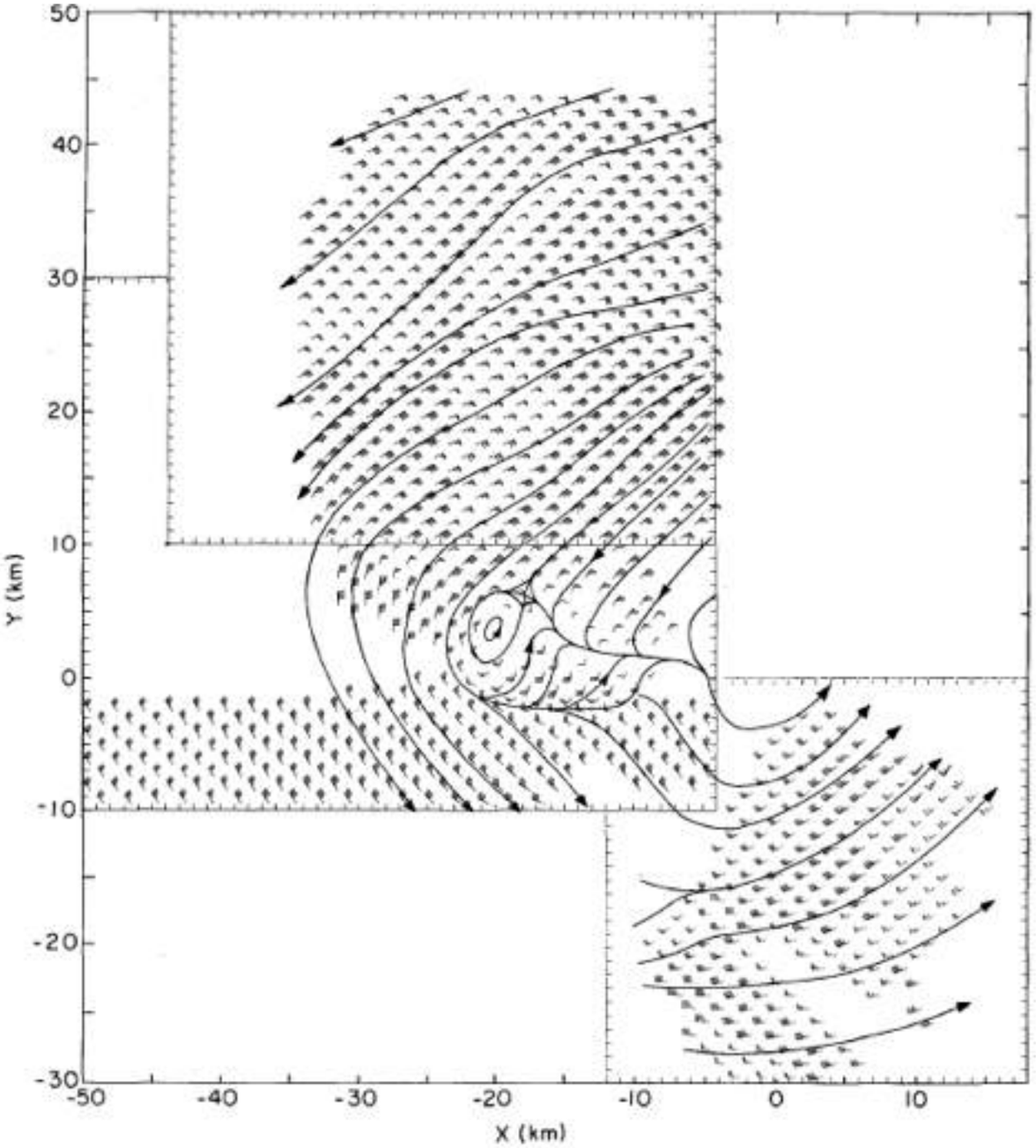

FIG. 7. Analysis of Doppler-derived winds at the 2.5 km level. The field is a mosaic of the wind patterns in Boxes 1, 3, and 4. Plotting convention same as in Fig. 2.

Airborne Doppler Radar Observations in Hurricane Debby

Frank D. Marks, Jr.[1] and
Robert A. Houze, Jr.[2]

Mobile Wx Radars

- Take the radar to the storm, but adds additional constraints on size, weight, and sampling requirements
- Mobility adds challenges to pointing angle determination and velocity recovery
- Move it, then park it
  – DOW, SMART-R, MWR-05XP, Umass X & W
- ***Fly it***
  – ARMAR, ELDORA, P3 Tail, WCR, EDOP

Problems in Raw Data

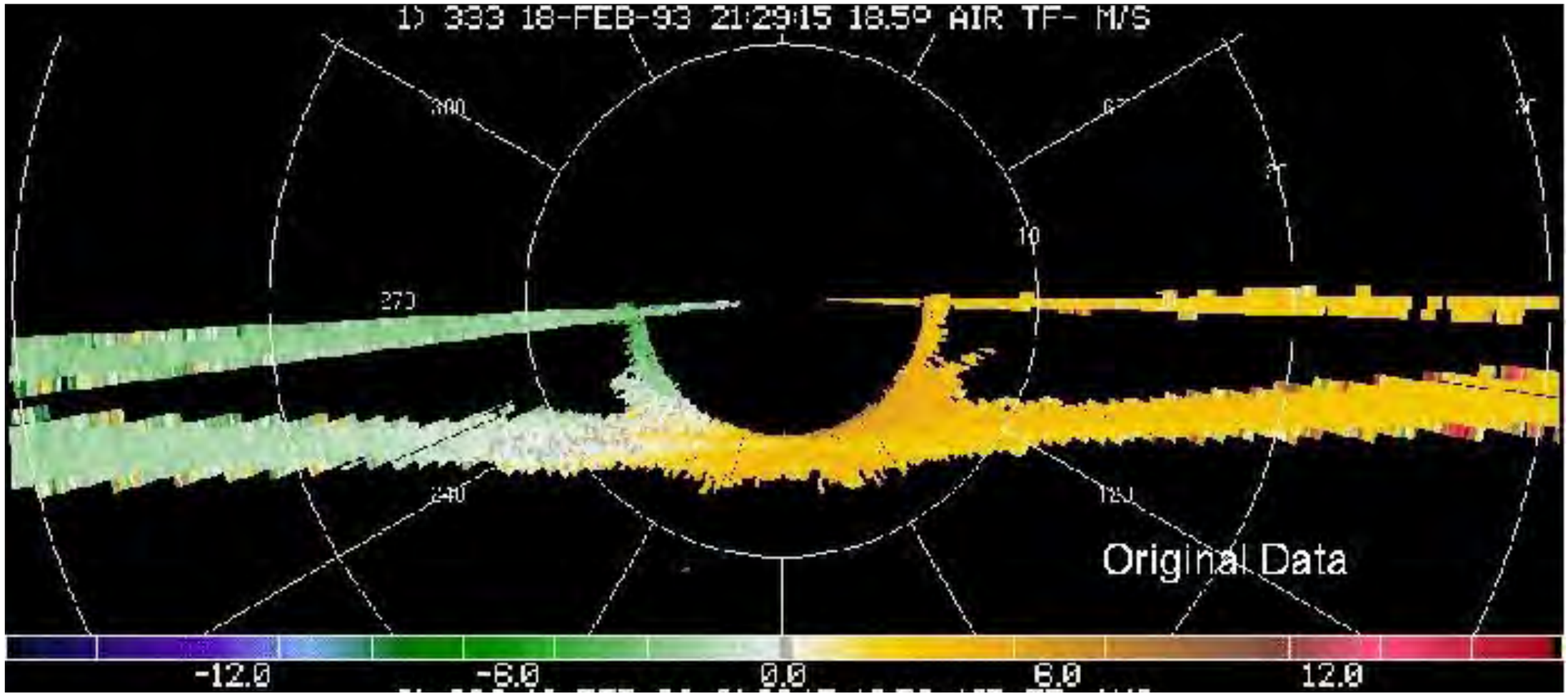

1. Earth surface is tilted.
2. Earth surface is not stationary.
3. Earth surface moves at different speeds.

Testud et al 1995

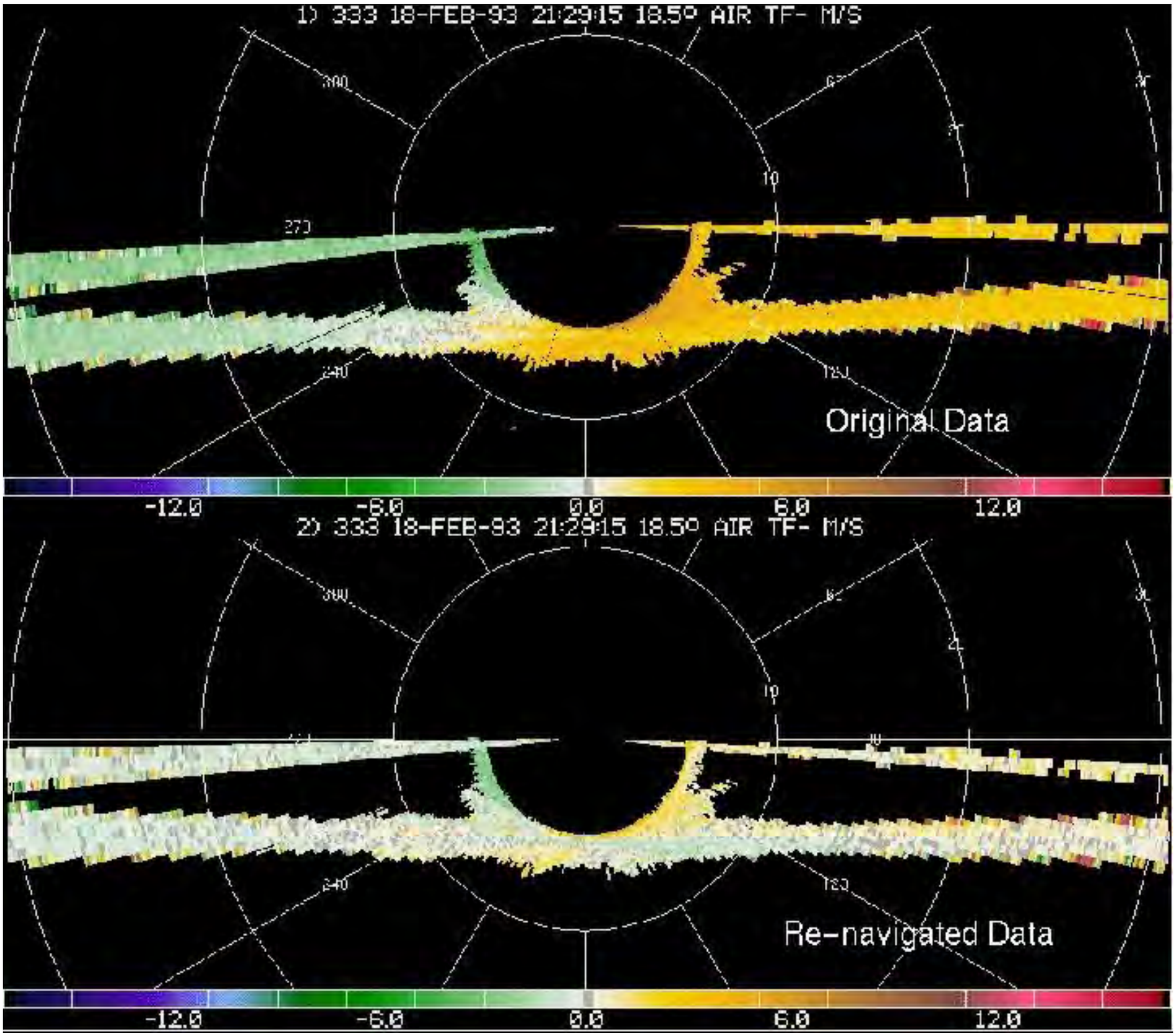
1) 333 18-FEB-93 21:29:15 18.5° AIR TF- M/S
300
270
240
210
180
150
120
90
60
30
0
10
20
Original Data
-12.0
-6.0
0.0
6.0
12.0
2) 333 18-FEB-93 21:29:15 18.5° AIR TF- M/S
Re-navigated Data

Dual-Doppler Flight Patterns

- ‘L’ pattern
- Cross-pattern
- F/AST Mode
- Stationary and steady assumptions apply

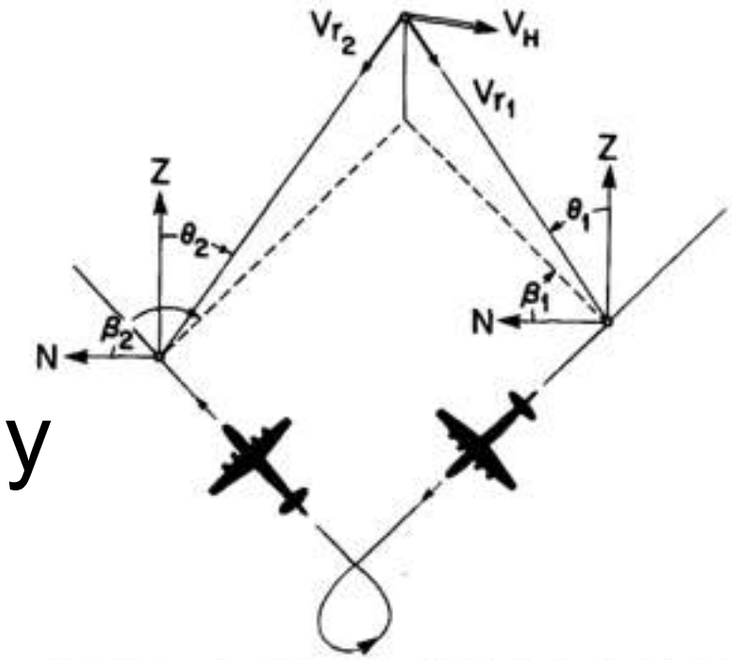

FIG. 2. Geometry of the pseudo-dual-Doppler horizontal wind calculation. Each point within the three-dimensional grid must be examined by two near-orthogonal rays of the vertically scanning tail Doppler radar. V_{r1} and V_{r2} are the two radial velocity components of the horizontal wind vector $\mathbf{V}_H$. θ is the elevation angle from the vertical and β the pointing angle from north (normally at right angle to the aircraft's track).

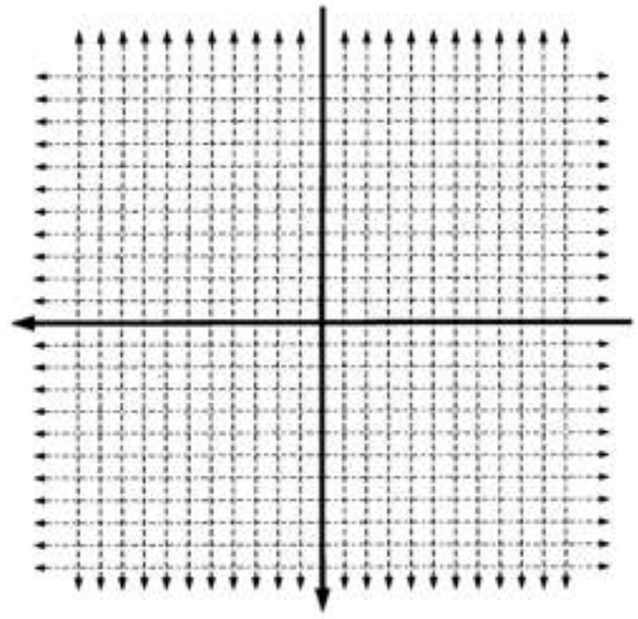

Jorgensen et al 1983; Gamache et al 1995

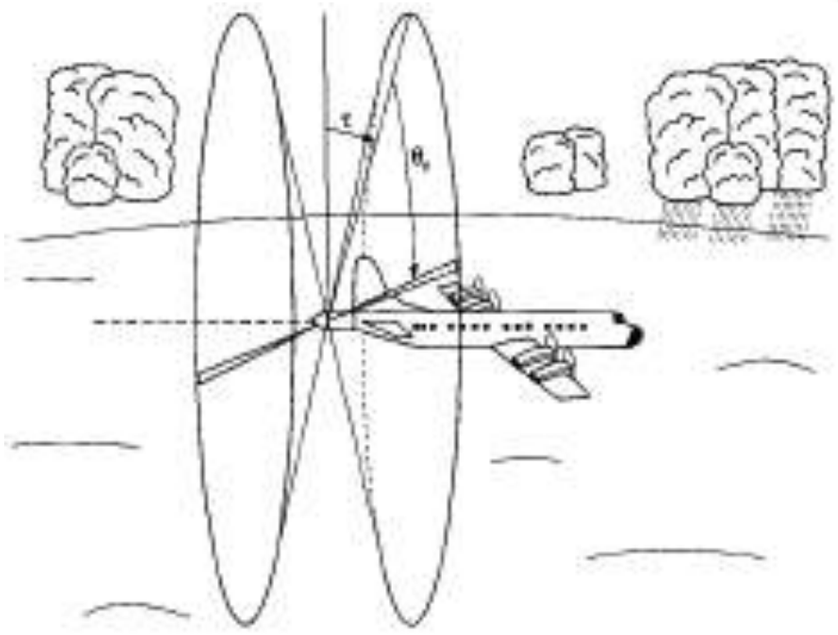

Hildebrand et al 1996

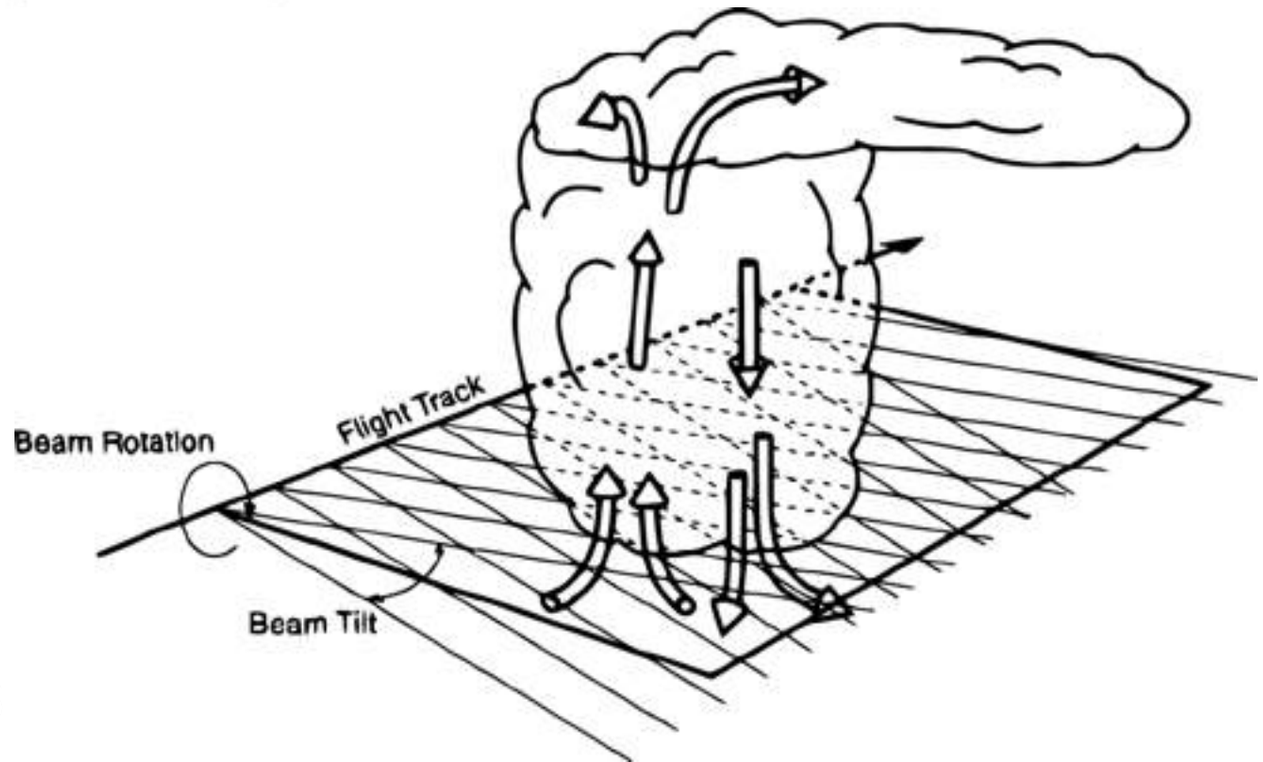

ELDORA Airborne Doppler Radar

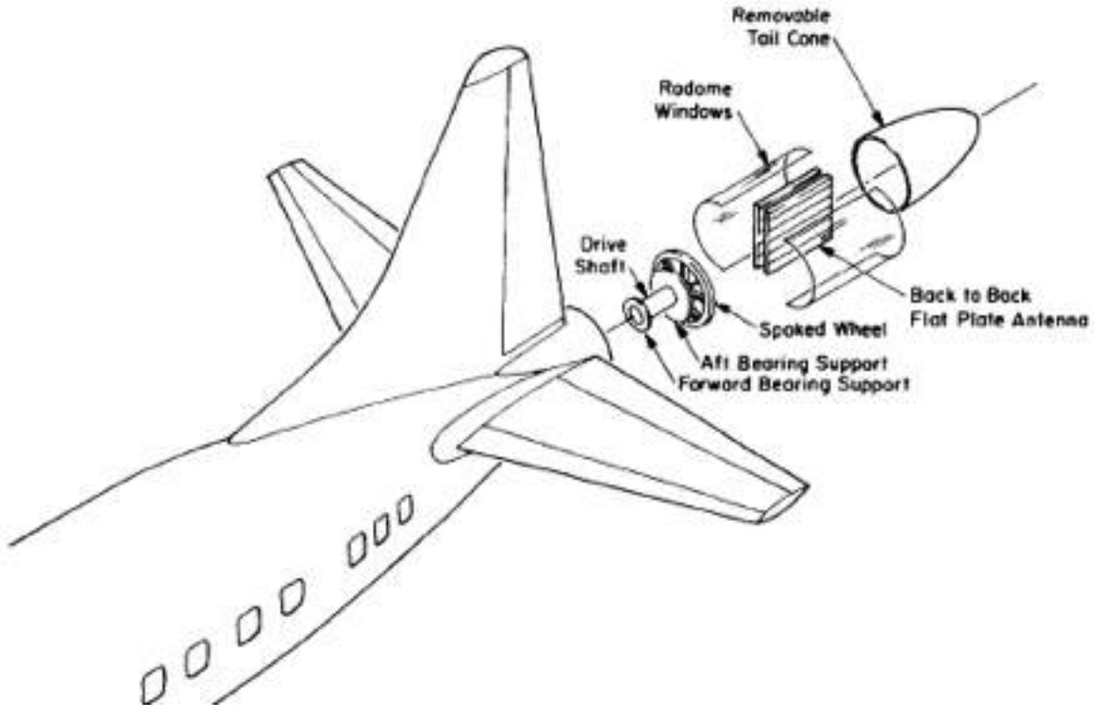

- NRL-P3 E~~Lectra DO~~ppler RAdar
  - 3.2 cm, 1.8° beam, 38.7 dB G
  - 2 Antennas & Tx
  - 35-40 kW Peak Power
  - 2 PRF in 4:5 ratio = >80 m/s NV
  - Scan rate up to 144°/s
  - Complex ‘chirp’ w/4 Freq.
  - ~400 m along track resolution
  - Unambig. Range ~60 km (Convective)
- TOGA COARE (93),VORTEX 95, LAKEICE (97/98), MAP (99), IHOP (02), CRYSTAL-FACE (02), BAMEX (03), RAINEX (05), TCS-08/TPARC (08)
- Retired after TPARC, to be replaced in ~2022 by APAR

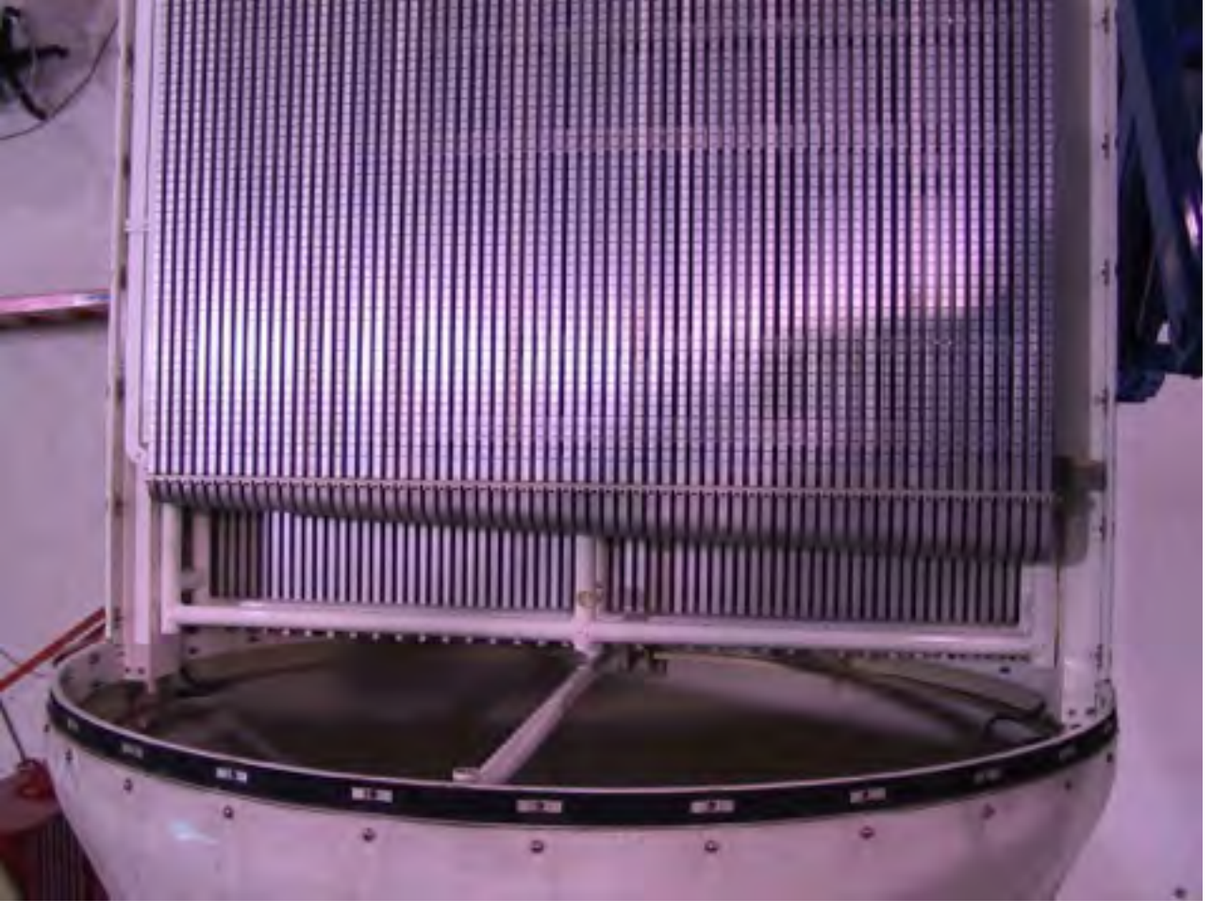

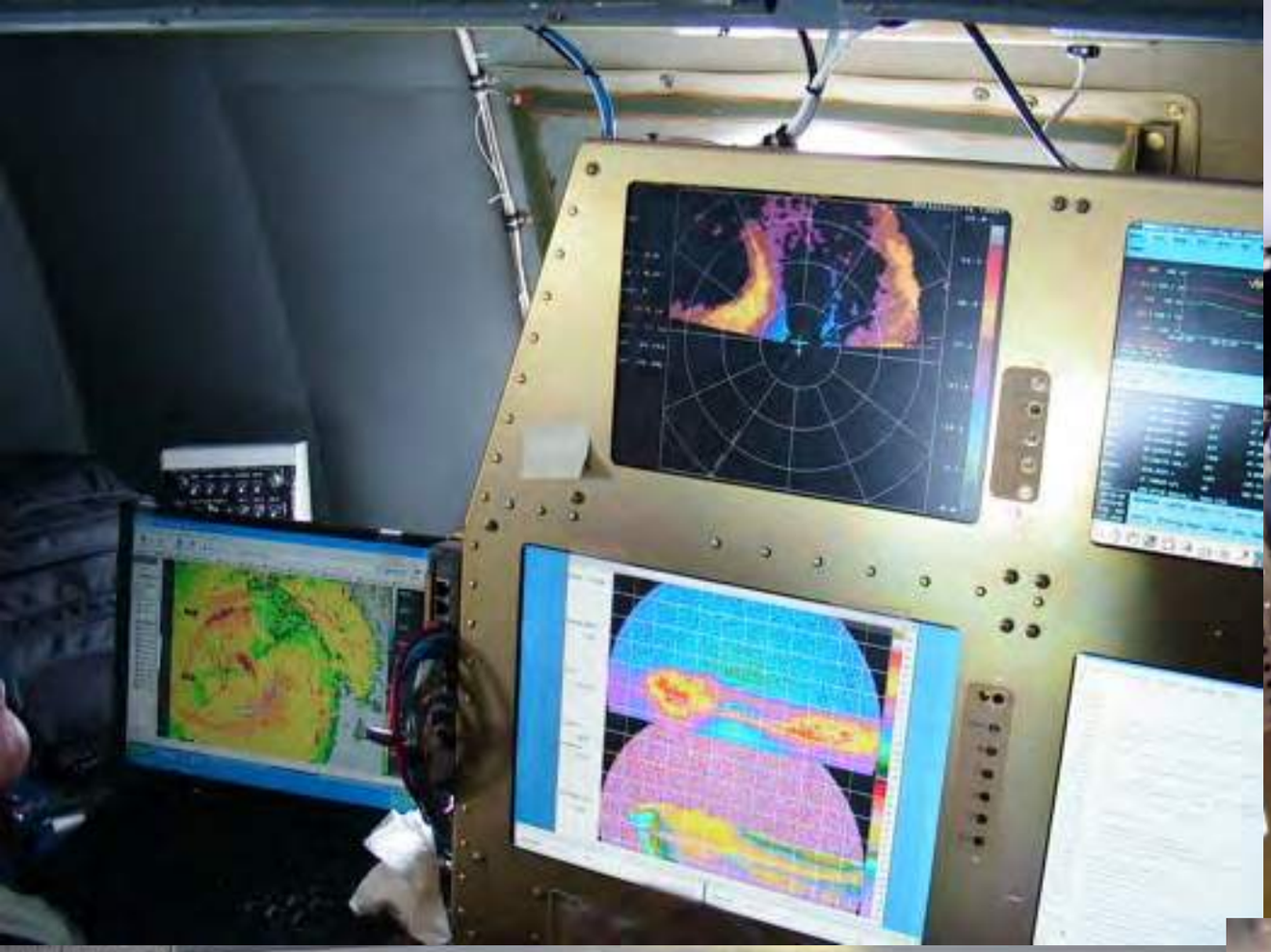


#7

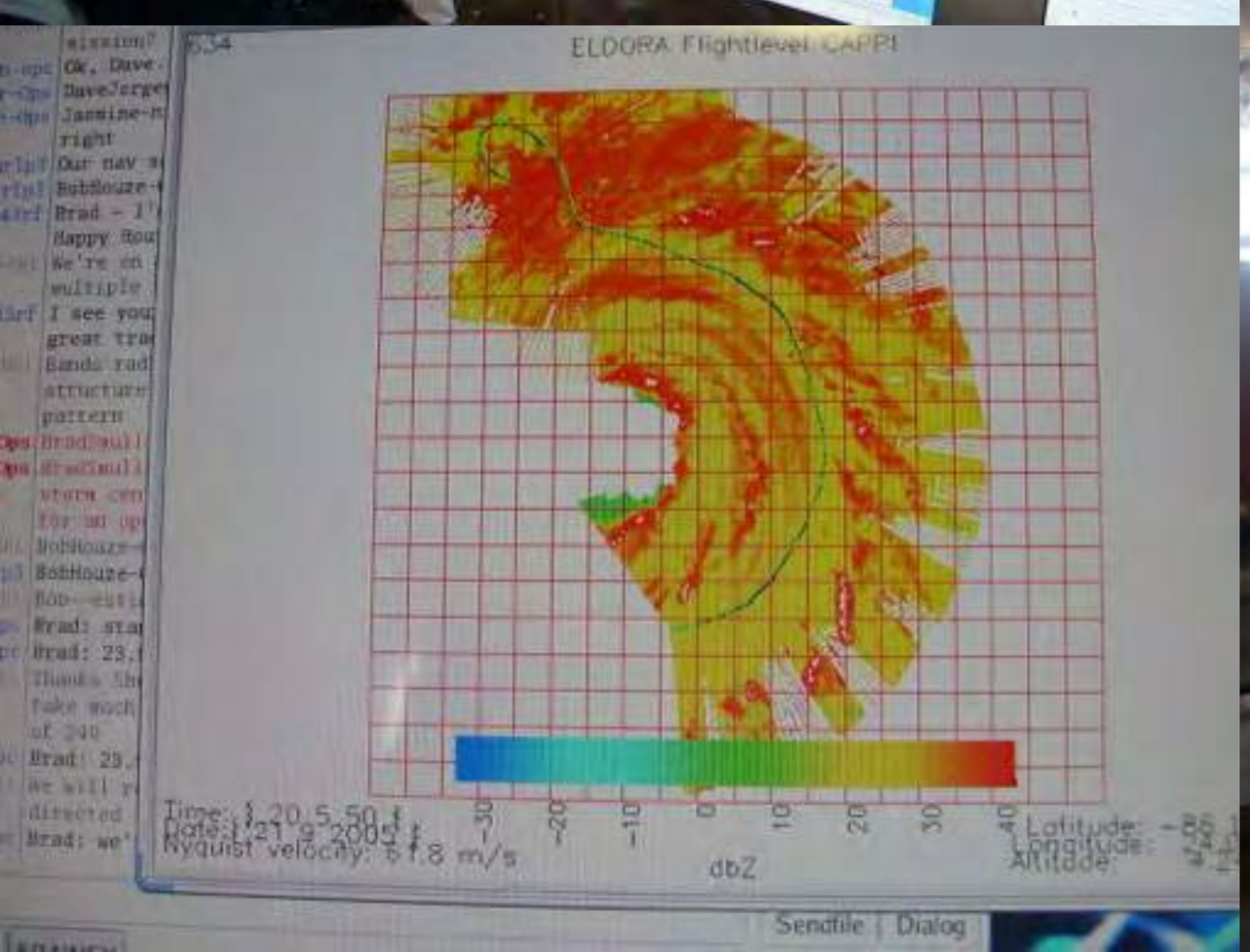
ELDORA Flightlevel CAPPI
Time:
Date:
Nyquist velocity:
dbZ
Latitude:
Longitude:
Altitude:
Sendfile
Dialog

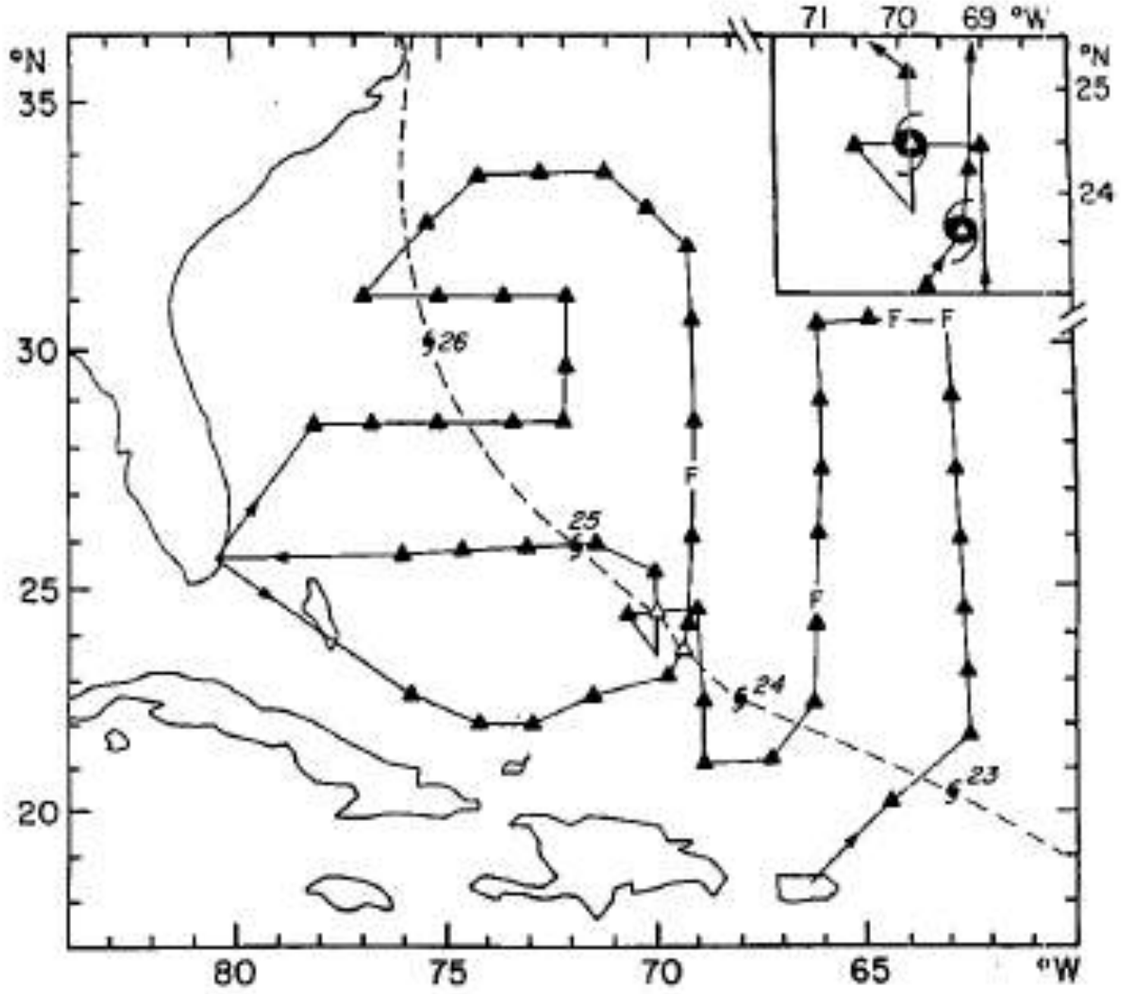

FIG. 2. Flight tracks for the Gloria synoptic flow experiment, 24–25 September 1985. Gloria's track is marked with a dashed line; hurricane symbols identify the 1200 UTC positions on the dates indicated. Successful ODW sounding locations are indicated by triangles; ODWs that failed are labeled "F." An expanded view of ODWs in the vicinity of Gloria's center is shown in the insert. Two ODW soundings in the eye are identified by open triangles.

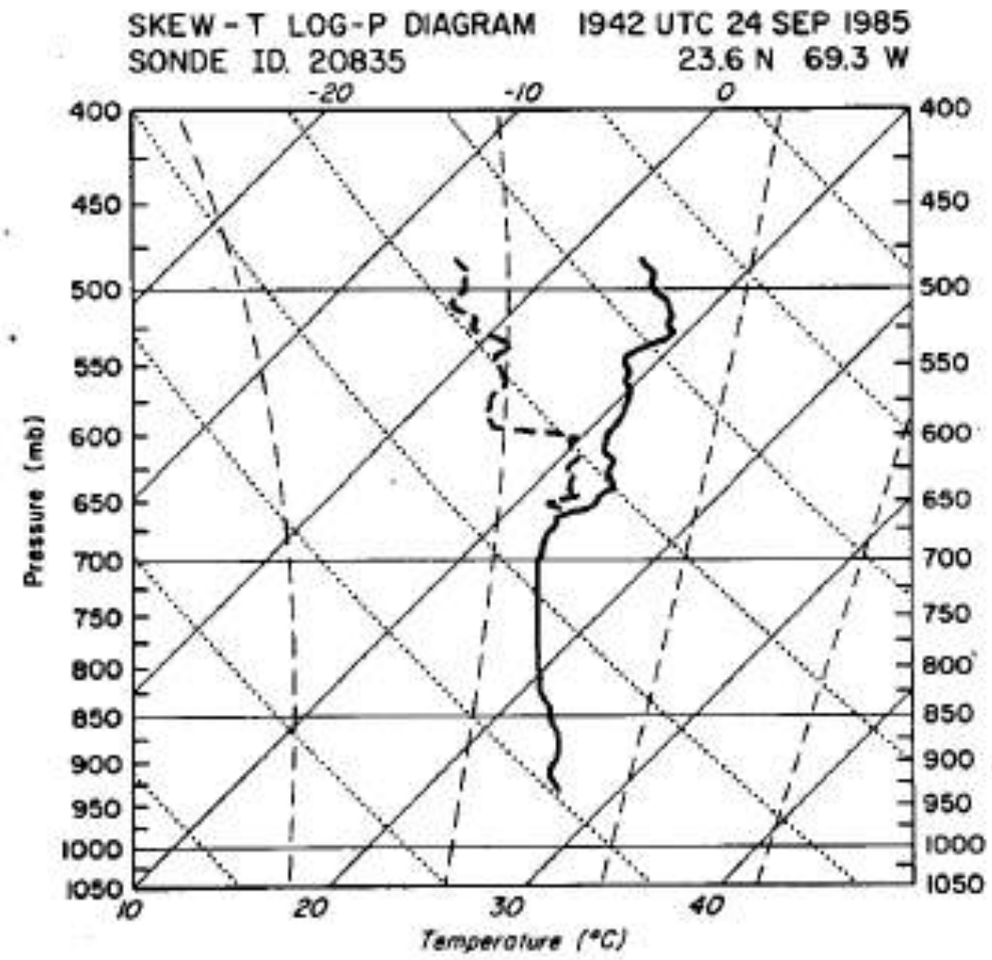

FIG. 3. Skew T–log$P$ thermodynamic diagram for ODW 1. Temperature is indicated by the thick solid line; dew point temperature by the thick dashed line. Isotherms are indicated by the sloping, thin solid lines. Dry and moist adiabats are indicated by the thin dashed and dotted lines, respectively. ODW wind estimates are plotted at 50 mb intervals in the standard fashion.

Dropwindsonde and Radar Observations of the Eye of Hurricane Gloria (1985)

JAMES L. FRANKLIN, STEPHEN J. LORD AND FRANK D. MARKS, JR.

NOAA/ERL/Atlantic Oceanographic and Meteorological Laboratory, Miami, Florida

3 August 1987 and 23 November 1987

Expendables

- Dropsonde, AXBT, AXCTD

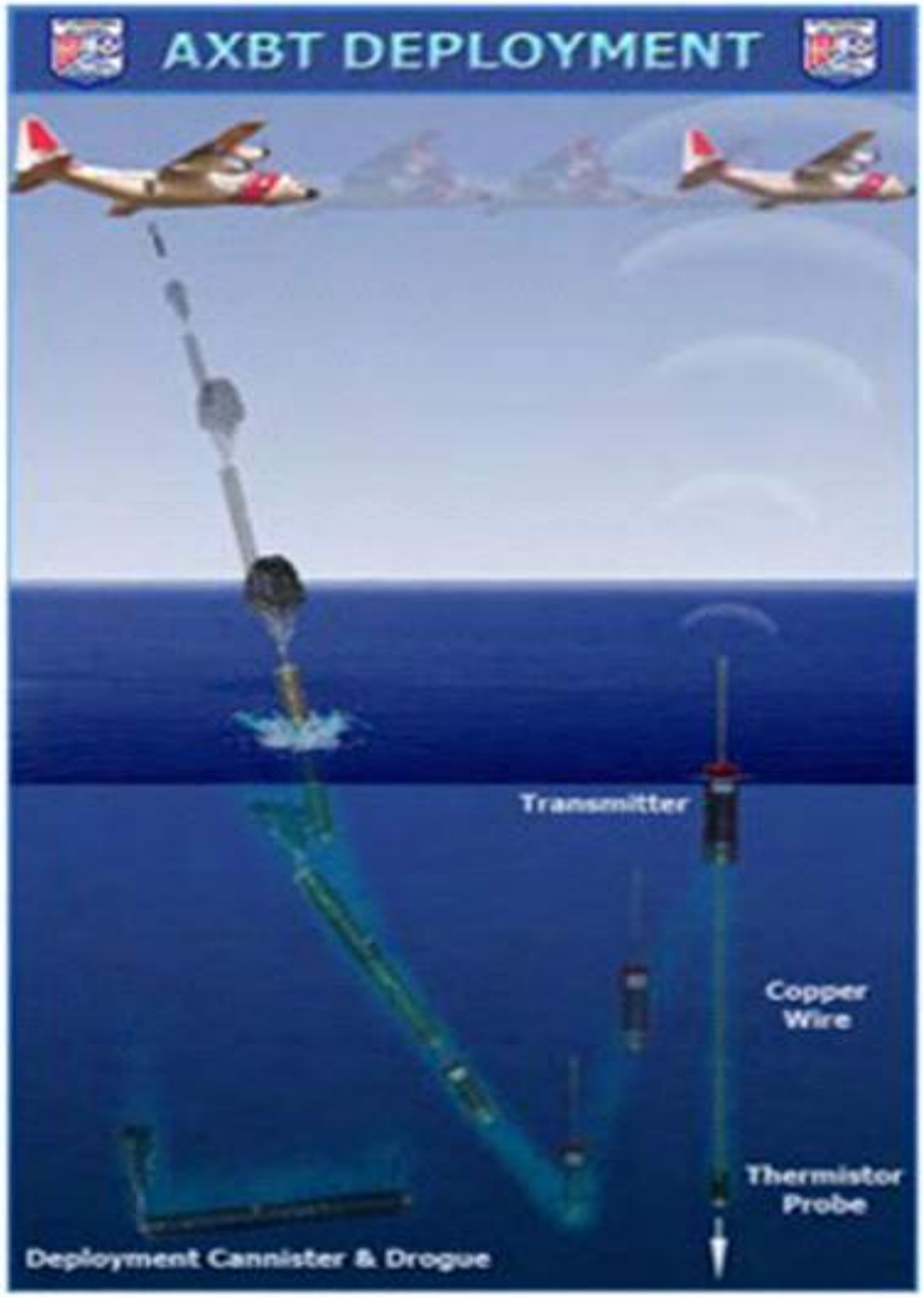

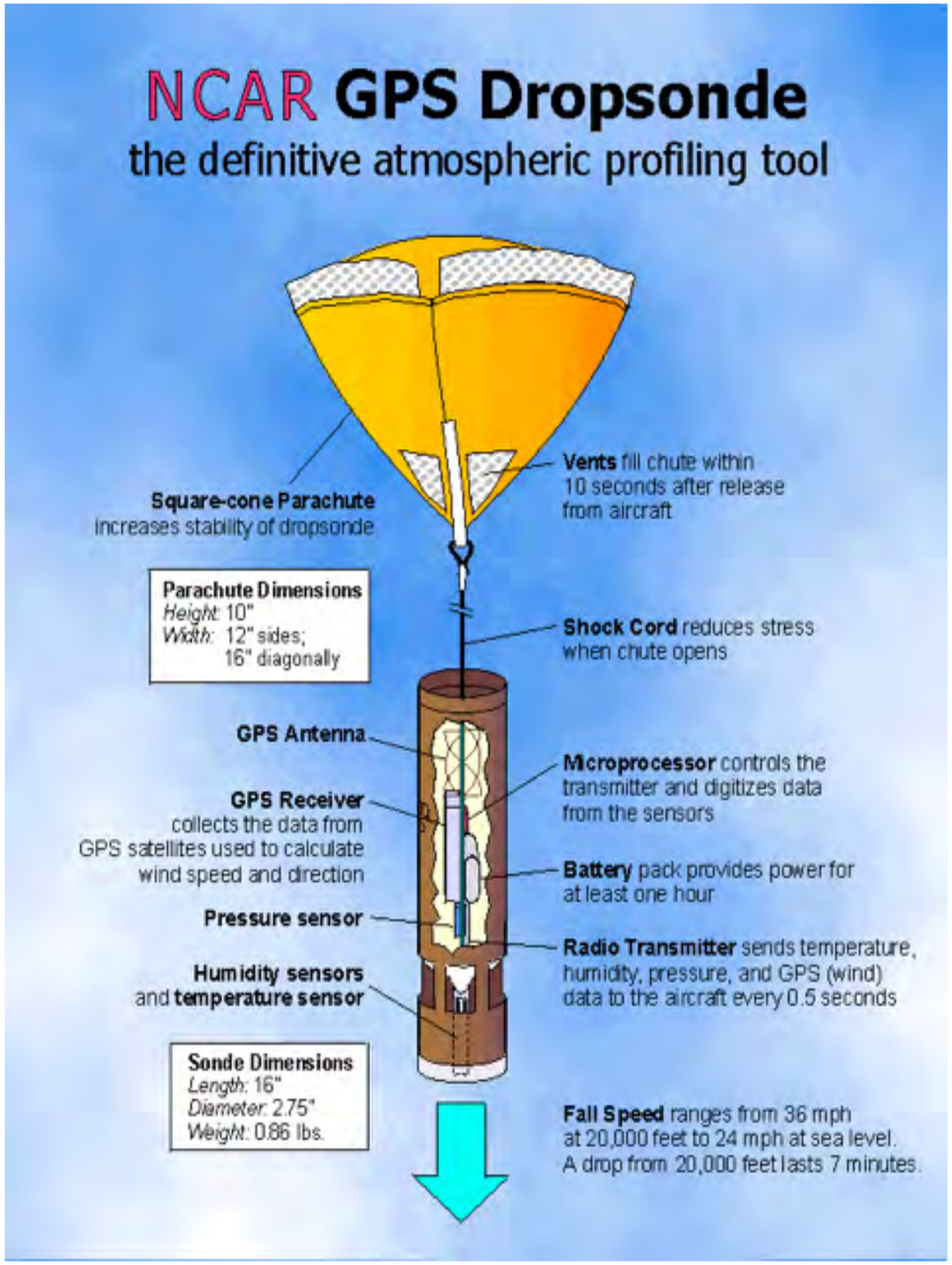

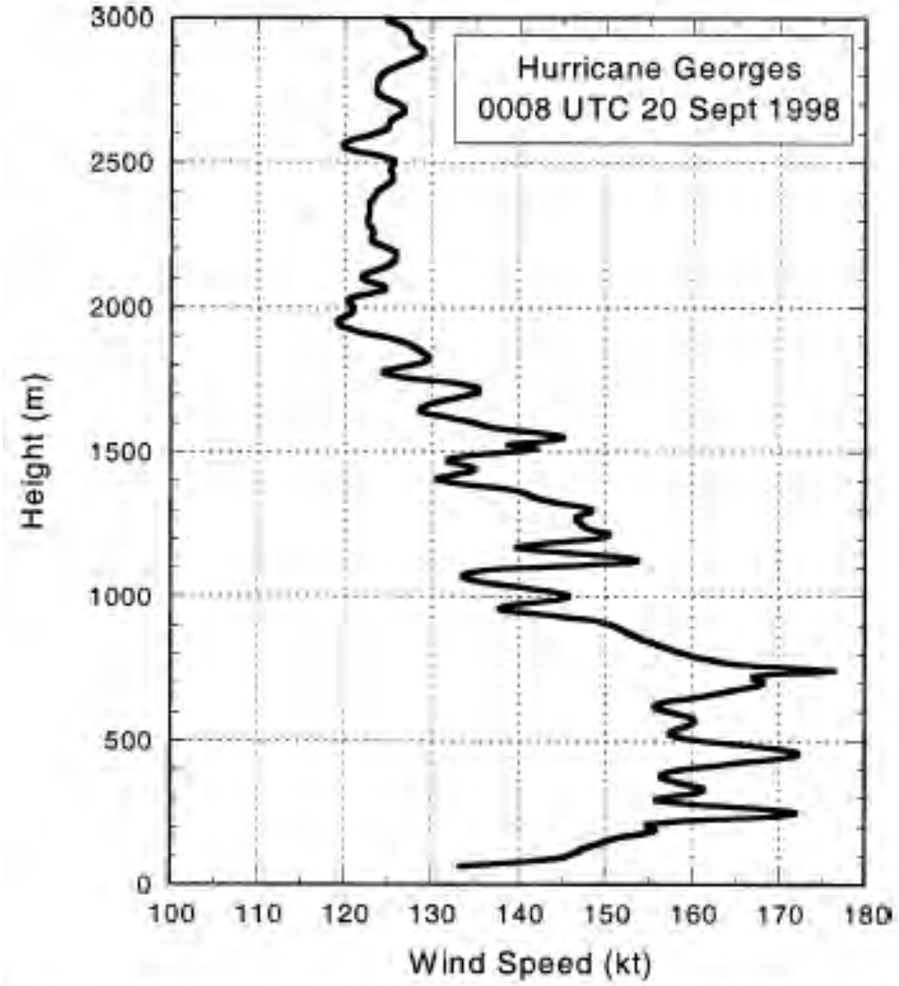

FIG. 3. Dropwindsonde wind speed profile from the eyewall of Hurricane Georges at 0008 UTC 20 Sep 1998.

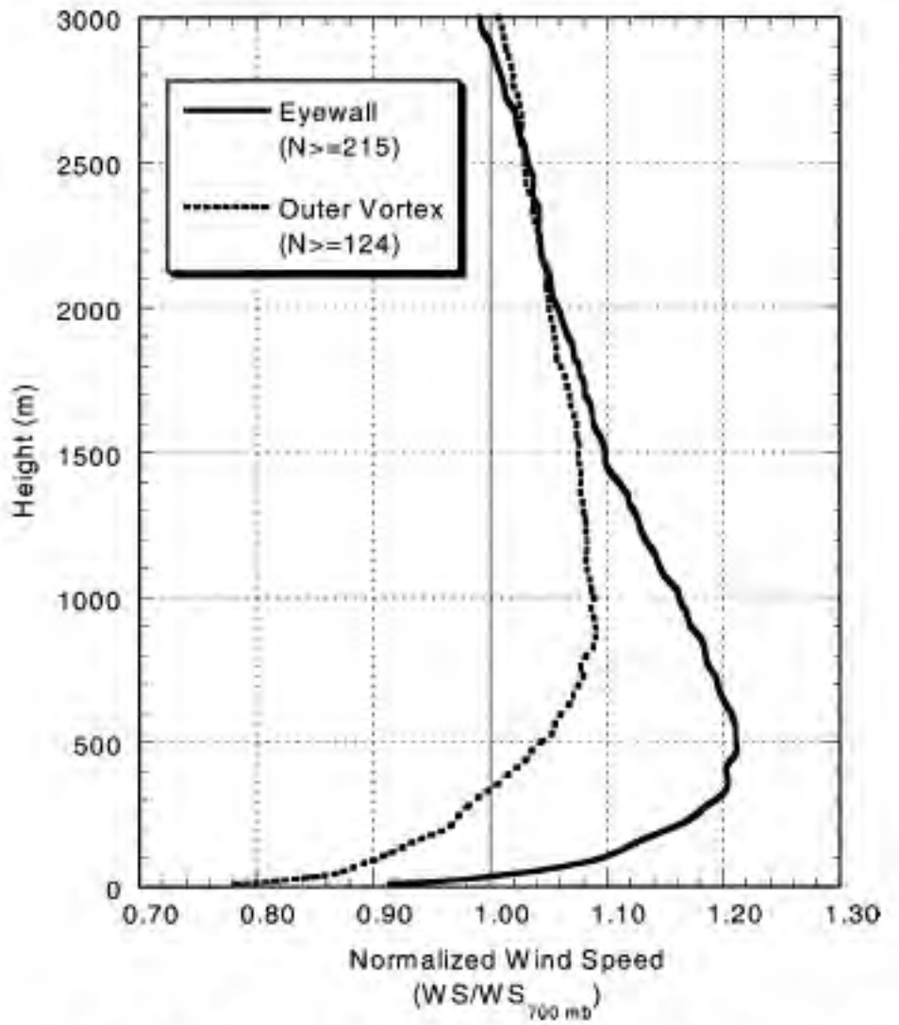

FIG. 8. Mean hurricane wind speed profiles for the eyewall and outer-vortex regions. Wind speeds are averaged and expressed as a fraction of the profile wind speed at 700 hPa. The minimum number of profiles used to construct the averages is also indicated.

GPS Dropwindsonde Wind Profiles in Hurricanes and Their Operational Implications

JAMES L. FRANKLIN

Tropical Prediction Center, National Hurricane Center, NOAA/National Weather Service, Miami, Florida

MICHAEL L. BLACK

Hurricane Research Division, NOAA/Atlantic Oceanographic and Meteorological Laboratory, Miami, Florida

KRYSTAL VALDE

Tropical Prediction Center, National Hurricane Center, NOAA/National Weather Service, Miami, Florida

(Manuscript received 9 June 2002, in final form 2 October 2002)

From Black et al. (2016)

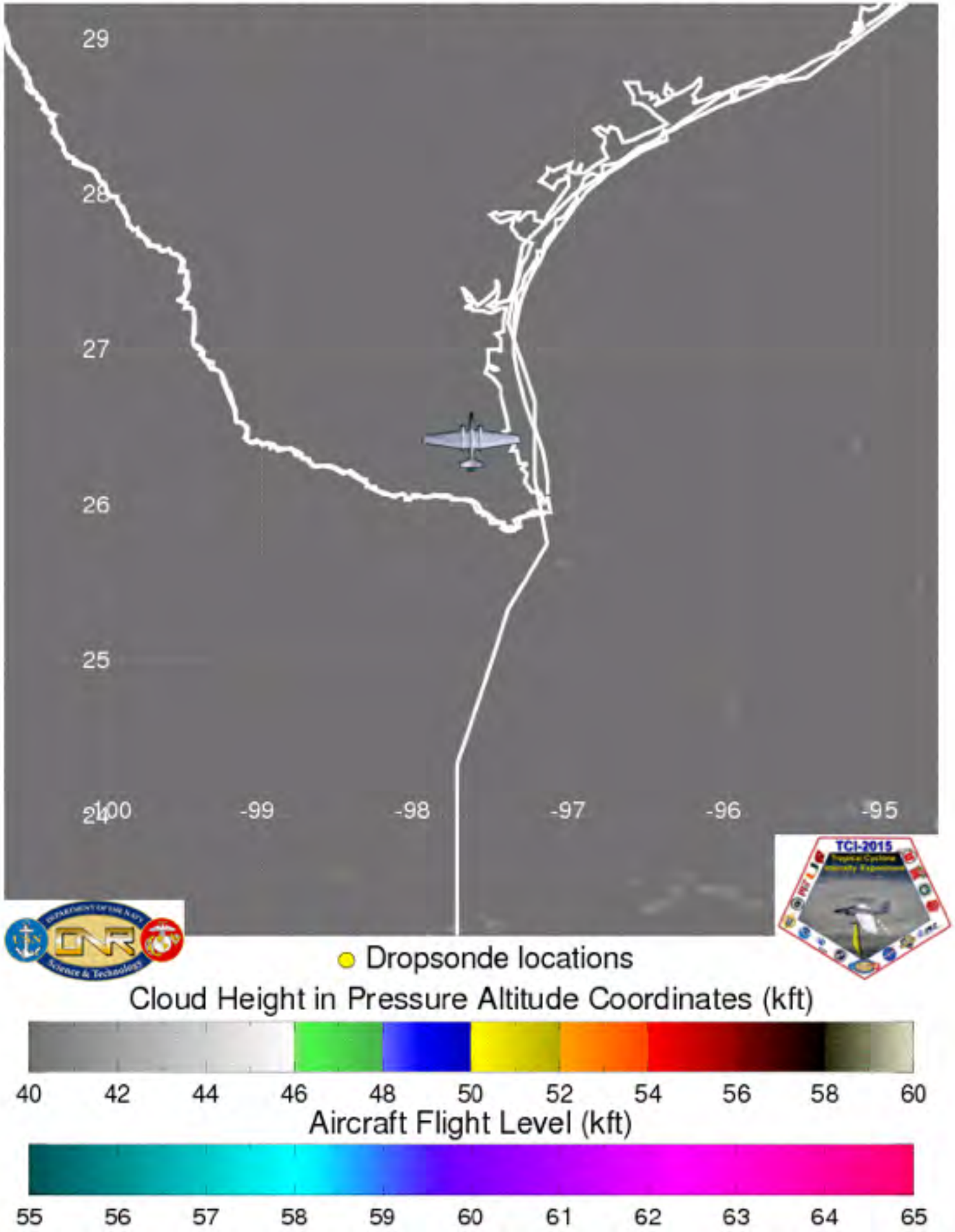

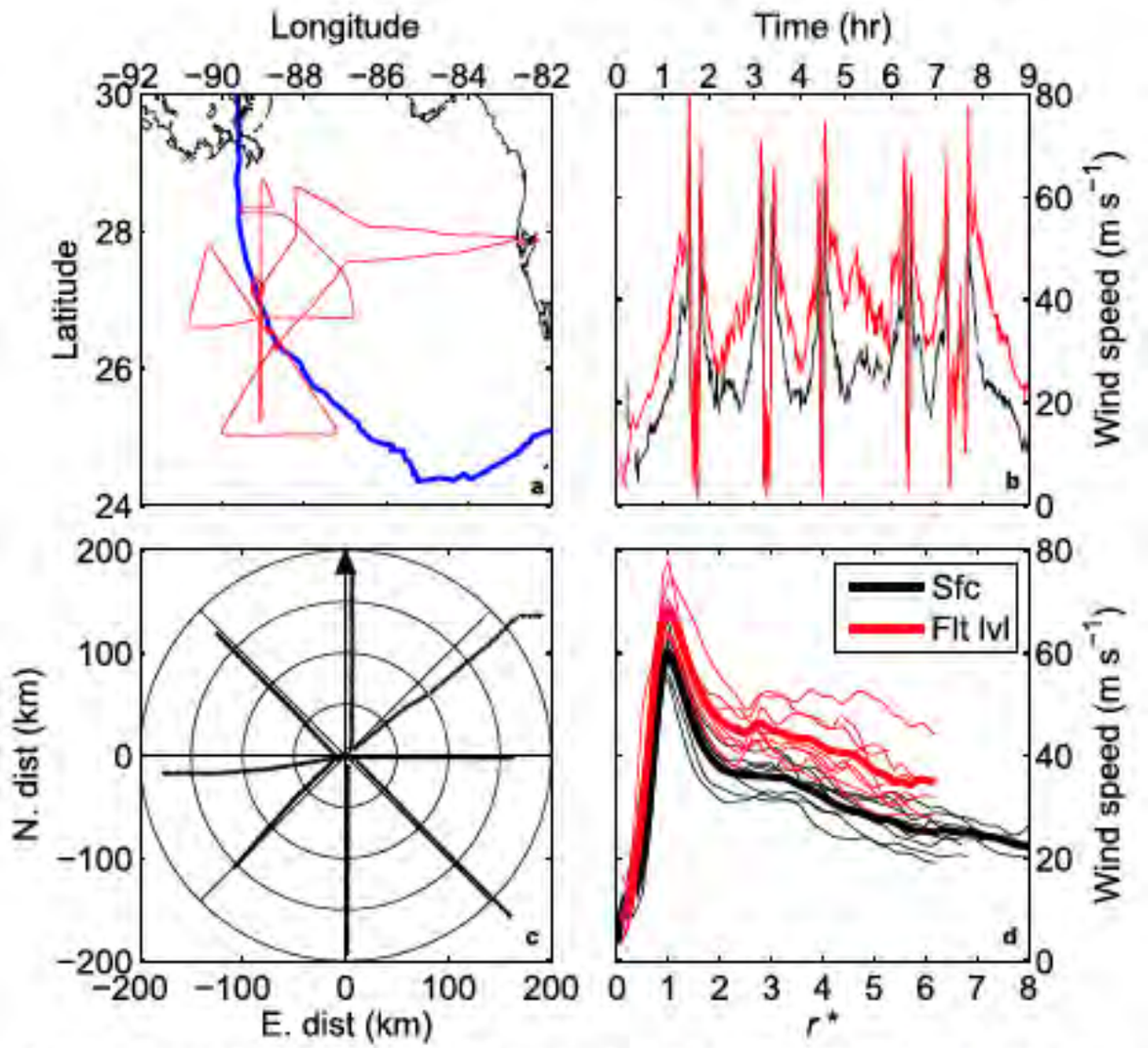

FIG. 4. (a) National Oceanic and Atmospheric Administration (NOAA) WP-3D flight track (red) and Hurricane Katrina storm track (blue), (b) surface (black) and 700-mb flight-level (red) wind speed time series for the flight duration, (c) observation locations relative to moving storm center, and (d) surface (black) and flight-level wind speeds as functions of normalized radial distance (r^*). In (c), the arrow points north.

Observed Hurricane Wind Speed Asymmetries and Relationships to Motion and Environmental Shear

ERIC W. UHLHORN

NOAA/AOML/Hurricane Research Division, Miami, Florida

BRADLEY W. KLOTZ

Cooperative Institute for Marine and Atmospheric Studies, Rosenstiel School of Marine and Atmospheric Science, University of Miami, Miami, Florida

TOMISLAVA VUKICEVIC, PAUL D. REASOR, AND ROBERT F. ROGERS

NOAA/AOML/Hurricane Research Division, Miami, Florida

(Manuscript received 6 June 2013, in final form 19 November 2013)

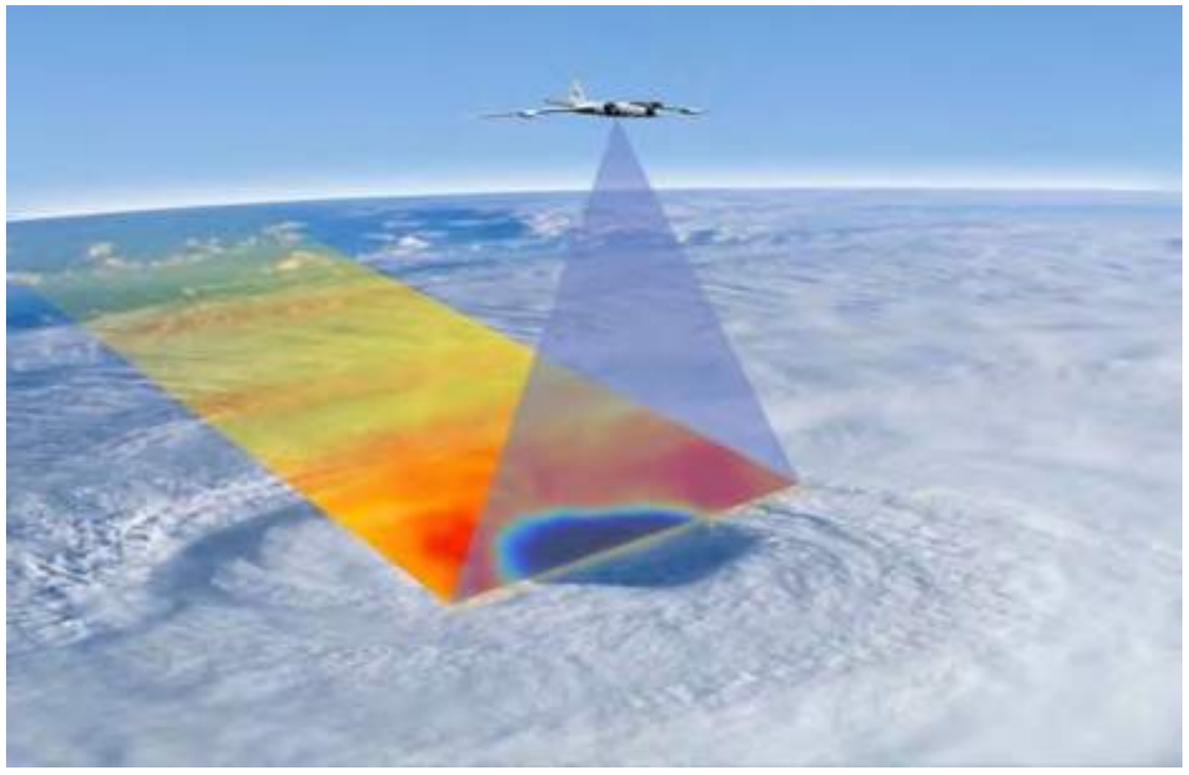

Hurricane Imaging Radiometer (HIRAD):

- Multi-frequency, passive C-band radiometer, that measures ocean surface winds through heavy rain
- NASA MSFC developed instrument (Dan Cecil, PI)

Criteria for TC Formation

1. Sea-surface temperature above 26.5-27 °C with a relatively deep oceanic mixed layer

2. Surface-based conditional instability

3. Weak to moderate vertical wind shear

4. Enhanced values of cyclonic low-level absolute vorticity

5. Organized deep convection in an area with large-scale mean ascent and high mid-level humidity

Criteria for TC Formation

1. Sea-surface temperature above 26.5-27 ^{o}C with a relatively deep oceanic mixed layer

2. Surface-based conditional instability

3. Weak to moderate vertical wind shear

4. Enhanced values of cyclonic low-level absolute vorticity

5. Organized deep convection in an area with large-scale mean ascent and high mid-level humidity

Only ~20% of pre-depression disturbances develop into TCs

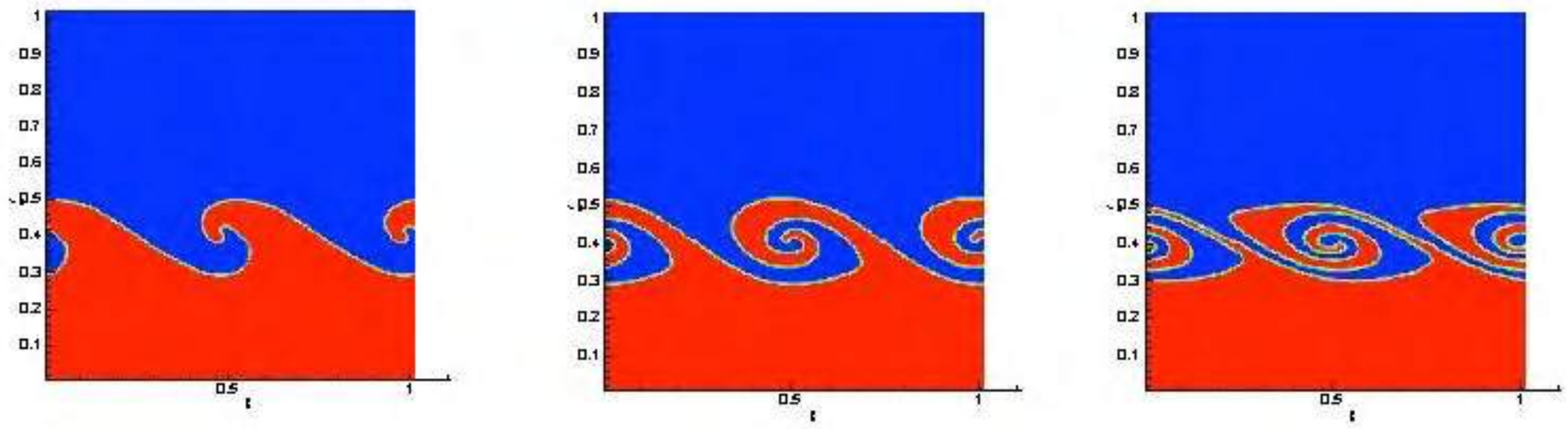

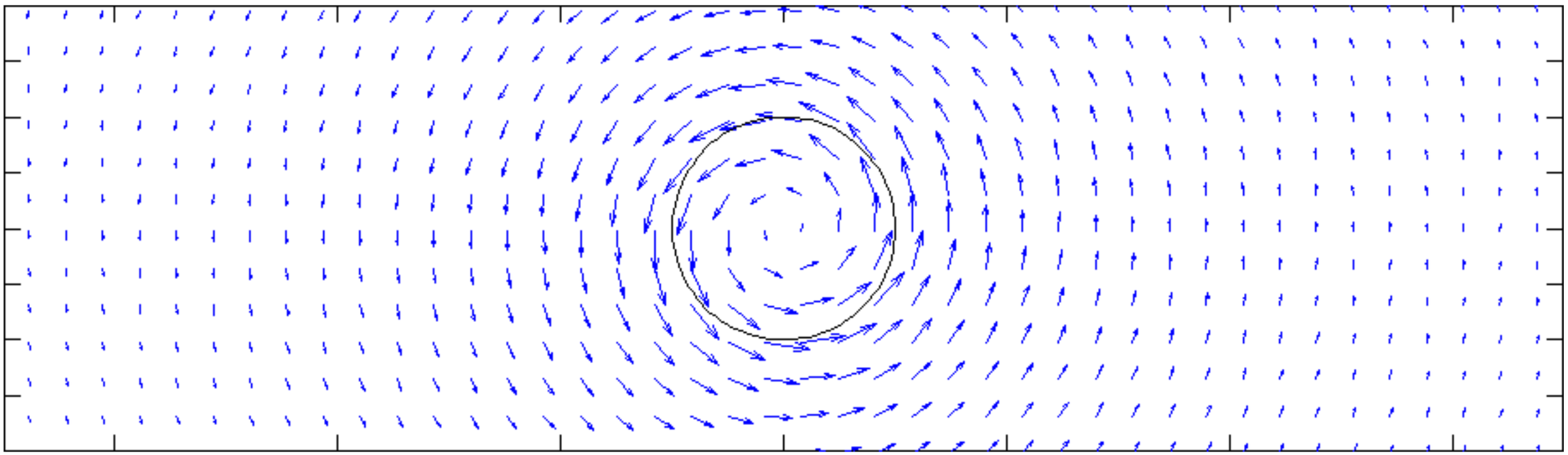

Pre-existing synoptic scale disturbance can provide initial meso-α scale vorticity and favorable environment for convection

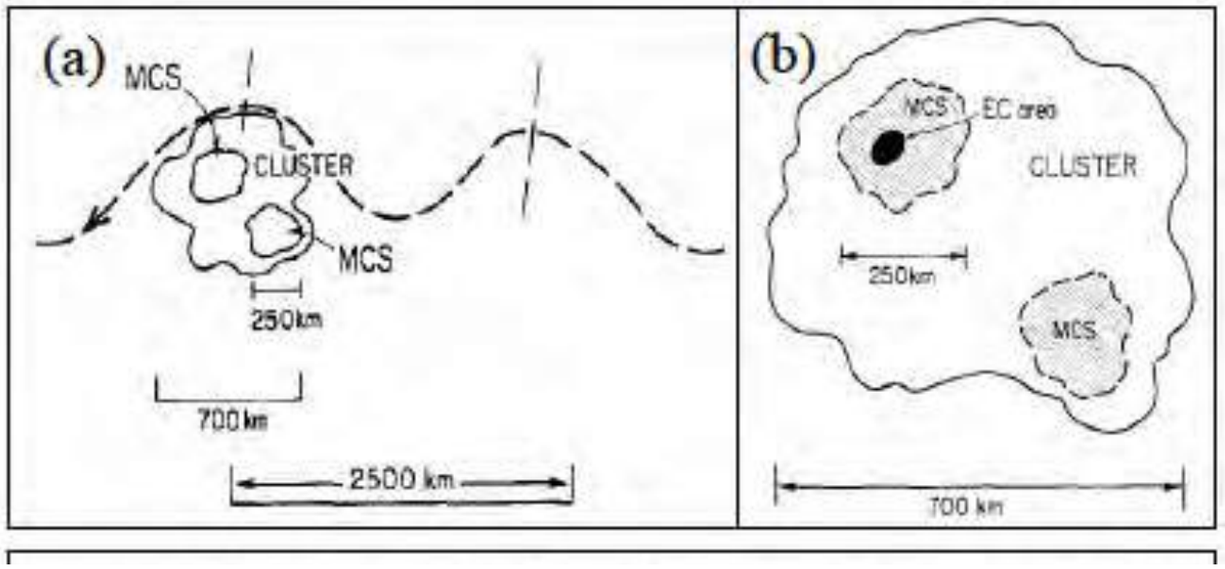

Gray (1998)

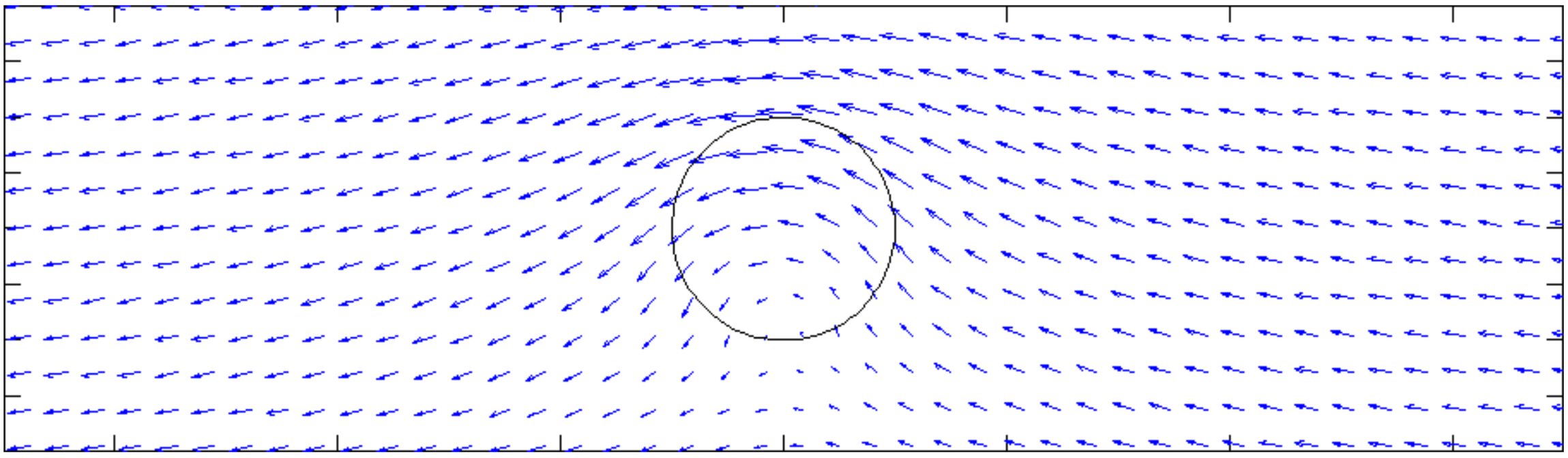

Pre-existing synoptic scale disturbance can provide initial meso-α scale vorticity and favorable environment for convection

Strong meso-α circulation helps to keep moisture and meso-β scale vorticity with the disturbance and protect it from drier environment

Dunkerton, Montgomery, and Wang (2009); Montgomery et al. (2012)

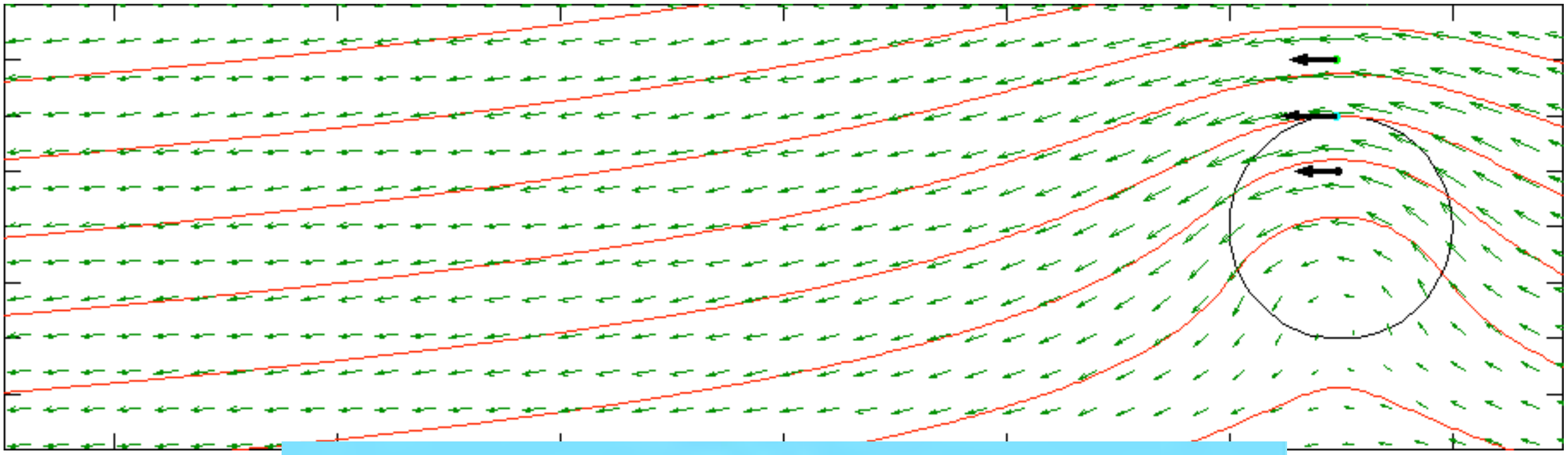

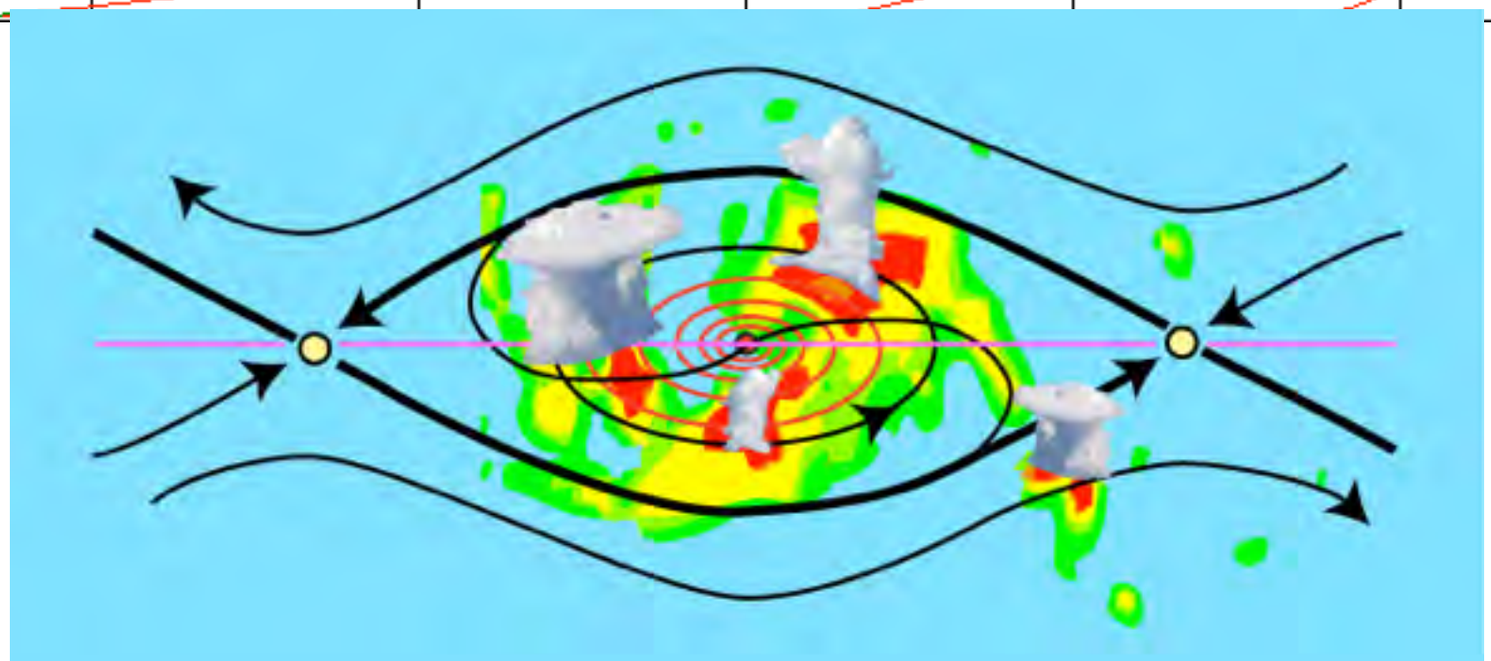

Animation From Dale Durran

- The cat's eye '**pouch**' is a region of approximately closed circulation, where air is repeatedly moistened by deep moist convection and protected to some degree from dry air intrusion
- "A deep wave pouch extending from the mid-troposphere (~600–700 hPa) down to the boundary layer is a necessary condition for tropical cyclone formation within an easterly wave. It is hypothesized also that a deep wave pouch together with other large-scale favorable conditions provides a sufficient condition for sustained convection and tropical cyclone formation." (Wang et al. 2012)

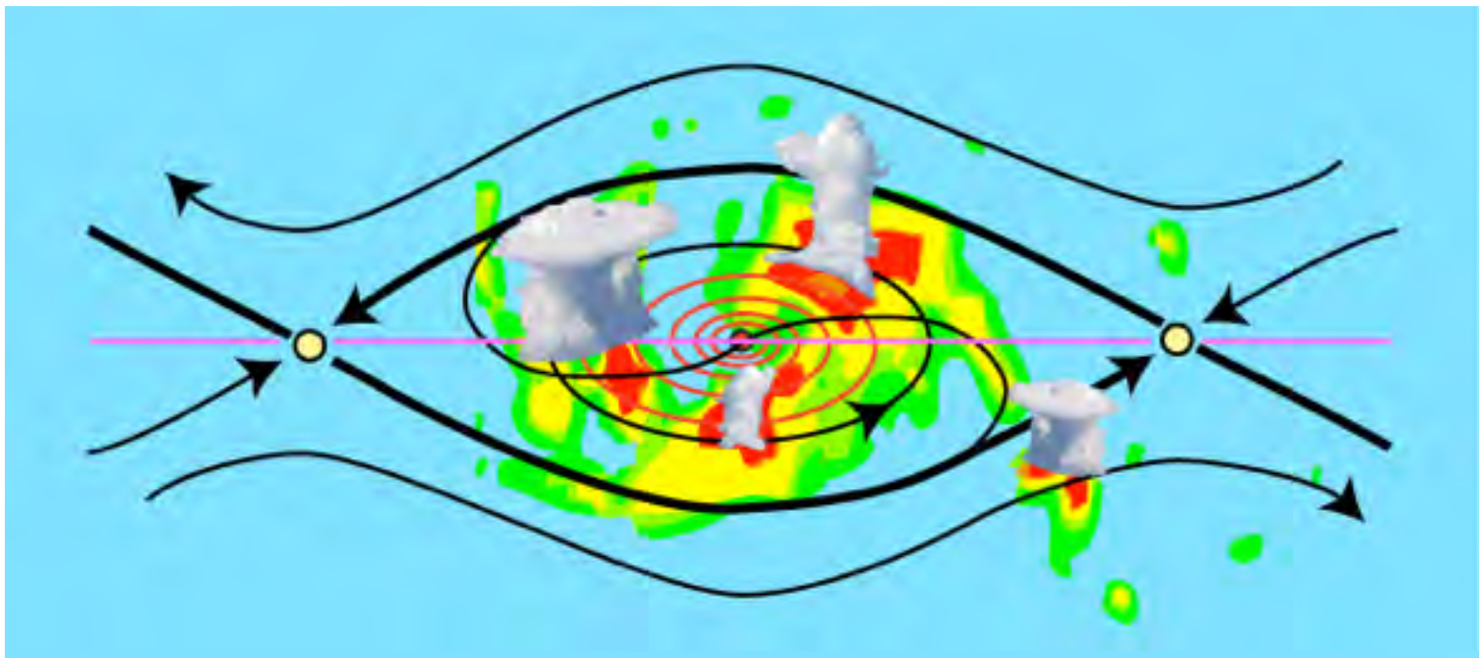

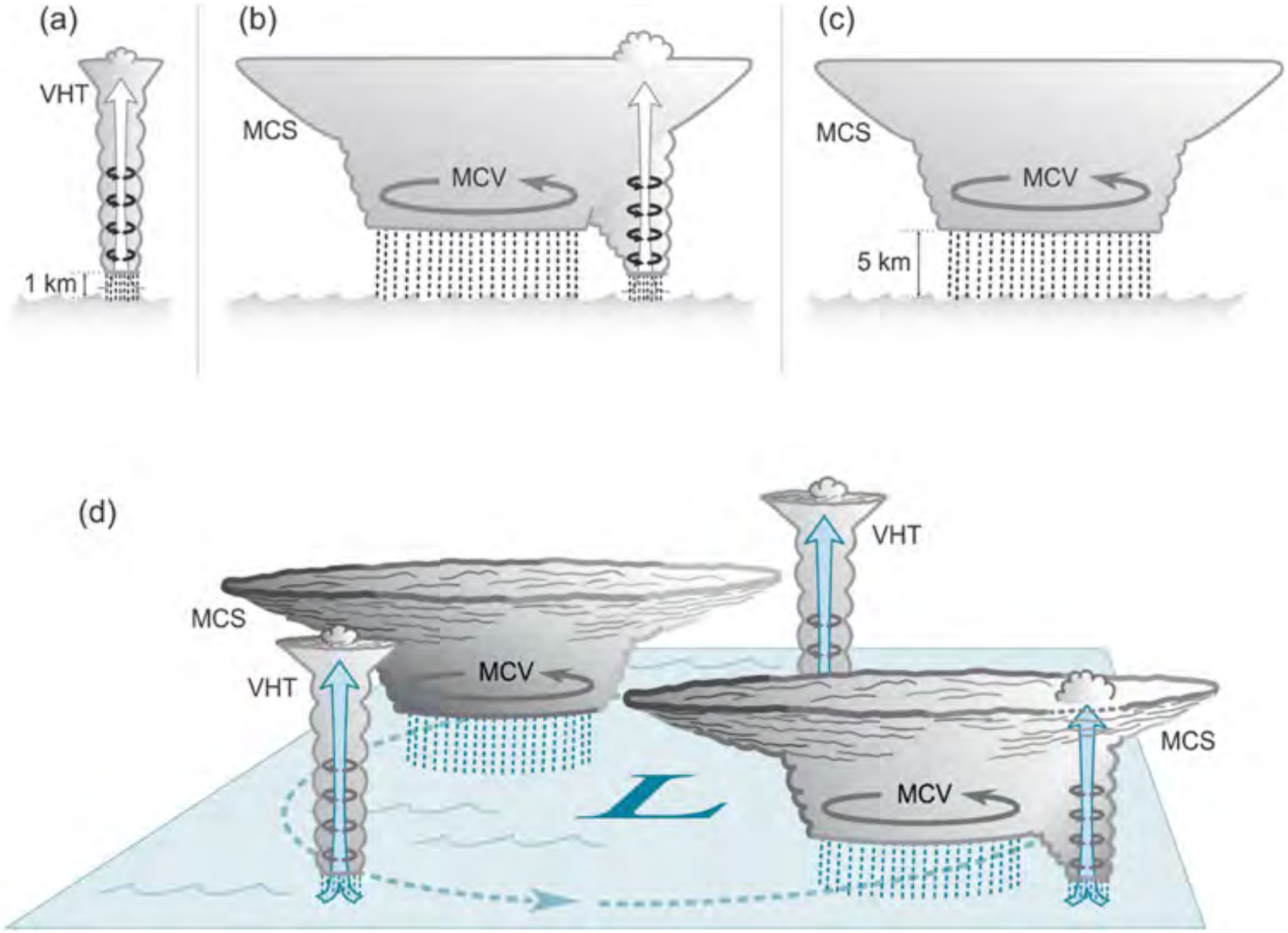
(a)
VHT
1 km
(b)
MCS
MCV
(c)
MCS
MCV
5 km
(d)
MCS
VHT
MCV
VHT
MCS
MCV
L

Convective and stratiform elements stretch vertical vorticity and can spin up the TC circulation

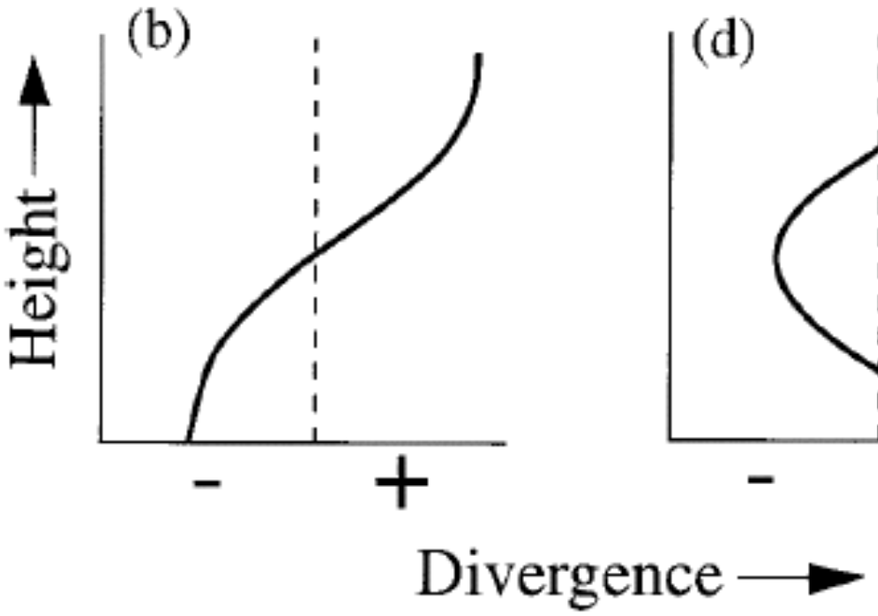

From Houze 1997

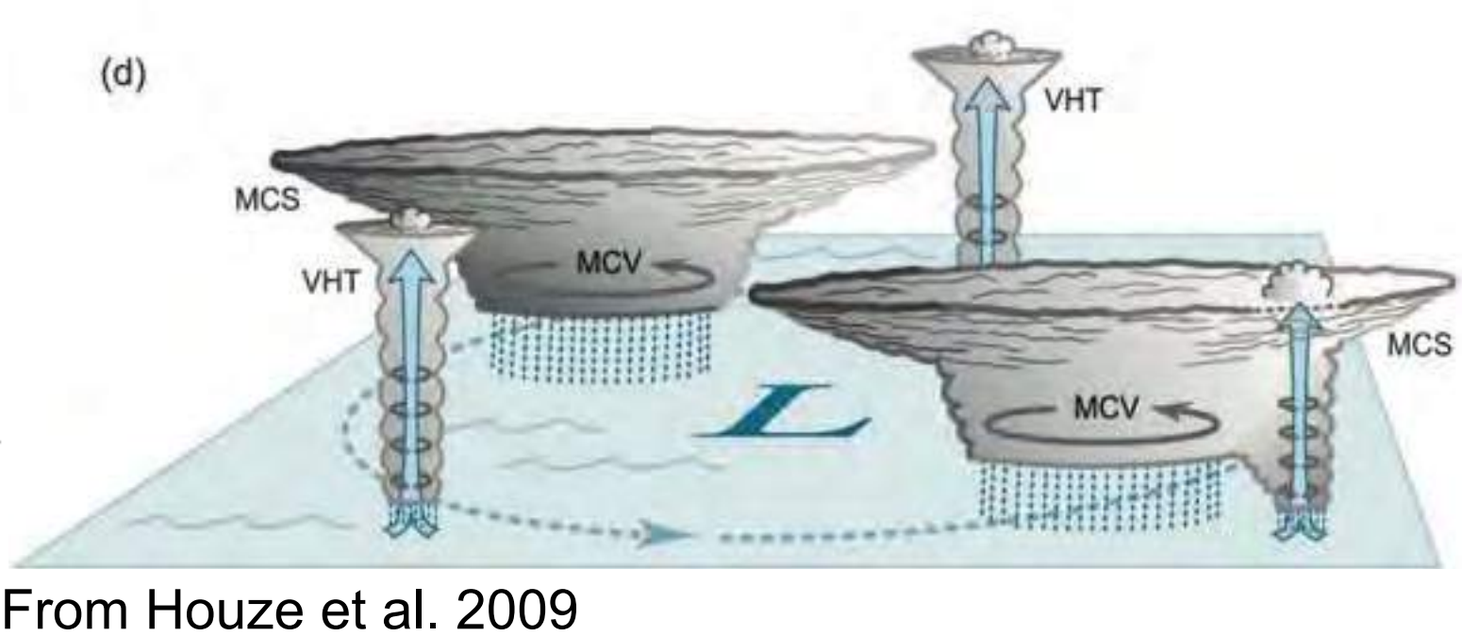

From Houze et al. 2009

$$\frac{\partial C}{\partial t} = -\bar{\eta}\tilde{\delta}A - \oint \eta' \mathbf{v}' \cdot \hat{\mathbf{n}}\, dl + \oint w \left(\hat{\mathbf{k}} \times \frac{\partial \mathbf{V}}{\partial p} \right) \cdot \hat{\mathbf{n}} dl + \oint \left(\hat{\mathbf{k}} \times \mathbf{F} \right) \cdot \hat{\mathbf{n}} dl$$

Mean Stretching

Horizontal Eddy Flux

Tilting

Friction

From Davis and Galarneau (2009)

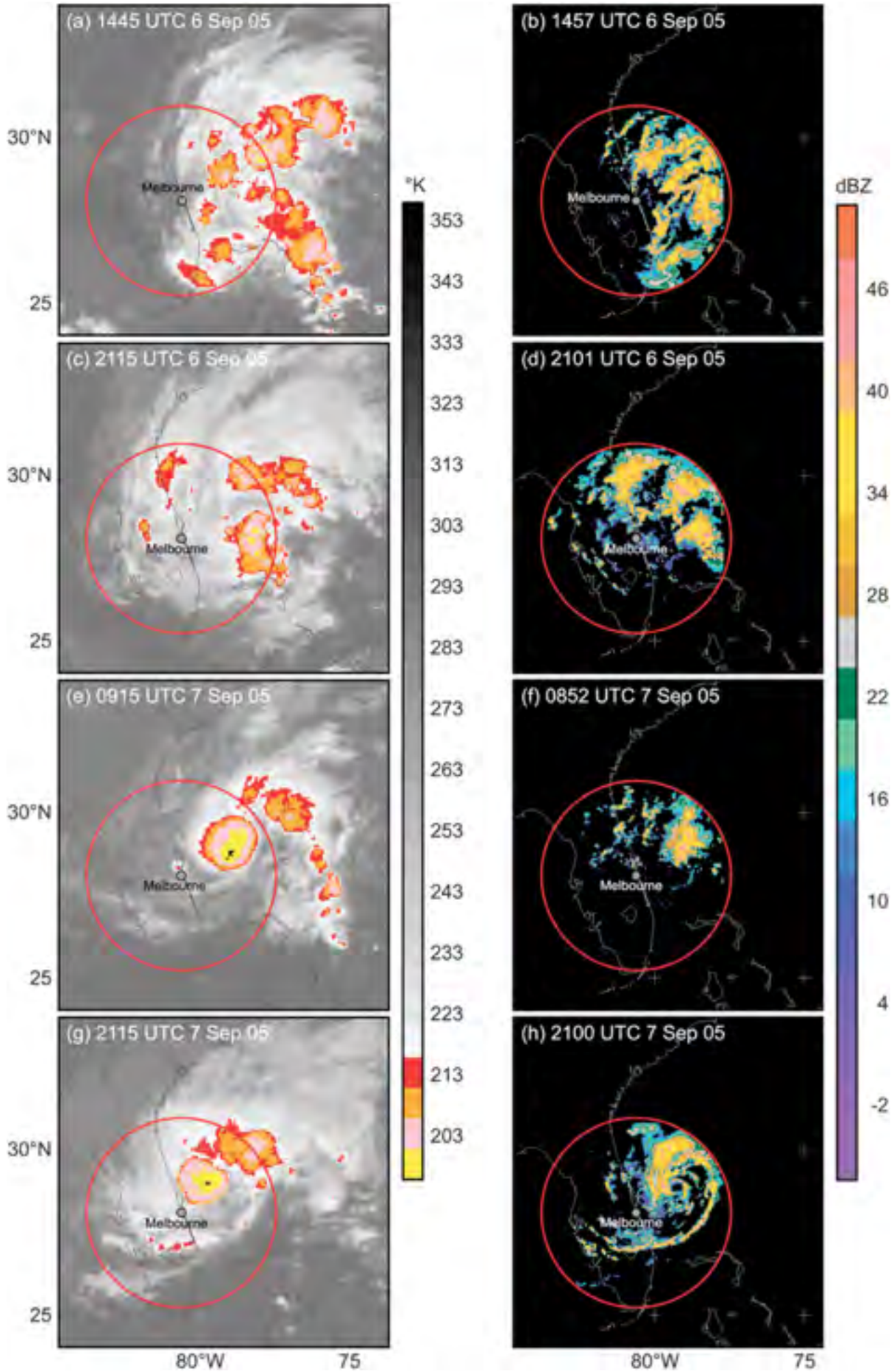

FIG. 4. Satellite and radar overview of the genesis of Ophelia. The circle shows maximum radar range. Satellite imagery shows infrared temperature from Geostationary Operational Environmental Satellite (GOES)-12**. Radar data are from the Melbourne Weather Surveillance Radar-1988 Doppler (WSR-88D). (Figure is from Houze et al. 2009.)**

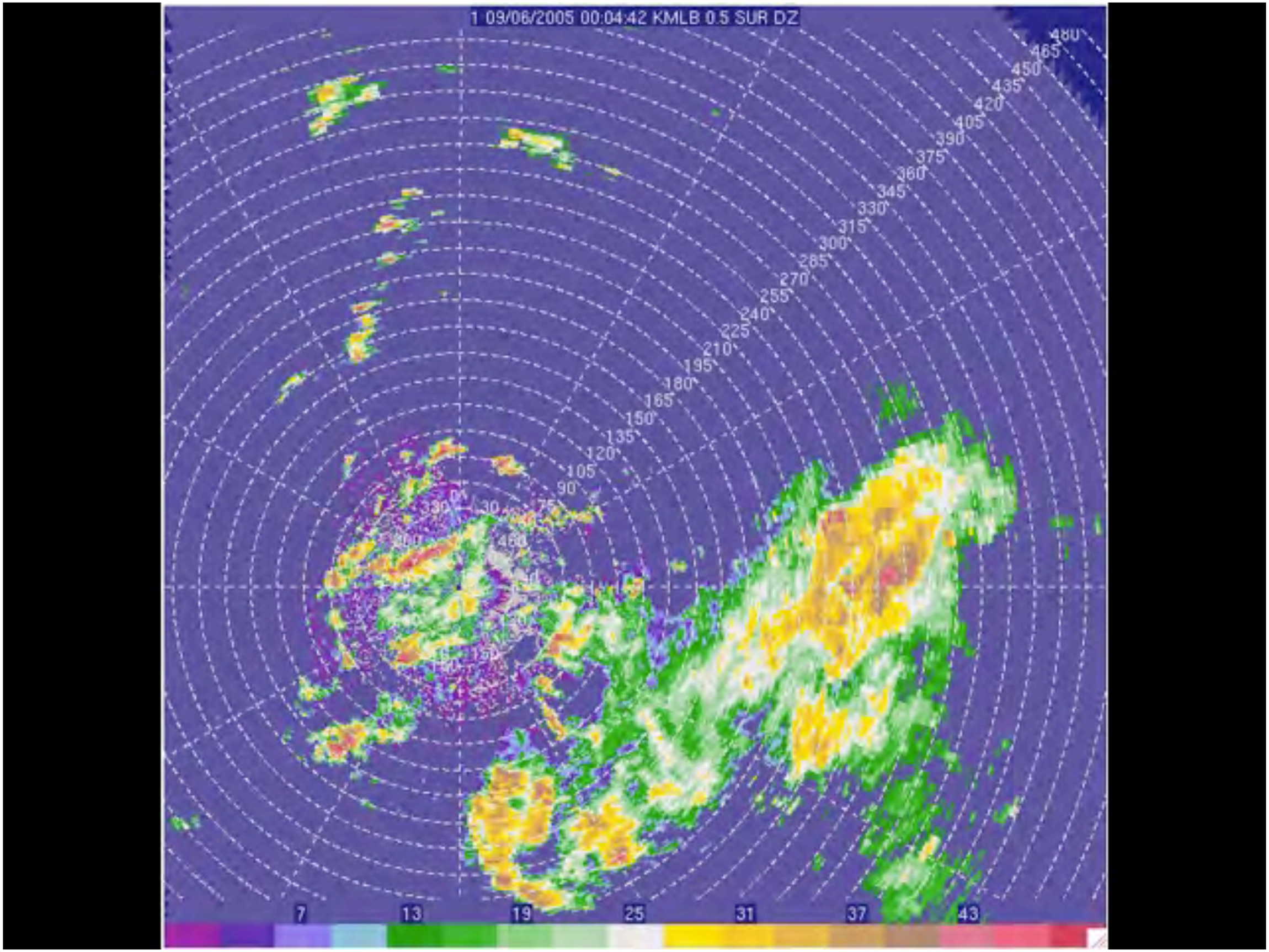
1 09/06/2005 00:04:42 KMLB 0.5 SUR DZ
480
465
450
435
420
405
390
375
360
345
330
315
300
285
270
255
240
225
210
195
180
165
150
135
120
105
90
7
13
19
25
31
37
43

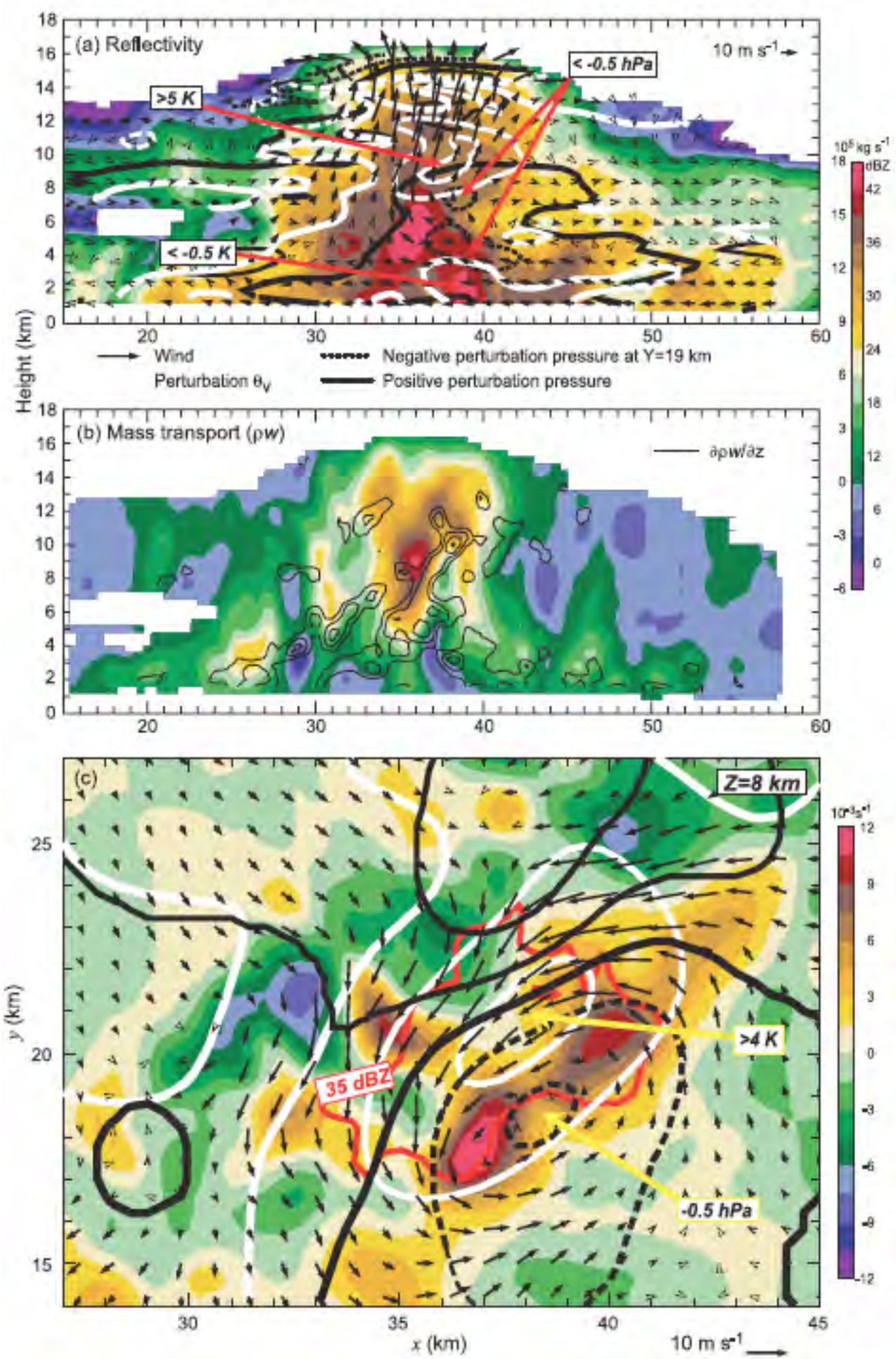

From Houze et al. (2009)

Typhoon Hagupit (2008)

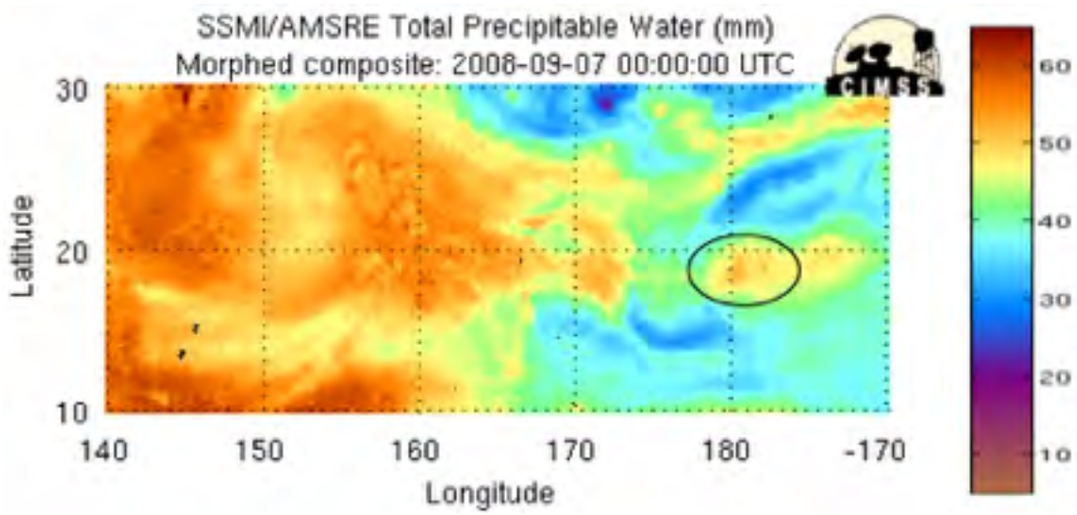

- A "pouch" was evident 10 days prior to the JTWC tropical cyclone formation alert
- 2 consecutive aircraft missions 4 days prior to genesis in TPARC/ TCS08 (Bell and Montgomery 2010)

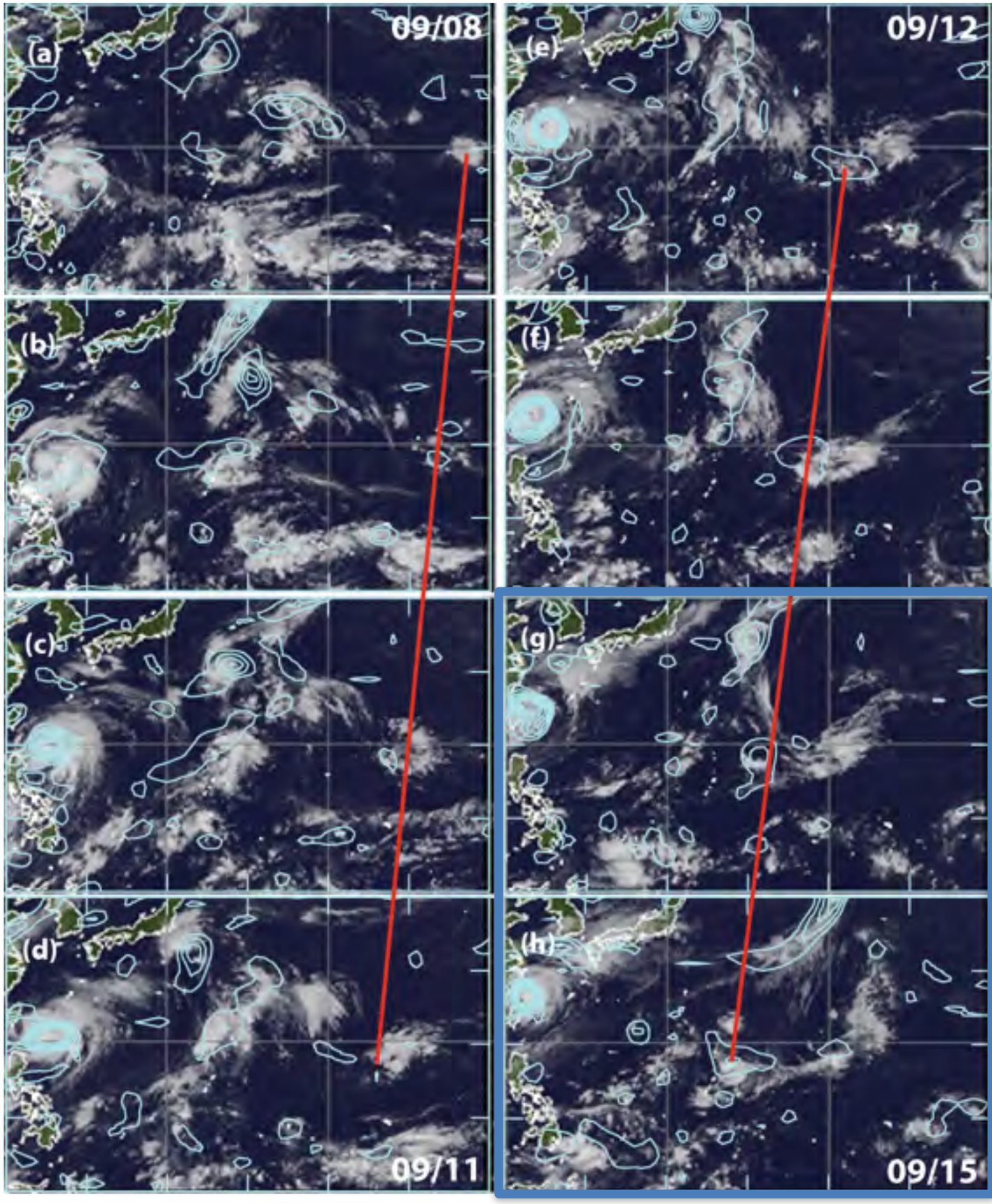

Research Flights ~00 UTC 14 & 15 Sept.

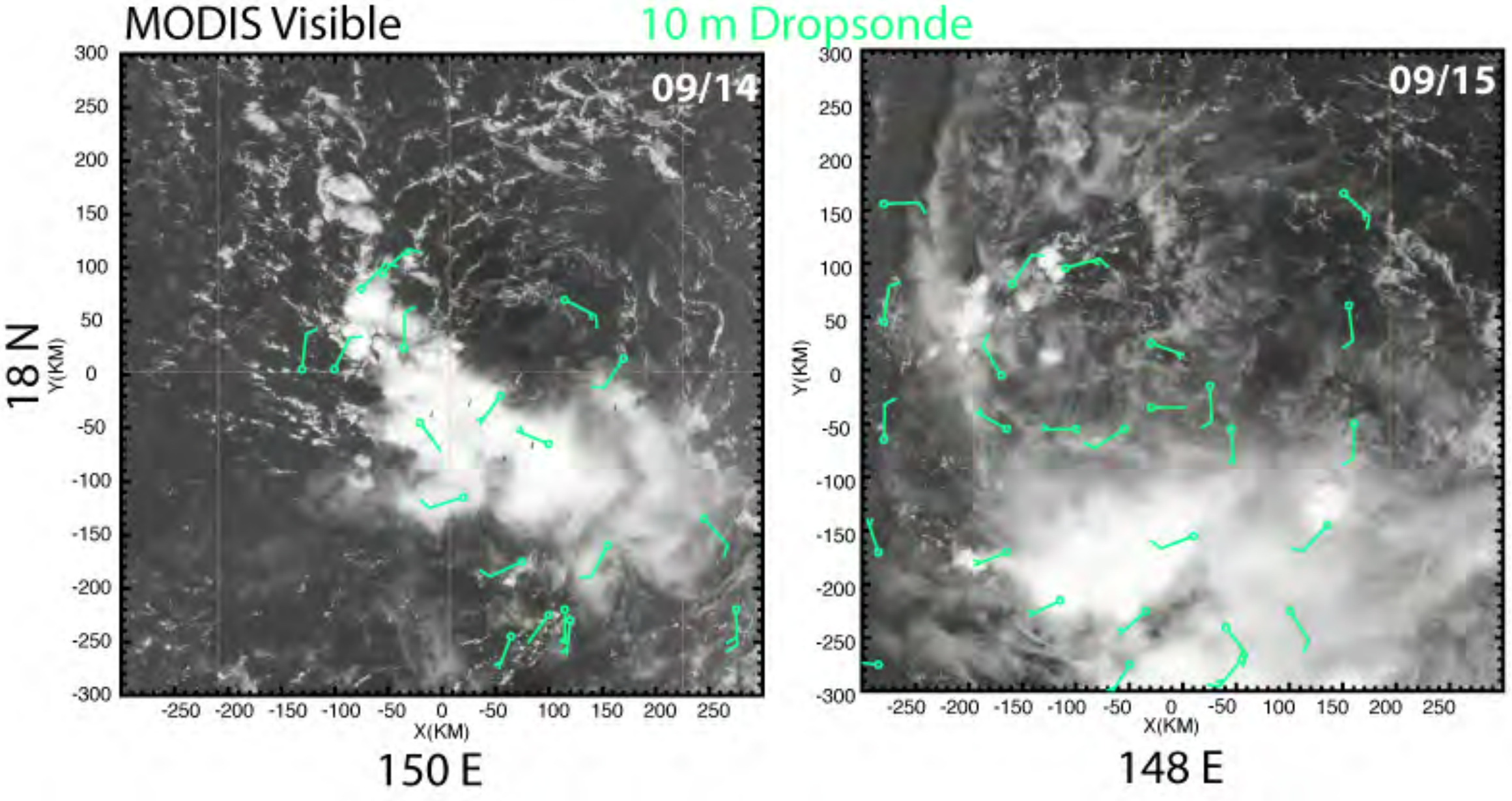

Bell and Montgomery (2010)

Research Flights ~00 UTC 14 & 15 Sept.

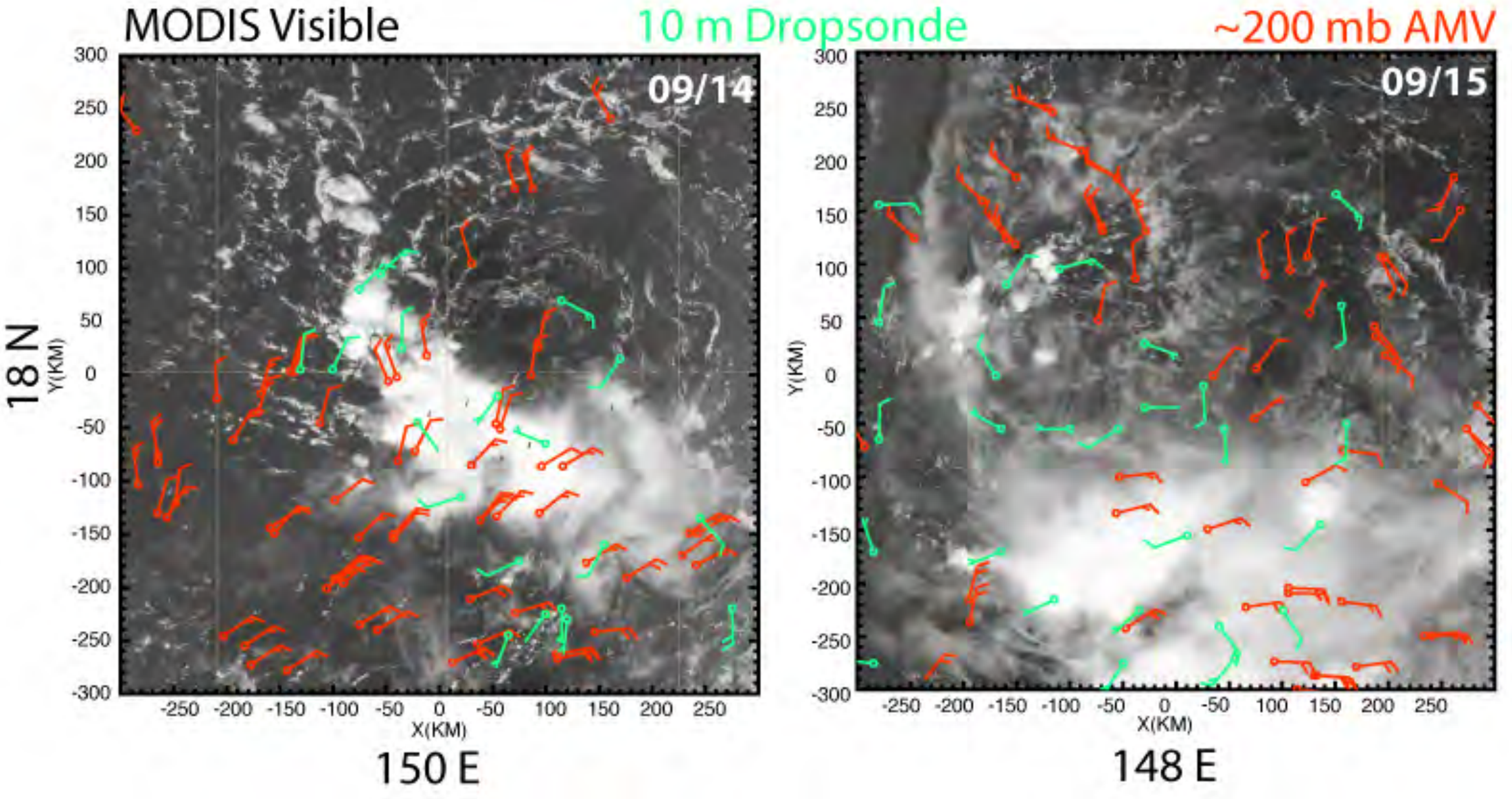

Bell and Montgomery (2010)

Research Flights ~00 UTC 14 & 15 Sept.

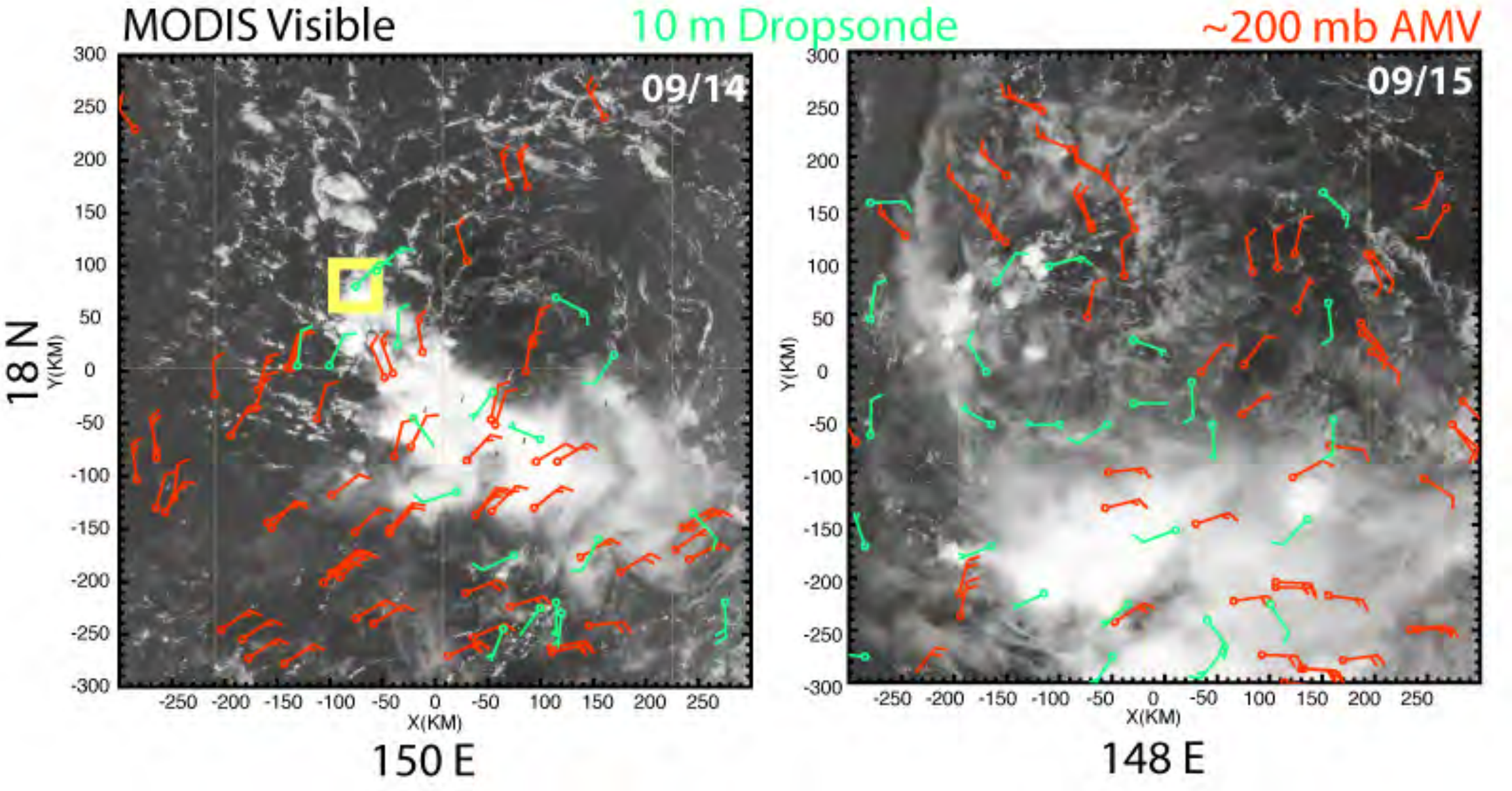

Bell and Montgomery (2010)

ELDORA Observations (0036 UTC)

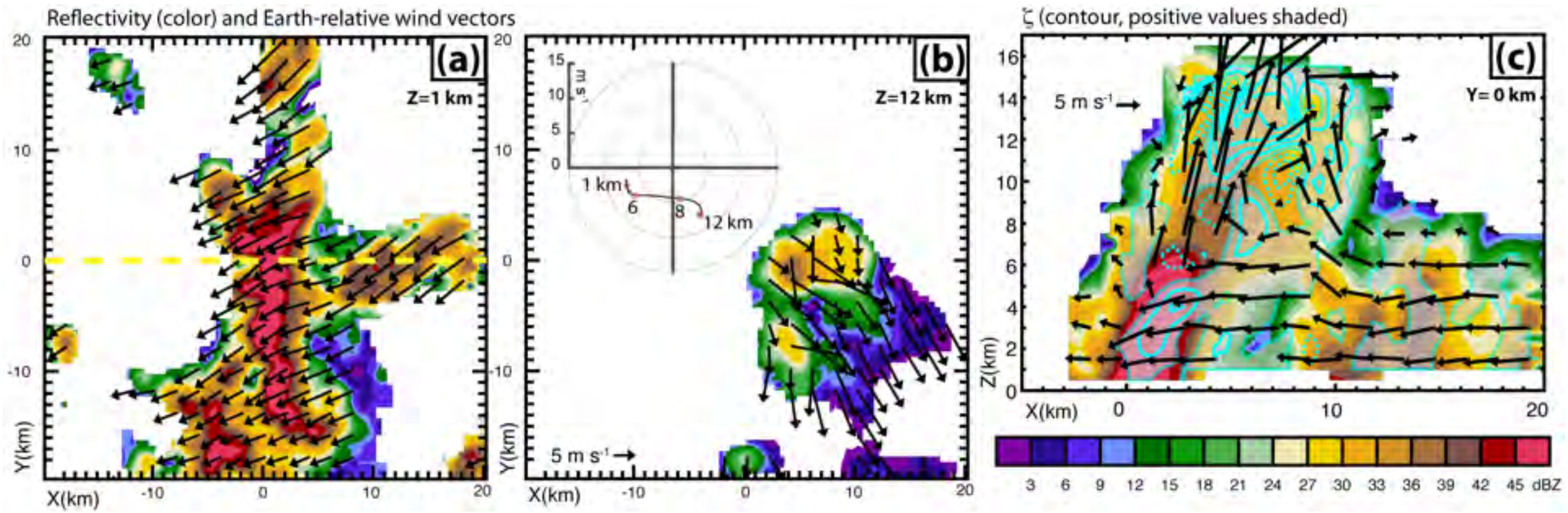

- Variational Doppler radar synthesis on a 500 m grid (Reasor et al. 2009)

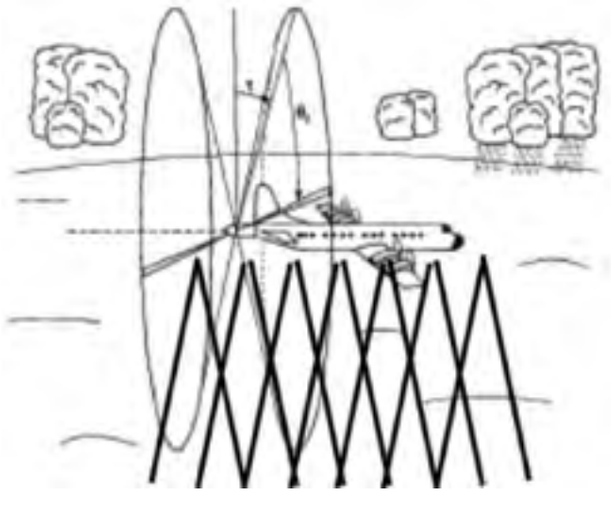

Bell and Montgomery (2010)

Research Flights ~00 UTC 14 & 15 Sept.

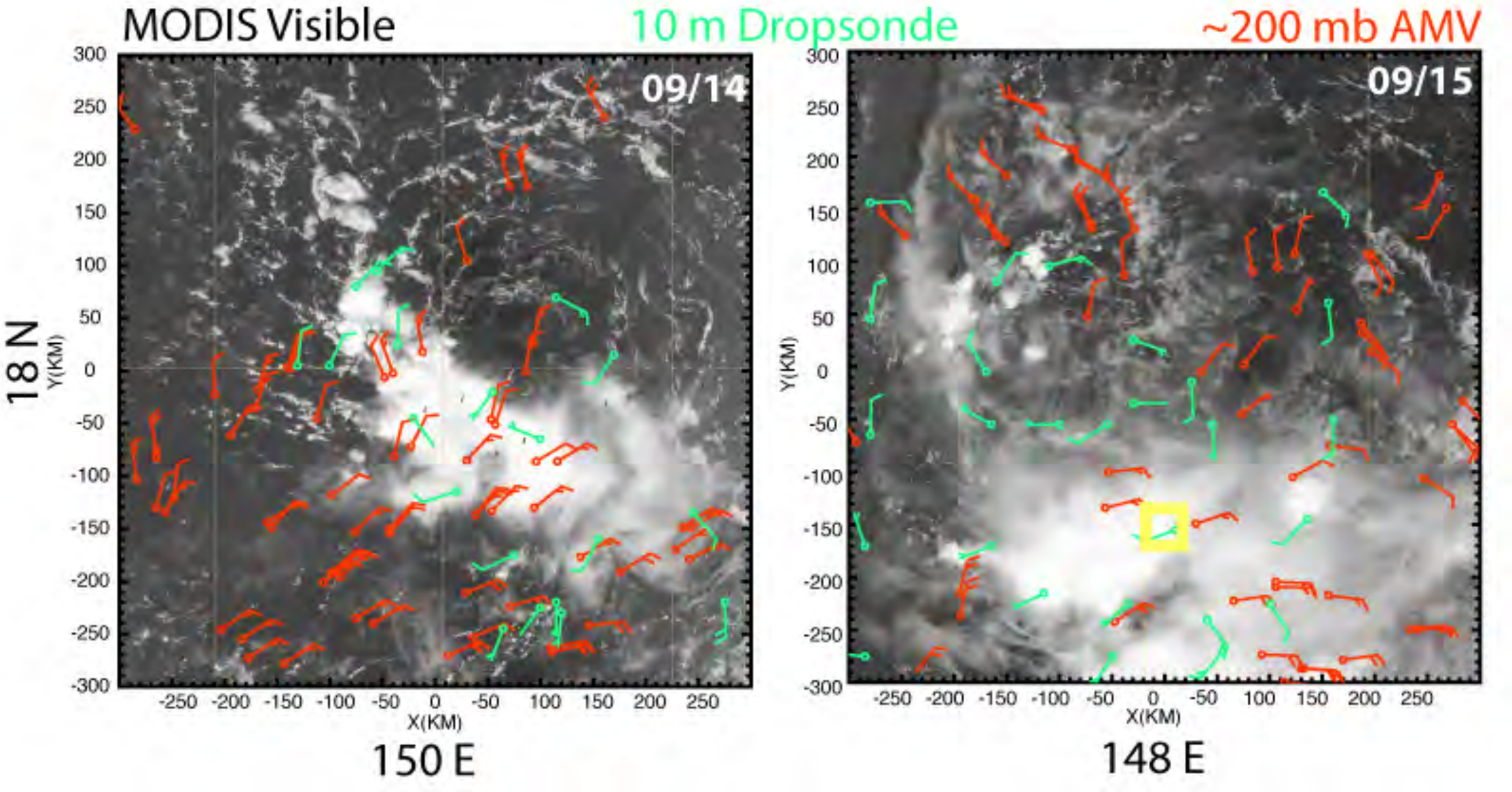

Bell and Montgomery (2010)

ELDORA Observations (2341 UTC 14 Sep)

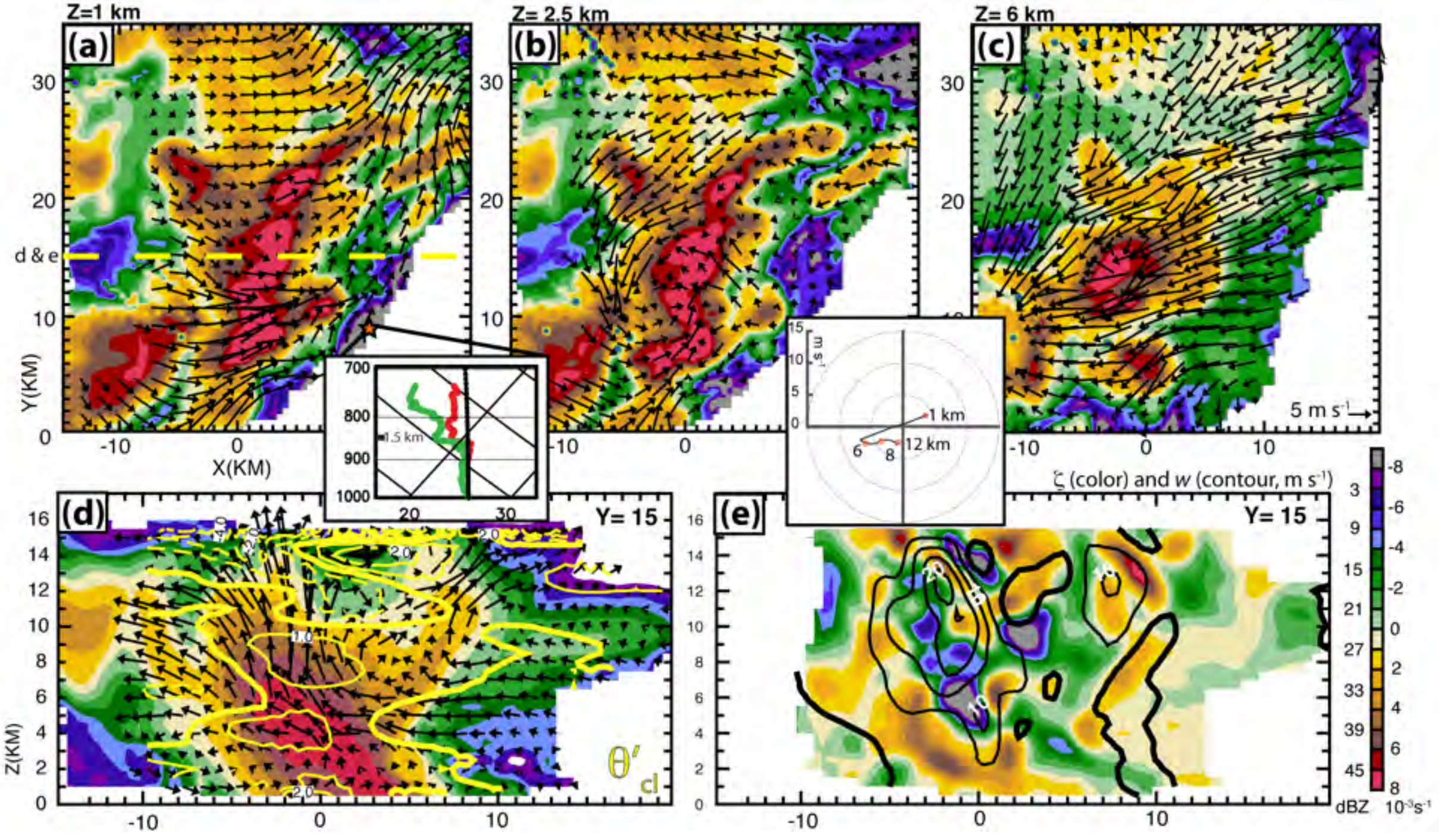

Bell and Montgomery (2010)

The vorticity concentrated through stretching outlives the deep convection that produced it

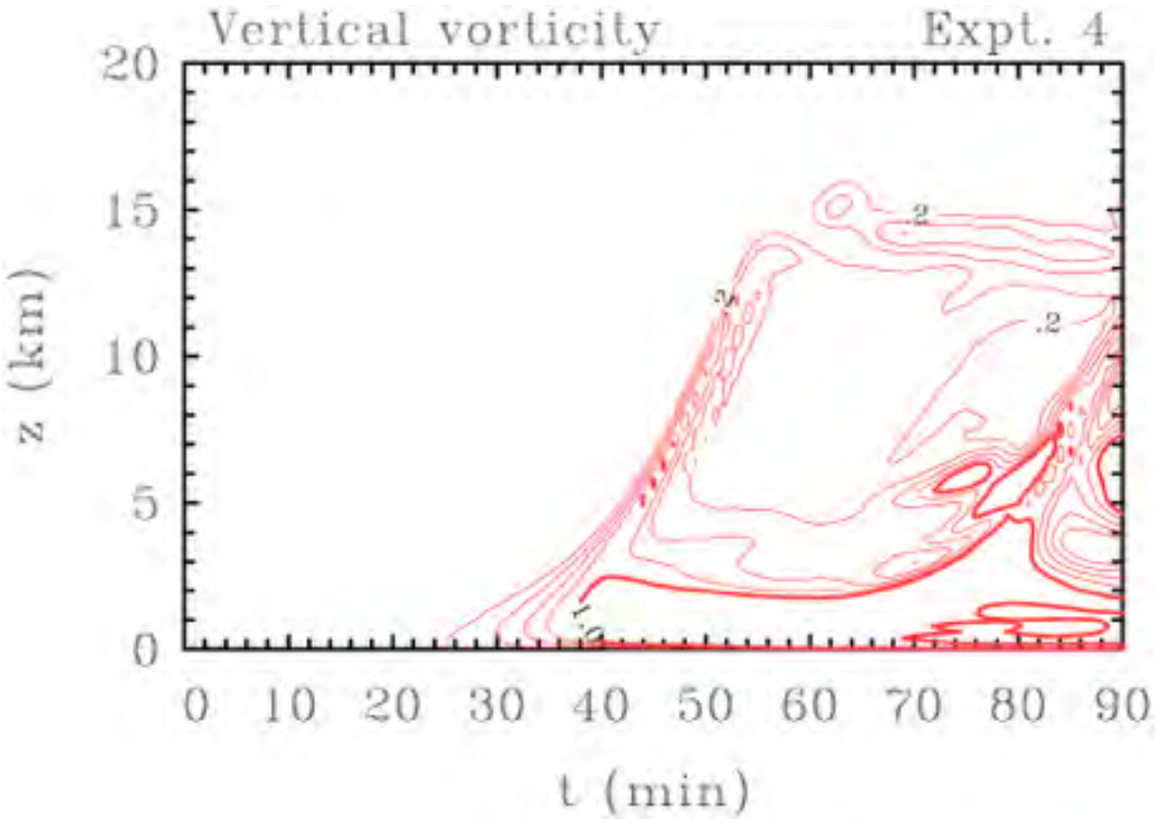

Wissmeier and Smith 2011

contour
1×10^{-3} s^{-1}, thin lines 2×10^{-4} s^{-1}

~40 × amplification

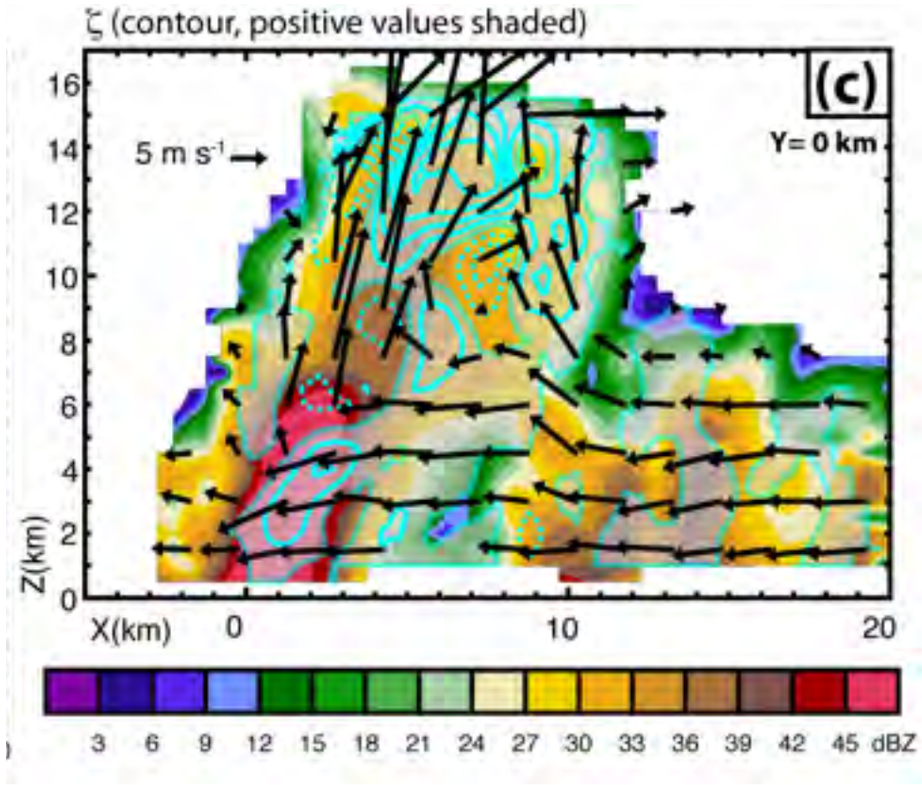

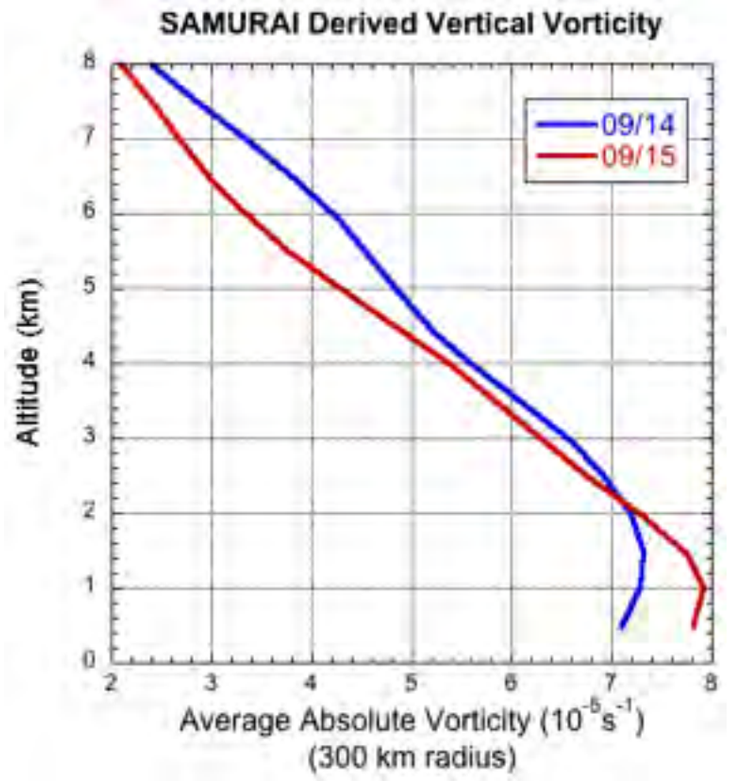

SAMURAI analysis methodology

- Spline Analysis at Mesoscale Utilizing Radar and Aircraft Instrumentation (Bell et al. 2012)
  - Tunable boundary conditions, error specifications, and filtering without balance constraints required for NWP
- 3D-VAR analysis using dropsonde, in situ, satellite vector winds, and Doppler radar data in inertial frame with or without background field
  - Meso-α (25 km) and meso-β (2 km)

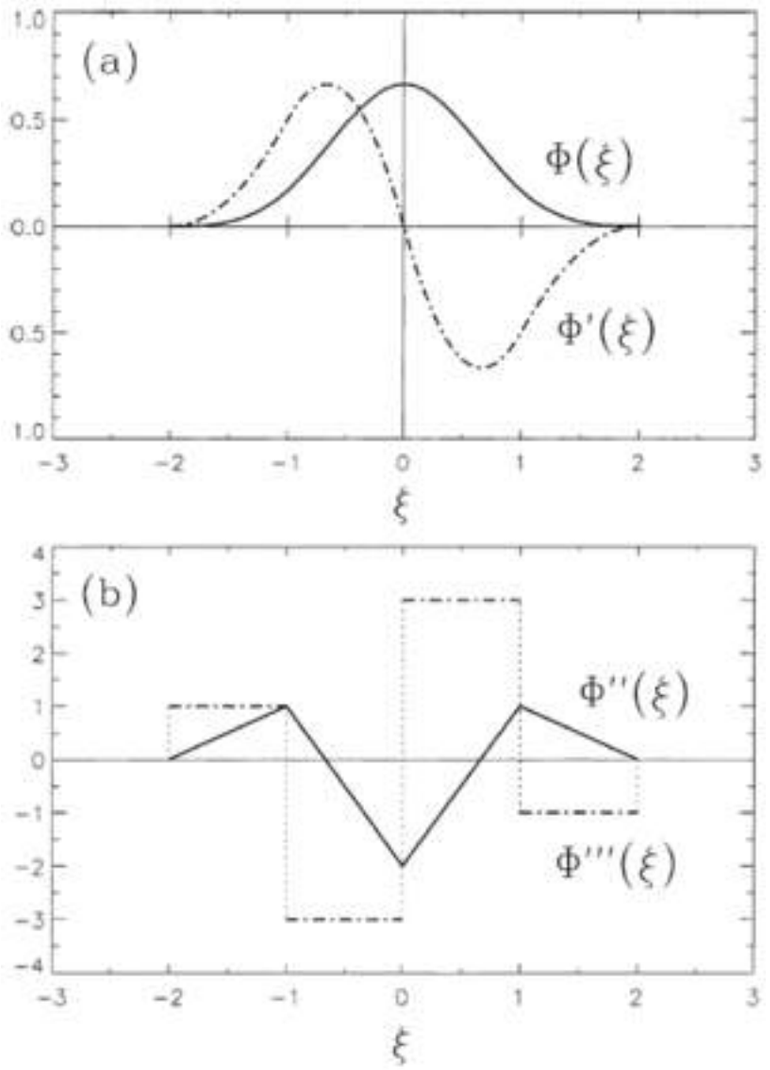

From Ooyama (2002)

$$\hat{x}(x,y,z) = \left\{\rho u, \rho v, \rho w, T', \rho_a', q_v'\right\}$$

Typhoon Nuri (2008)

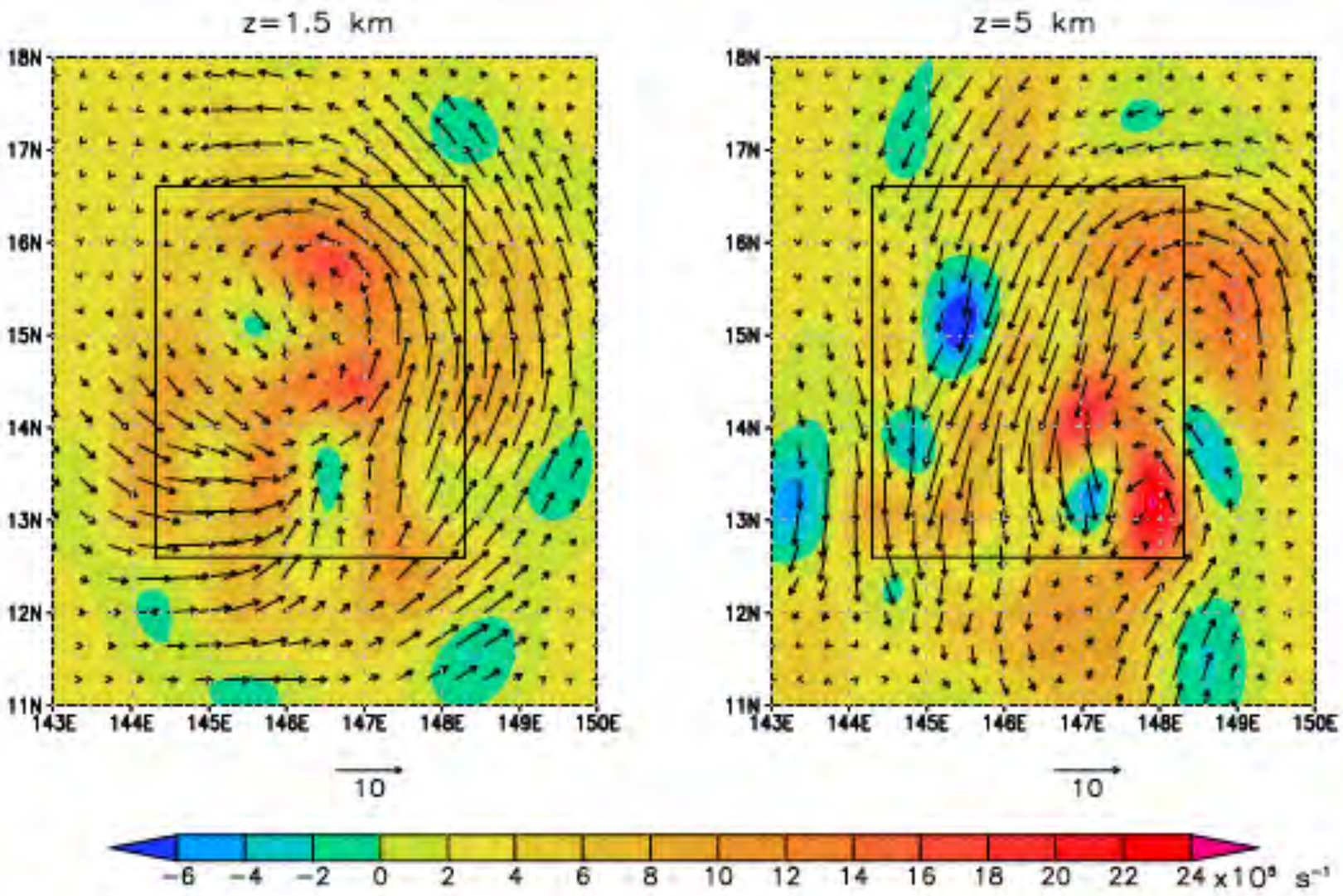

Figure 7. Two-panel plot of absolute vorticity (shaded) and wind vectors (co-moving) for Nuri 1 at 1.5 km (left) and 5 km (right) height from the 10 km SAMURAI analyses. The black box is the four-degree length box centered on the 25 km analysis 1.5 km altitude sweet spot position and is for reference only. The abscissa is longitude and the ordinate is latitude.

Lussier et al. (2014)

Typhoon Nuri (2008)

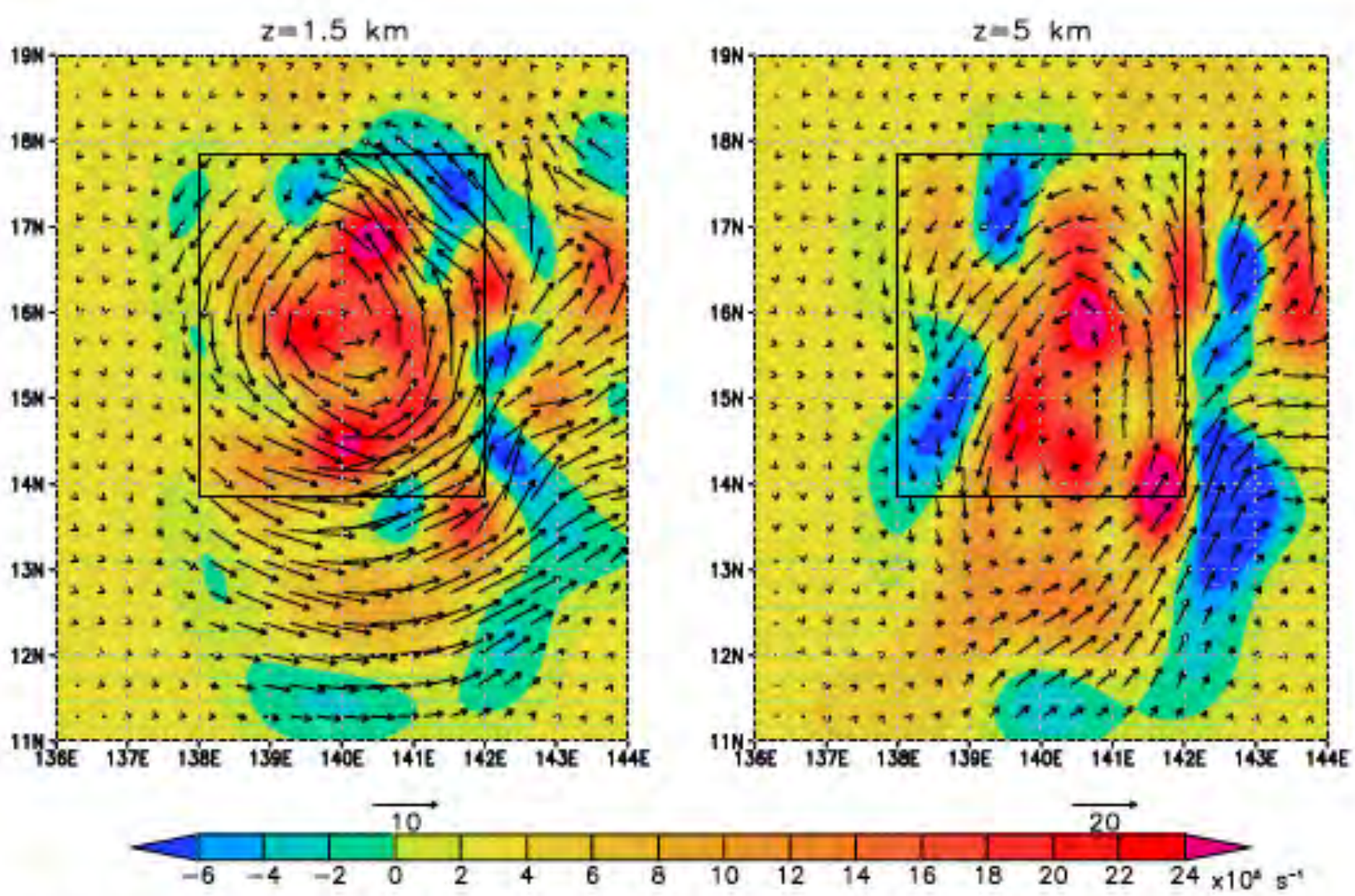

Figure 8. Two-panel plot of absolute vorticity (shaded) and wind vectors (co-moving) for Nuri 2 at 1.5 km (left) and 5 km (right) height from the 10 km SAMURAI analyses. The black box is the four-degree length box centered on the 25 km analysis 1.5 km altitude sweet spot position and is for reference only. The abscissa is longitude and the ordinate is latitude.

Lussier et al. (2014)

Typhoon Nuri (2008)

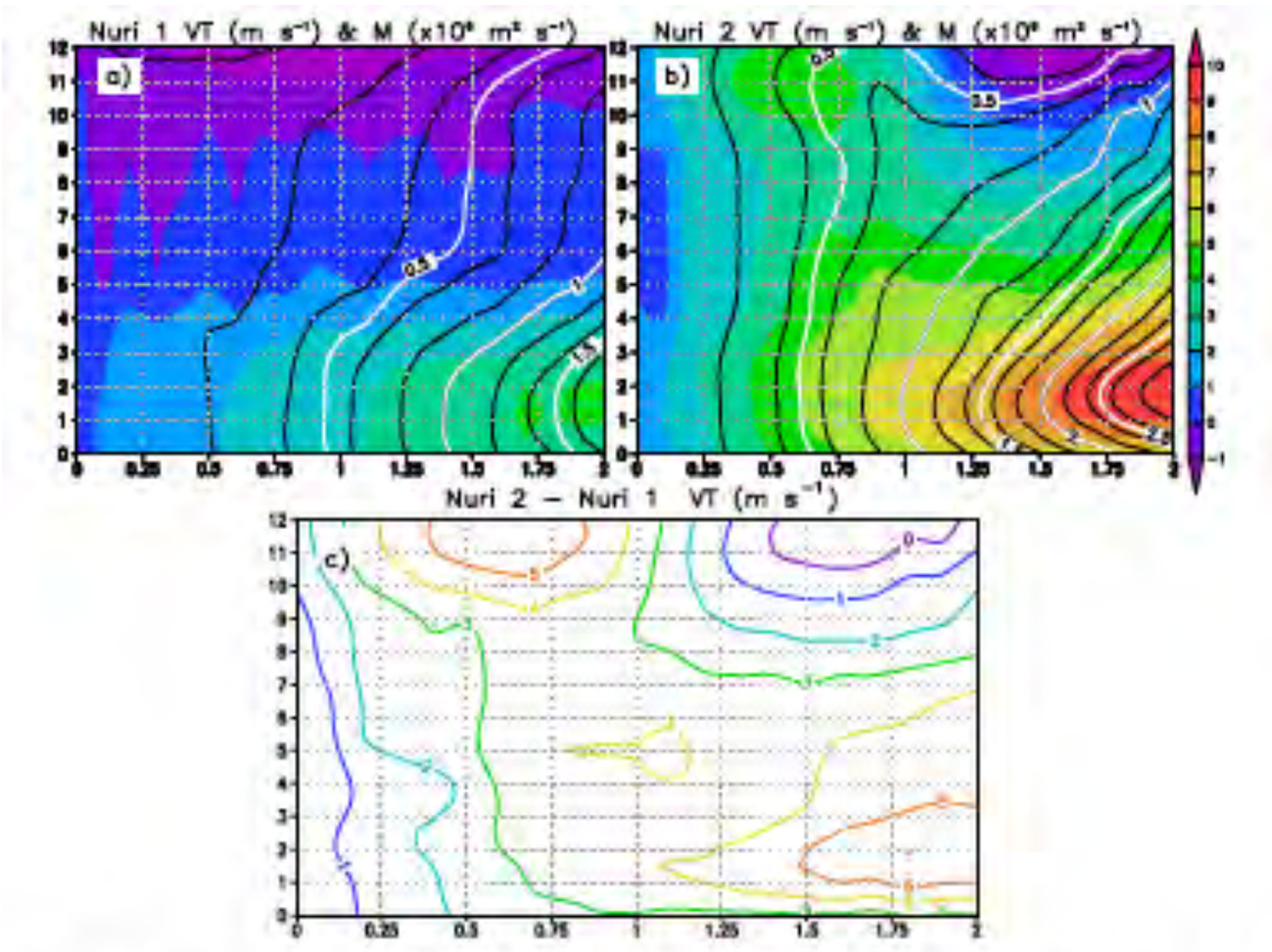

Figure 13. Three-panel plot of tangential wind (top, shaded) and absolute angular momentum (top, contours) for Nuri 1 (**a**) and Nuri 2 (**b**). Angular momentum surfaces are plotted at $0.2 \times 10^6\ m^2\ s^{-1}$ contours (black) and are highlighted (white) at $0.5 \times 10^6\ m^2\ s^{-1}$ intervals. The difference in tangential wind speed between Nuri 2 and Nuri 1 is plotted in (**c**). The abscissa is radial distance (degrees) from the 1.5 km sweet spot position. The ordinate is height (km).

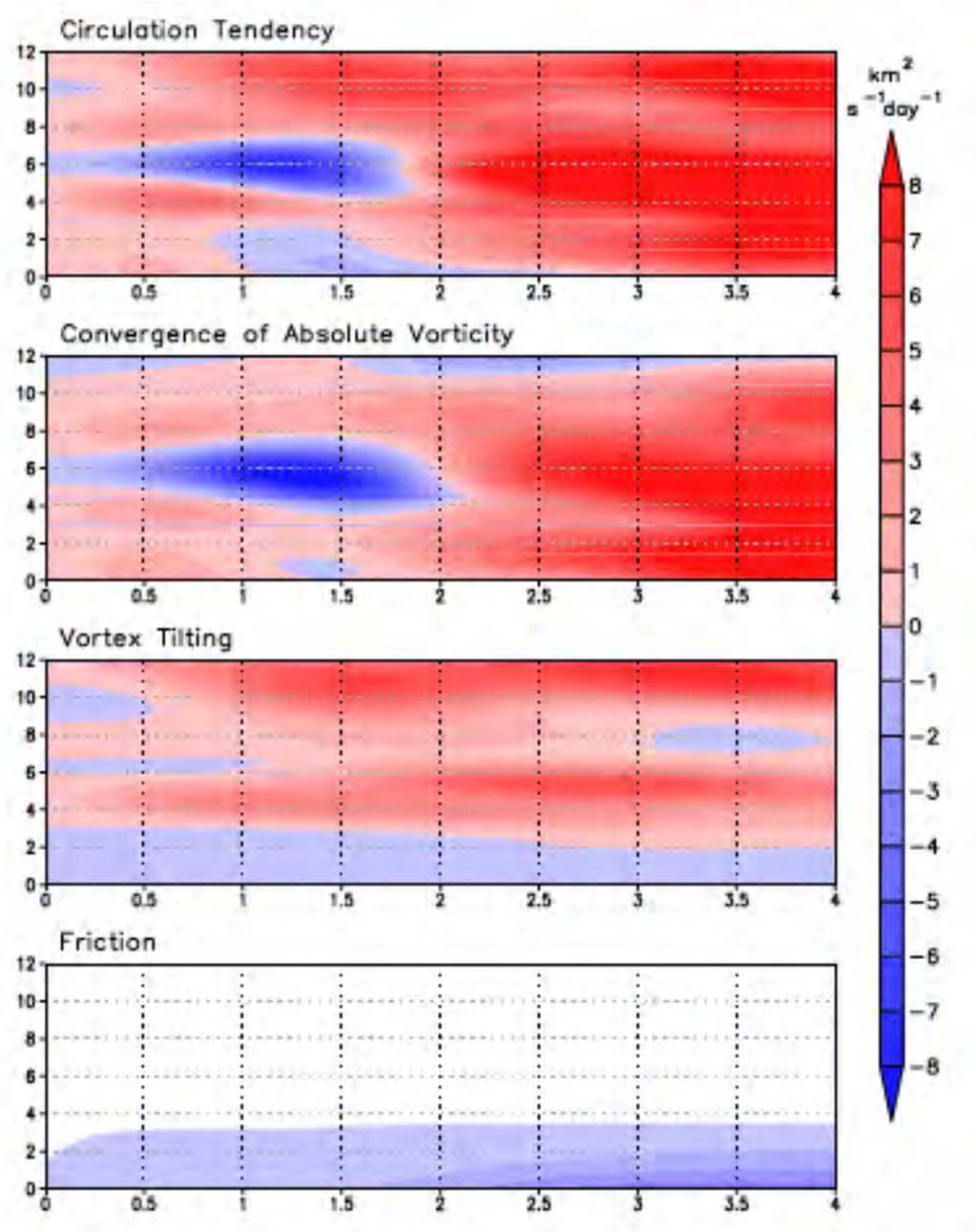

Figure 12. Four-panel height/distance cross section of each term from the circulation tendency equation (Eq. 7) for Nuri 1. The abscissa is the length of the box (degrees) on which the integration is performed and is centered on the 1.5 km sweet spot position. The ordinate is height (km).

Lussier et al. (2014)

Non-developing Disturbance TCS-025

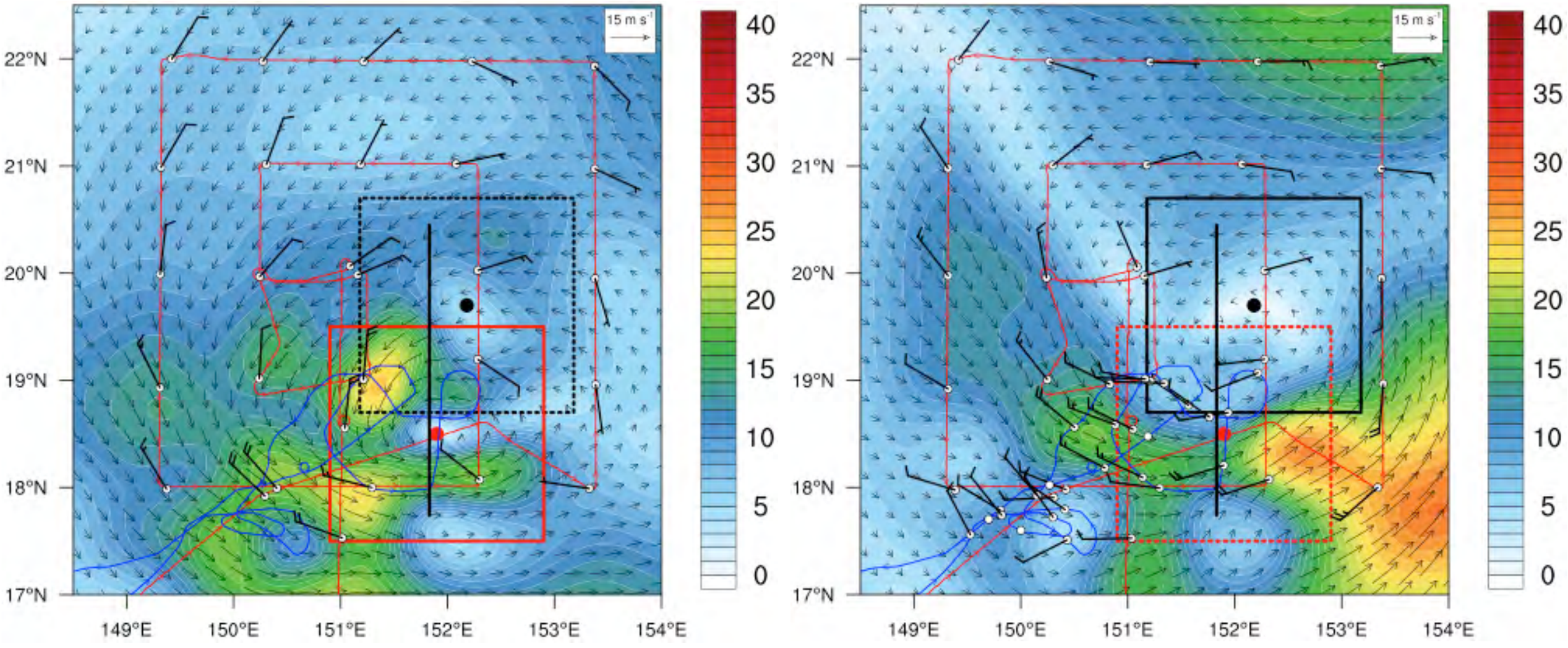

Storm-relative wind speed (kt, shading) and vectors (m s^{-1}) at (a) 5 km and (b) 1.5 km from the 5-km SAMURAI analysis valid at 0000 UTC 28 August. The WC-130J track for flight 0325W is in red and the P-3 track for flight 0225W is in blue. Black wind barbs (1 full barb = 10 kt) correspond to dropwindsonde winds corrected for storm motion. Solid black line denotes location of the cross-section in next slide. The 2 x 2 black and red boxes are centered on the circulation center positions at 1.5 (black dot) and 5 km (red dot),

Penny et al. (2015)

Non-developing Disturbance TCS-025

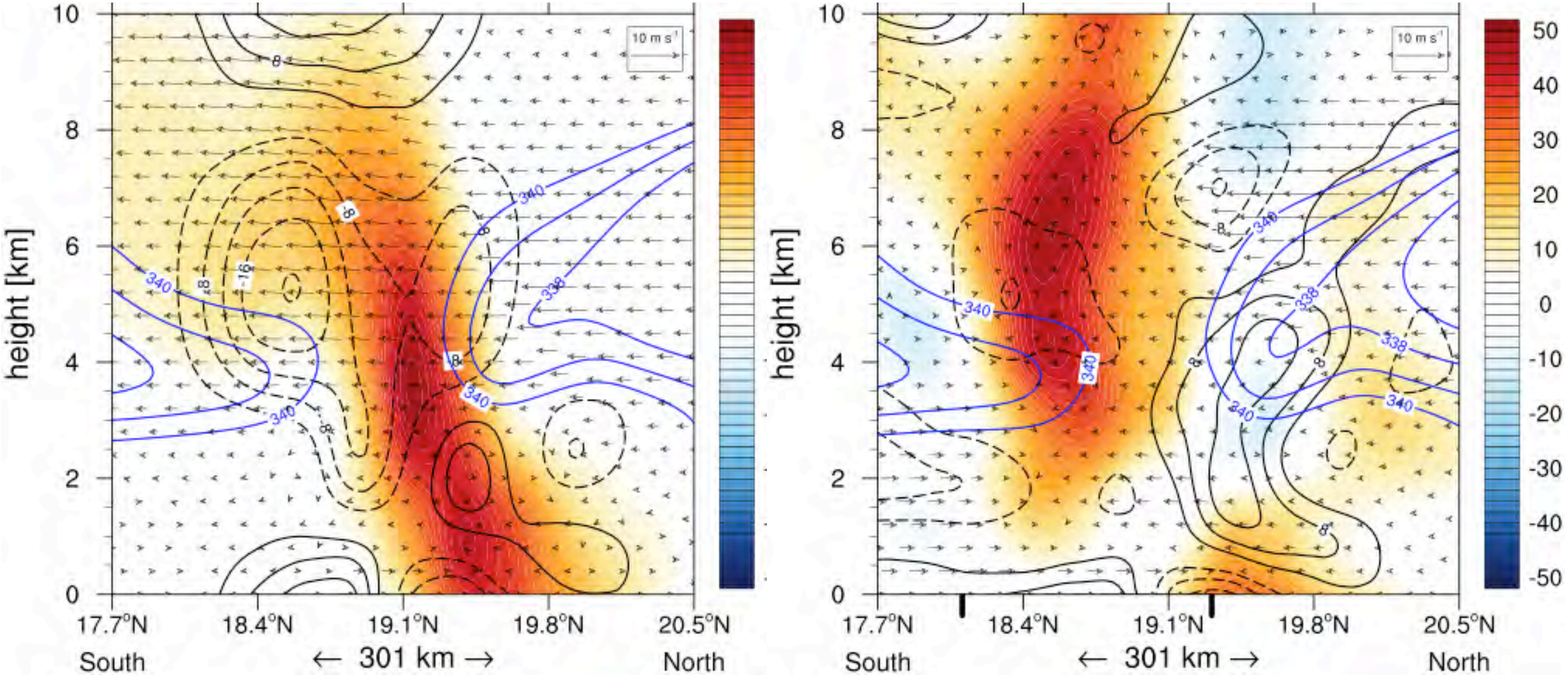

South-to-north oriented vertical cross section of relative vorticity (10^{-5} s^{-1}, shading), divergence (10^{-5} s^{-1}, black contours at 4.0×10^{-5} s^{-1} intervals with negative values dashed), θ_e (K, blue contours for θ_e <= 340 K), and wind vectors in the plane of the cross section (m s^{-1}) constructed from (a) the ECMWF background field and (b) the SAMURAI analysis with 5-km grid spacing valid at 0000 UTC 28 August. The location of cross section corresponds to solid black lines shown in previous slide.

Penny et al. (2015)

Square spiral was generally a better flight pattern than the lawnmower in PREDICT

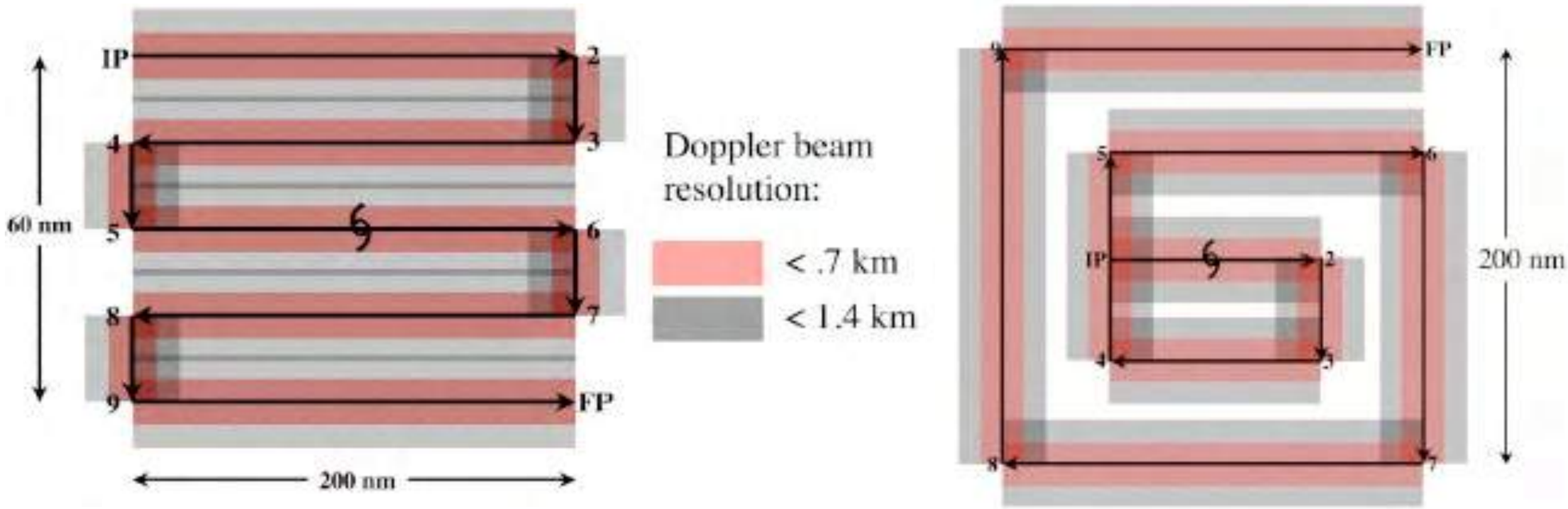

- Square spiral is good for a high-altitude meso-alpha scale flight pattern with
- Data coverage is similar to lawnmower, but offers more flexibility and less convective penetration

Square Spiral in pre-Fiona was a textbook example of the pattern

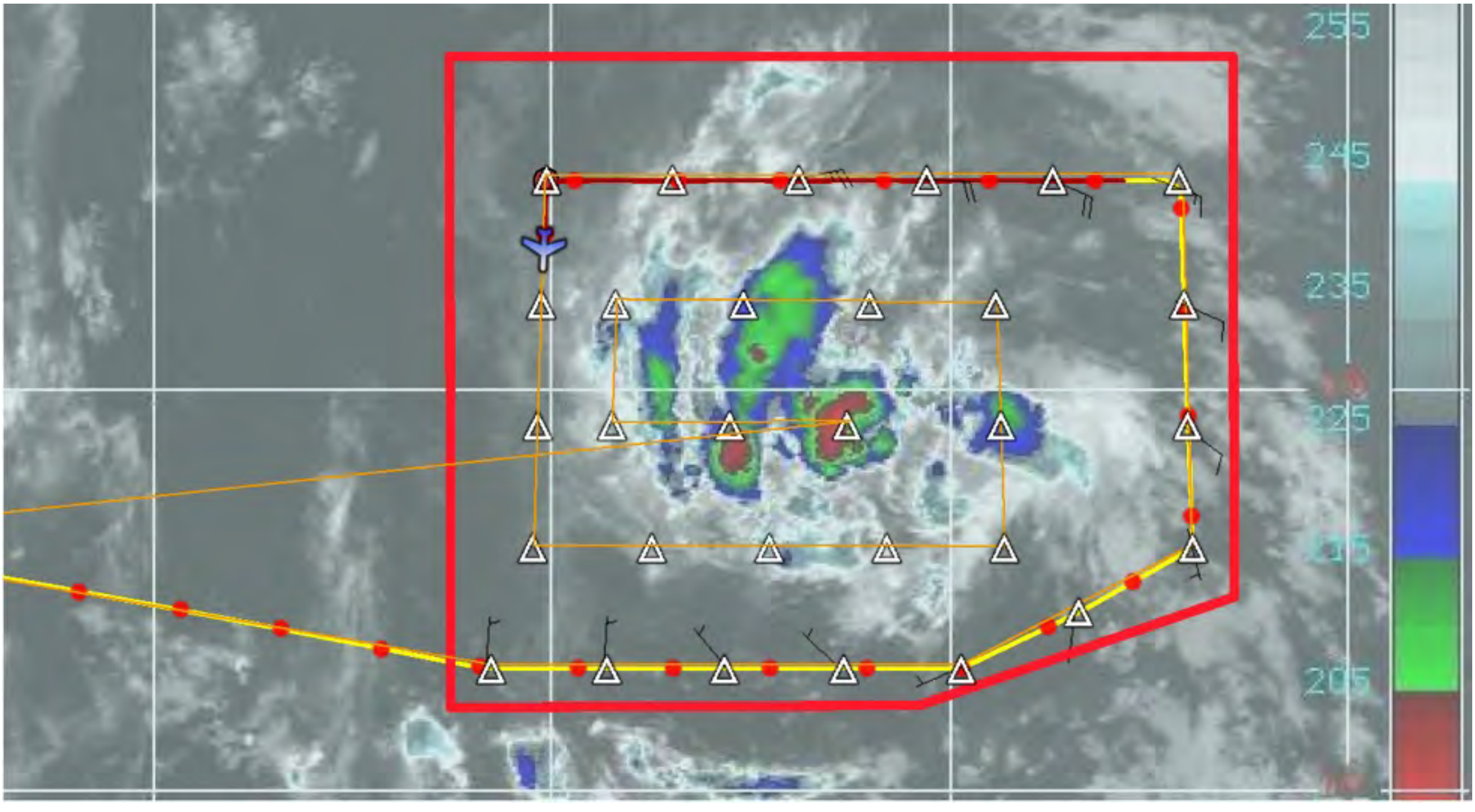

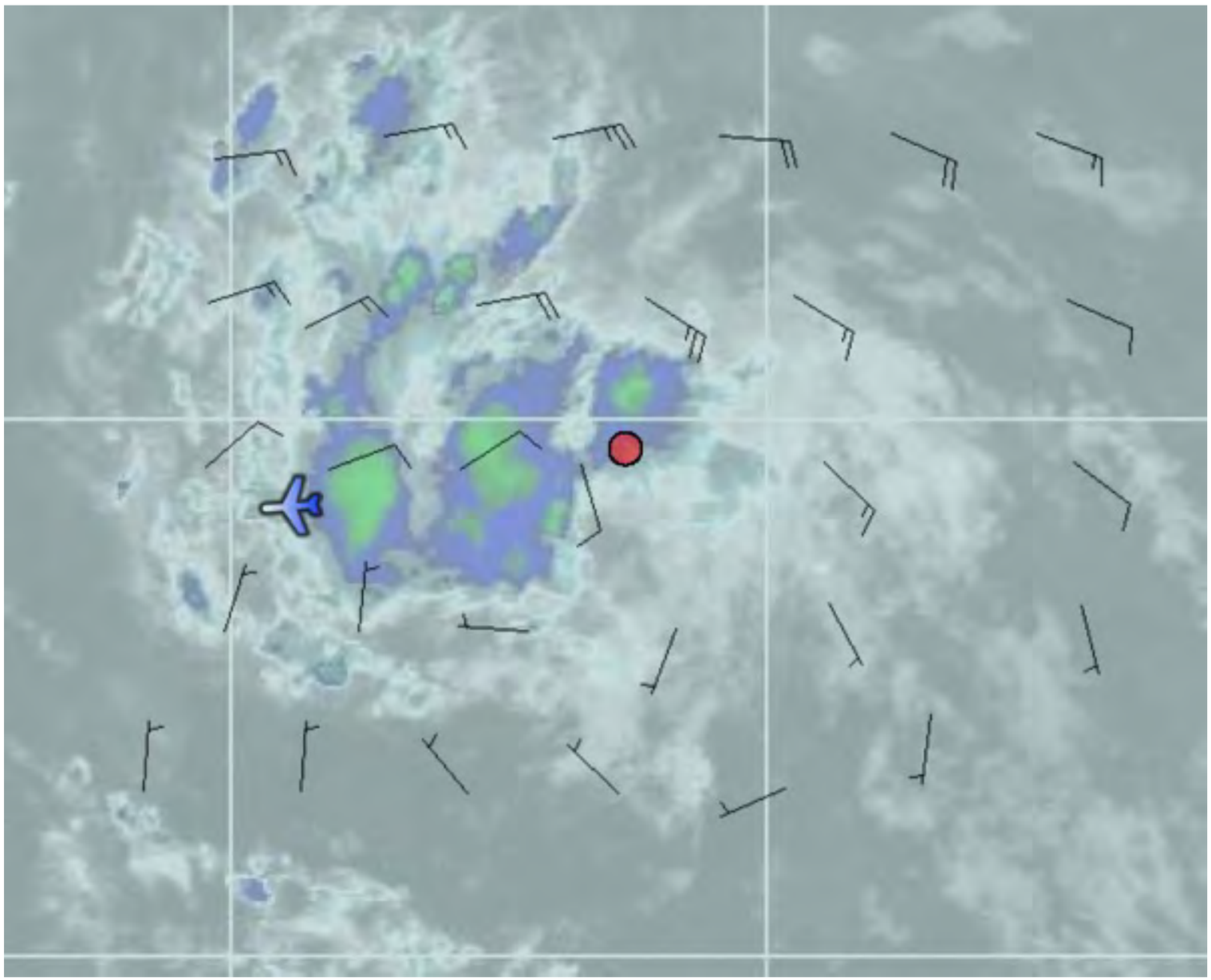

EARLIER TODAY...ABOUT 30 DROPSONDES WERE RELEASED DURING A G-V RESEARCH MISSION BEING CONDUCTED BY THE NATIONAL CENTER FOR ATMOSPHERIC RESEARCH NEAR THE AREA OF LOW PRESSURE LOCATED ABOUT 800 MILES EAST OF THE LESSER ANTILLES. ONE OF THE DROPSONDES MEASURED A SURFACE WIND OF 35 KT APPROXIMATELY 120 N MI TO THE NORTHEAST OF THE ESTIMATED CENTER. THIS MEASUREMENT AGREES WITH AN ASCAT PASS FROM 1208 UTC...WHICH SHOWED A SWATH OF 30-35 KT WINDS IN THAT SAME AREA. CONVECTION HAS BEEN A LITTLE THIN FOR MOST OF THE DAY...BUT BANDING FEATURES HAVE RECENTLY BECOME MORE PROMINENT MAINLY OVER THE WESTERN SEMICIRCLE. GIVEN THE INCREASE IN CONVECTION AND SINCE TROPICAL STORM FORCE WINDS ARE ALREADY OCCURRING...THE SYSTEM IS BEING DIRECTLY UPGRADED TO TROPICAL STORM FIONA.

Lawnmower in pre-Karl was difficult

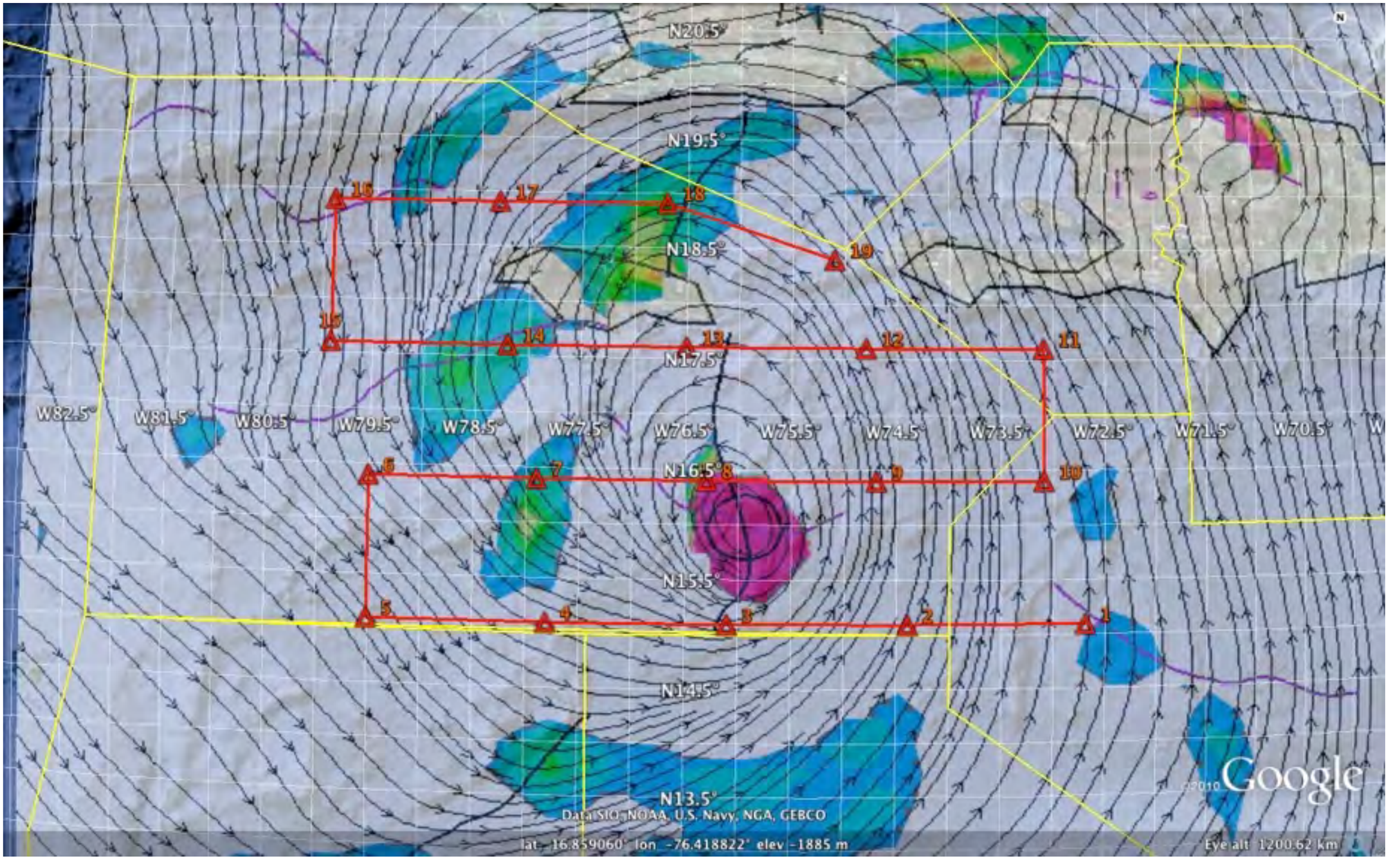

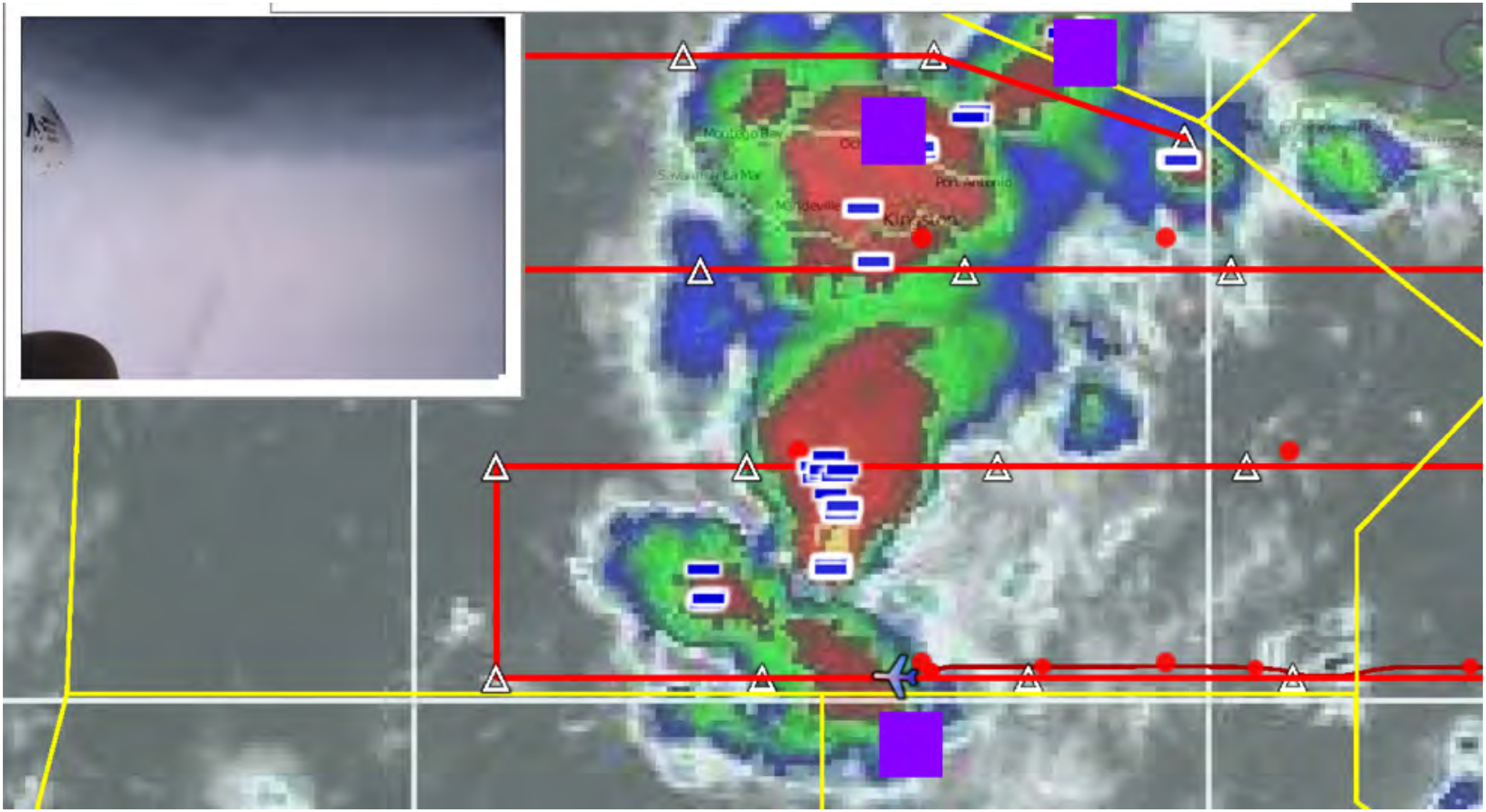
Montego Bay
Ocho Rios
Port Antonio
Mandeville
Kingston

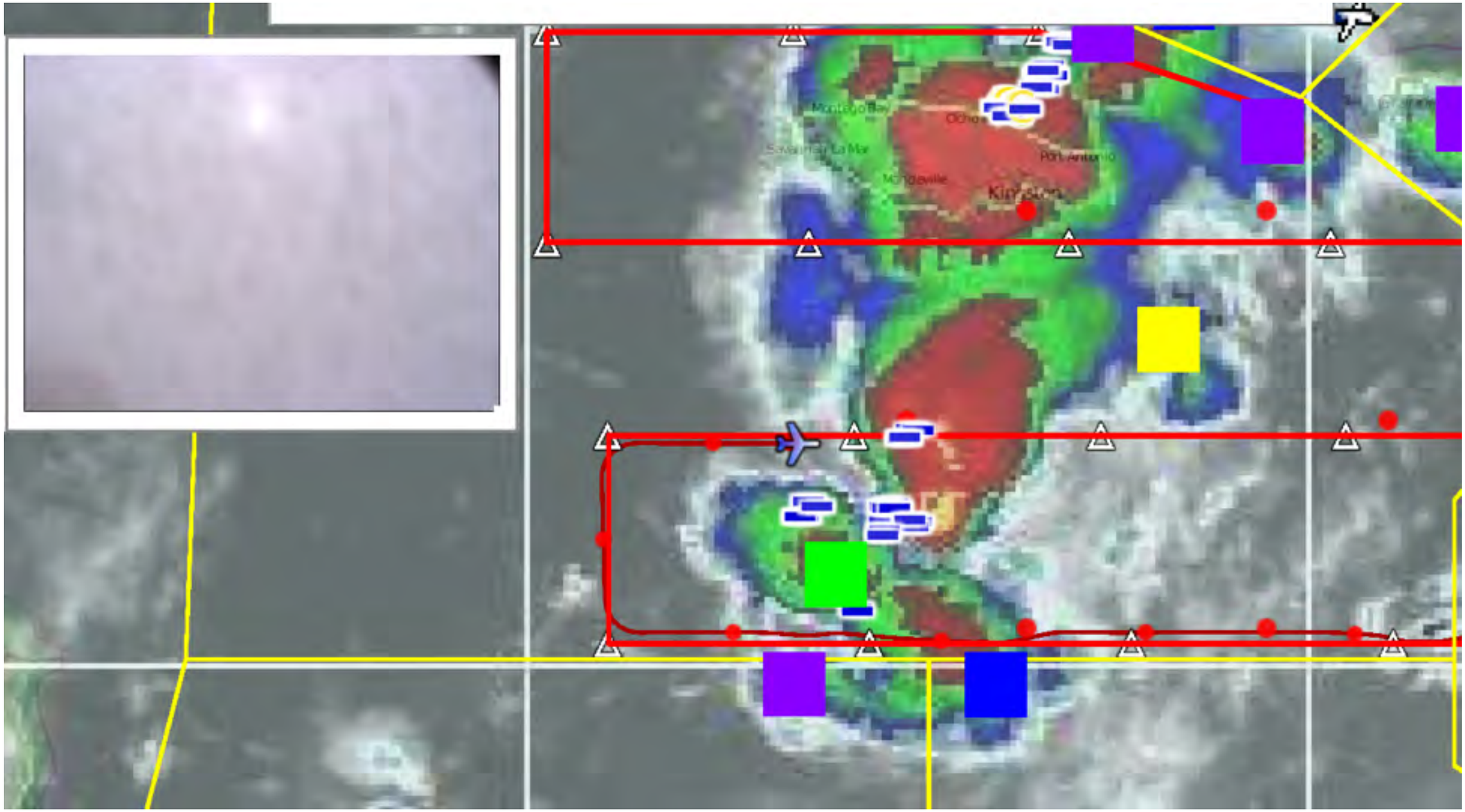
Montego Bay
Ocho Rios
Savanna-la-Mar
Port Antonio
Mandeville
Kingston

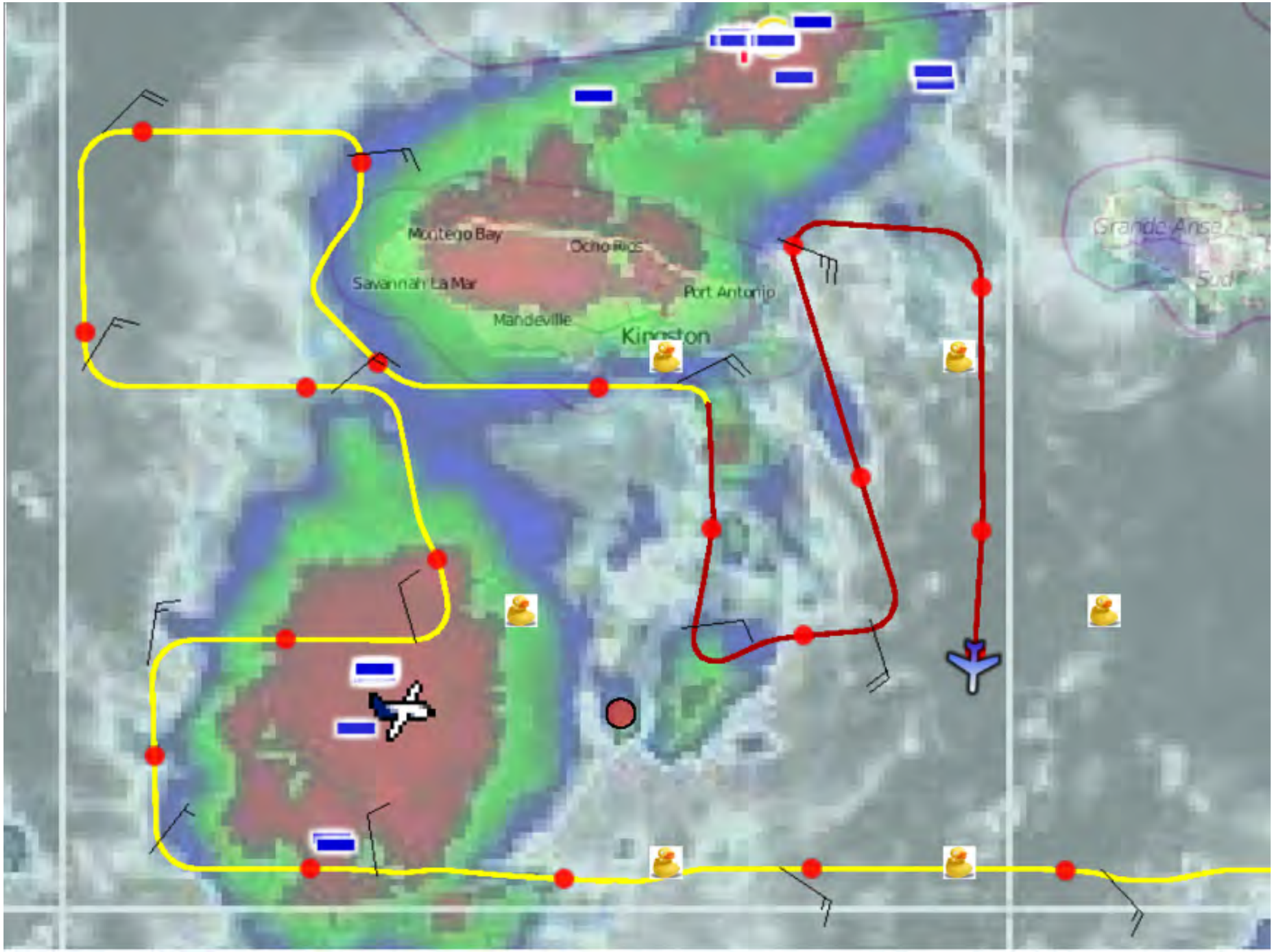
Montego Bay
Ocho Rios
Savannah La Mar
Port Antonio
Mandeville
Kingston
Grande Anse
Sud

Real-time adjustments led to a great dataset

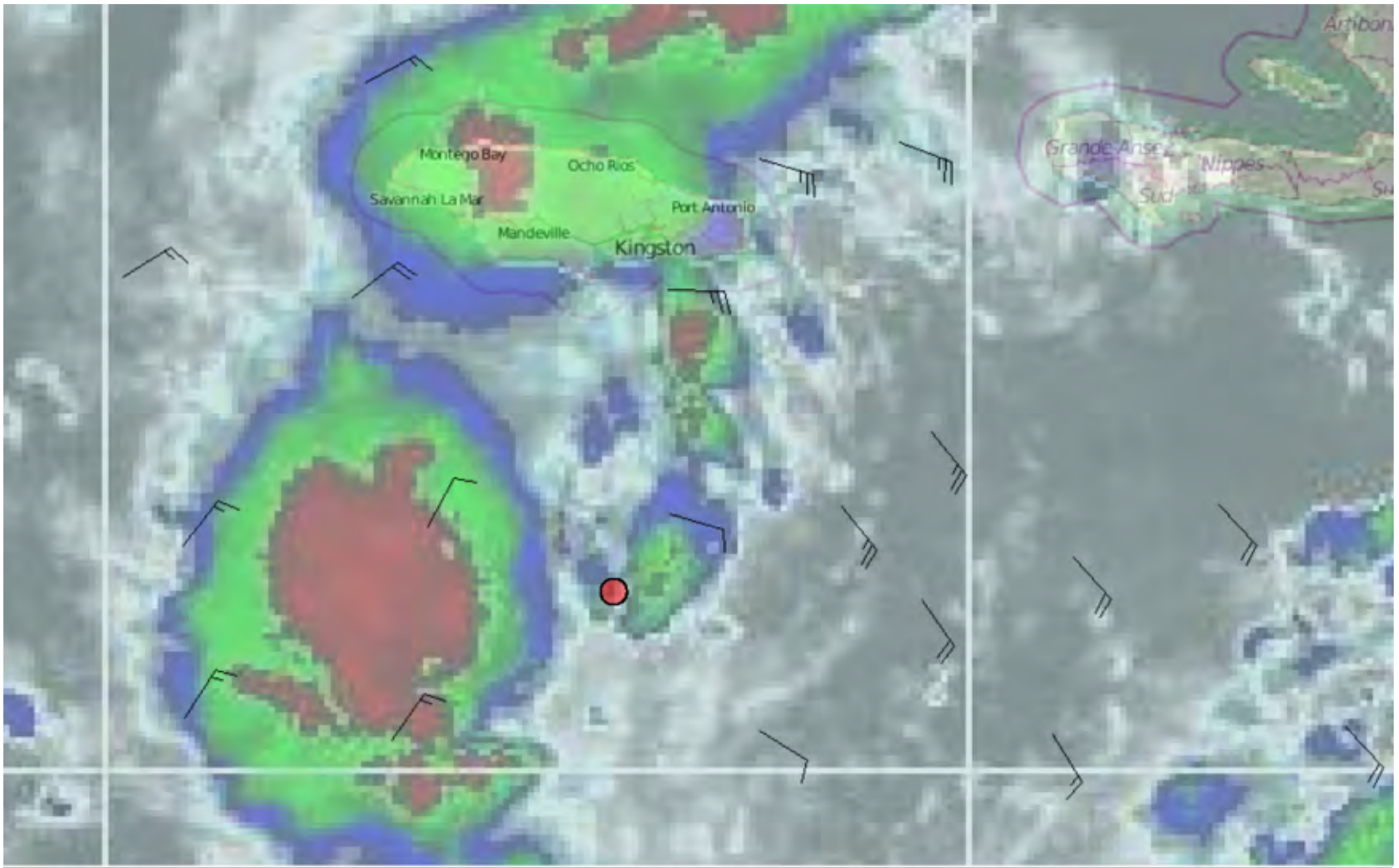

Genesis of Hurricane Karl (2010)

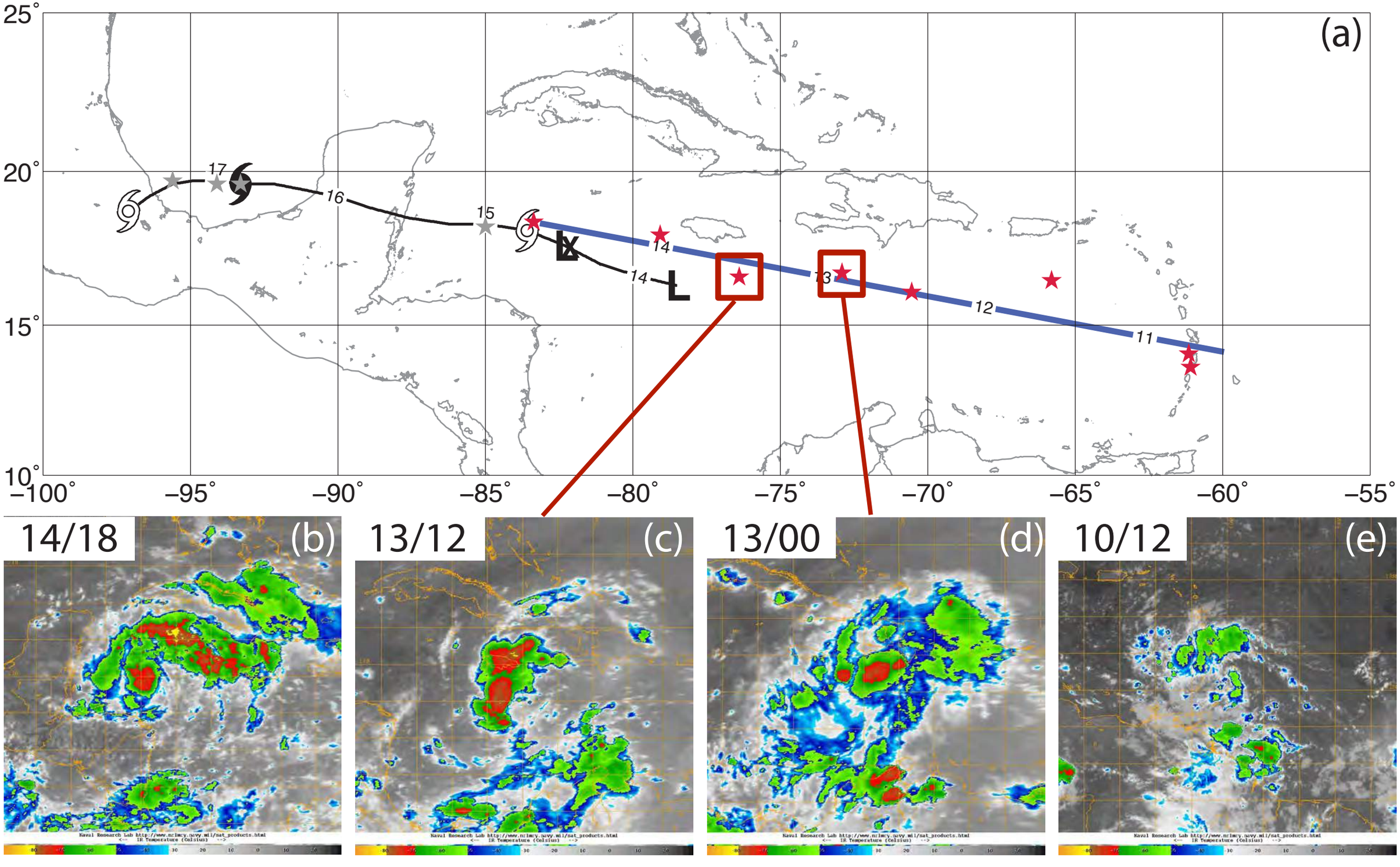

Bell and Montgomery (2016)

Stratiform precipitation spins-up mid-levels
Convective burst spin-ups low-levels

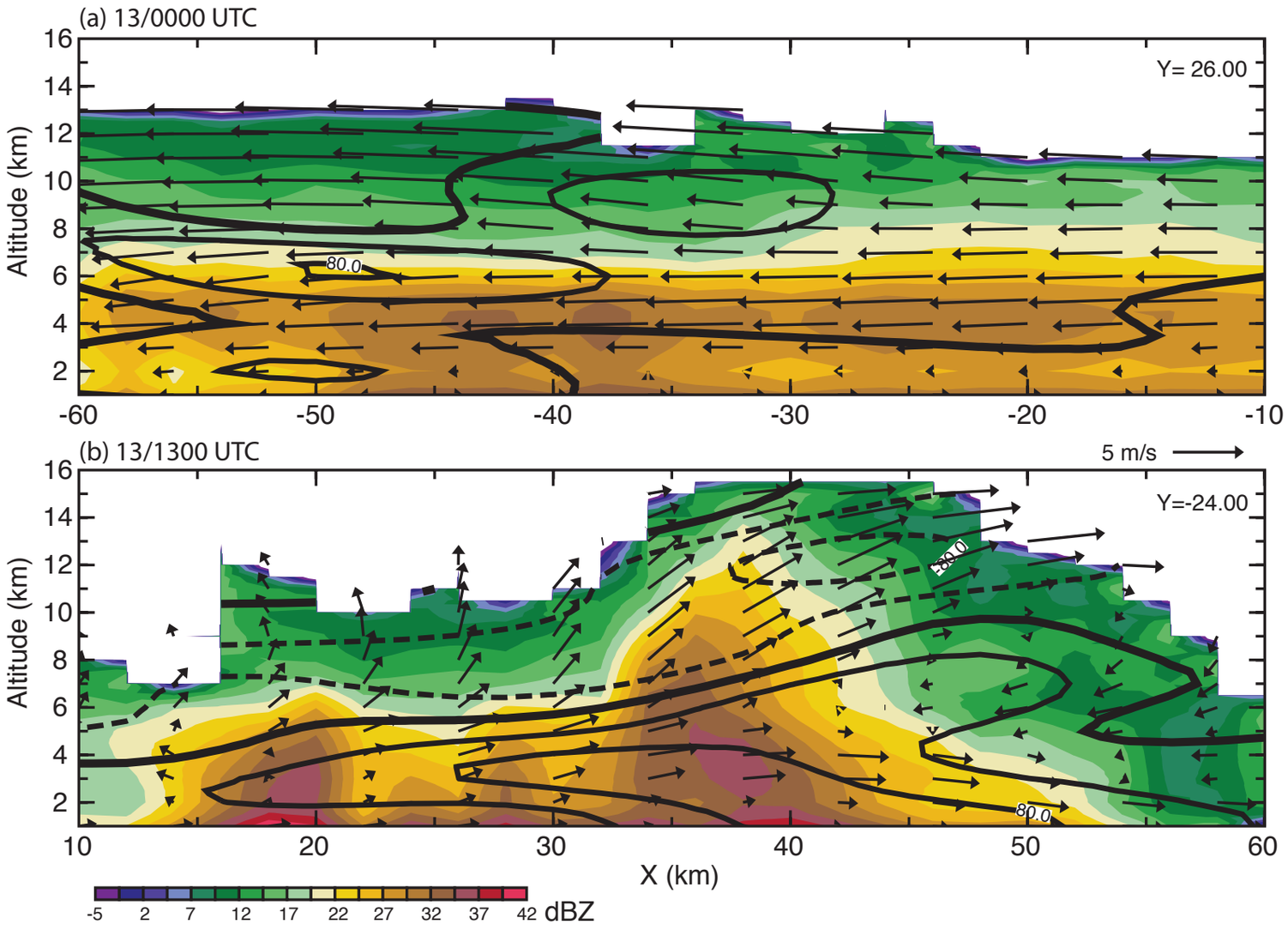

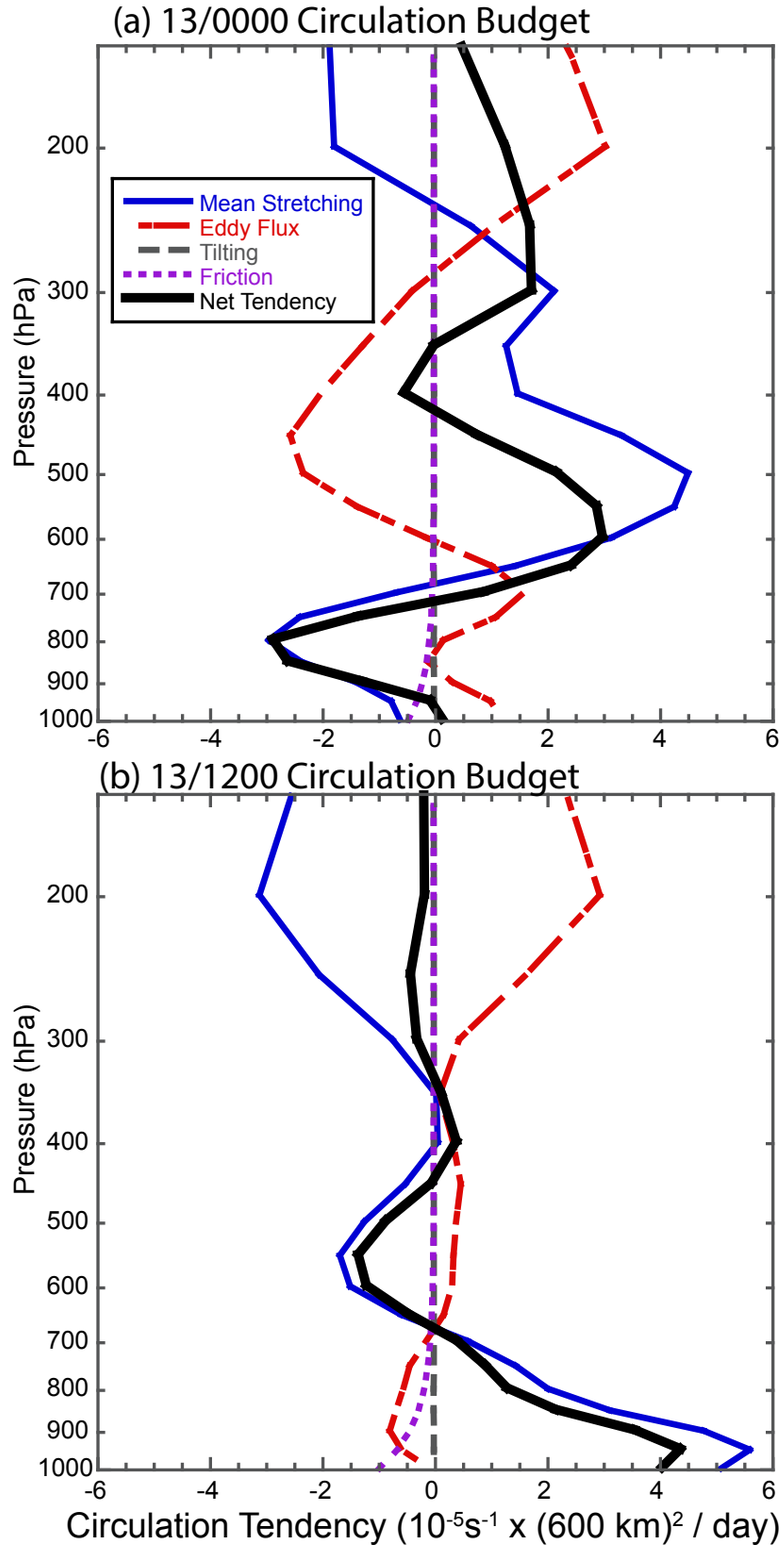

Bell and Montgomery (2016)

Stratiform precipitation spins-up mid-levels
Convective burst spin-ups low-levels

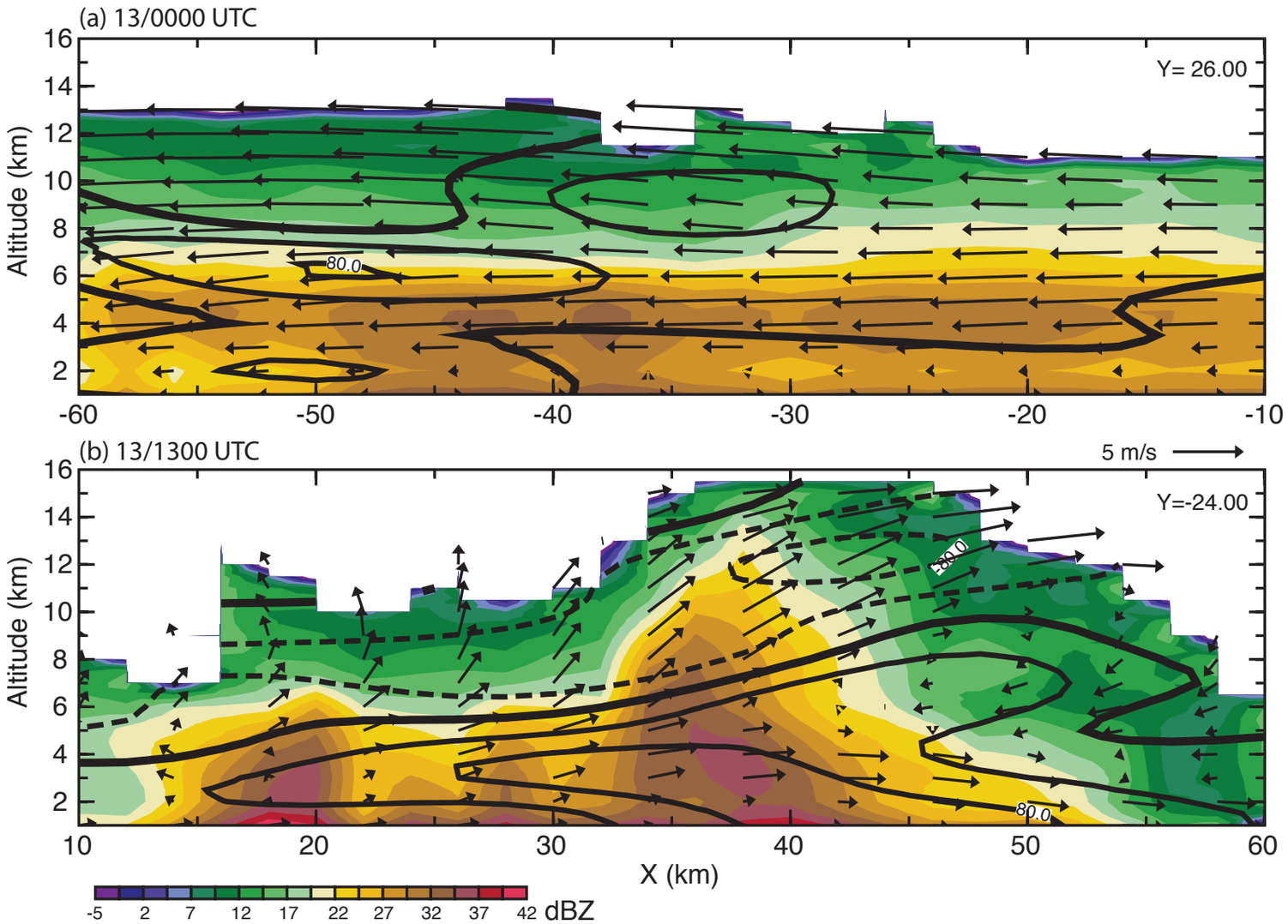

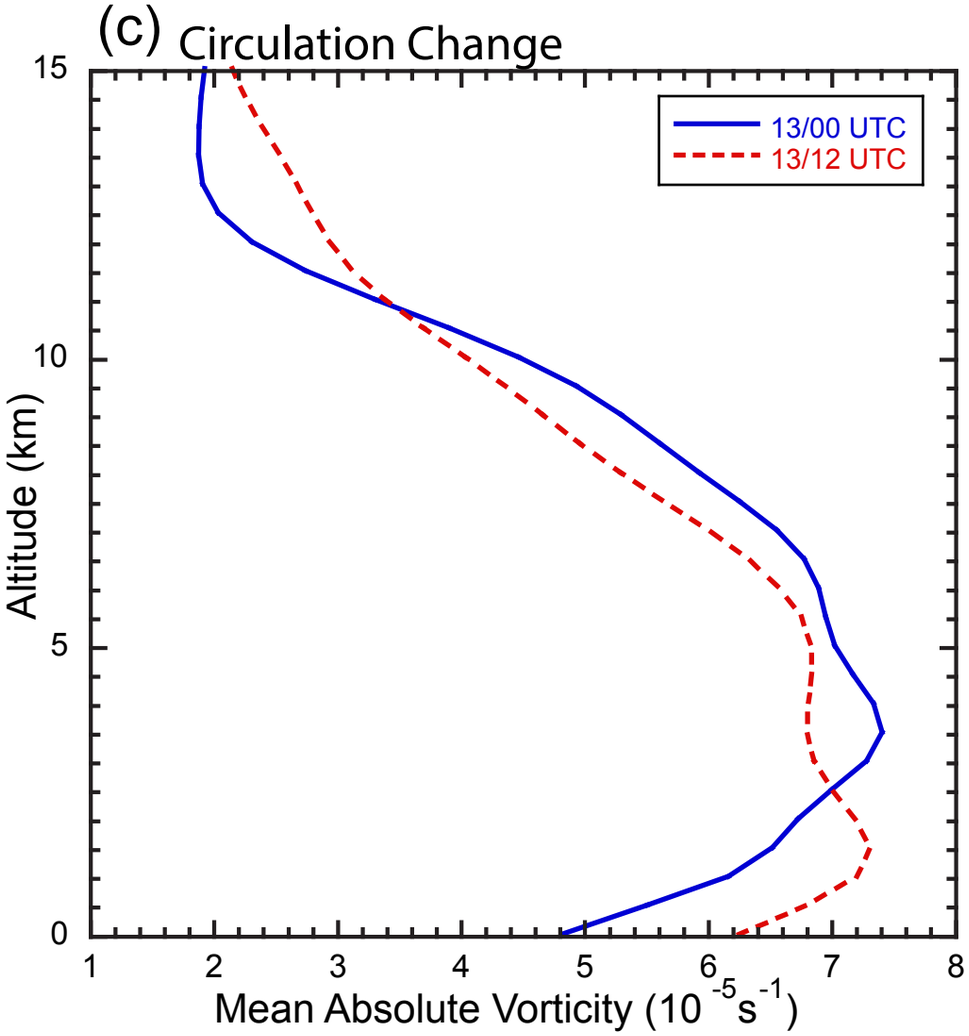

Bell and Montgomery (2016)

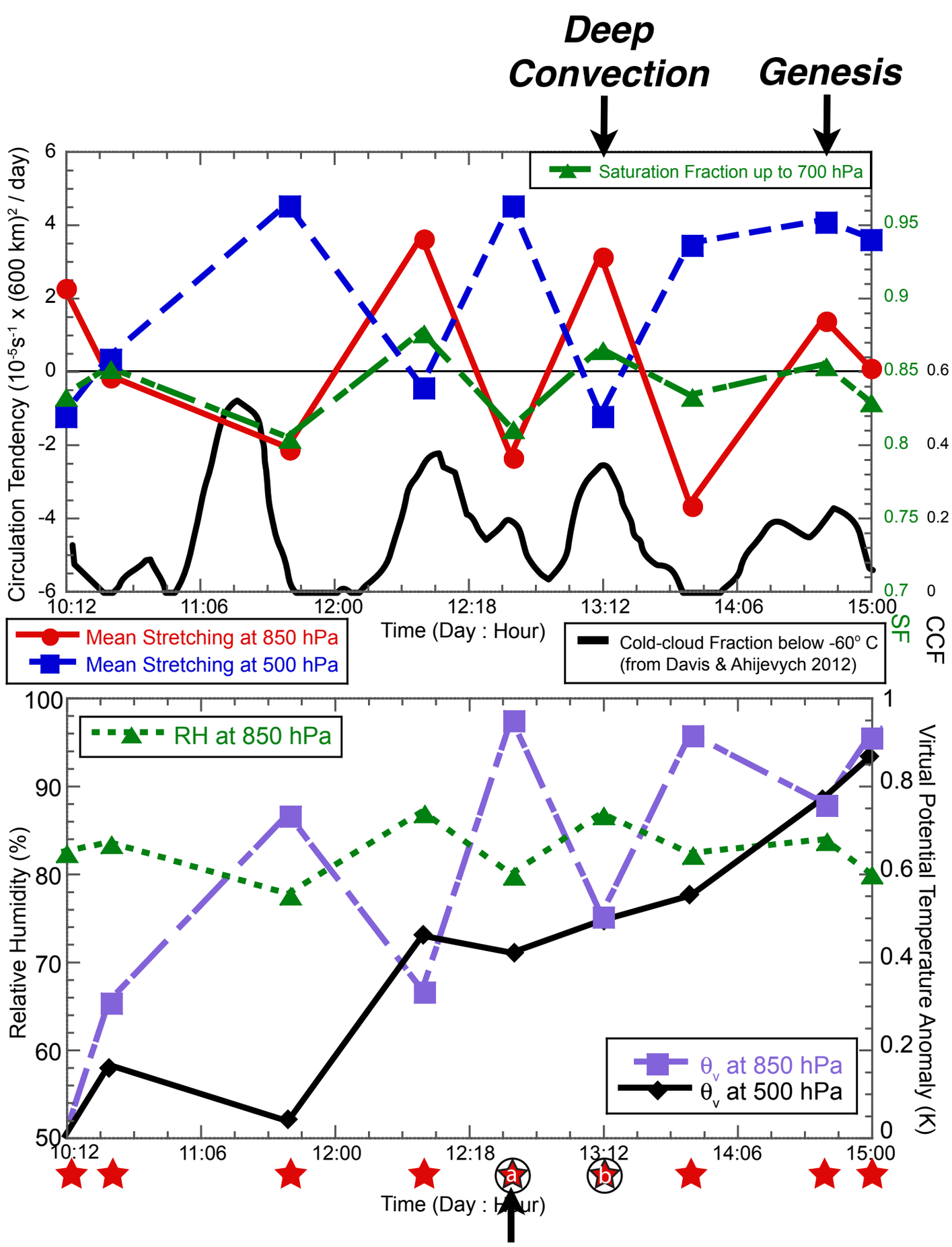

Bell and Montgomery (2016)

Results from PREDICT (2010)

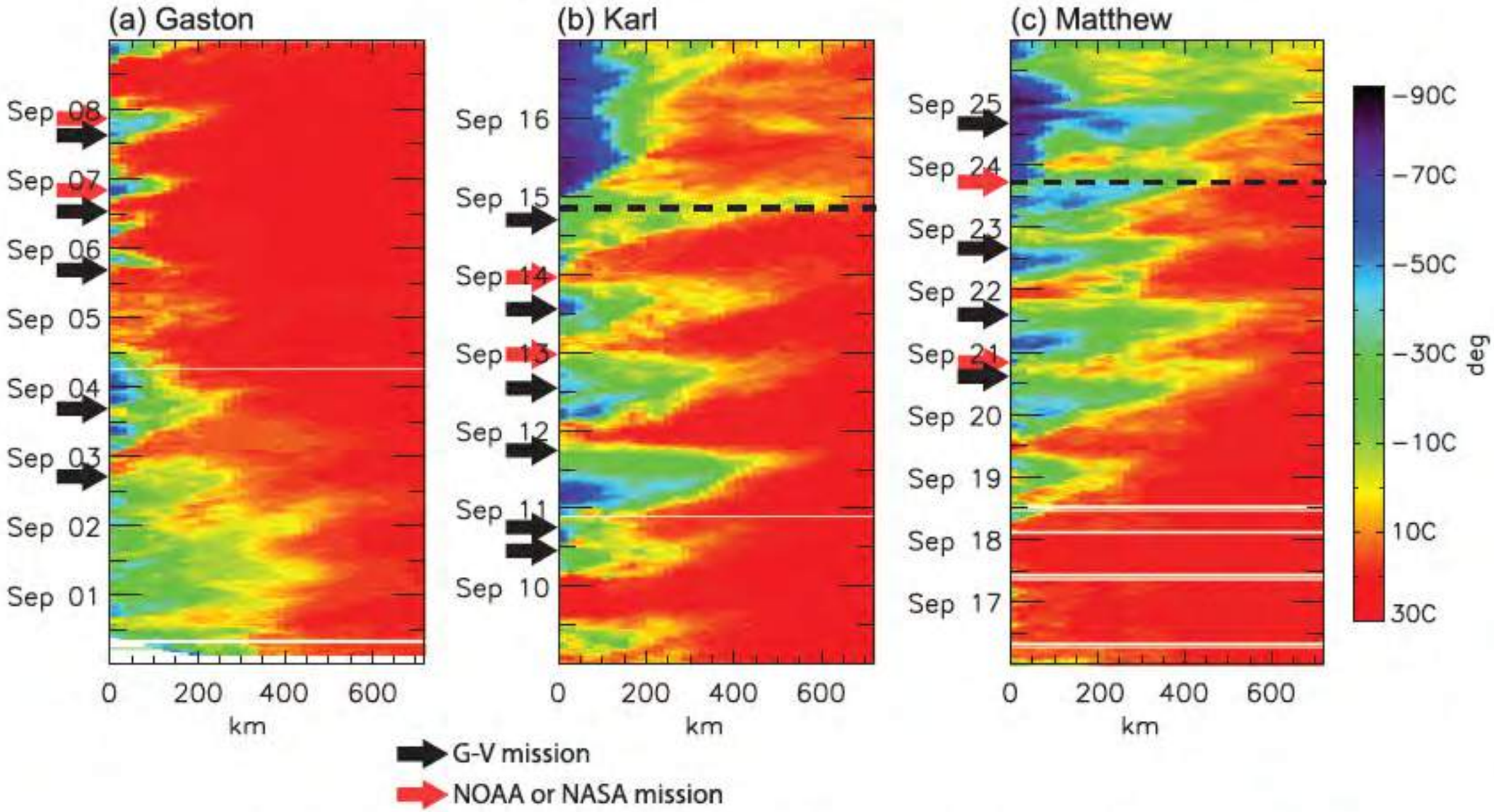

FIG. 3. Time–radius diagrams of cloud-top temperature derived from Geostationary Operational Environmental Satellite (GOES) IR data, where the 75th percentile temperature within each radial ring of 20-km width is plotted. Arrows indicate when dropsonde missions occurred (black for GV, red for NOAA or NASA). Dashed lines denote time of tropical storm formation for Karl and Matthew.

Davis and Ahijeyvich (2012)

Results from PREDICT (2010)

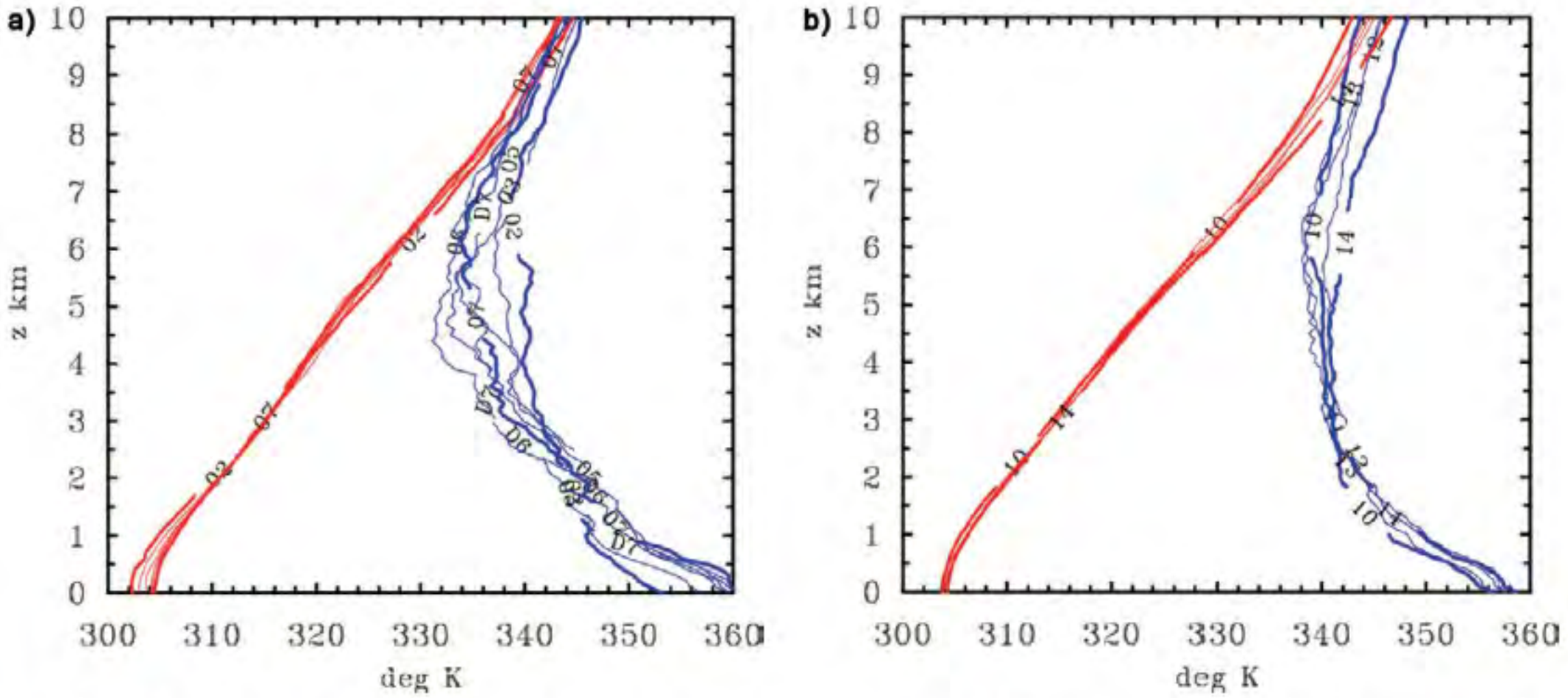

FIG. 14. Comparison of pouch-mean soundings of virtual potential temperature (θ_v) (red) and pseudo-equivalent potential temperature (θ_e) (blue) as a function of height derived from the NSF GV and NASA DC8 dropsondes in (a) the pouch of PGI38 (ex-Gaston) that failed to redevelop and (b) the pouch of PGI44 (pre-Karl) that did develop. Numbers on curves refer to the day of the flight mission in Sep 2010. The thick curves mark the first and last days of the GV flights. Curves for the NASA DC8 flights are denoted with the prefix D.

Montgomery et al. (2012)

Summary Part I

- **Field observations and modeling suggest a deep, moist pouch is a necessary, and perhaps sufficient condition for genesis**
  - Developing TCs are characterized by a vertically aligned, strong low and mid-level meso-α circulation, with higher moisture in the mid-troposphere above the boundary layer
- **Observations suggest that active deep convection within the larger scale recirculation region is a primary low-level intensification mechanism**
  - Repeated bursts of deep convection spin-up the low-level circulation primarily through vortex stretching
  - Stratiform precipitation spins down the low-level circulation, but deepens and broadens the mid-level circulation and helps thermodynamically
  - Shallow and cumulus congestus may also play an important role in pre-conditioning the environment

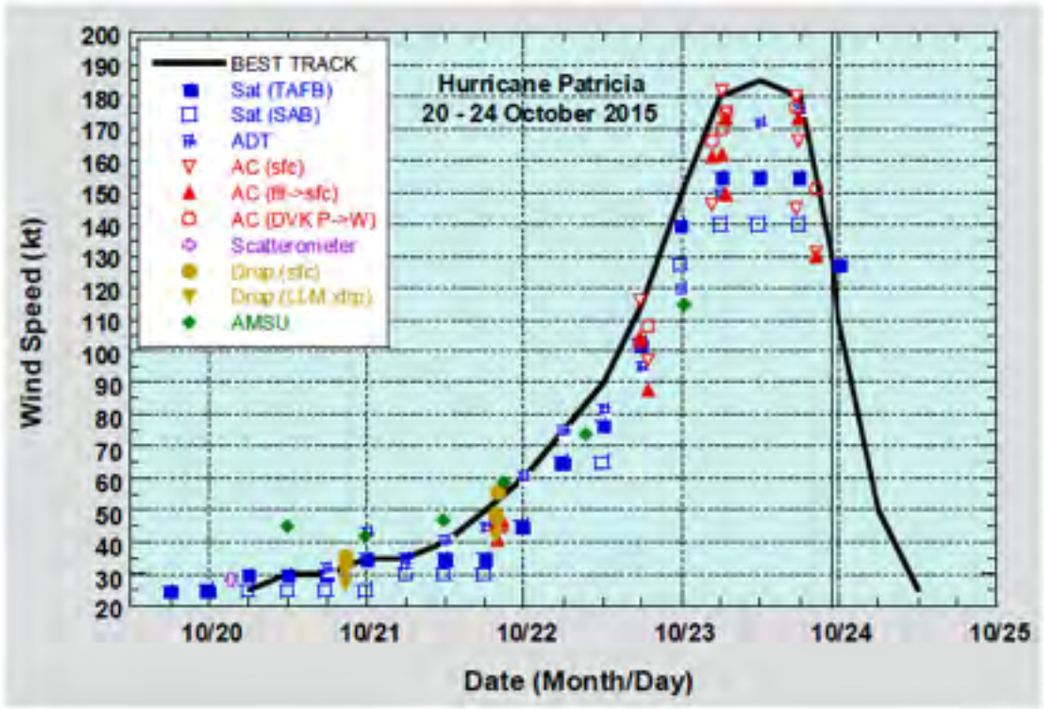

Hurricane Patricia (2015) set a new bar for rapid intensification and challenge for forecast skill

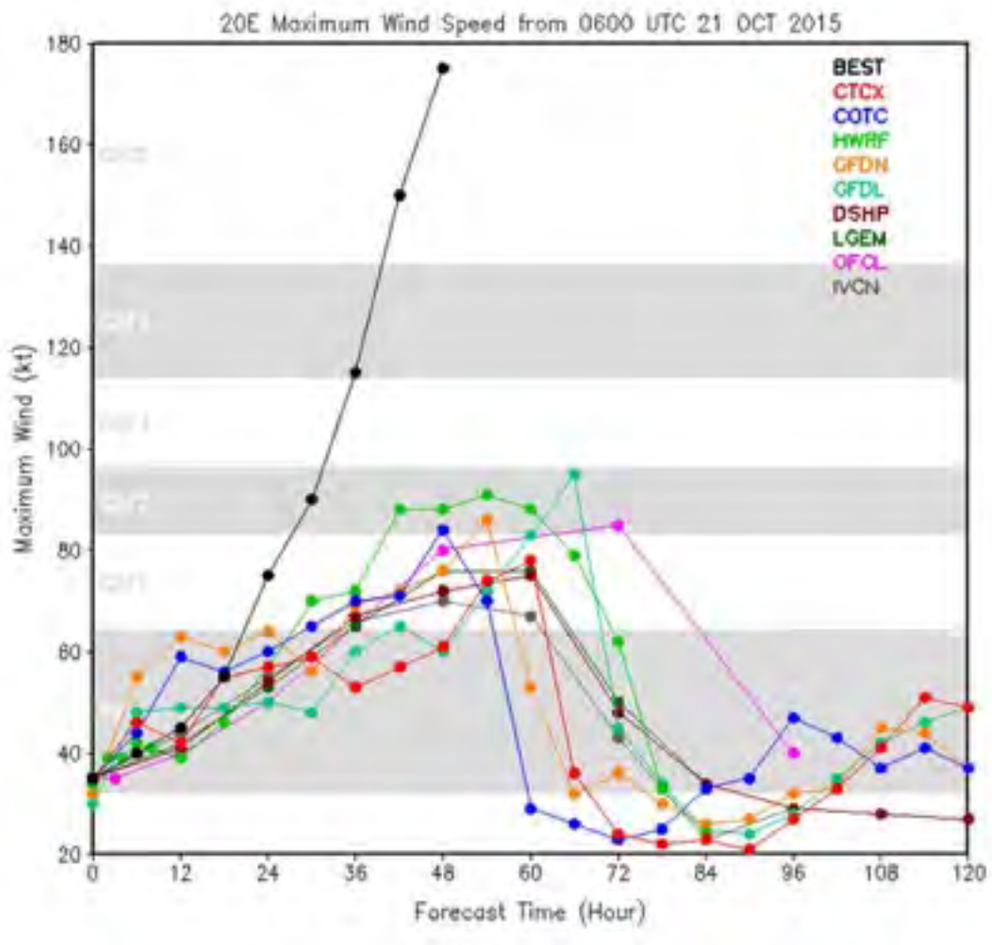

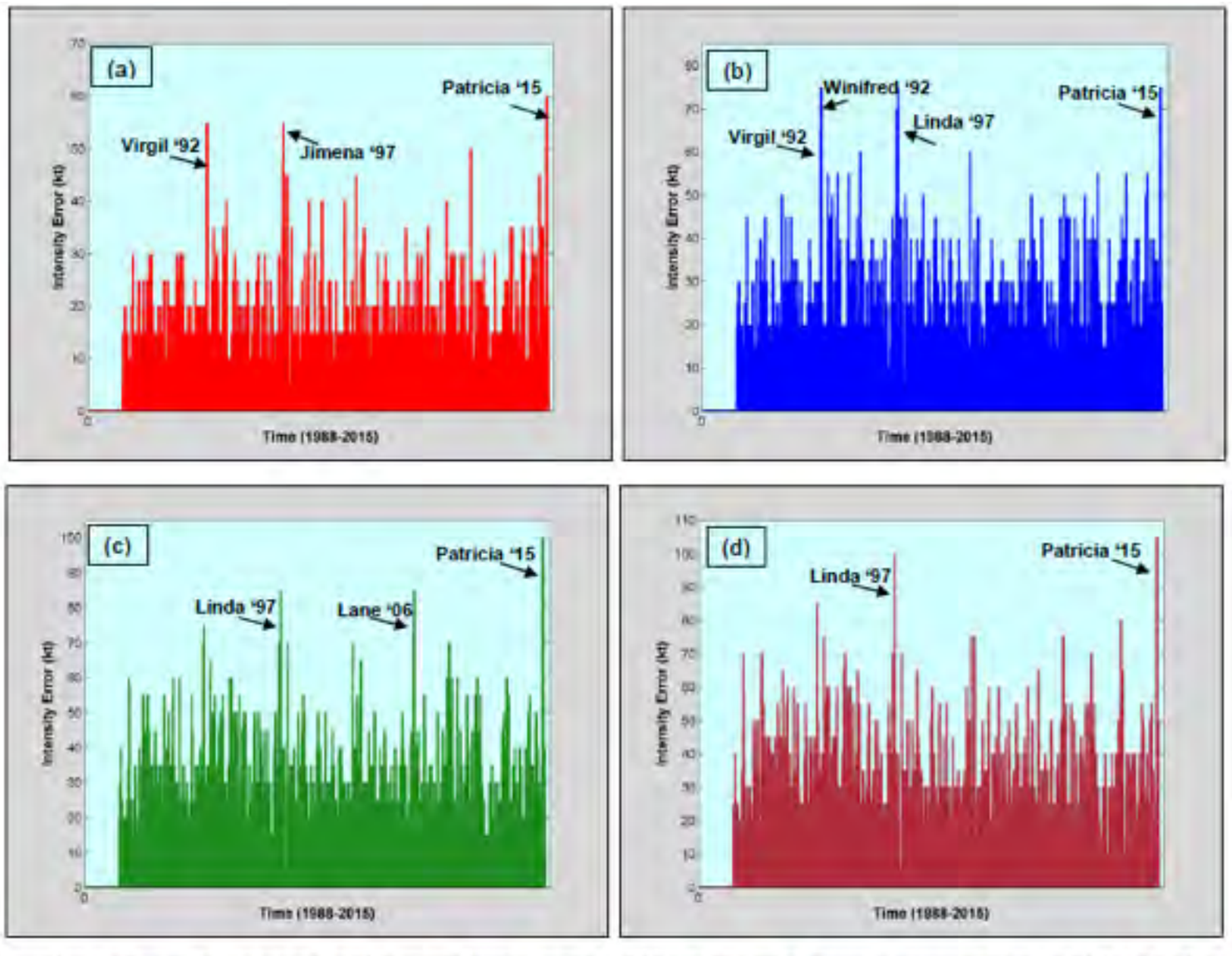

Figure 12. Distribution of all individual NHC eastern North Pacific (1988-2015) official intensity errors at a) 12 h, b) 24 h, c) 36 h, 48 h.

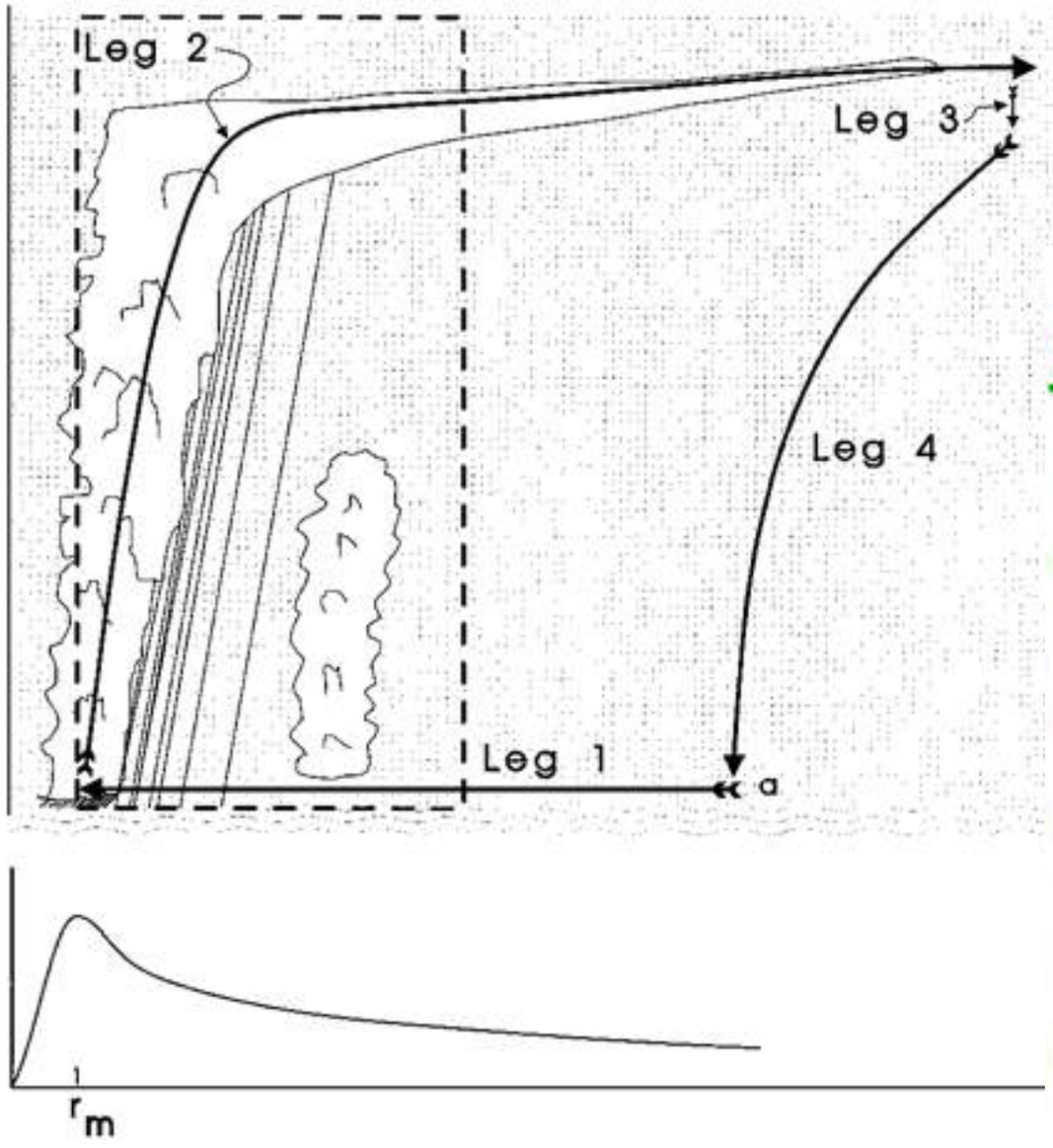

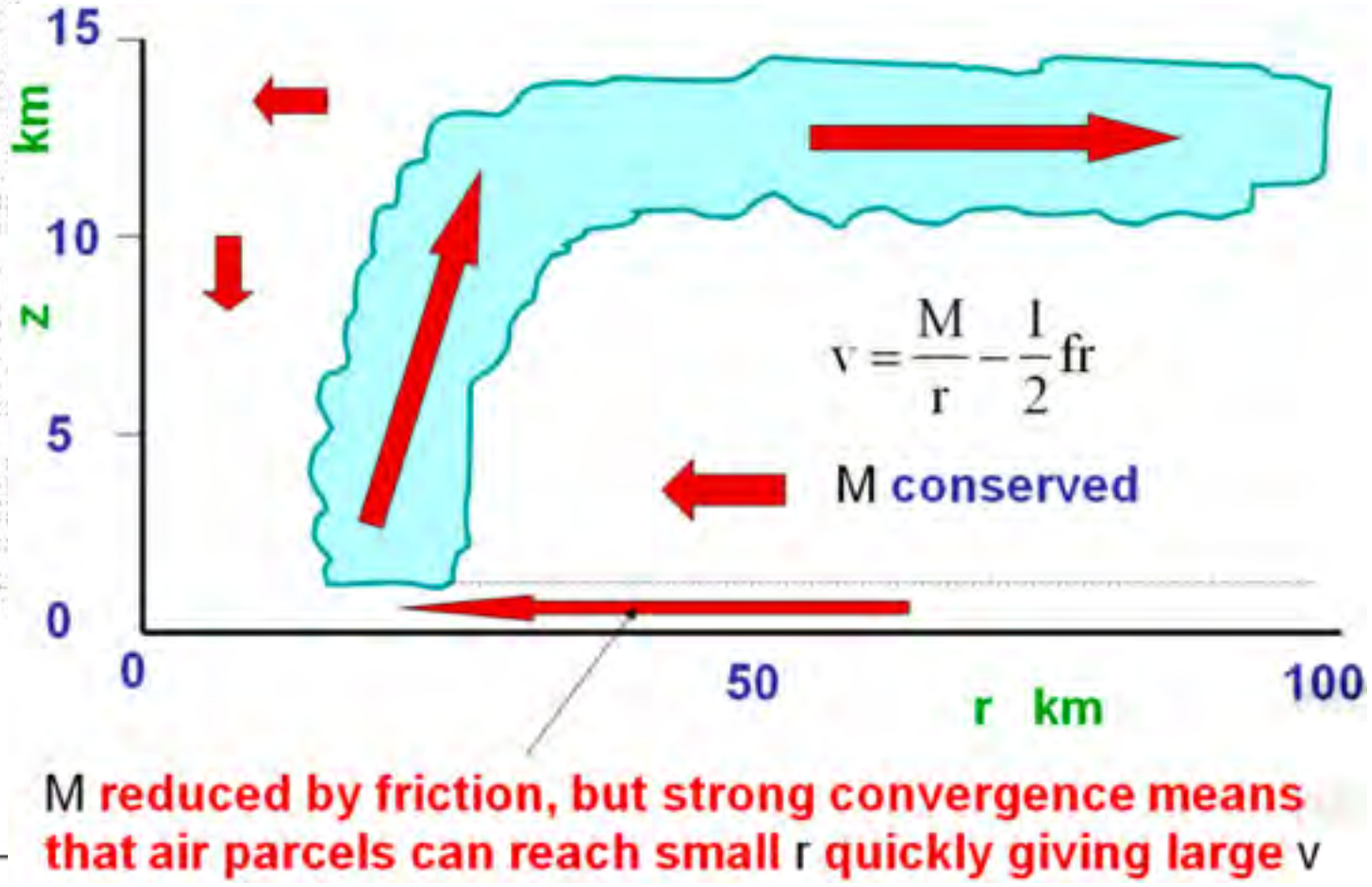

Emanuel (1997)

Smith and Montgomery (2015)

- Axisymmetric
- Gradient Wind Balance
- Hydrostatic Balance

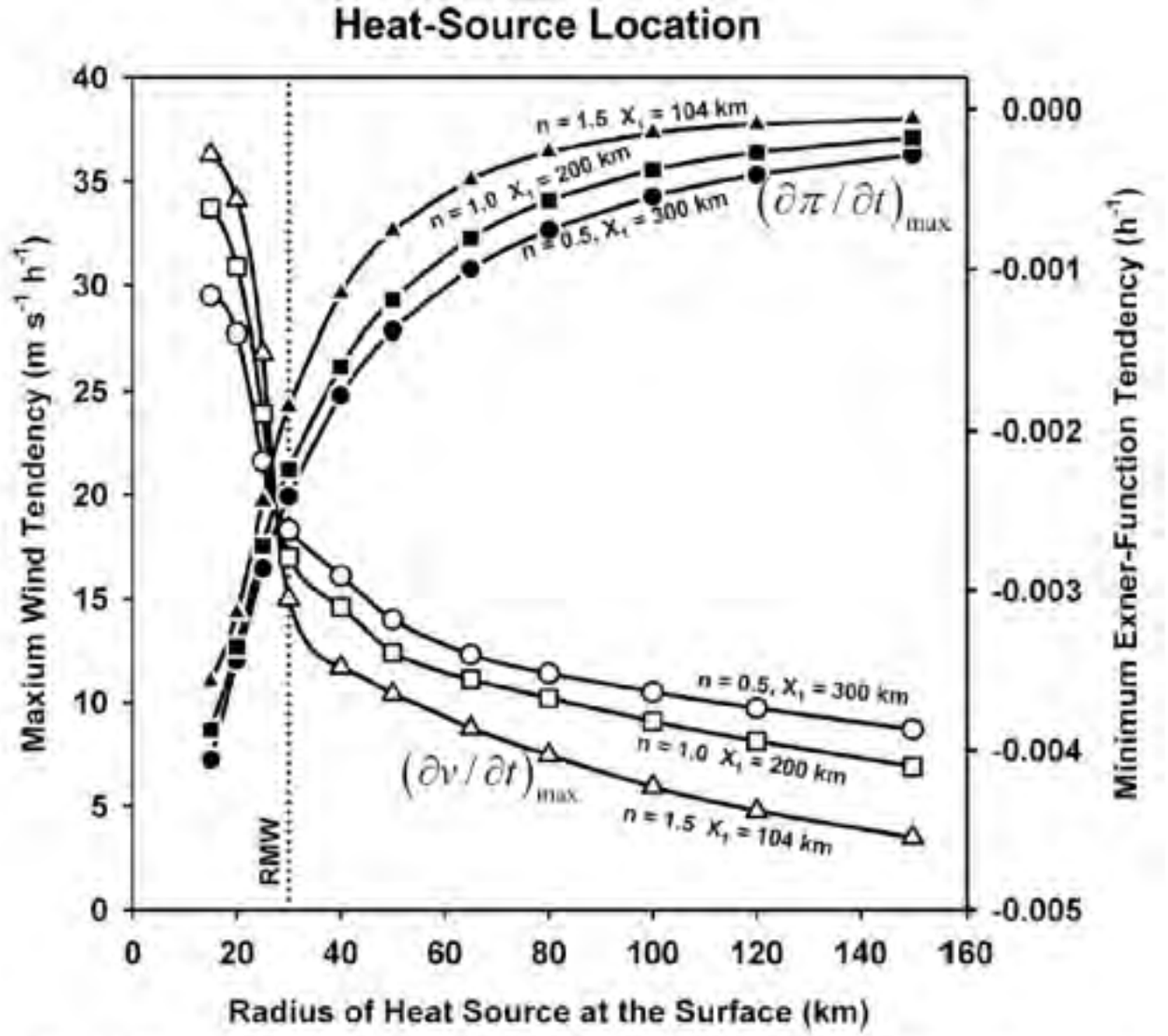

FIG. 12. Maximum rates to change of Exner function and swirling as a function of heat source radius for sharp ($n = 1.5$ and $X_1 = 104$ km), medium ($n = 1.0$ and $X_1 = 200$ km), and broad ($n = 0.5$ and $X_1 = 300$ km) vortex wind profiles.

Pendergrass and Willoughby (2009)

Vigh and Schubert (2009)

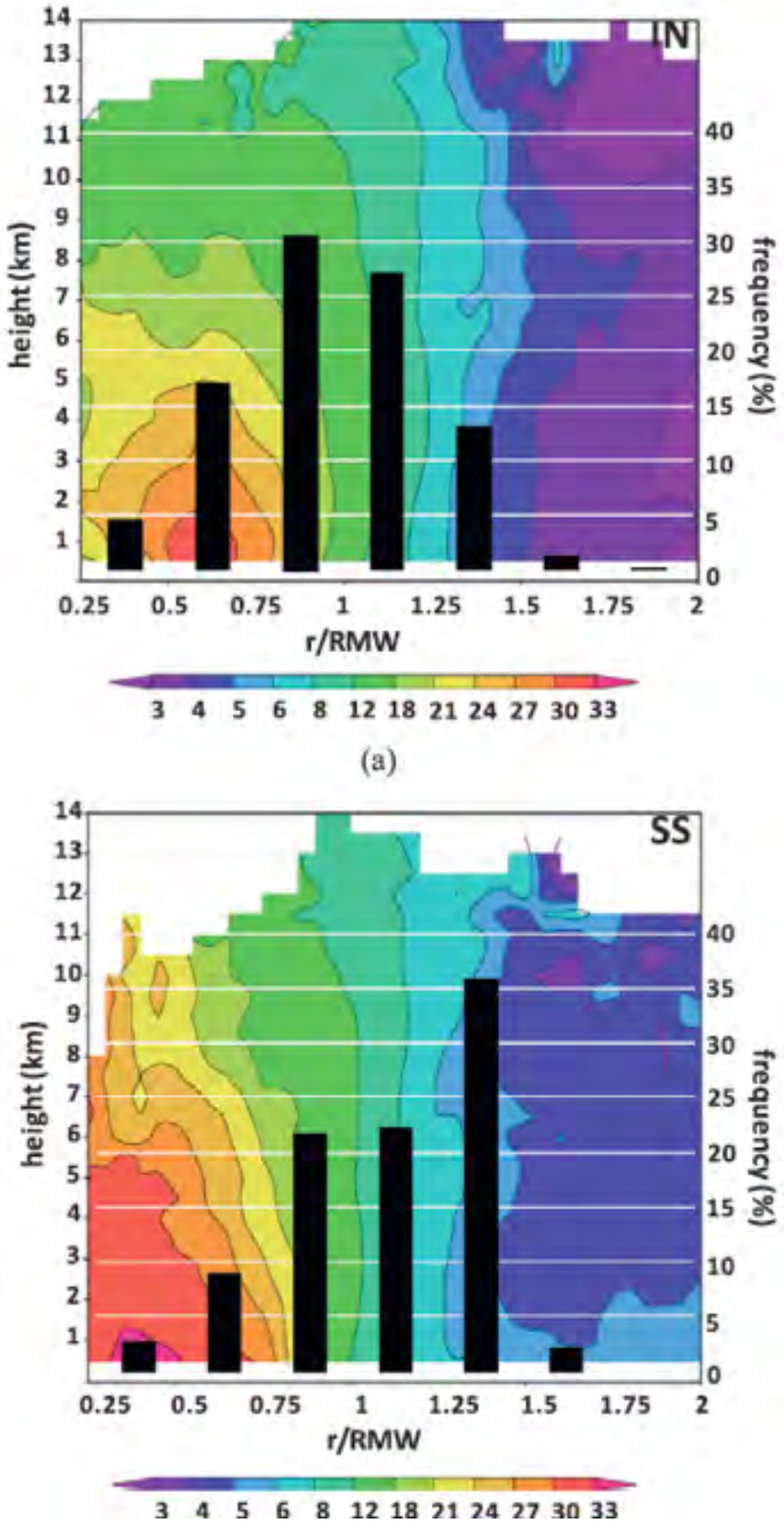

Rogers et al. (2013)

Hurricane Rita (2005)
Rapid Intensification

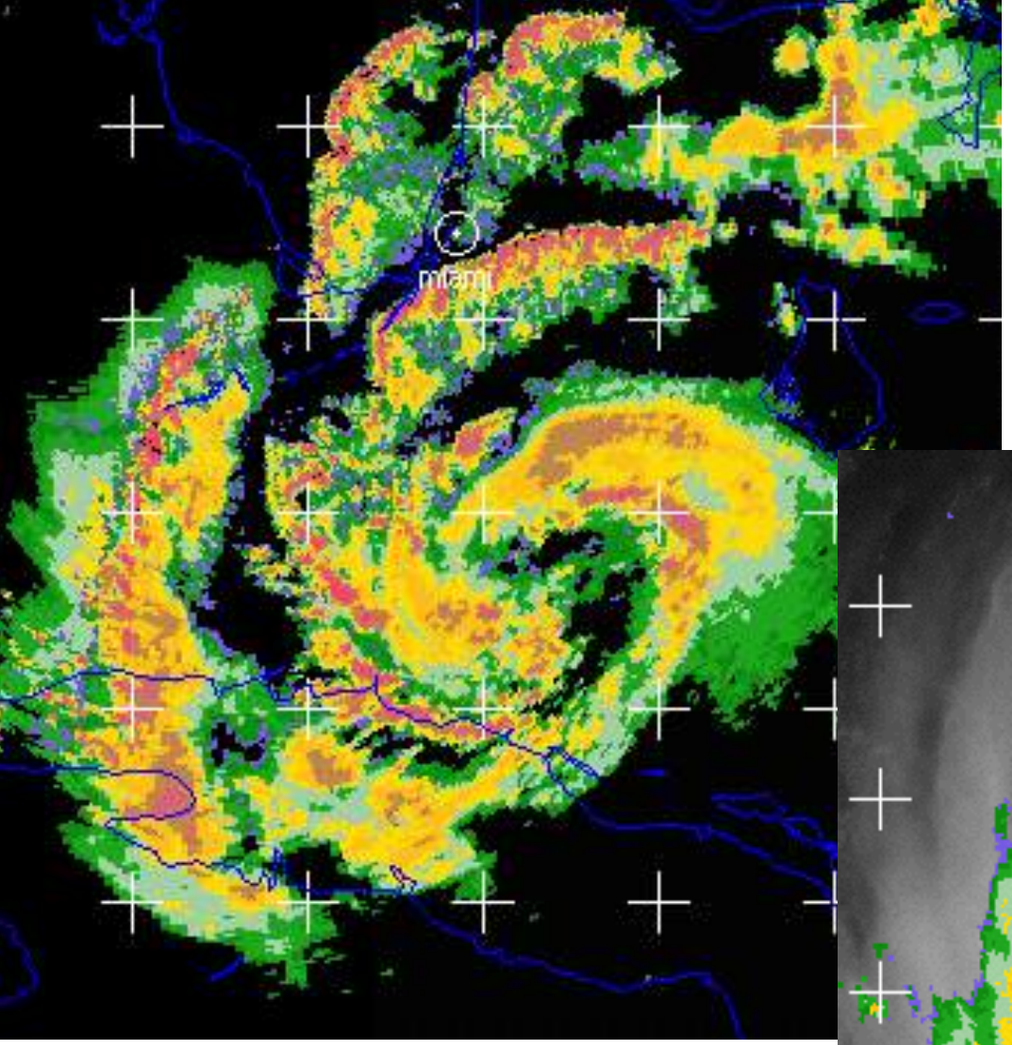

20/09 UTC

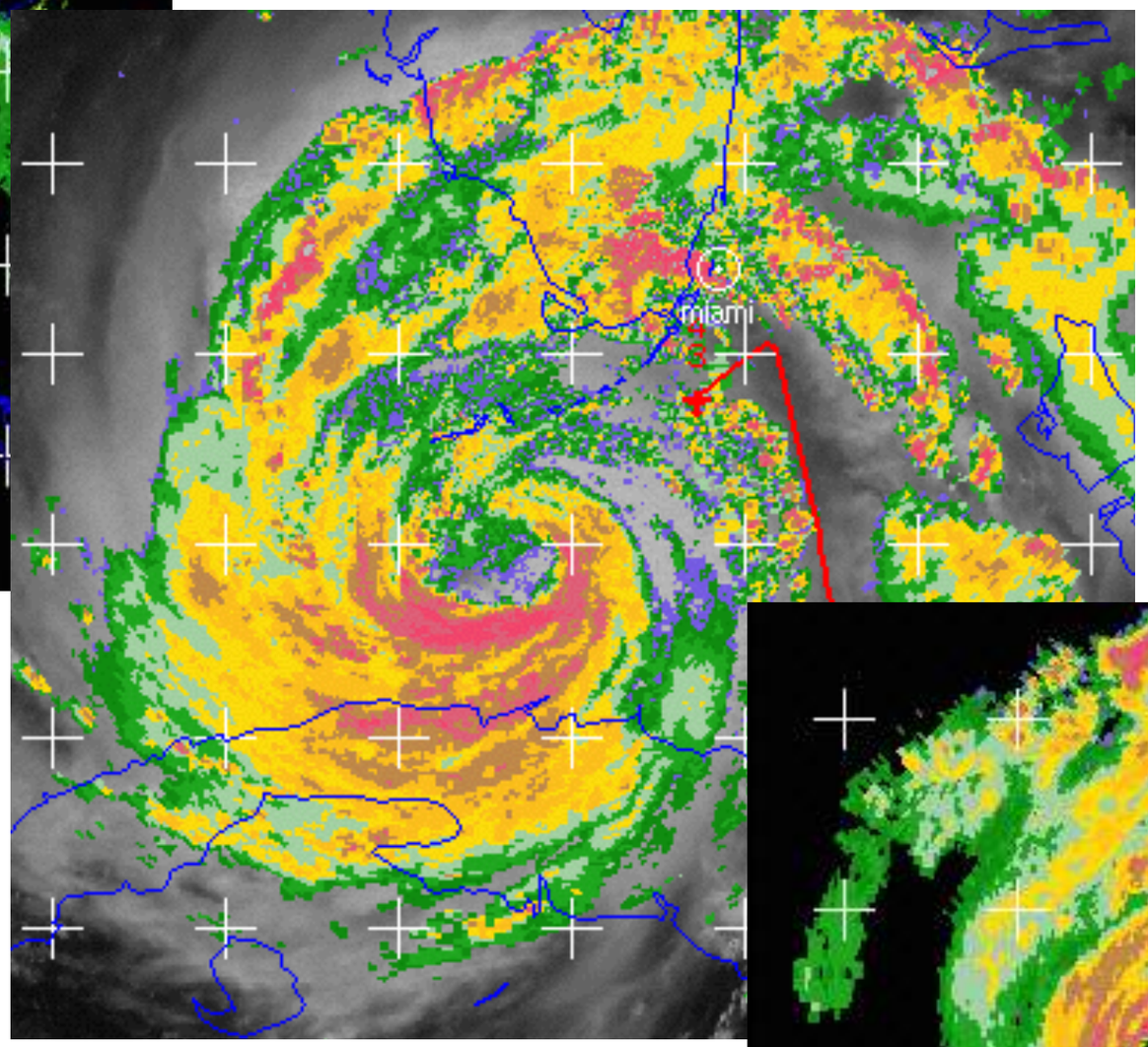

20/17 UTC

21/02 UTC

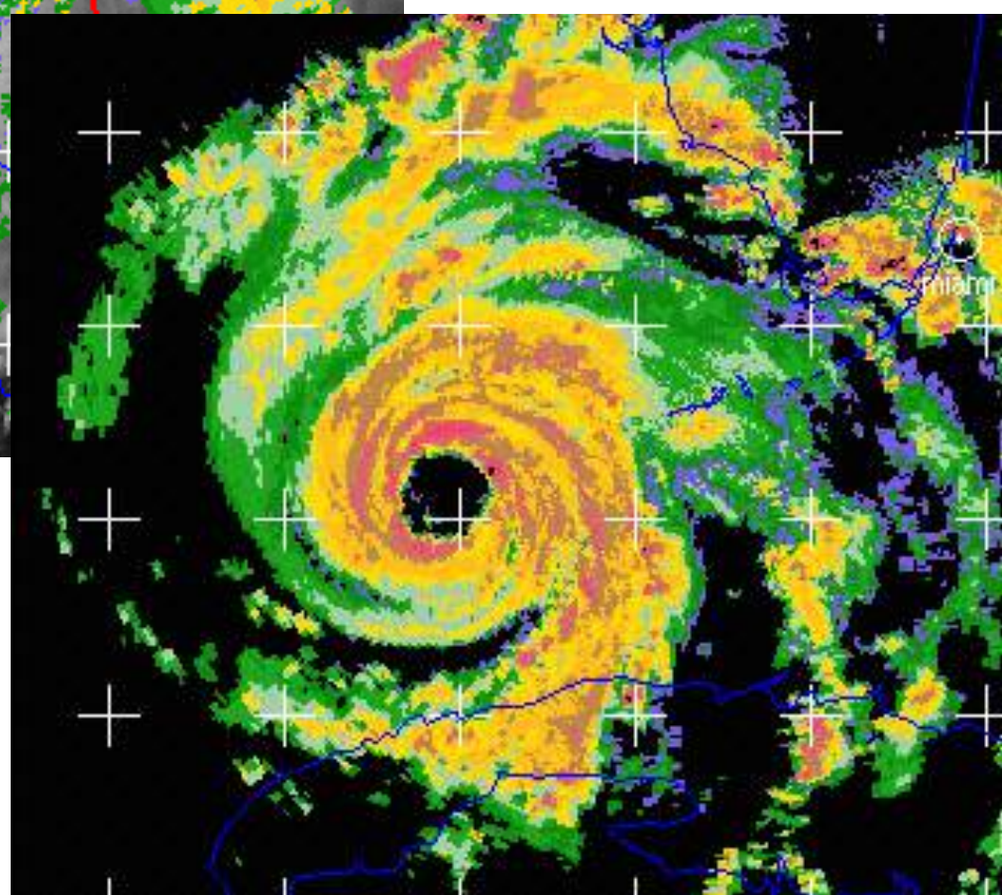

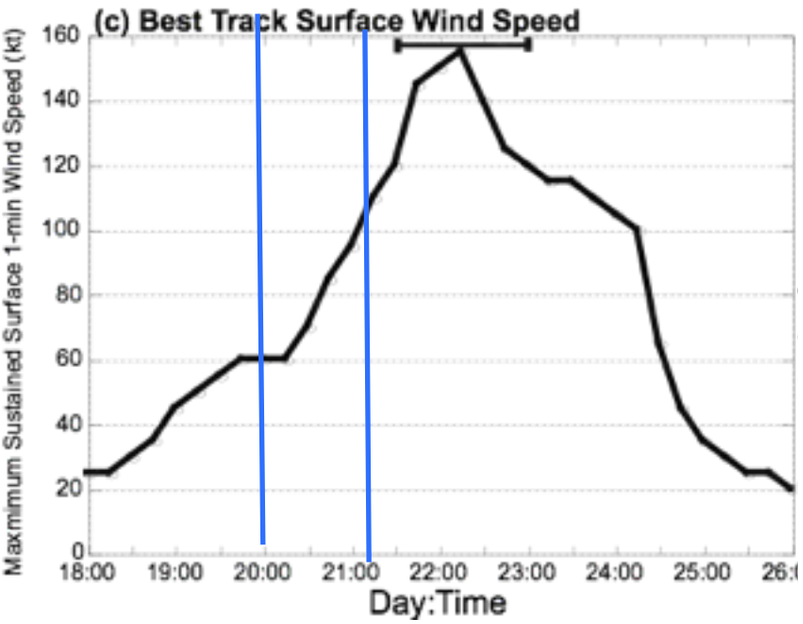

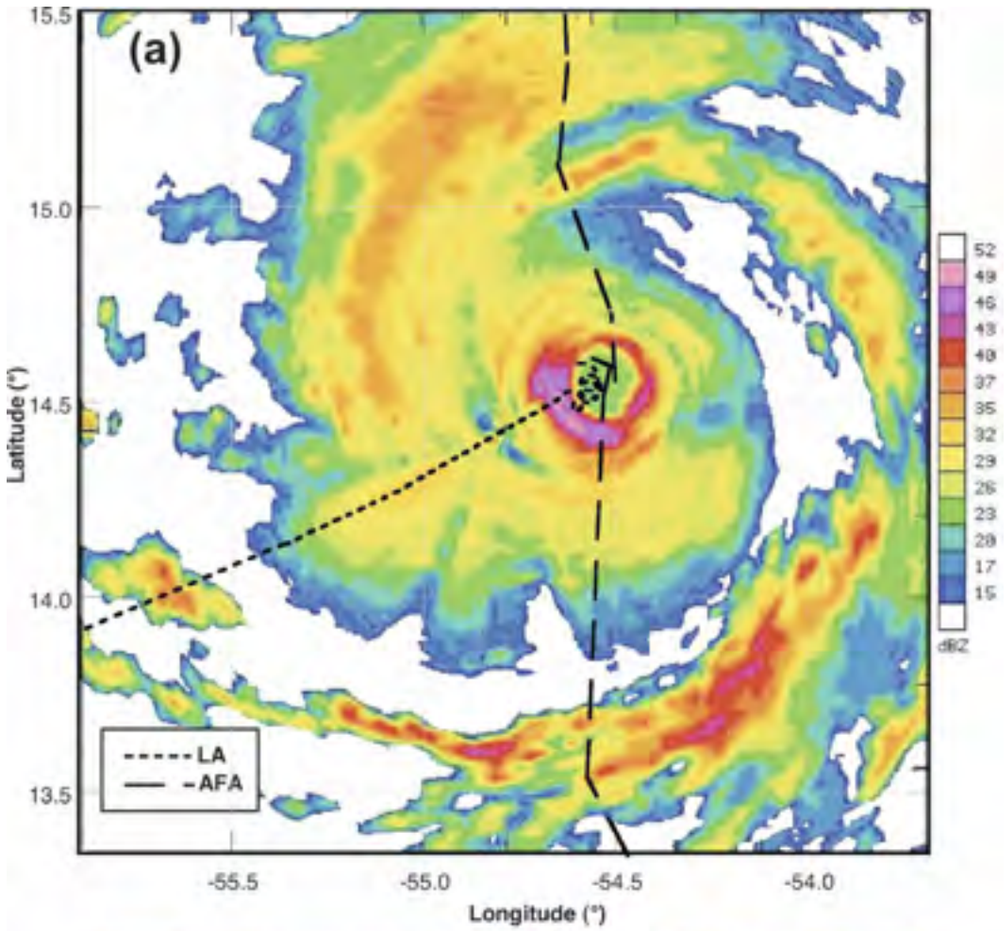

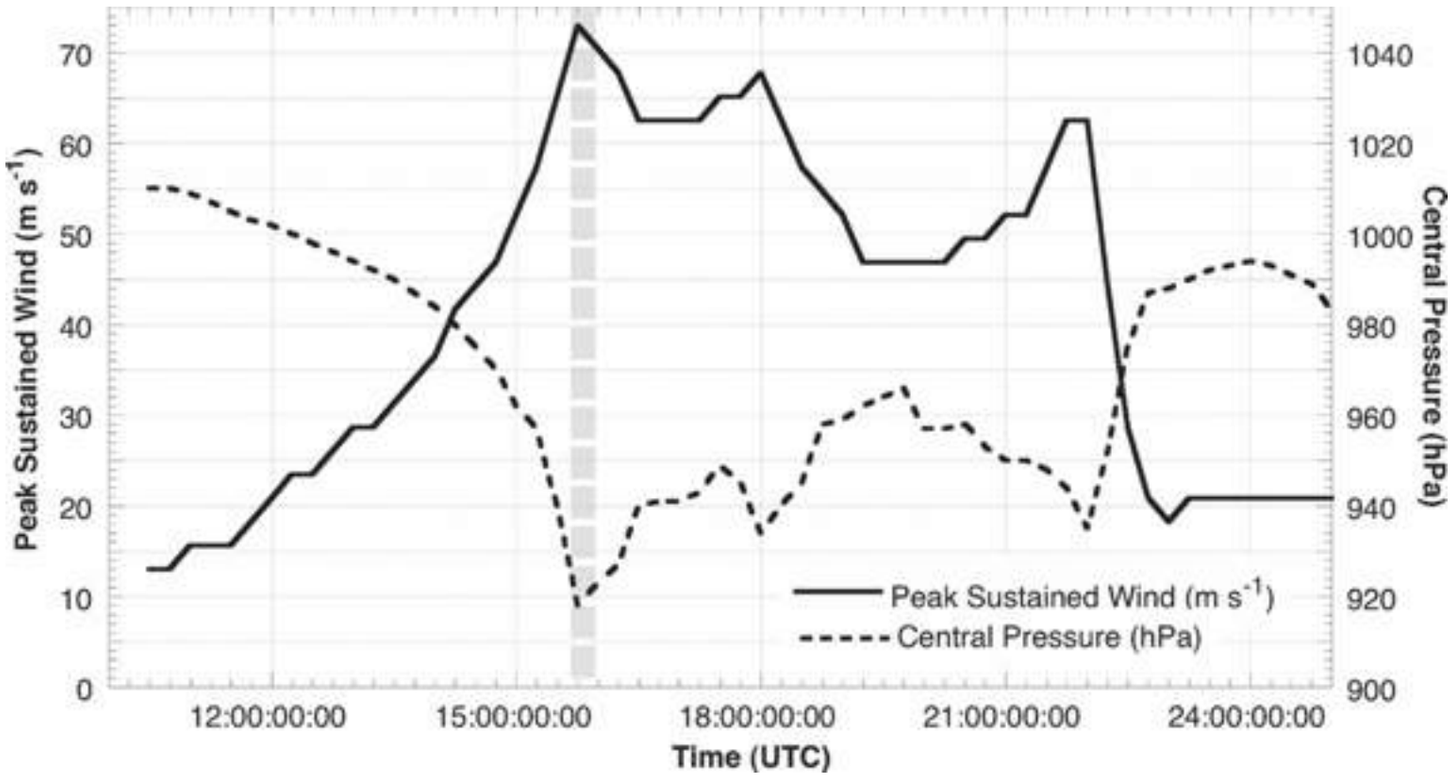

FIG. 1. Time series of the estimated P_{SC} and the V_{max} in Hugo for 10–24 Sep 1989. The vertical dashed line denotes the time of the LA flight on 15 Sep.

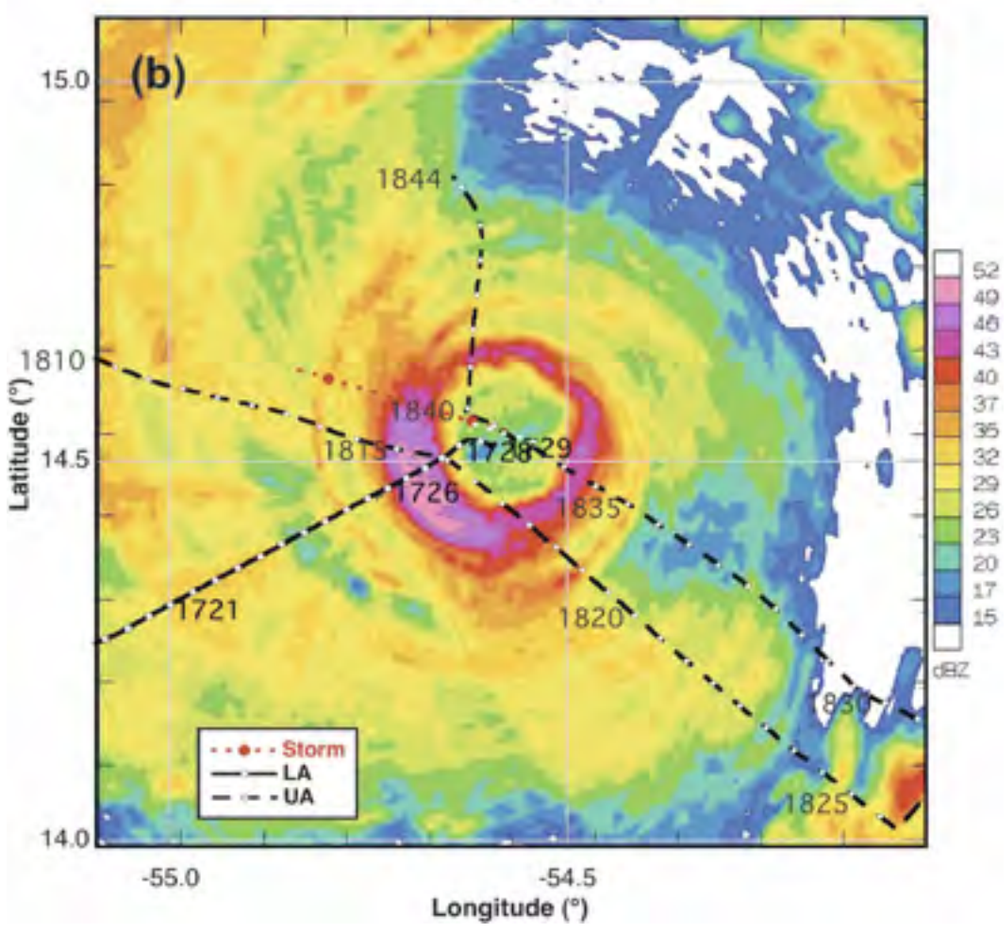

FIG. 2. (a) Ground tracks for LA from 1710 to 1738 UTC and AFA from 1723 to 1805 UTC,
and LA lower fuselage radar image for 1724:50 UTC. The radar image domain is 240 km x 240 km. The short- and long-dashed line depict the LA and AFA flight tracks, respectively. (b) The storm-relative aircraft track for LA from 1719 to 1730 UTC and UA from 1810 to 1844 UTC superimposed on radar data for 1726 UTC. The composite domain is 120 km x 120 km. The solid line depicts the LA track, and the dashed line depicts the UA track, with circles at 30-s intervals. The red dotted line is the storm track from 1715 to 1845 UTC. In both images the reflectivity is denoted by colors (dBZ).

From Marks et al. (2008)

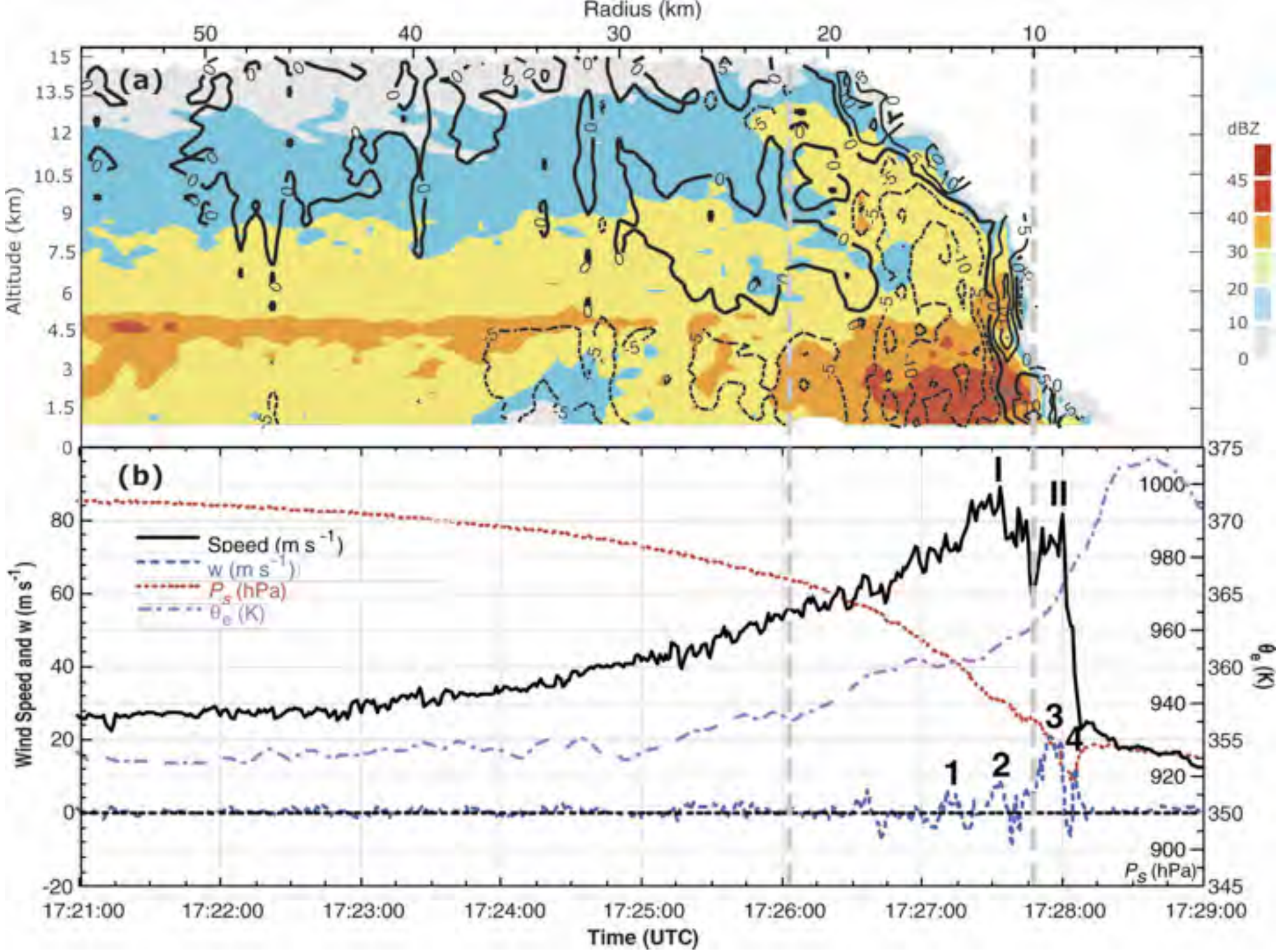

FIG. 3. (a) Time–height cross section of vertical incidence tail radar reflectivity (dBZ) from LA for 1721–1728 UTC. The LA flight track was at 450 m. Solid and dashed lines denote vertical velocity, and radar reflectivity is denoted by colors using the color scale on the right. (b) Time series plots of w, horizontal wind speed, Ps, and theta_e for the period 1721–1730 UTC. Updrafts labeled 1, 2, 3, and 4 and wind speed peaks I and II are described in the text. The thick dashed lines in (b) approximately delineate the outer and inner radii of strong eyewall reflectivity maxima in the lower troposphere (1 - 5-km altitude).

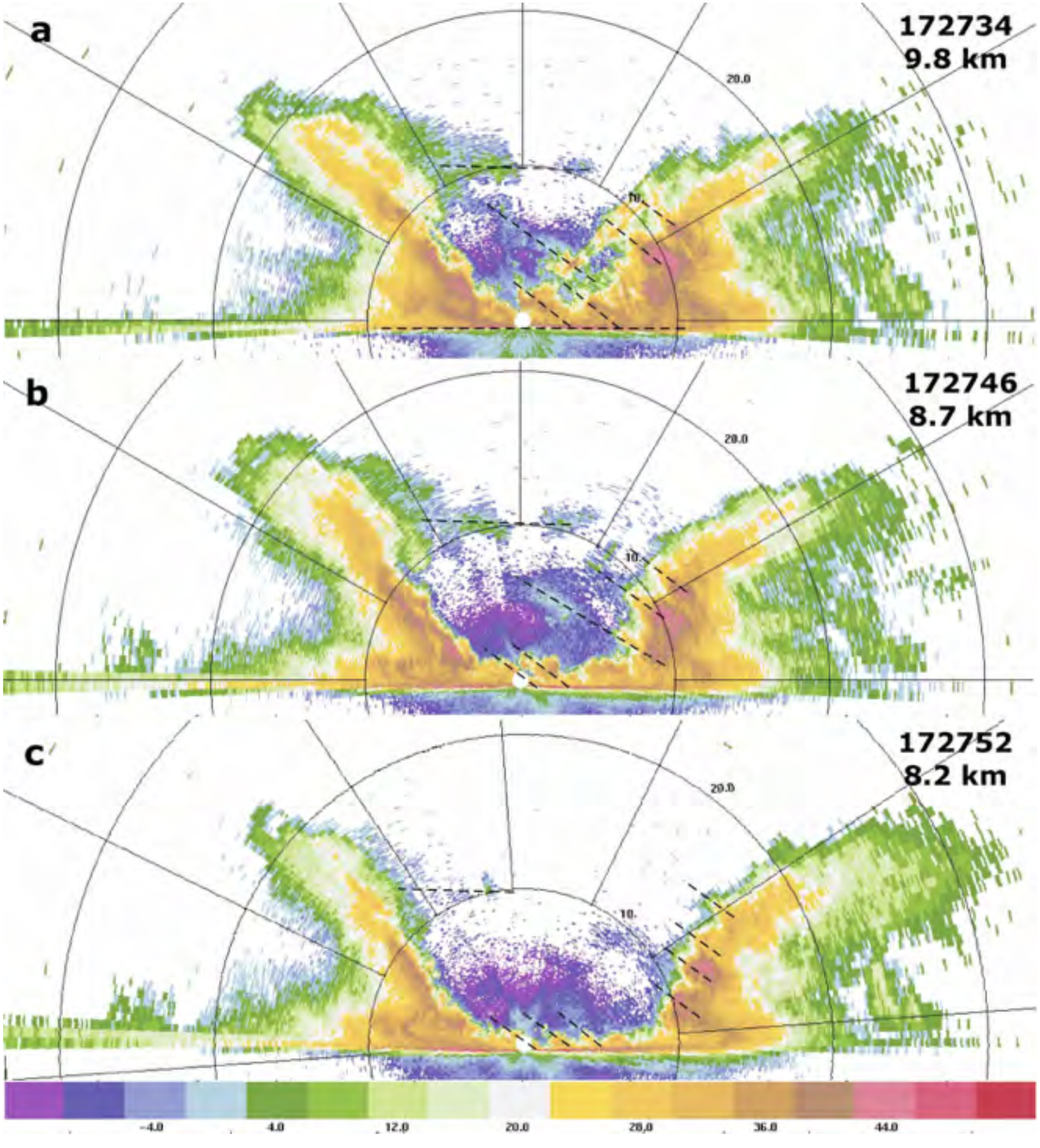

FIG. 4. Vertical cross sections of reflectivity (dBZ) from the tail radar at (a) 1727:34, (b) 1727:46 (8.7 km), and (c) 1727:52 (8.2 km) oriented perpendicular to the plane in Fig. 3a and the aircraft ground track in Fig. 2a. The aircraft radial distance (km) from the wind circulation center (computed as in section 2b) for each image is listed below the time, e.g., (a) 9.8-, (b) 8.7-, and (c) 8.2-km radius. The aircraft is located at the origin (white square) with range rings from the radar at 10-km intervals. The color scale at the bottom of the figure denotes reflectivity thresholds. Dashed lines denote reflectivity maxima discussed in the text.

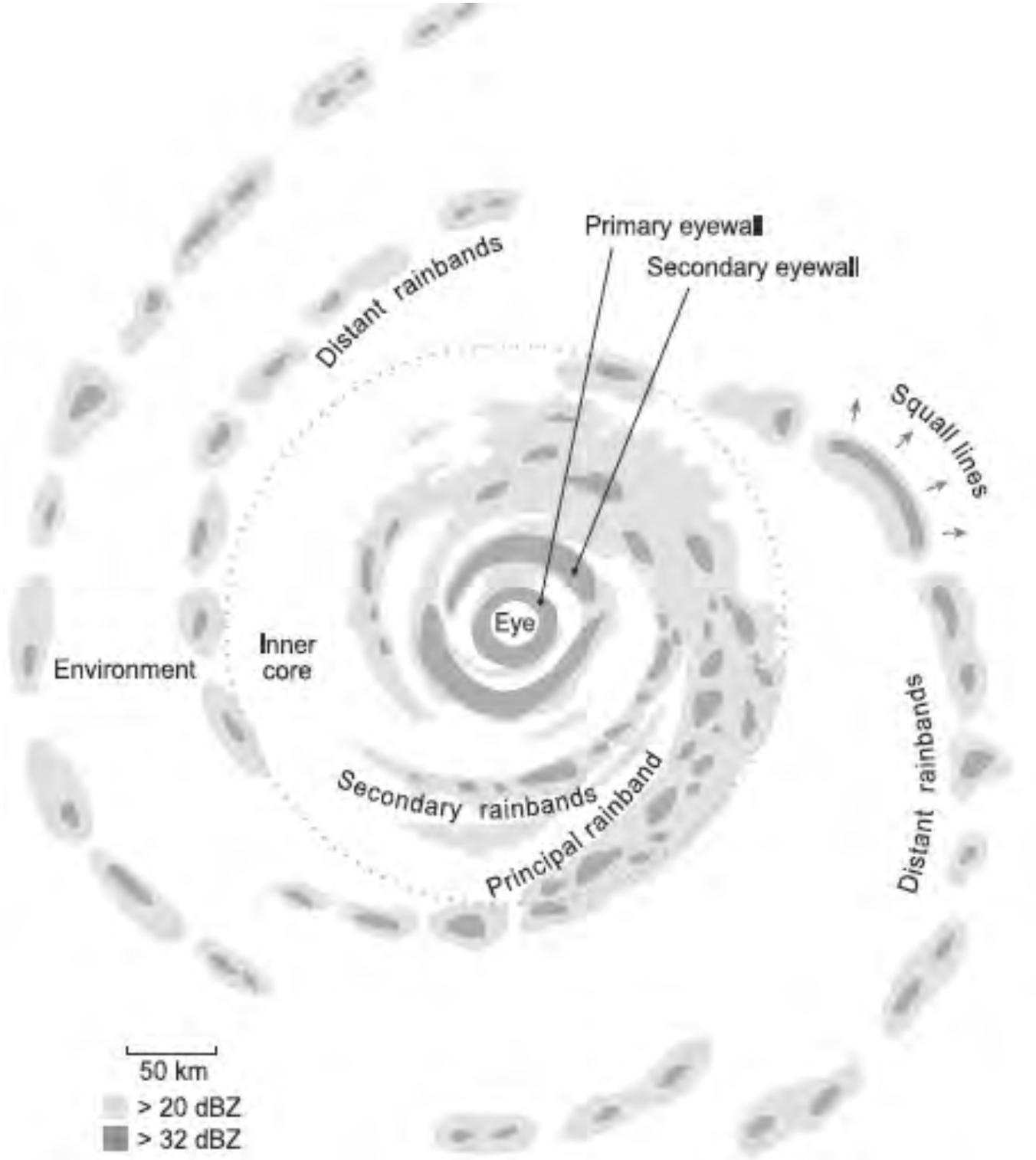

FIG. 30. Schematic illustration of radar reflectivity in a Northern Hemisphere tropical cyclone with a double eyewall. (Adapted liberally from Willoughby 1988.)

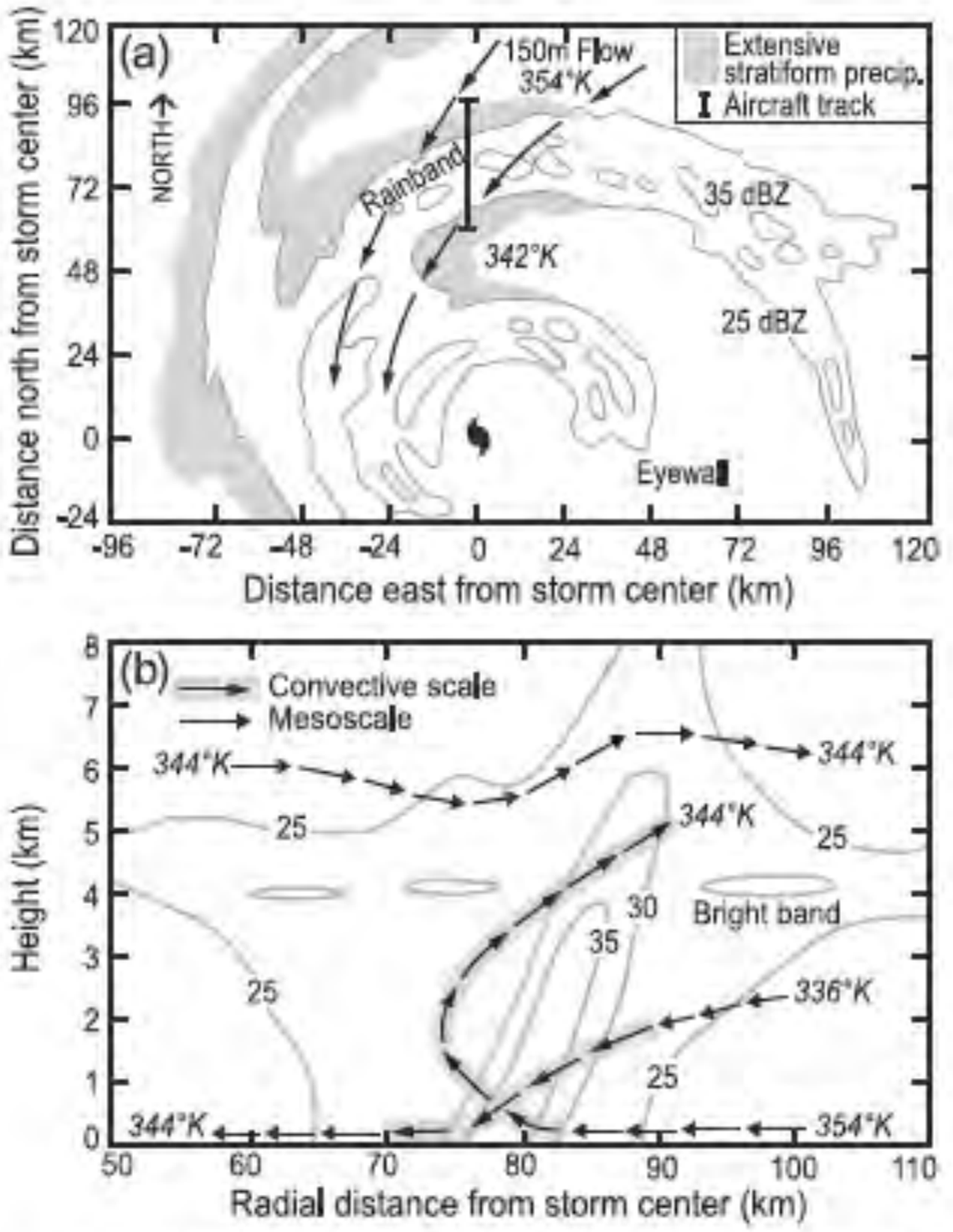

FIG. 34. Rainband observed by aircraft penetration of Hurricane Floyd (1981). (a) A horizontal projection of the data, showing the track. (b) A vertical cross section taken along the aircraft track, which was across the axis of the rainband. In (a) and (b), contours show radar reflectivity (dBZ), temperatures refer to values of equivalent potential temperature, and arrows indicate airflow (on either the convective scale or mesoscale, as indicated by the style of arrow). (From Barnes et al. 1983.)

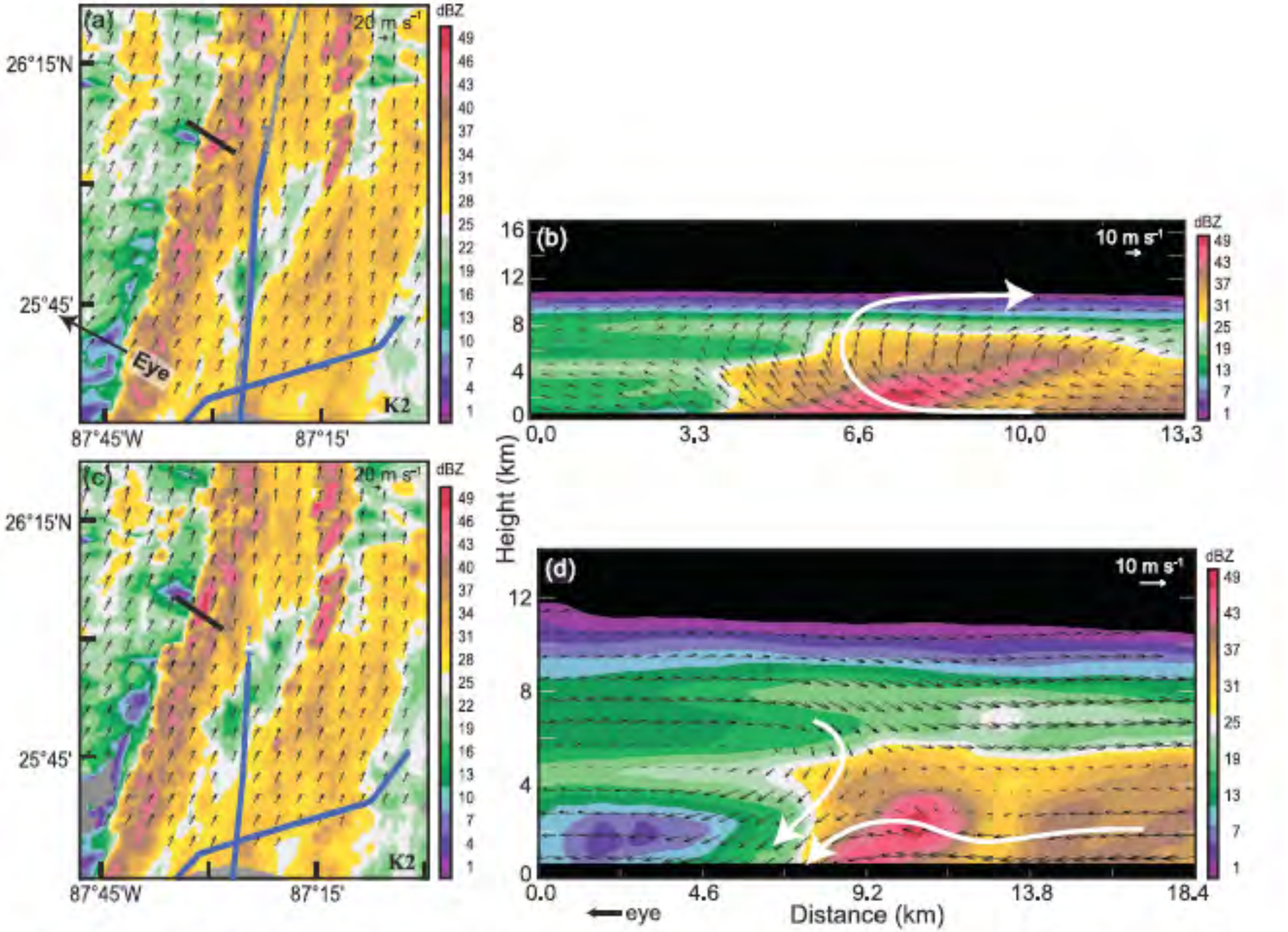

FIG. 35. Composite of Doppler radar data collected in Hurricane Katrina by an aircraft during 2026–2036 UTC 28 Aug 2005 showing the structure of the principal rainband when the storm was at category-5 intensity. (a) Plan view showing the reflectivity pattern (color shading) and Doppler-derived airflow (vectors) at the 3.5-km level observed while the aircraft was flying along the track shown by the blue line. The straight black line passes through a convective-scale updraft associated with one of the intense reflectivity cells. (b) The reflectivity and Doppler-radar-derived airflow in the plane of the cross section along the black line in (a). (c) Plan view showing the reflectivity pattern and Doppler-derived airflow at the 2.0-km level observed while the aircraft was flying along the track shown by the blue line. (d) The reflectivity and Doppler-radar-derived airflow in the plane of the cross section along the black line in (c). (Adapted from Hence and Houze 2008.)

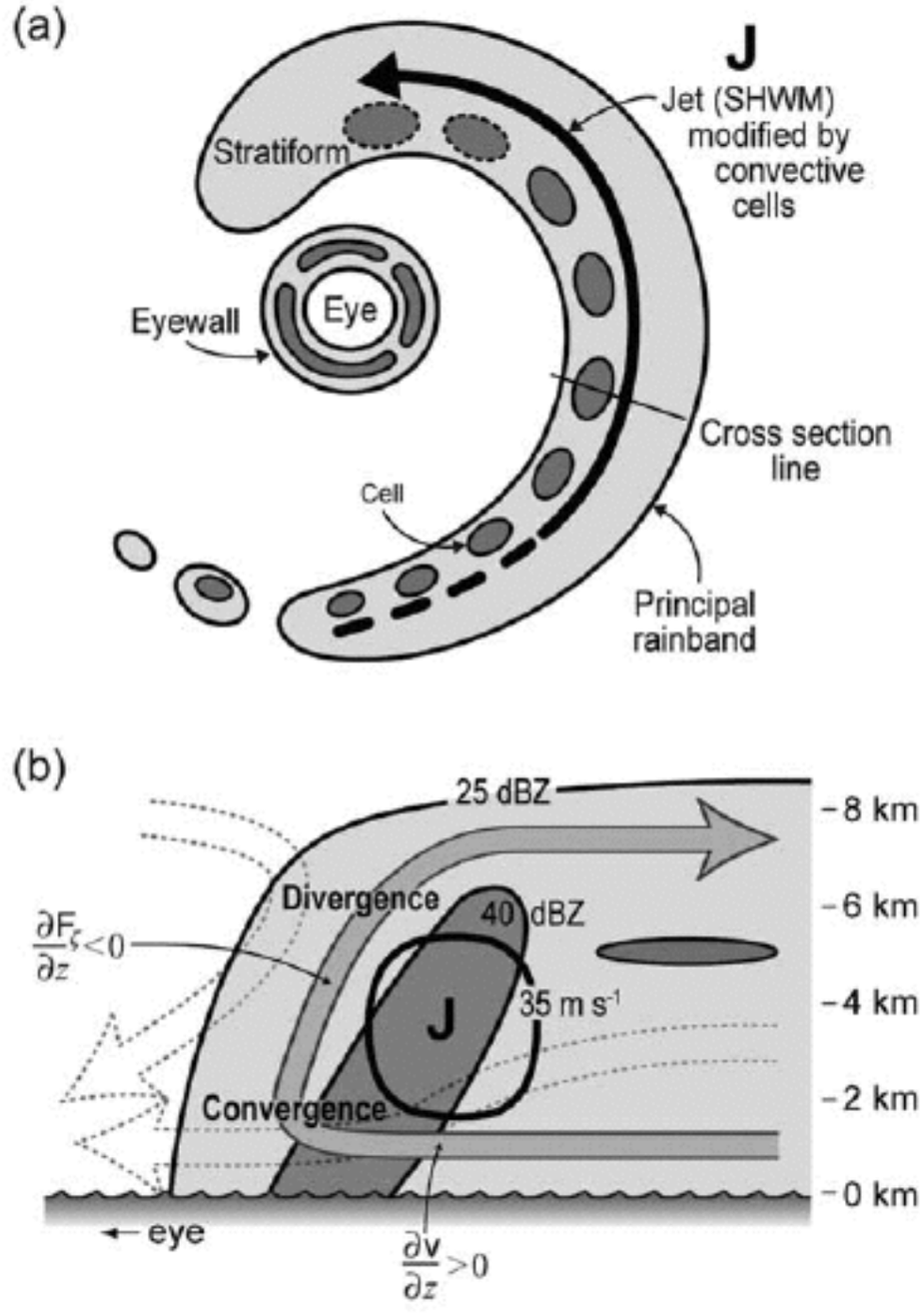
(a)
J
Jet (SHWM)
modified by
convective
cells
Stratiform
Eye
Eyewall
Cross section
line
Cell
Principal
rainband
(b)
25 dBZ
8 km
Divergence
40 dBZ
6 km
$\frac{\partial F_\zeta}{\partial z}<0$
35 m s^{-1}
J
4 km
Convergence
2 km
0 km
eye
$\frac{\partial v}{\partial z}>0$

Hurricane Rita (2005)
Eyewall Replacement

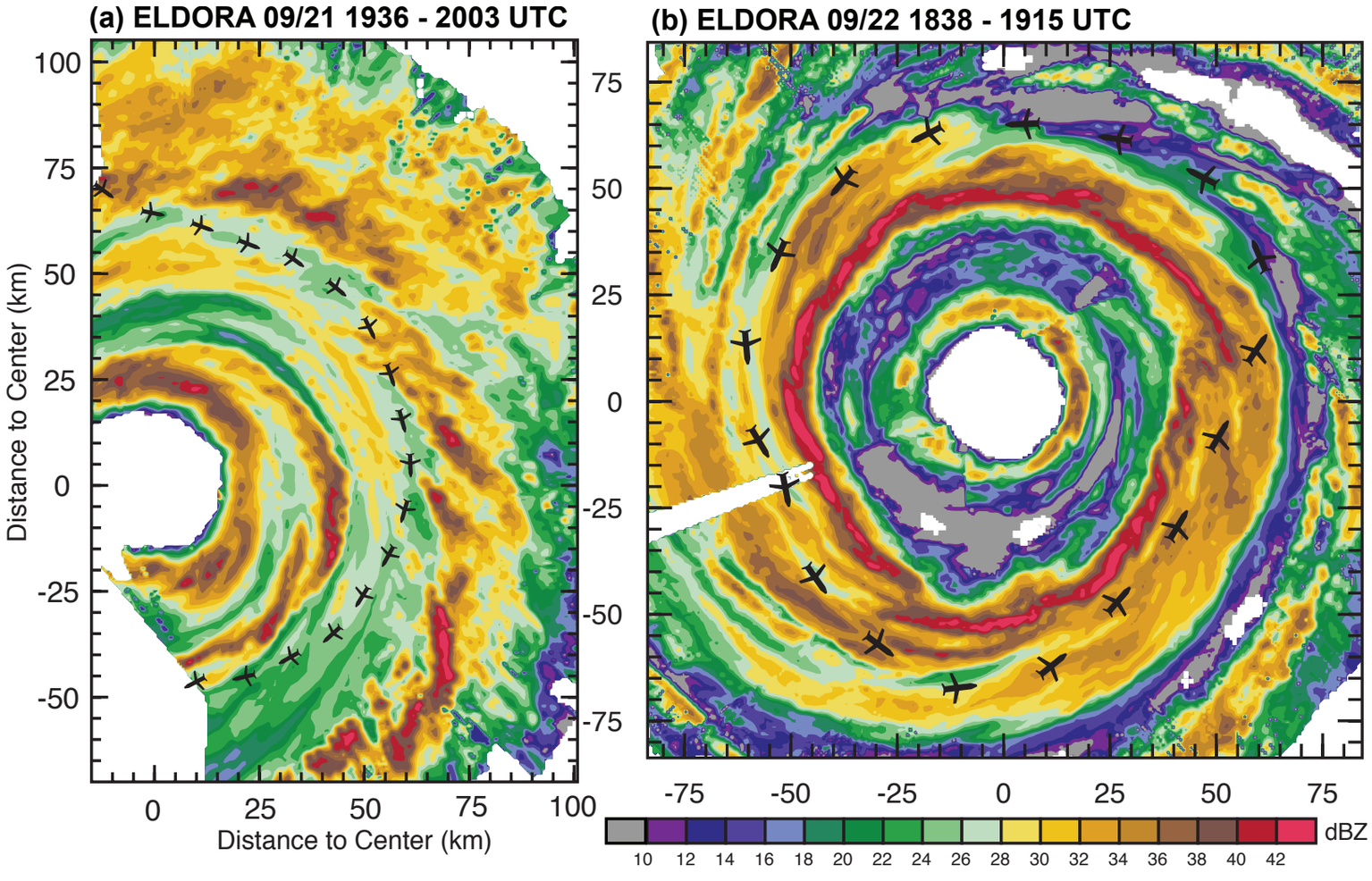

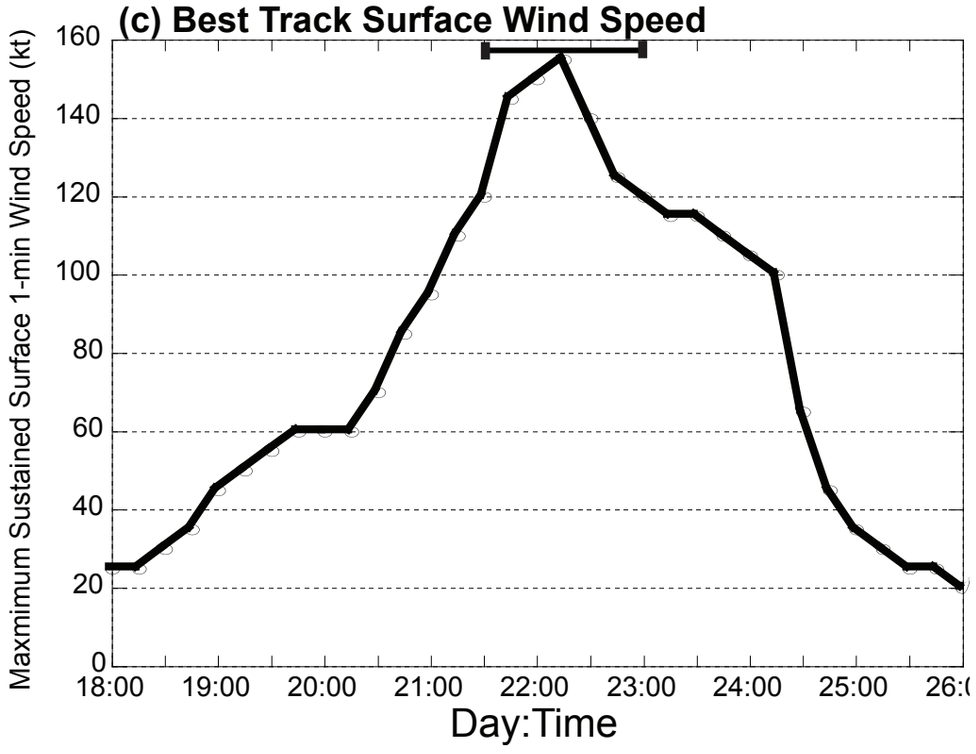

Bell et al. (2012)

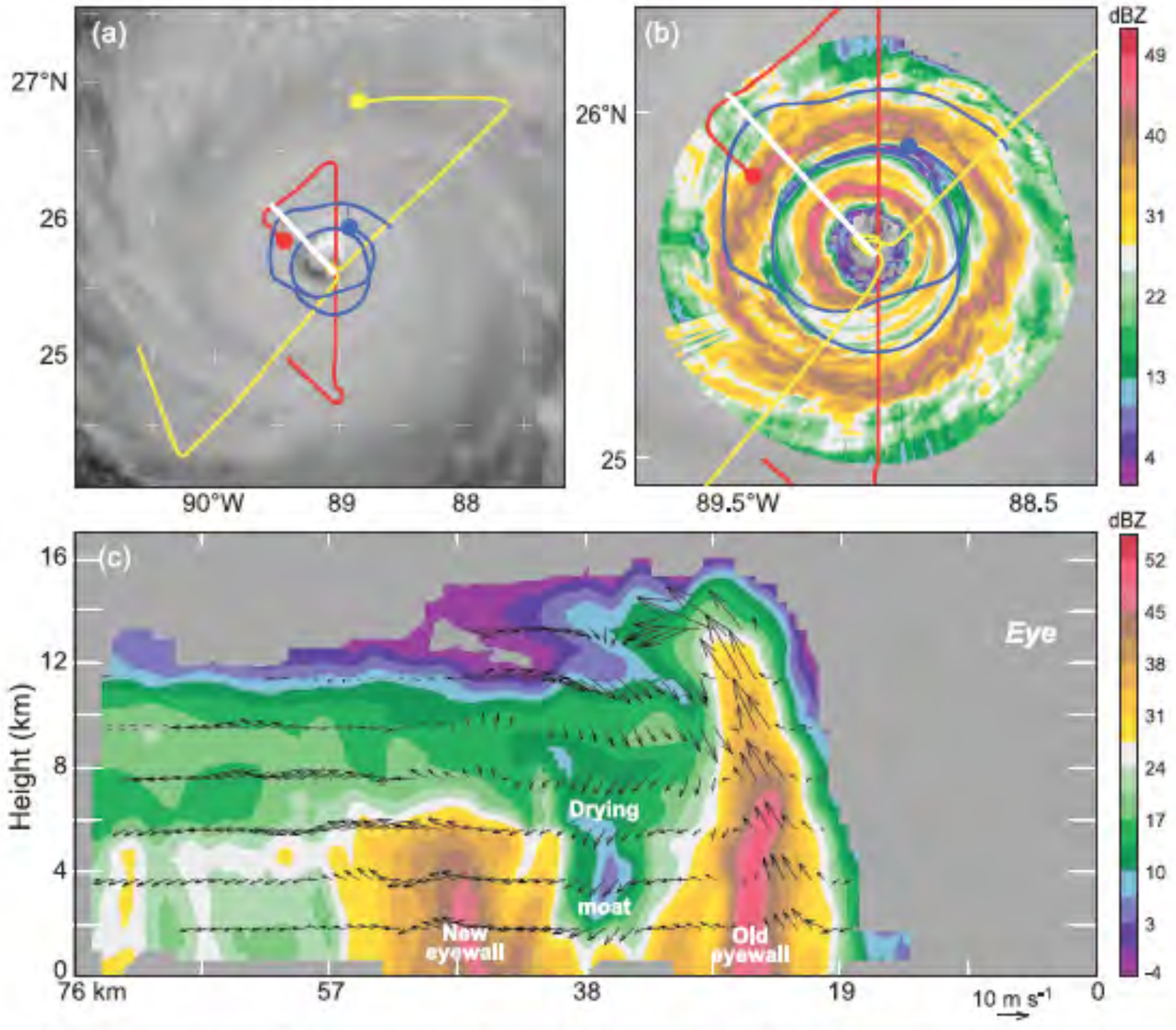

FIG. 41. Aircraft data collected in Hurricane Rita (2005) between 1800 and 1820 UTC 22 Sep. (a),(b) Plan views; (c) vertical cross section across the northwest side of the storm (along the white line in the plan views). Colored lines in (a) denote the flight tracks of three aircraft. The dots show aircraft locations as of 1830 UTC. The yellow track segment is for the 80 min preceding that time; the red and blue track segments are for the preceding 45 min. The yellow track was part of a wide pattern to determine the broadscale structure of the cyclone vortex. The red track was part of an intermediate pattern, with shorter legs across the center of the storm to monitor the two eyewalls. The blue track was a circumnavigation that obtained the key radar and sounding data shown in (b) and (c). The color shades in (b) and (c) correspond to values of radar reflectivity (a measure of precipitation intensity). Vectors in (c) show the component of air motions within the cross sections. [From Houze et al. (2007). Reproduced with permission from the American Association for the Advancement of Science.]

Houze et al 2007

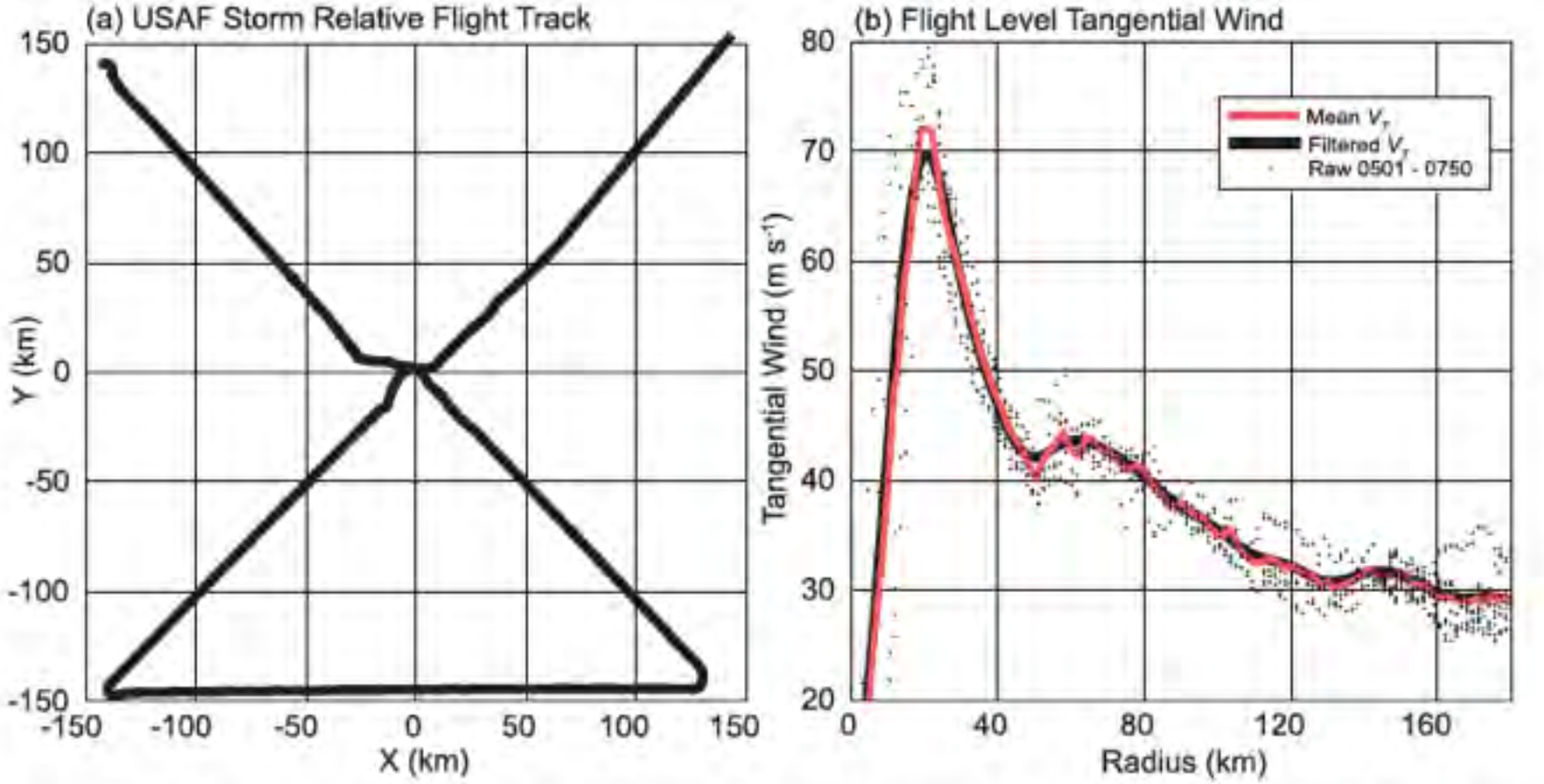

FIG. 4. U.S. Air Force flight track and tangential wind from 0501 to 0750 UTC 22 Sep. (a) The storm-relative "figure four" flight track used to compute the azimuthal mean structure. (b) The tangential wind V_T (m s^{-1}) from the raw in situ data (dots), azimuthal mean (red line), and scale filtered mean (black line).

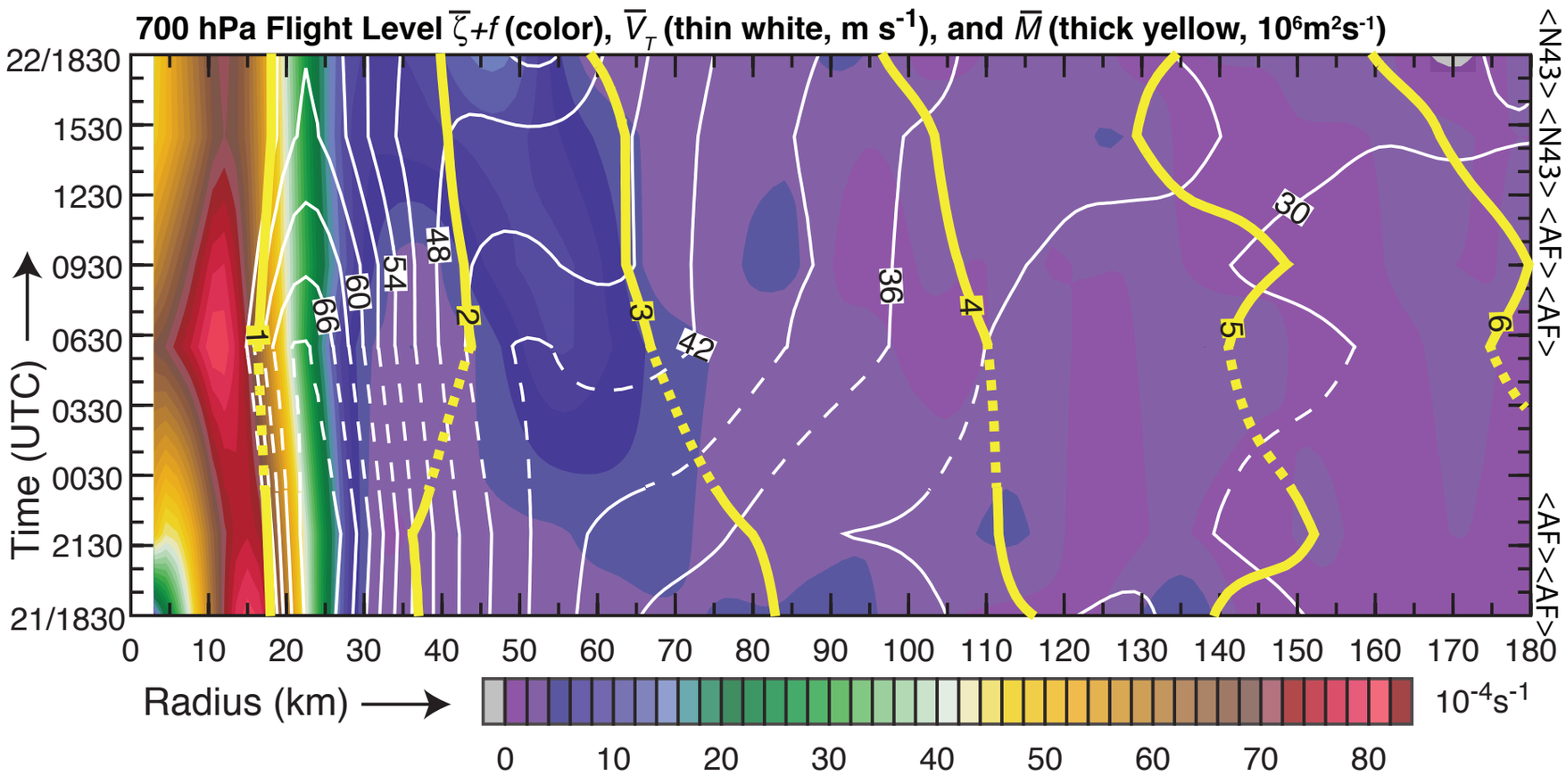

Bell et al. (2012)

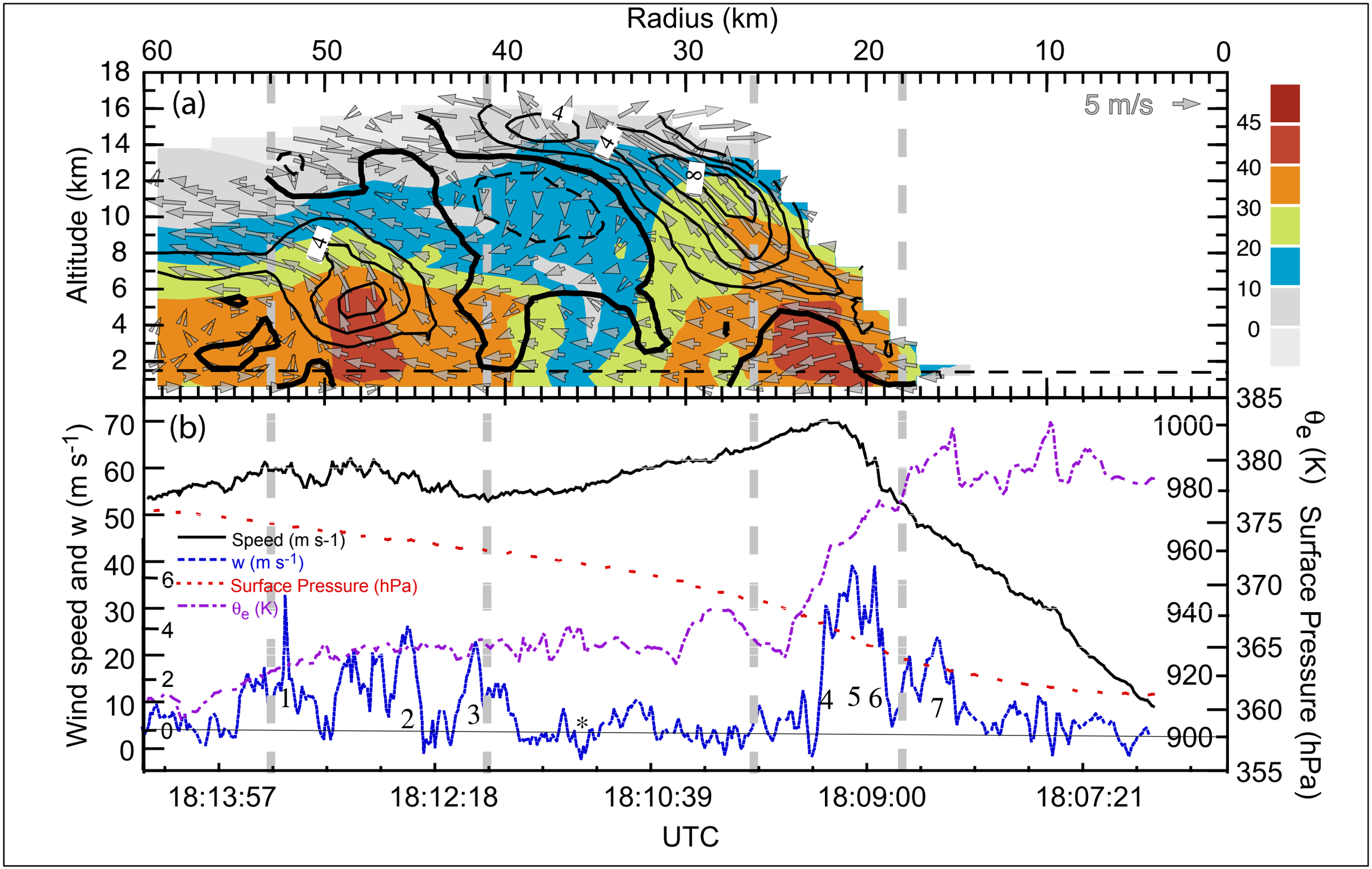

FIG. 8. North–south vertical cross section of quad-Doppler radar analysis from N42 and ELDORA and in situ flight level data at 1.5 km from N42. (a) Radar reflectivity (color), vertical velocity (contour, m s^{-1}), and secondary circulation (vector); (b) wind speed, vertical velocity, surface pressure, and pseudoequivalent potential temperature. Note that axes are reversed to indicate a north–south vertical cross section, not an axisymmetric mean.

From Bell et al. (2012)

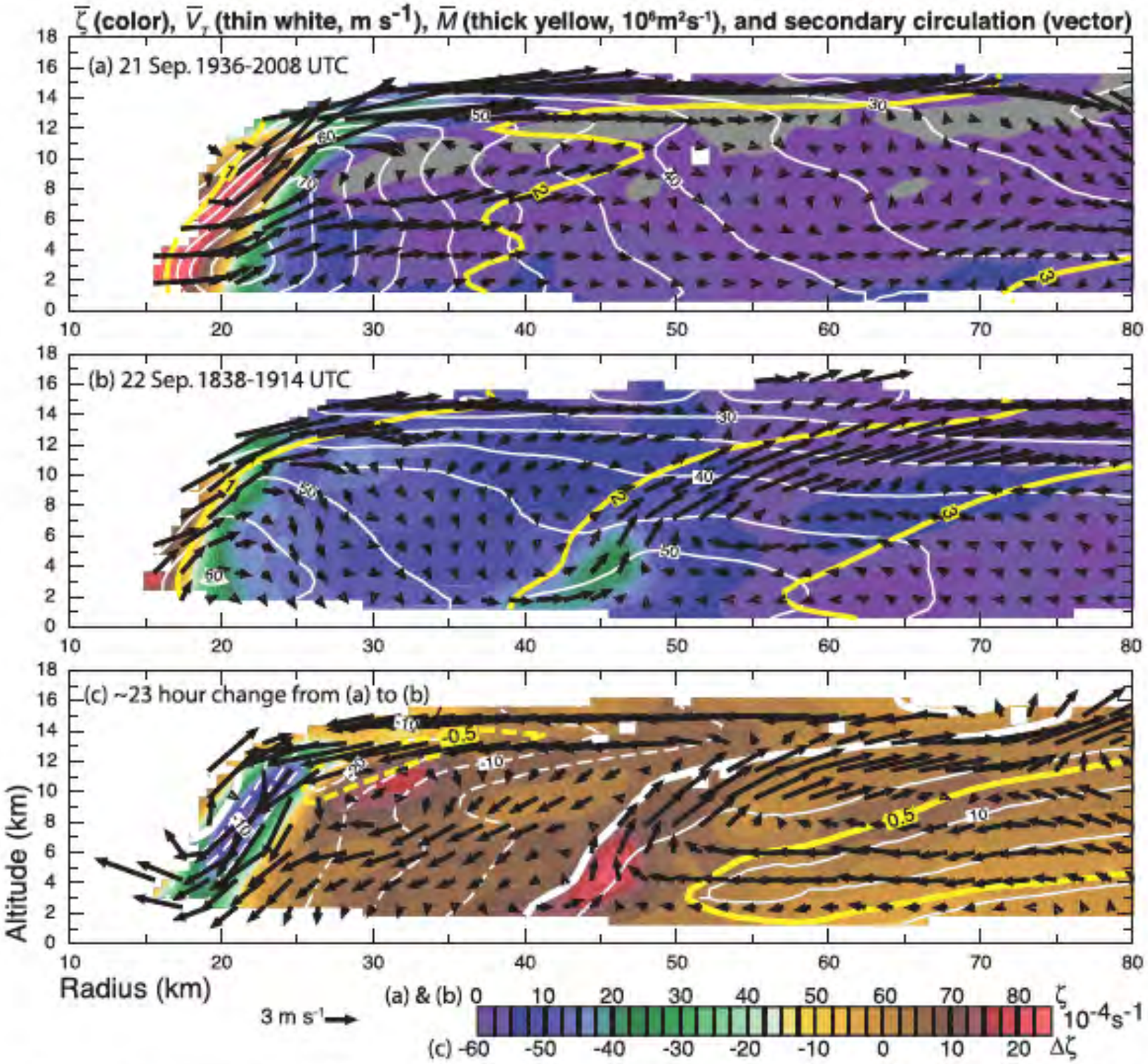

FIG. 6. Axisymmetric relative vorticity (color, 10^{-4} s^{-1}), tangential wind (contour, m s^{-1}), and secondary circulation (vector) derived from ELDORA. (a),(b) Flight patterns and times shown in Fig. 1, and (c) the change between the two analysis times. Dashed contours in (c) indicate a negative change of tangential wind and absolute angular momentum, thick contours indicate zero change, and solid contours indicate positive change. Vorticity change in (c) is indicated by the numbers on the bottom of the color bar.

Bell et al. (2012)

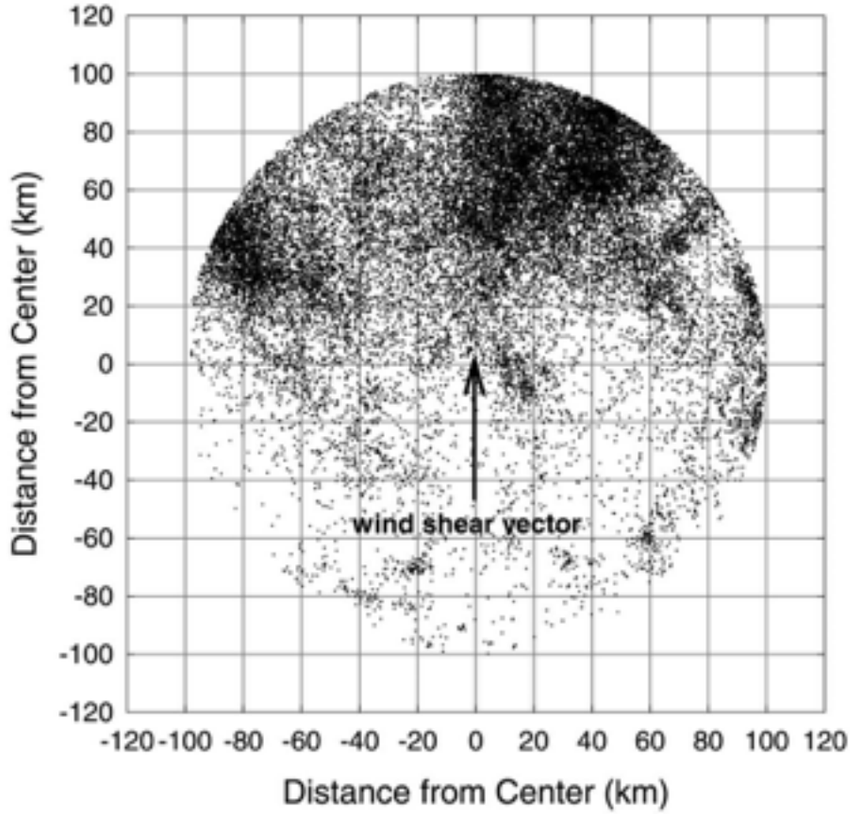

Corbosiero and Molinari (2002)

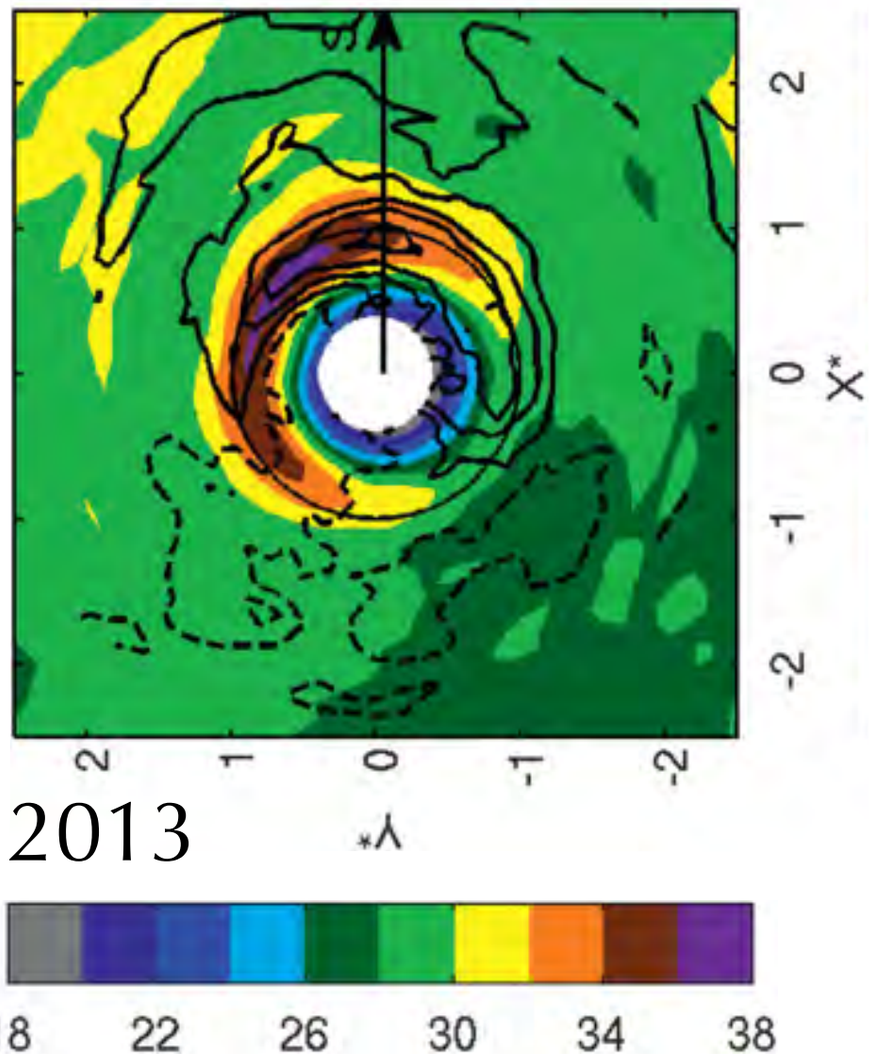

Reasor et al. 2013

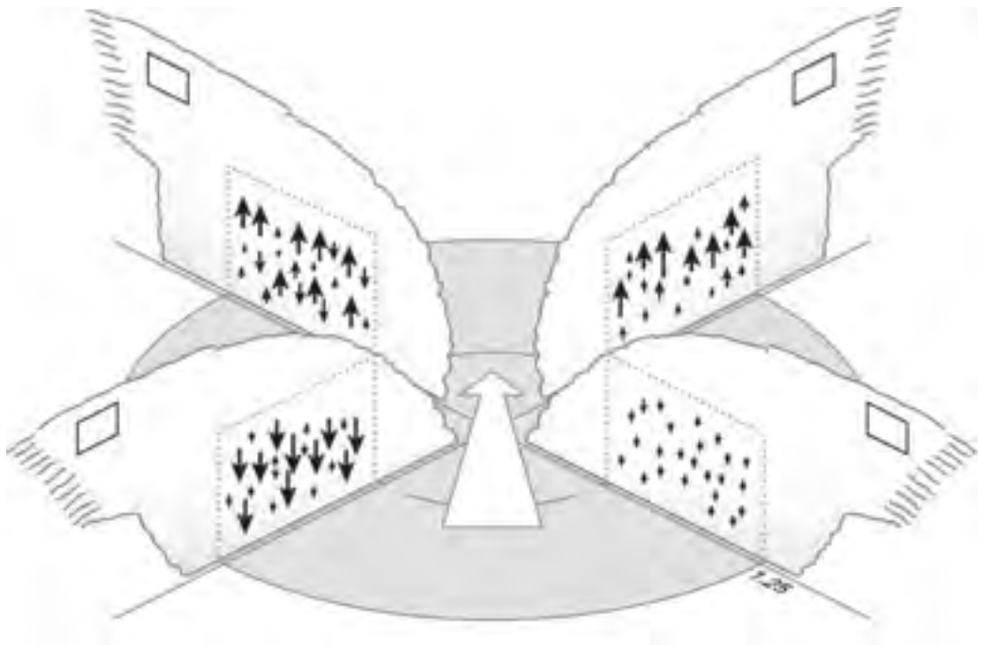

DeHart et al. 2014

Storm	Ocean basin	Lat (°N)	Wind [kt ($m\,s^{-1}$)]
Jimena	East Pacific	13.4	114 (59)
Olivia	East Pacific	17.5	115 (59)
Guillermo	East Pacific	13.6	123 (63)
Sinlaku	West Pacific	33.0	68 (35)

Typhoon Sinlaku (2008) near Extratropical Transition

Foerster et al. 2014

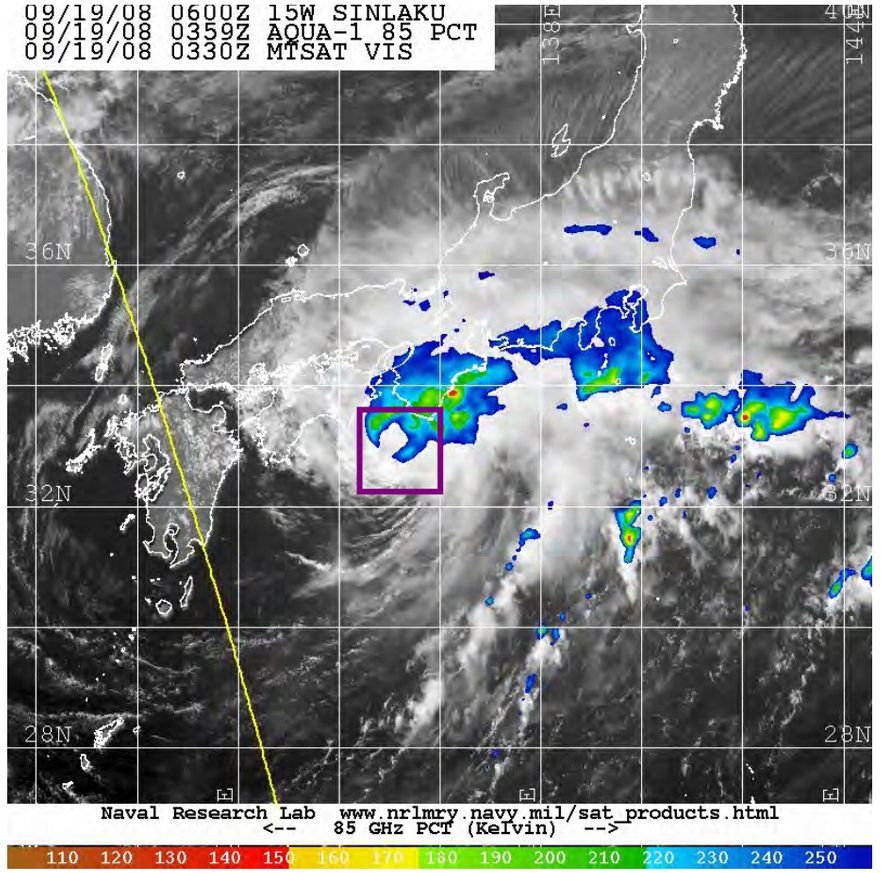

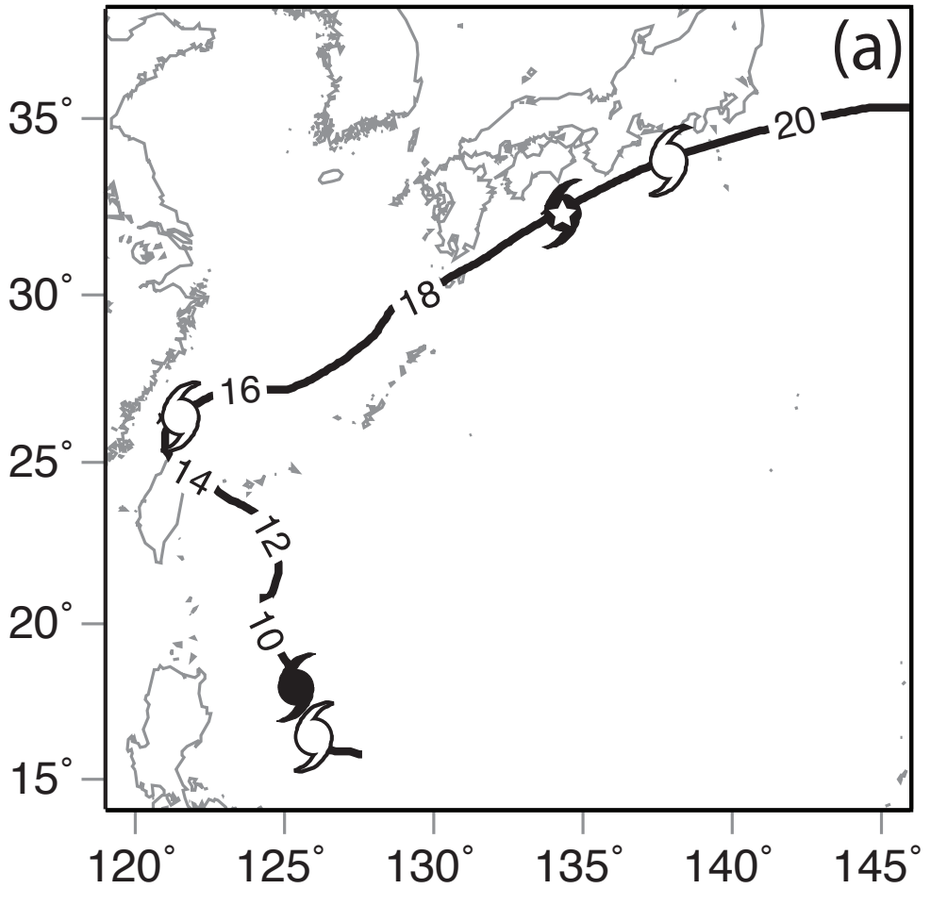

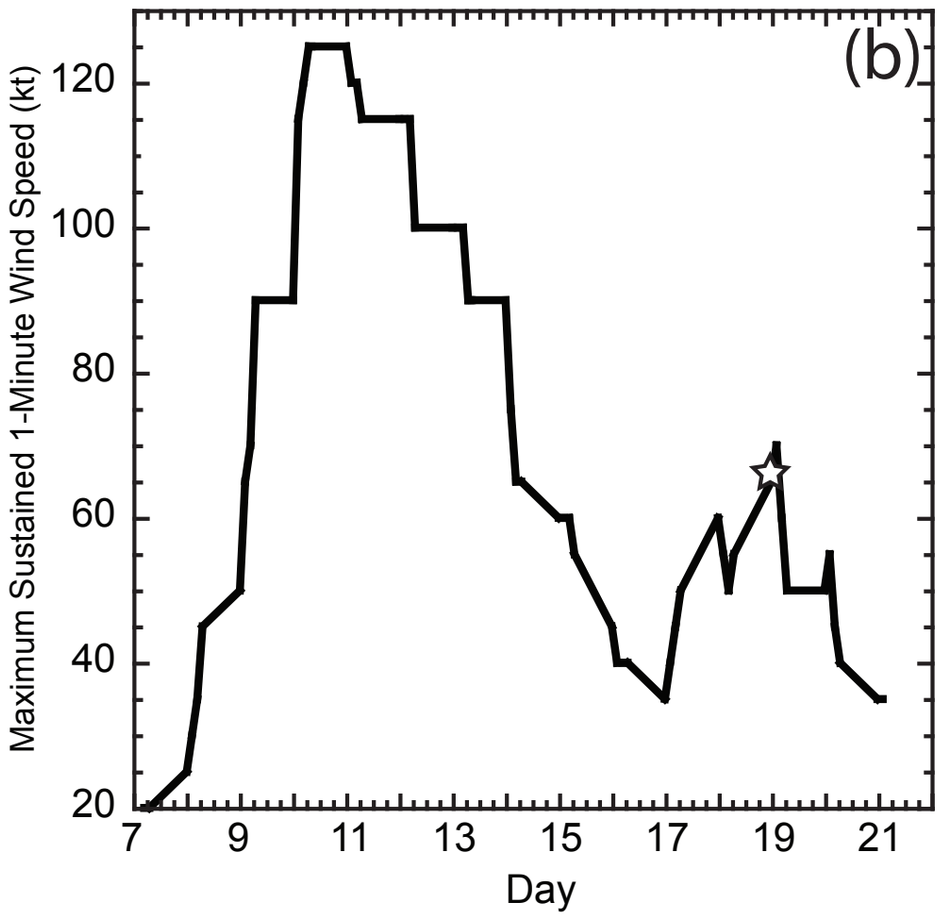

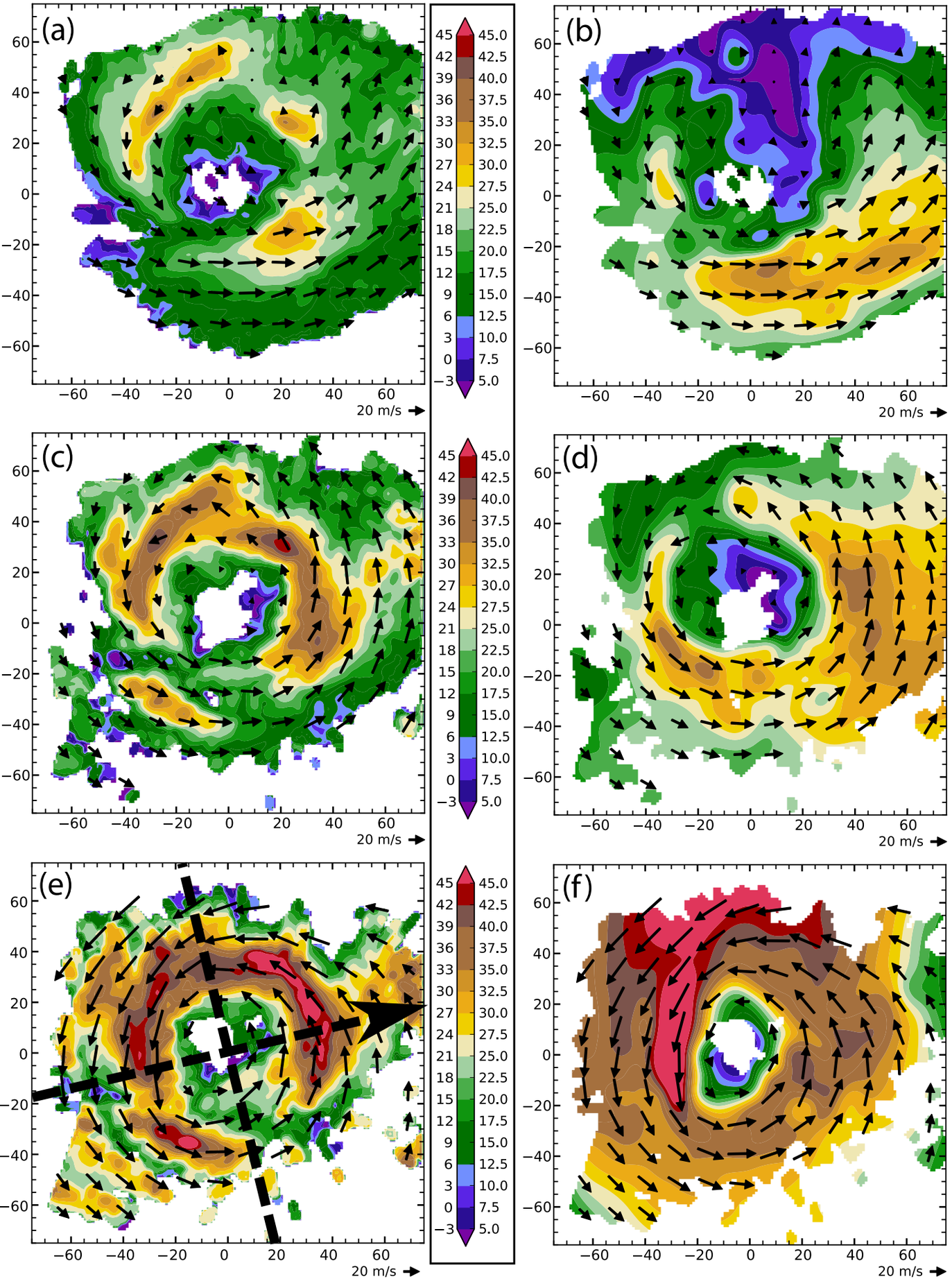

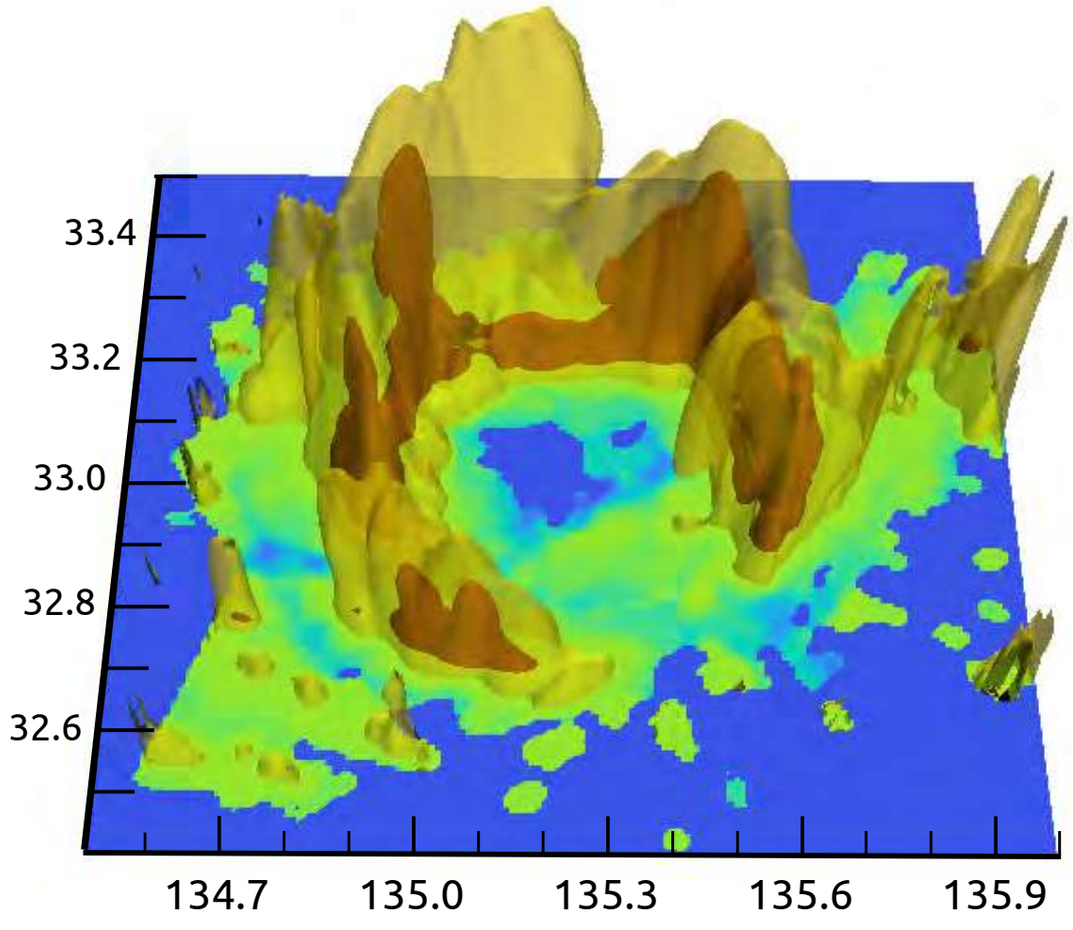

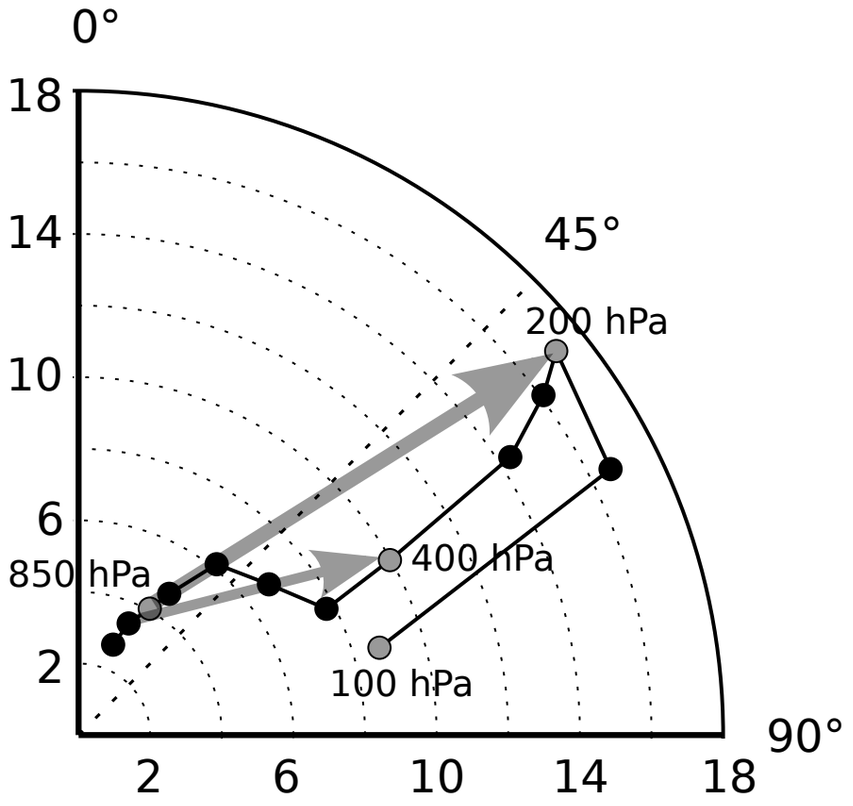

Foerster et al. (2014)

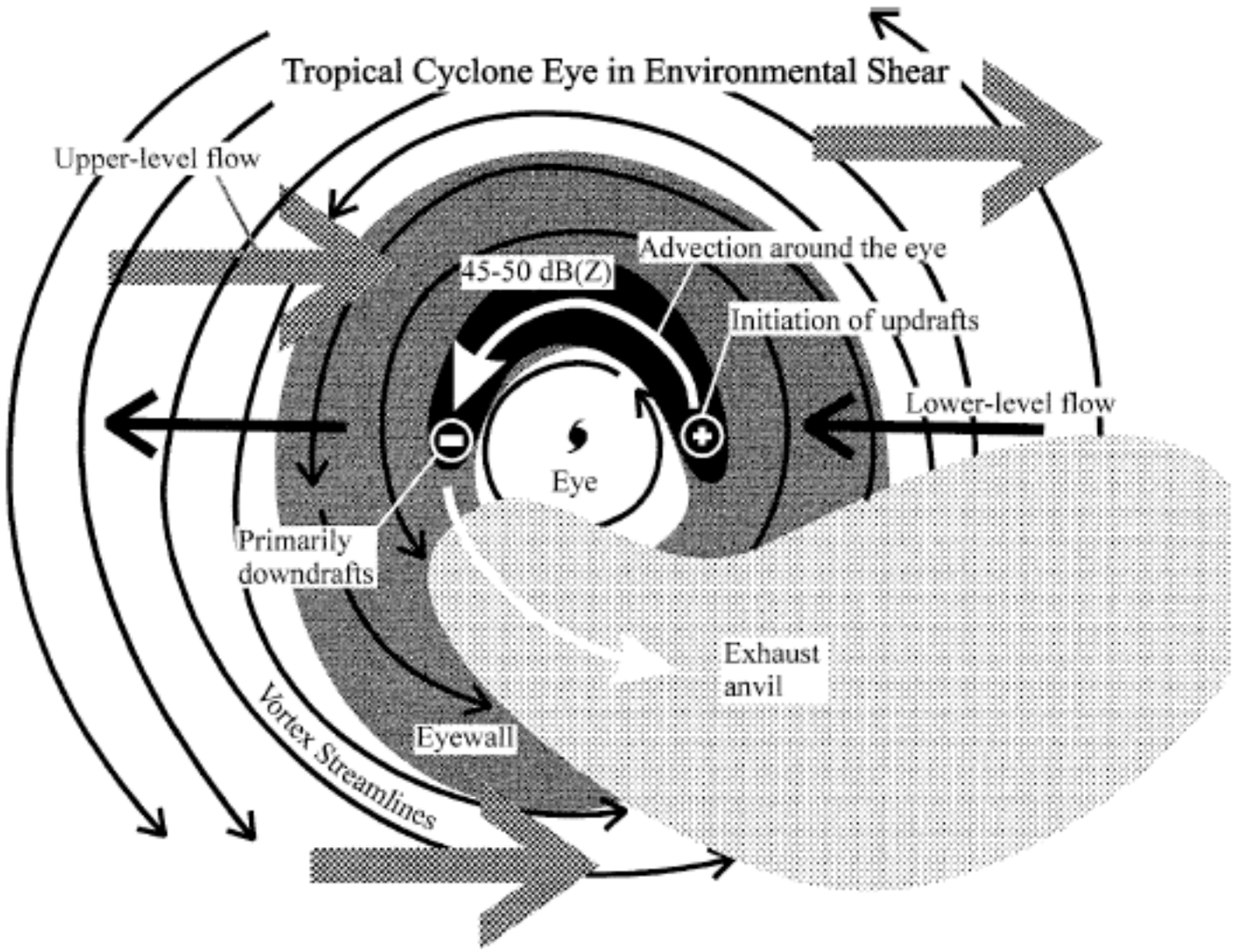

From Black et al. (2002)

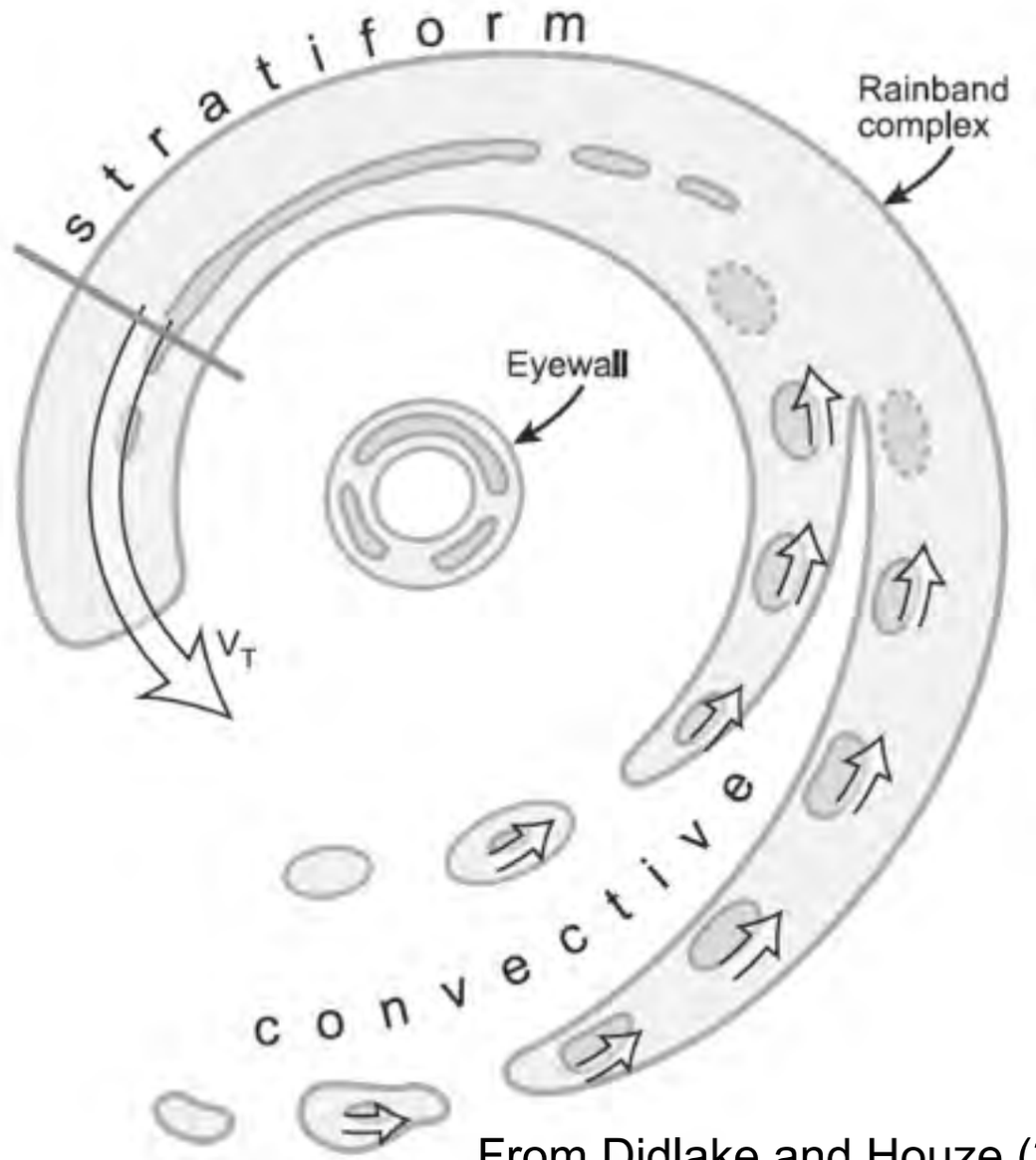

From Didlake and Houze (2013)

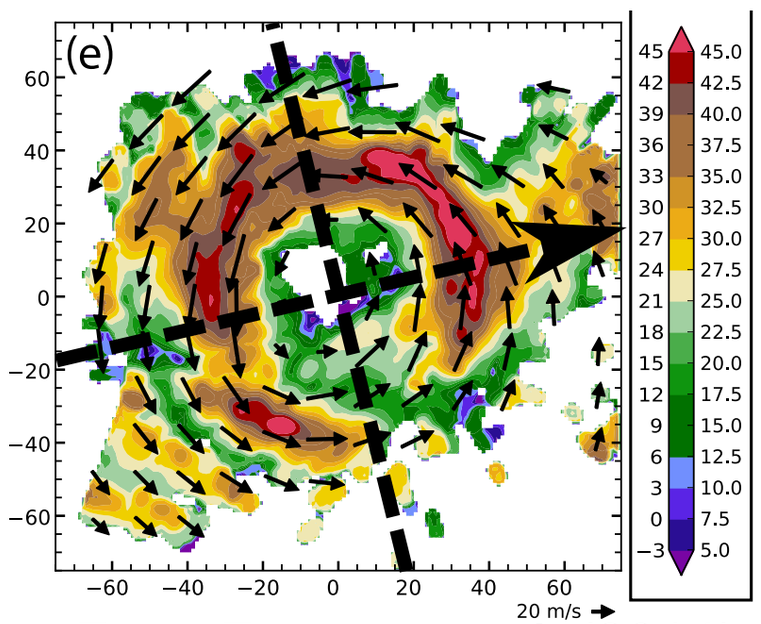

From Foerster et al. (2014)

Convective initiation DR, Maturing deep convection DL, Transition to stratiform UL, decay in UR

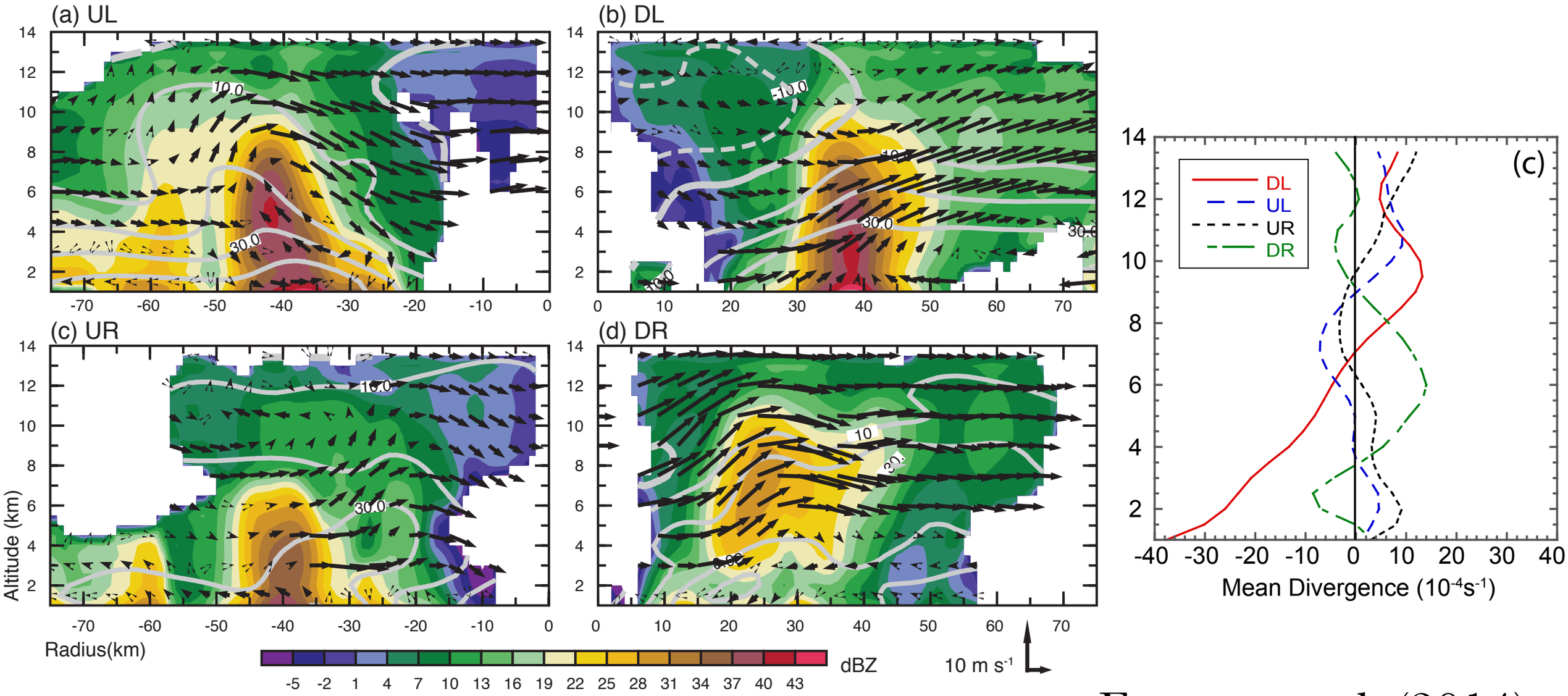

Foerster et al. (2014)

- Strong downdrafts on inside edge of eyewall, still warm-core system
- Extratropical transition began 24 hours later (Quinting et al. 2014)

Convective initiation DR, Maturing deep convection DL, Transition to stratiform UL, decay in UR

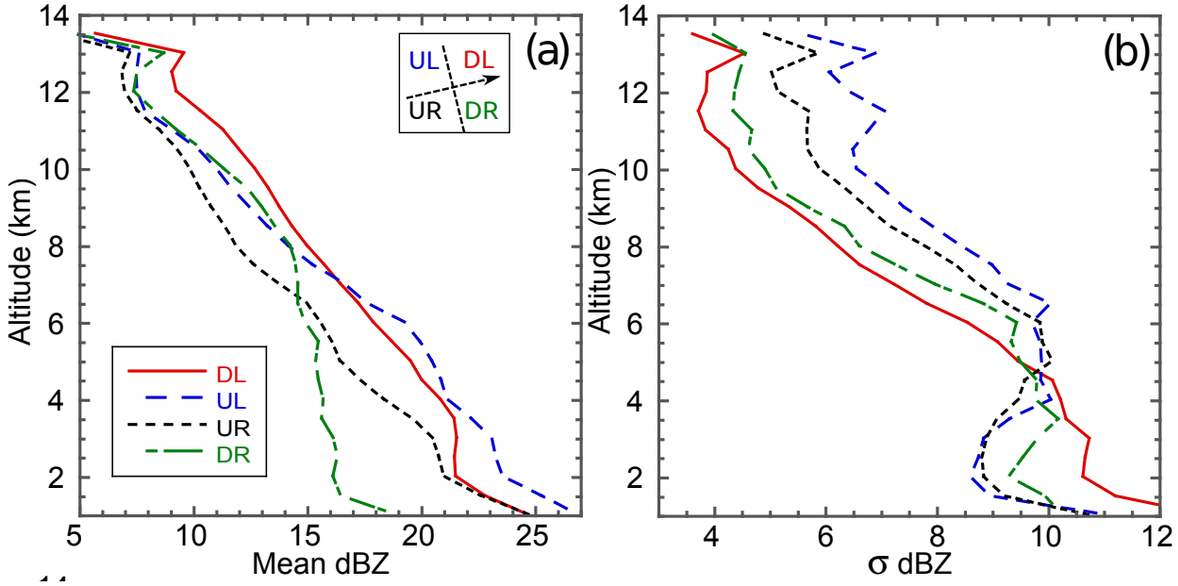

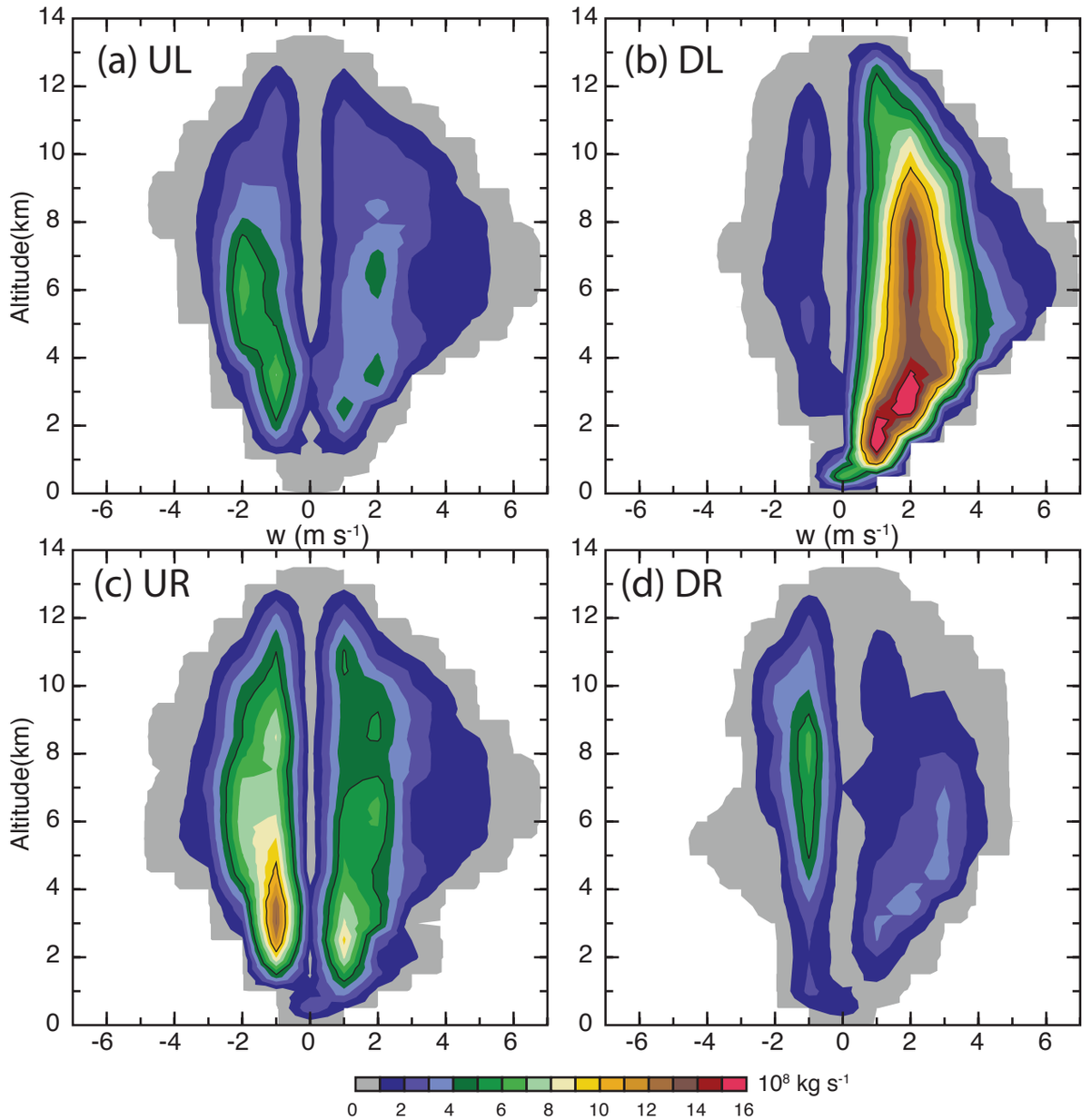

Foerster et al. (2014)

A composite approach to understanding TC structure and intensity change

- Previous studies have considered either intensity (Mallen et al. 2005) or intensity change (Shea and Gray 1973; Kossin and Eastin 2001; Rogers et al. 2013)

- Consider TC intensity and centered 12 h intensity change

- Create kinematic and thermodynamic composites with in situ (flight level) observations

- Identify structural differences between composites stratified by intensity and intensity change

From Martinez (2016)

Datasets used in the analysis

1) National Hurricane Center's Best Track (BT) dataset
   - "Fixes" at synoptic reference times
   - TC intensity and centered 12 h intensity change

2) Statistical Hurricane Intensity Prediction Scheme (SHIPS)
   - Determine TC's distance to land

3) FLIGHT+: The Extended Flight Level Dataset for Tropical Cyclones (Version 1.0; Vigh et al. 2016)
   - Radially binned in situ data collected at 700 hPa
   - Determine the azimuthal mean structure of each flight

Computing the azimuthal mean structure

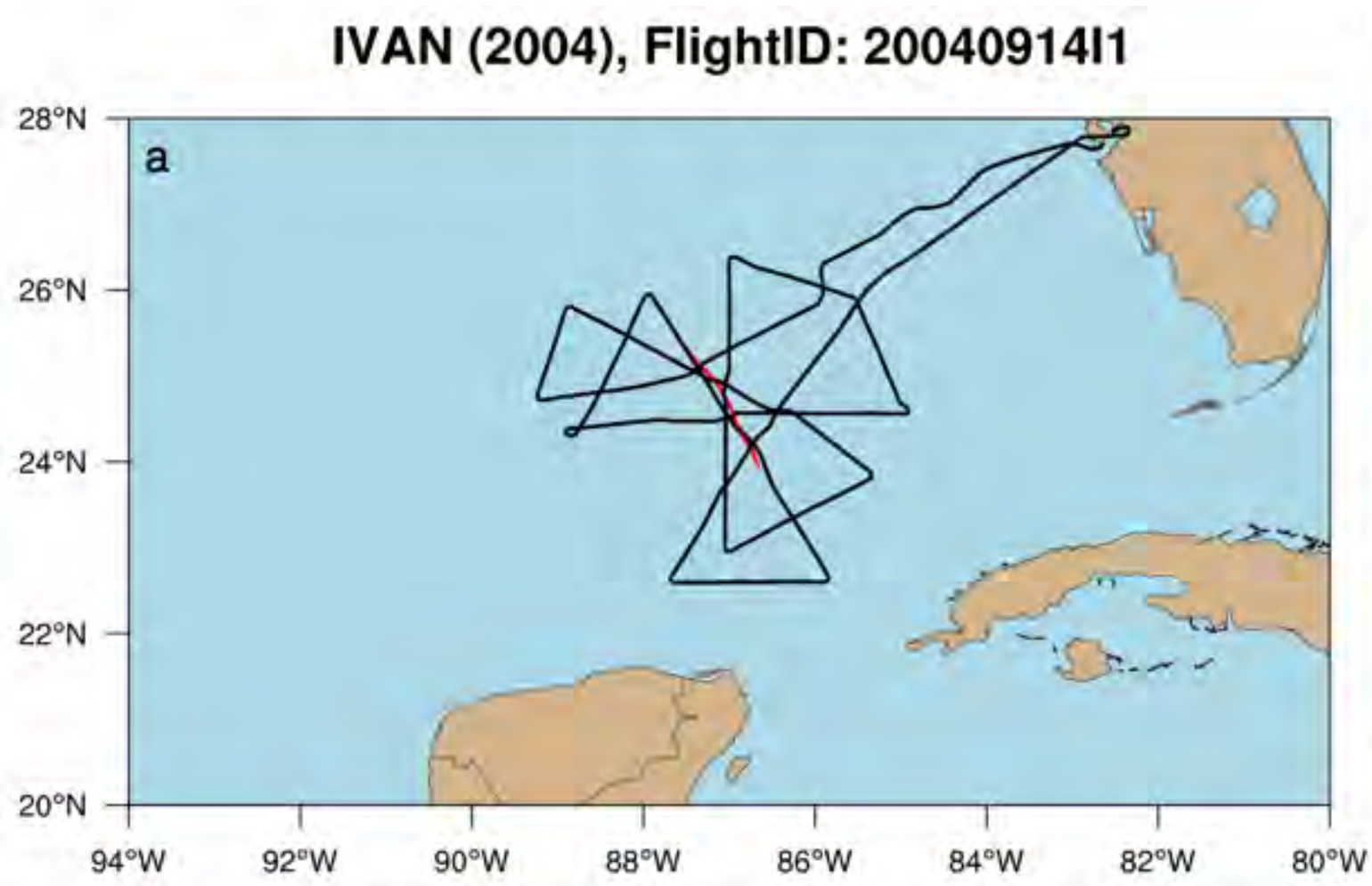

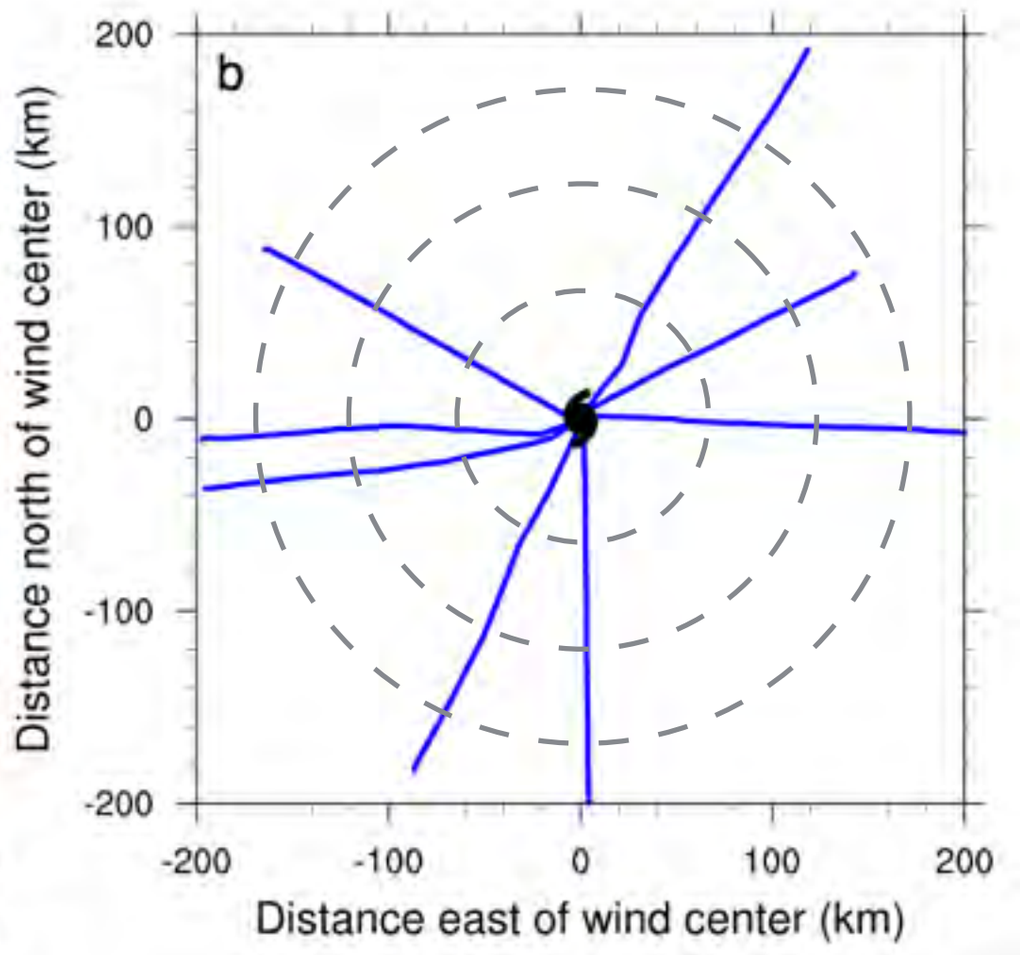

- Average all radial legs in a given flight over all radial points
- Round the average flight time to nearest synoptic reference time

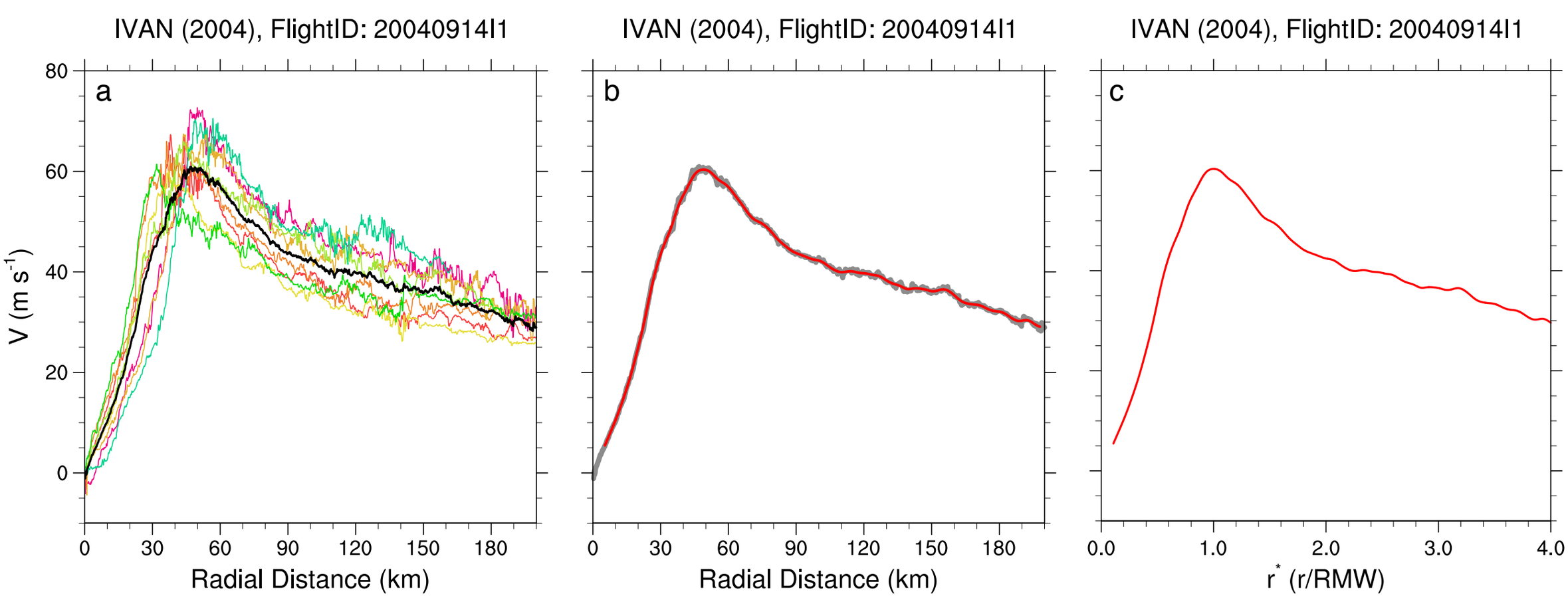
IVAN (2004), FlightID: 20040914I1
a
b
c
V (m s-1)
80
60
40
20
0
0
30
60
90
120
150
180
Radial Distance (km)
0.0
1.0
2.0
3.0
4.0
r* (r/RMW)

Number of flights matched to binned BT fixes

Storm Intensity

Centered 12 h Intensity Change	Hurricane (64 < V ≤ 95)	Major Hurricane (V > 95 knots)
Weakening (WK) ≤ -10 kts/12h	23	31
Steady State (SS) -5 to 5 kts/12h	48	46
Intensifying (IN) ≥ 10 kts/12h	44	41
Total	115	118

Tangential Wind

Hurricanes

Major Hurricanes

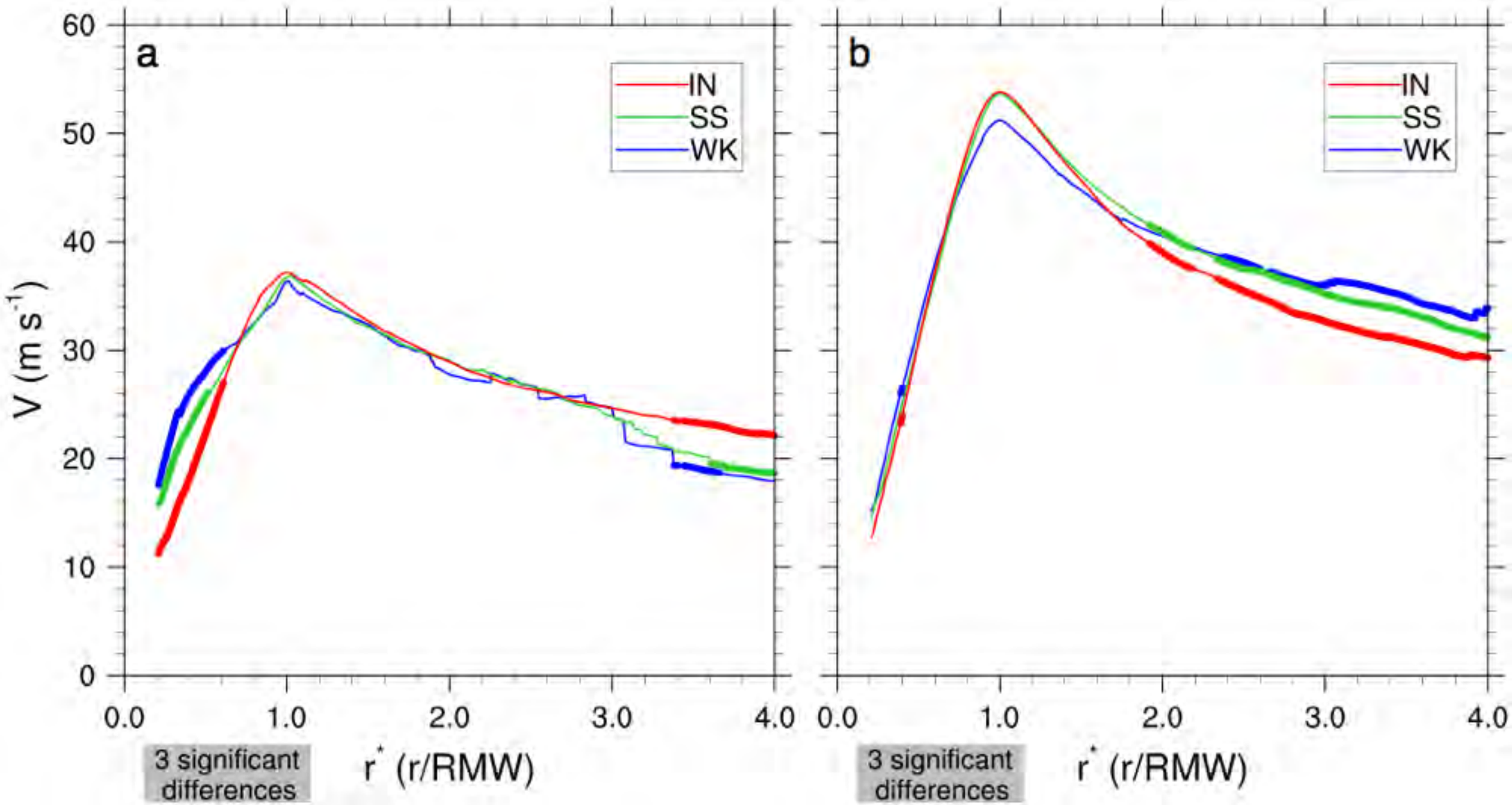

Tangential Wind

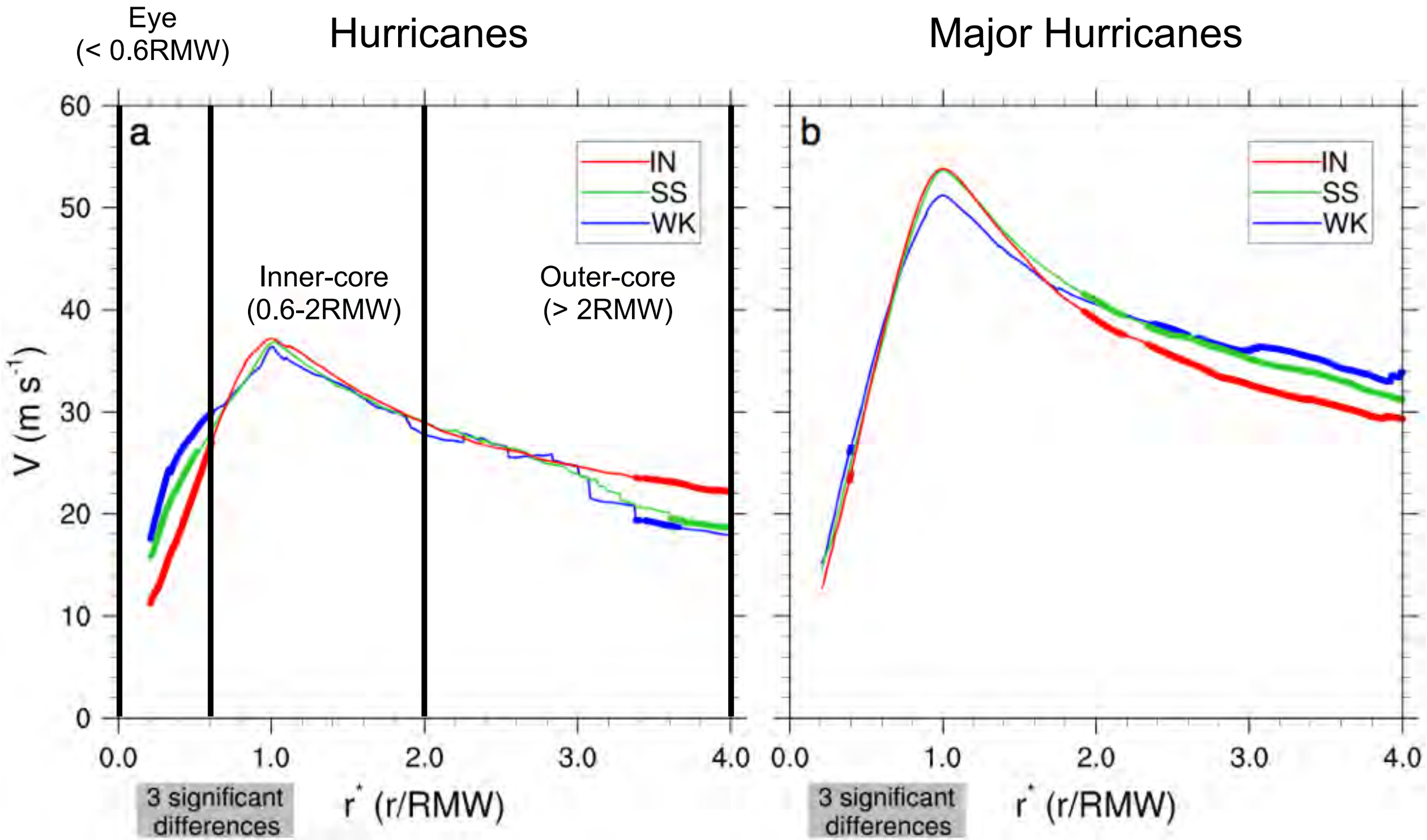

Tangential Wind

Hurricanes

Major Hurricanes

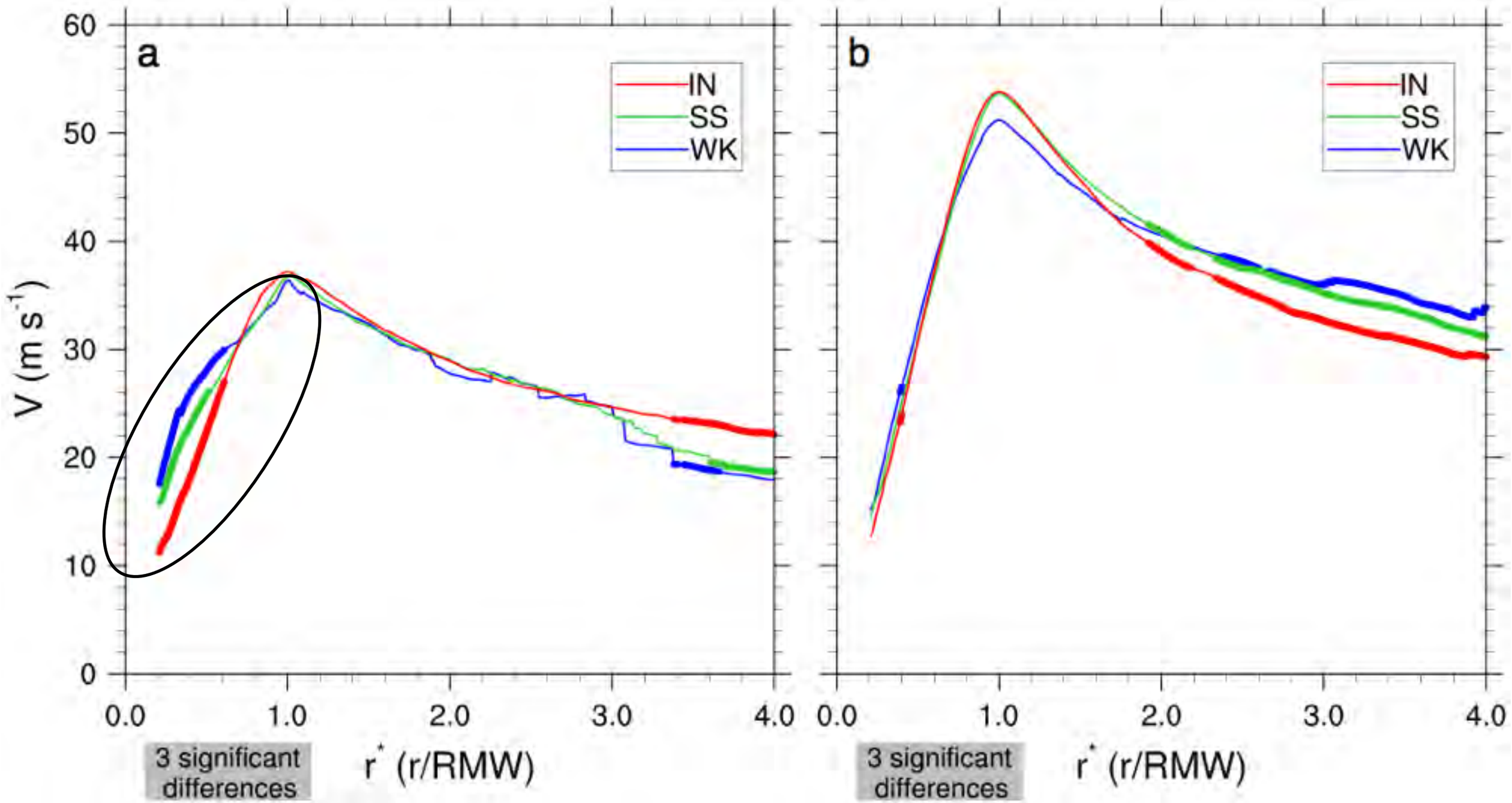

Tangential Wind

Hurricanes

Major Hurricanes

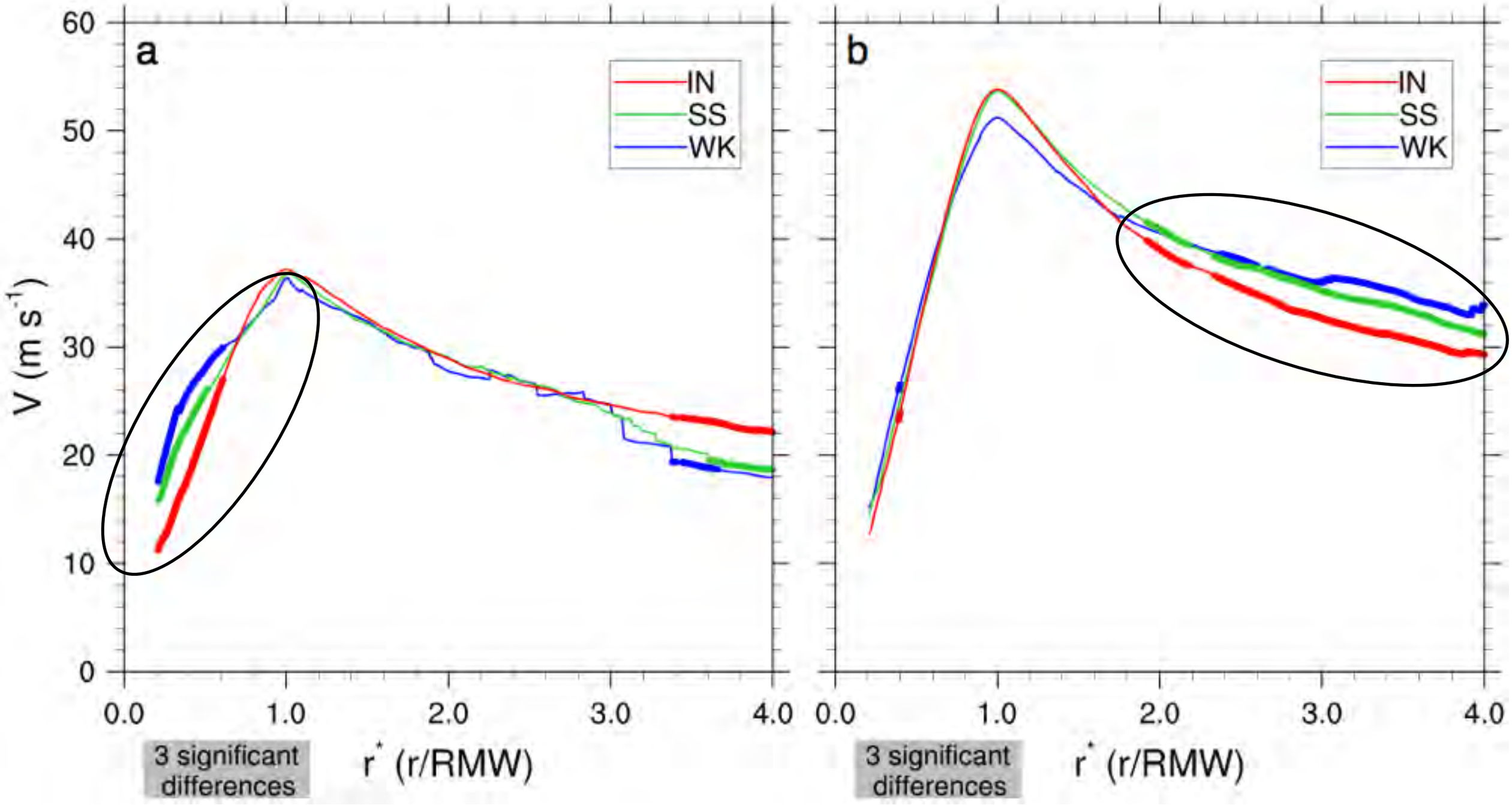

Vertical Vorticity

Hurricanes

Major Hurricanes

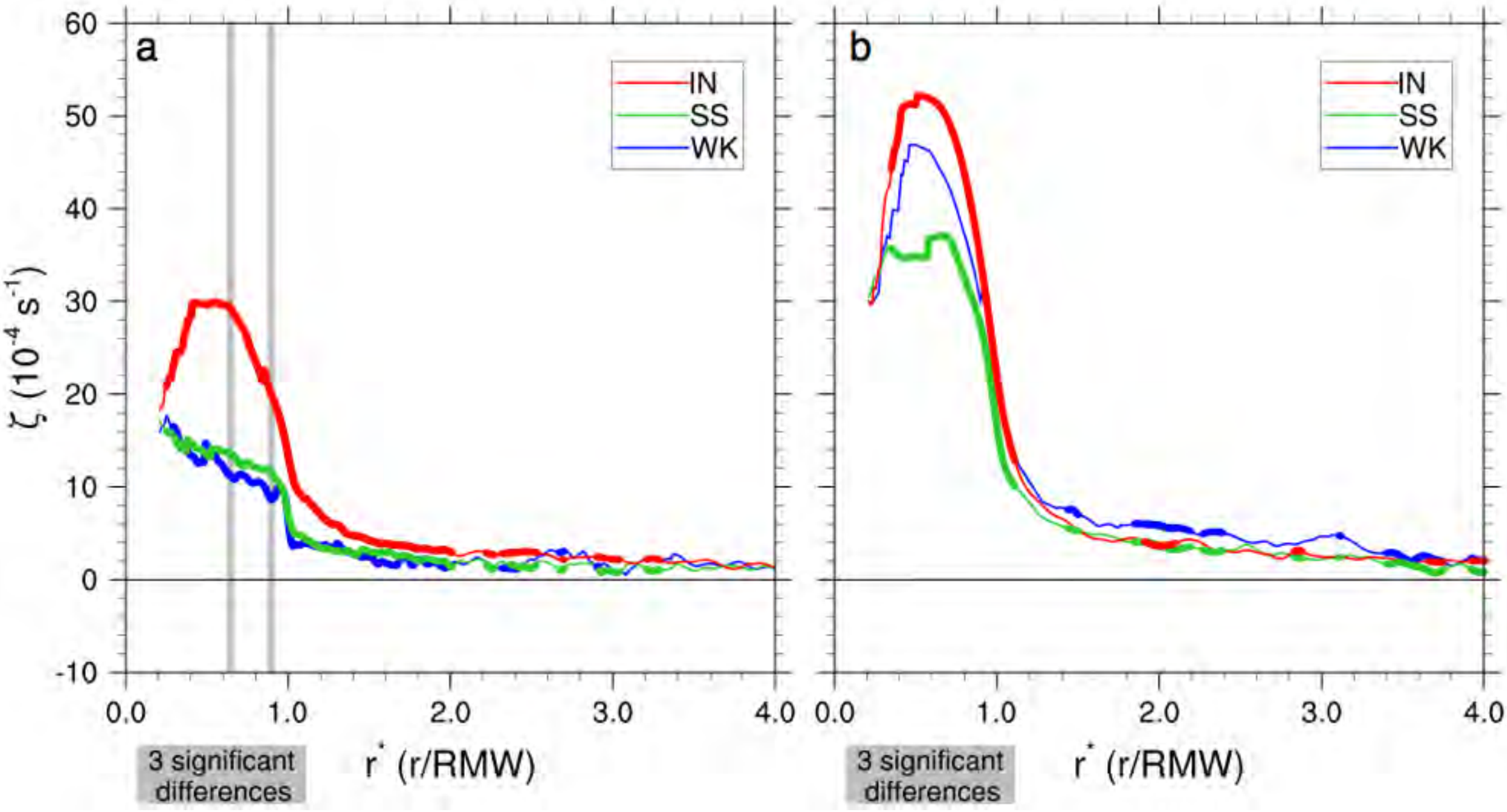

Dewpoint Depression

Hurricanes

Major Hurricanes

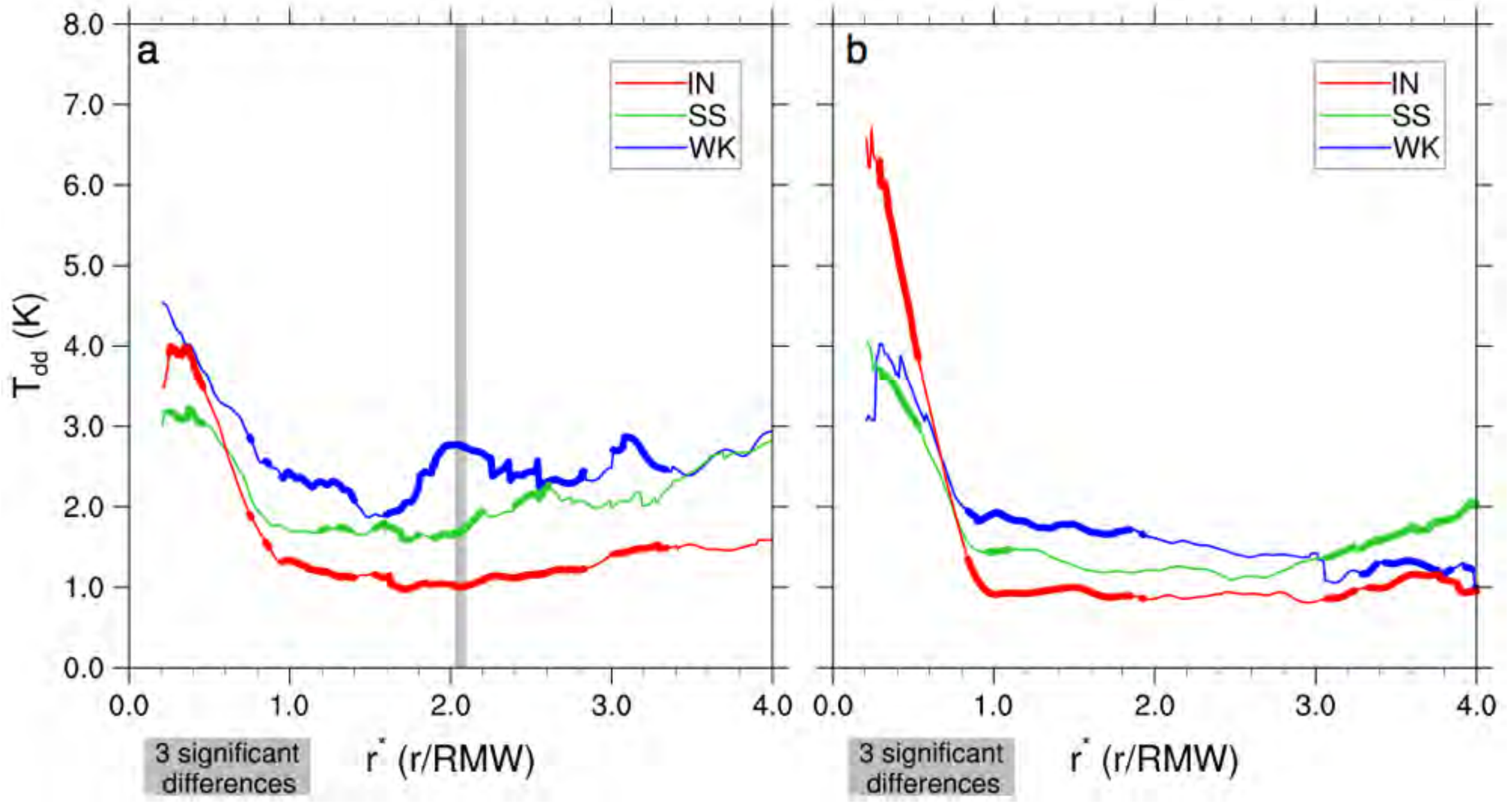

Intensity and intensity change are linked to TC structure

- **IN** TCs possess the steepest tangential wind gradients inside and outside the RMW
  - Vorticity ring structure with vorticity maximized inside RMW

- **WK** major hurricanes also exhibited a vorticity ring structure
  - Barotropic instability may have led to weakening state

- **SS** TCs possess flat profiles of vorticity inside the RMW

- **IN** TCs possess higher moisture in the inner and outer-core regions compared to **SS** or **WK** TCs

- Hurricanes exhibited more kinematic structural differences in the eye compared to outer-core region for major hurricanes

Large Scale Statistics

Bin	$RSST(C)$	$RHLO(\%)$	$SHDC(kt)$	$T200(C)$	$f(10^{-5}s^{-1})$
Hurricanes					
WK	28.56 (0.96)	63.52 (7.97)	17.67 (8.88)	-51.01 (1.77)	6.64 (1.40)
SS	28.84 (0.78)	67.30 (6.18)	15.50 (9.06)	-51.17 (1.30)	6.54 (1.10)
IN	29.13 (0.82)	68.70 (8.82)	13.62 (5.82)	-52.17 (1.28)	5.29 (1.30)
Major Hurricanes					
WK	29.04 (0.48)	67.03 (6.22)	10.87 (4.86)	-51.57 (1.24)	5.47 (1.24)
SS	29.07 (0.48)	67.85 (6.10)	11.10 (7.05)	-51.52 (1.04)	5.39 (0.88)
IN	29.04 (0.60)	68.51 (7.69)	9.48 (5.78)	-52.17 (1.13)	5.05 (1.15)

- Major hurricanes are found in similar, favorable environments
  - Observed structural differences likely caused by vortex or convective scale processes

- Hurricanes found in more variable environments
  - Environmental conditions may play more of a role

Tropical Cyclone Intensity (TCI)

Background

Role of Outflow in TC Intensification Has Been Relatively Unexplored

➢ Few detailed observations of outflow layer coordinated with inner core observations

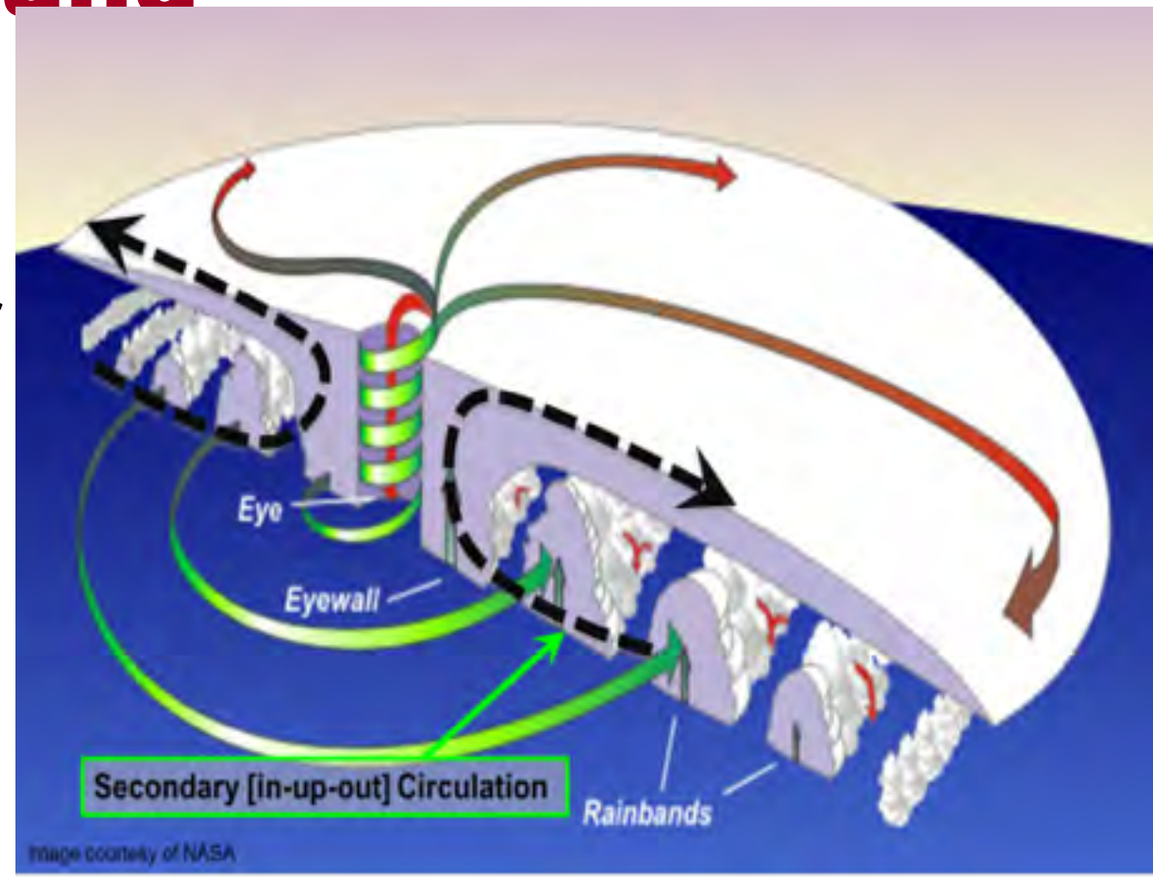

Key Science Issues

1) Document the inner-core at high-resolution, and the larger-scale outflow
2) Understand the role of outflow during TC intensity change
3) Explore air-sea interaction processes
4) Understand the impact of inner core and outflow observations on TC intensity and structure predictions.

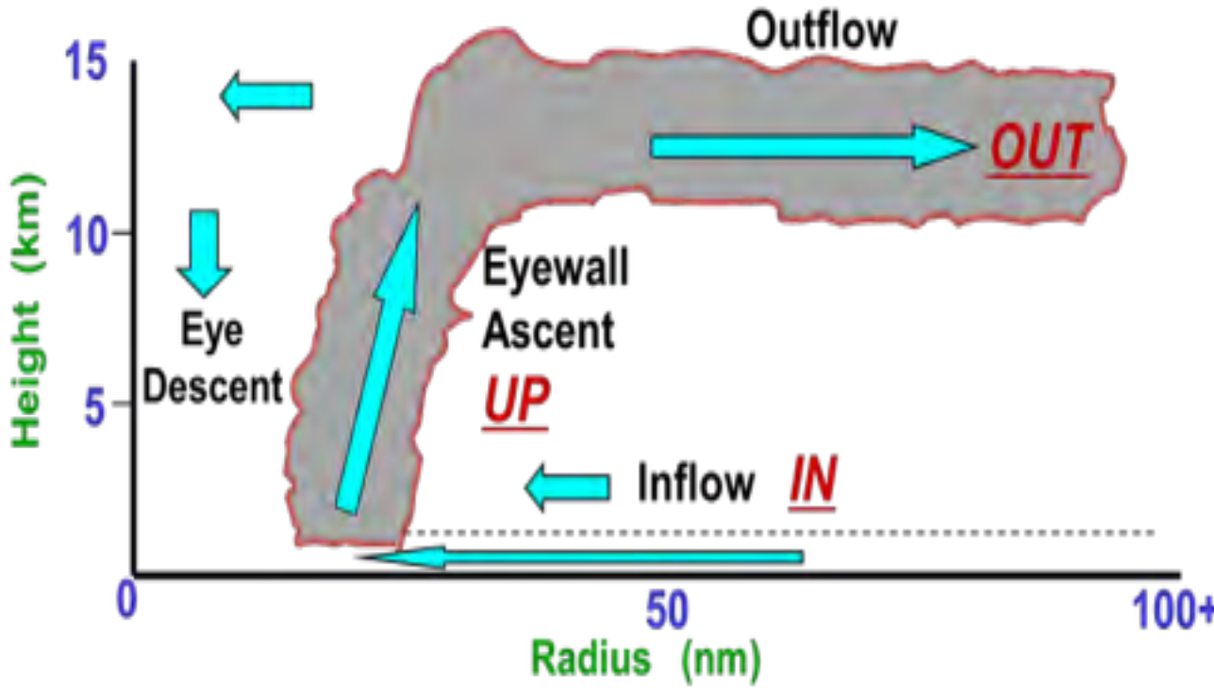

Slides courtesy Jim Doyle NRL

Tropical Cyclone Intensity (TCI)

Background

NASA WB-57 Aircraft:

- Duration ~6 h, range ~2000 nm, speed ~400 kt; cruise altitude > 60,000 ft.
- Based at Ellington AFB, TX; deployed to: i) Harlingen, TX (EPAC); ii) Warner Robbins AFB, GA (WATL)
- Coordination: NASA GH, NOAA P-3, AF C-130 - C-130 deployed AXBTs in TROPIC (Beth Sanabia)

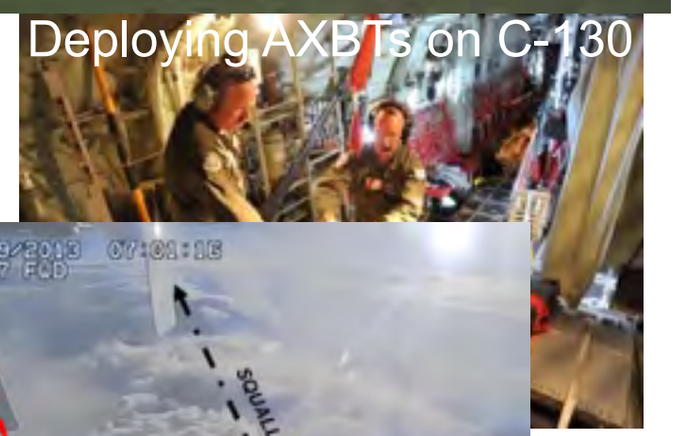

High Definition Sounding System (HDSS):

- Innovative eXpendable Digital Dropsonde (XDD) atmospheric profiling system (YES, Mark Beaubien)
- Profiles of pressure, temp., RH, winds, SST
- Capable of rapid sonde deployment (>80)

Hurricane Imaging Radiometer (HIRAD):

- Multi-frequency, passive C-band radiometer, that measures ocean surface winds through heavy rain
- NASA MSFC developed instrument (Dan Cecil, PI)

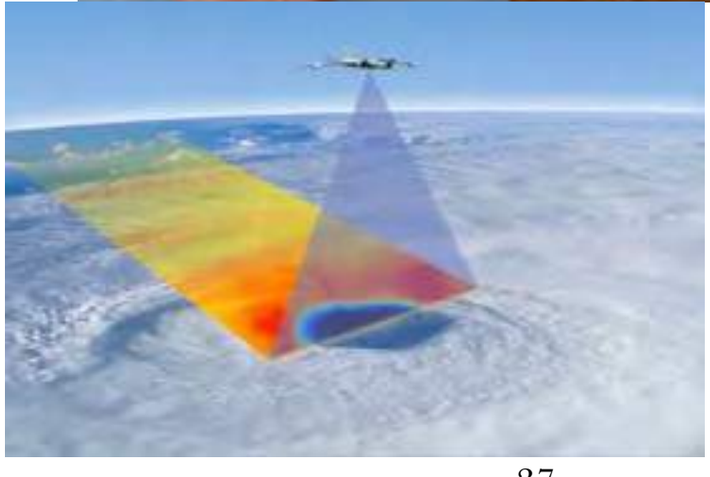

Tropical Cyclone Intensity (TCI)

Observations of 4 Unique TCs

- 2014: 3 WB-57 flights over Hurr Gonzalo (YES, HIRAD, HIWRAP)
- 2015: Unprecedented set of dropsonde and HIRAD observations in Hurricanes Marty, Joaquin, Patricia, and Tropical Storm Erika
  - ➢ TCI Ops Center at NRL (Monterey); Flight Ops Center at aircraft.
  - ➢ ~800 dropsondes deployed in 4 TCs in 11 WB-57 flights
  - ➢ Dropsondes & AMVs (UW) in real time (NCAR catalog, NASA MTS)
- HDSS sondes now QCed (team of 10 TCI scientists led by M. Bell)

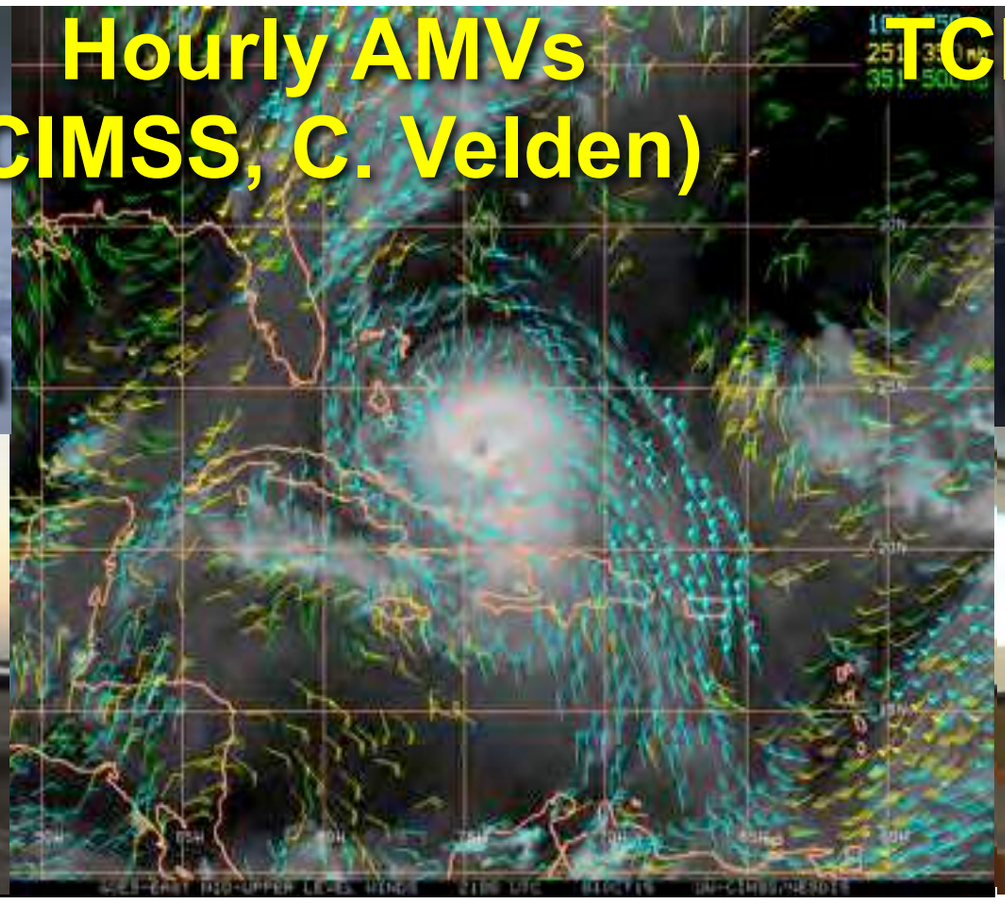

Tropical Cyclone Intensity (TCI)

Satellite-Derived Atmos. Motion Vectors (AMVs)

Processed at hourly intervals by the Univ. Wisc.-CIMSS TC Group
for the duration of the TCI field campaign (Chris Velden)

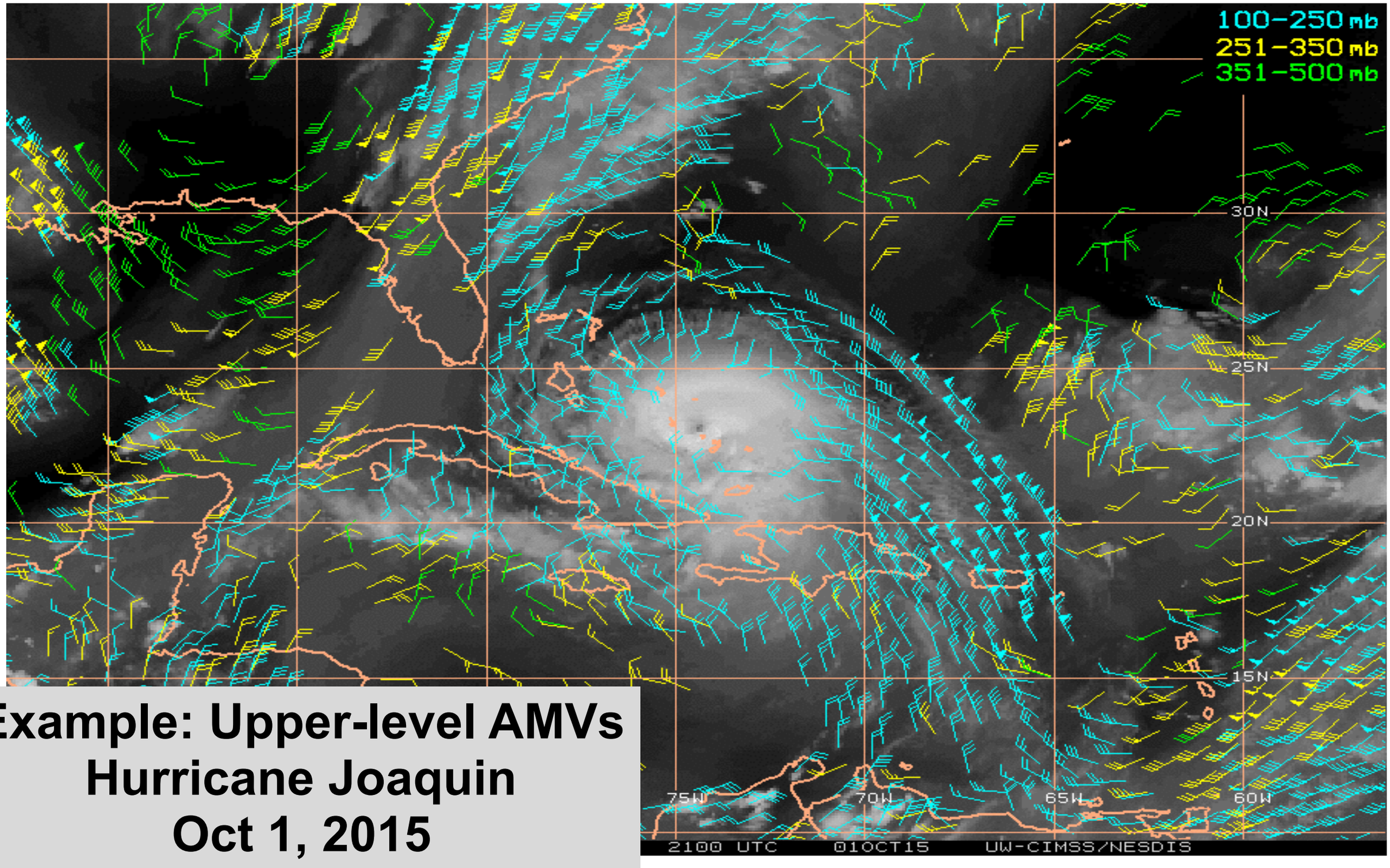

Example: Upper-level AMVs
Hurricane Joaquin
Oct 1, 2015

Tropical Cyclone Intensity (TCI)

Forecasting and Deployment

- Decision to forward-deploy the WB-57 needed to be made 3-5 days before the first science flight, to reposition the aircraft & personnel
- TCI mission scientists, forecast team, aircraft team, and NASA met daily
- Forecasts and real time obs in NCAR Field Catalog, access to NASA MTS.

Joaquin Deployment Decision

- On Sept 28, TD 11L was a 30 kt depression.
- CTCX and HWRF indicated the potential for significant intensification, as did the 12z EC and ~20% of the EC ensemble (see below)
- The forecast track of the TC was highly uncertain, but appeared to be close enough to the east coast for multiple flights

2015092800 EC ensemble
(Sharan Majumdar, U. Miami)

We decided to deploy the WB-57 to Georgia for what became a sequence of 4 flights into Joaquin

Joaquin Forecasts

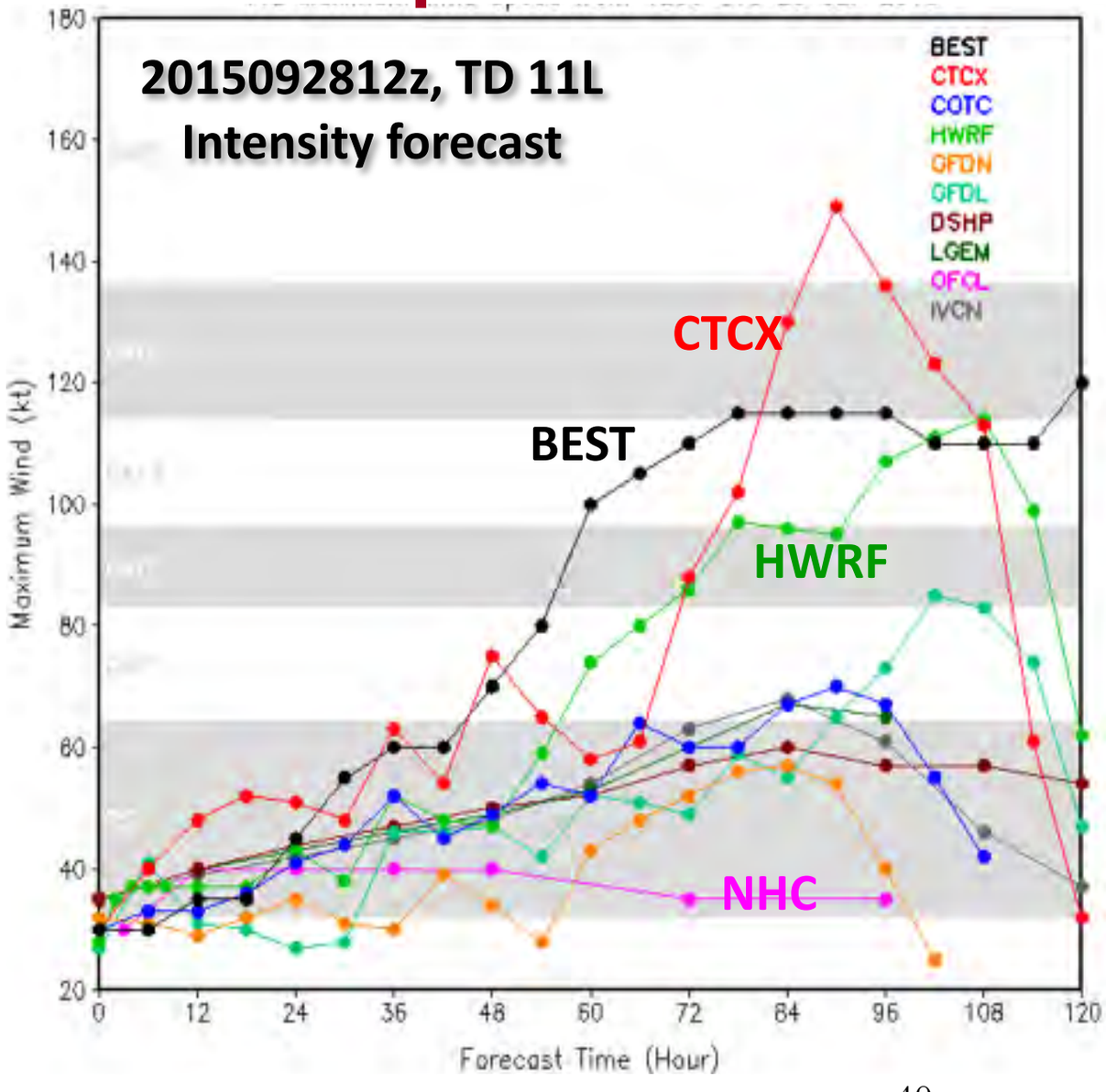

Tropical Cyclone Intensity (TCI)

Hurricane Marty (Sep 27-28)

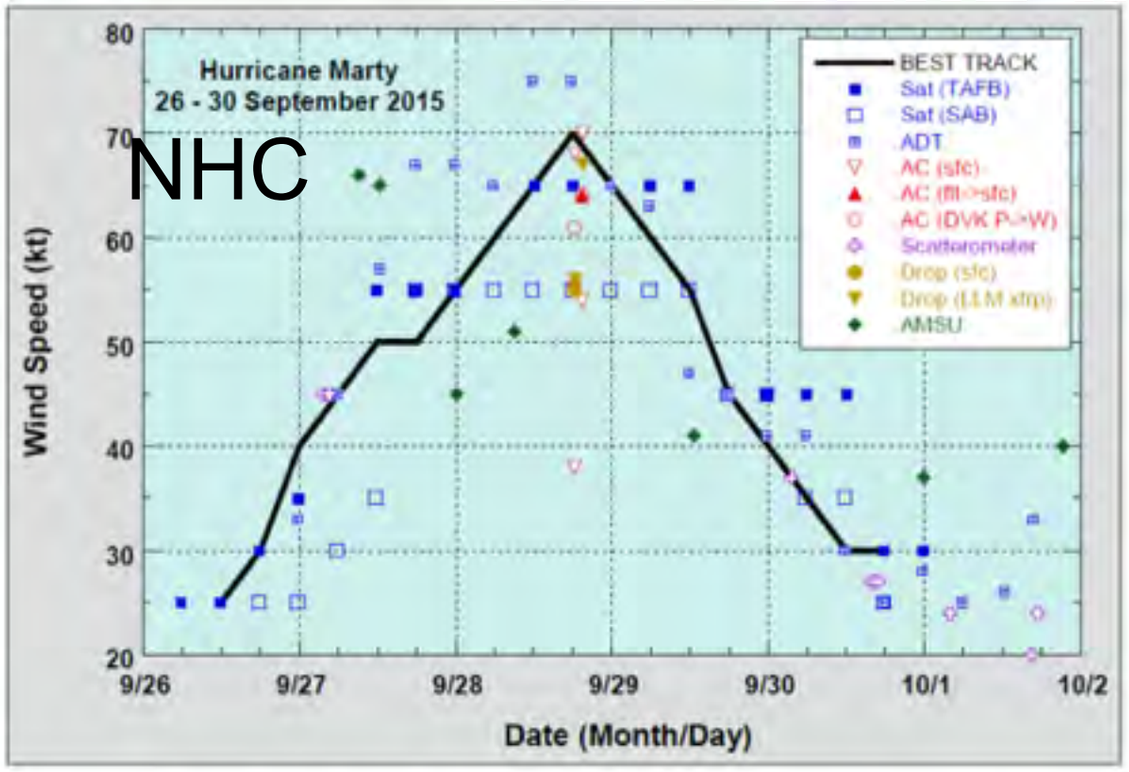

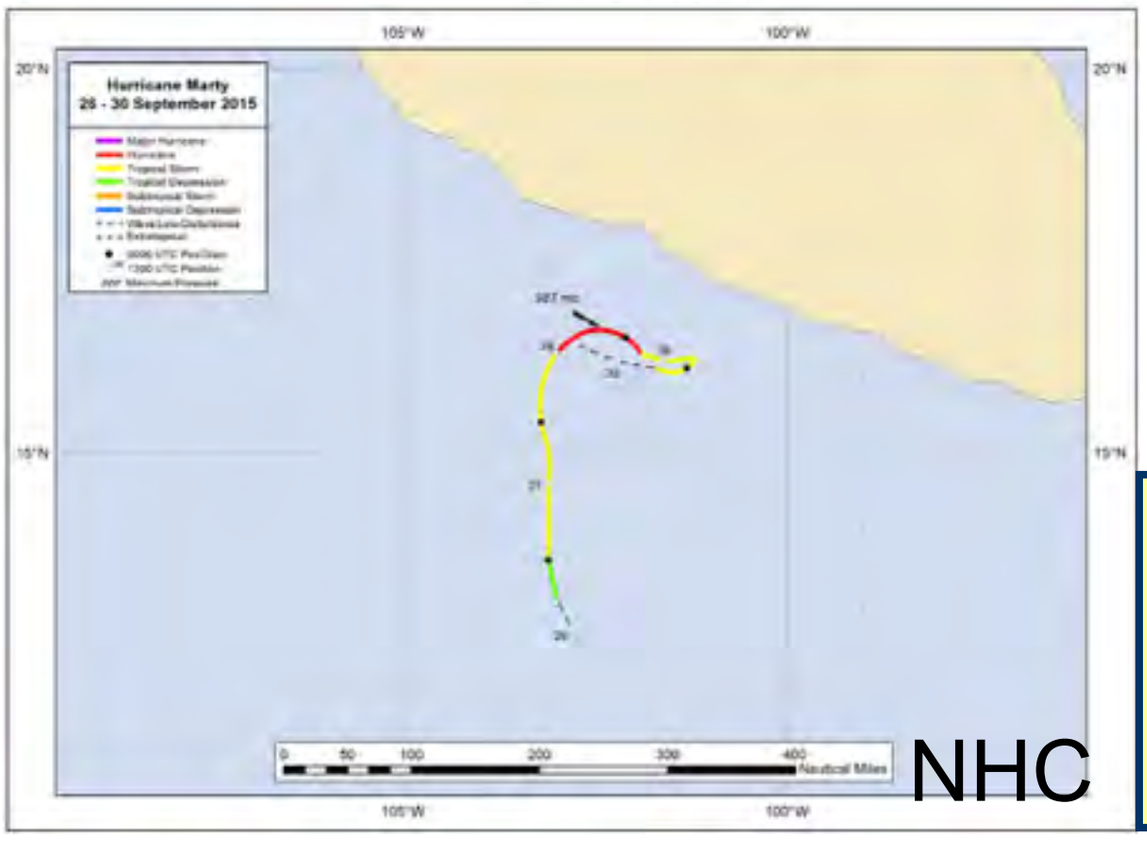

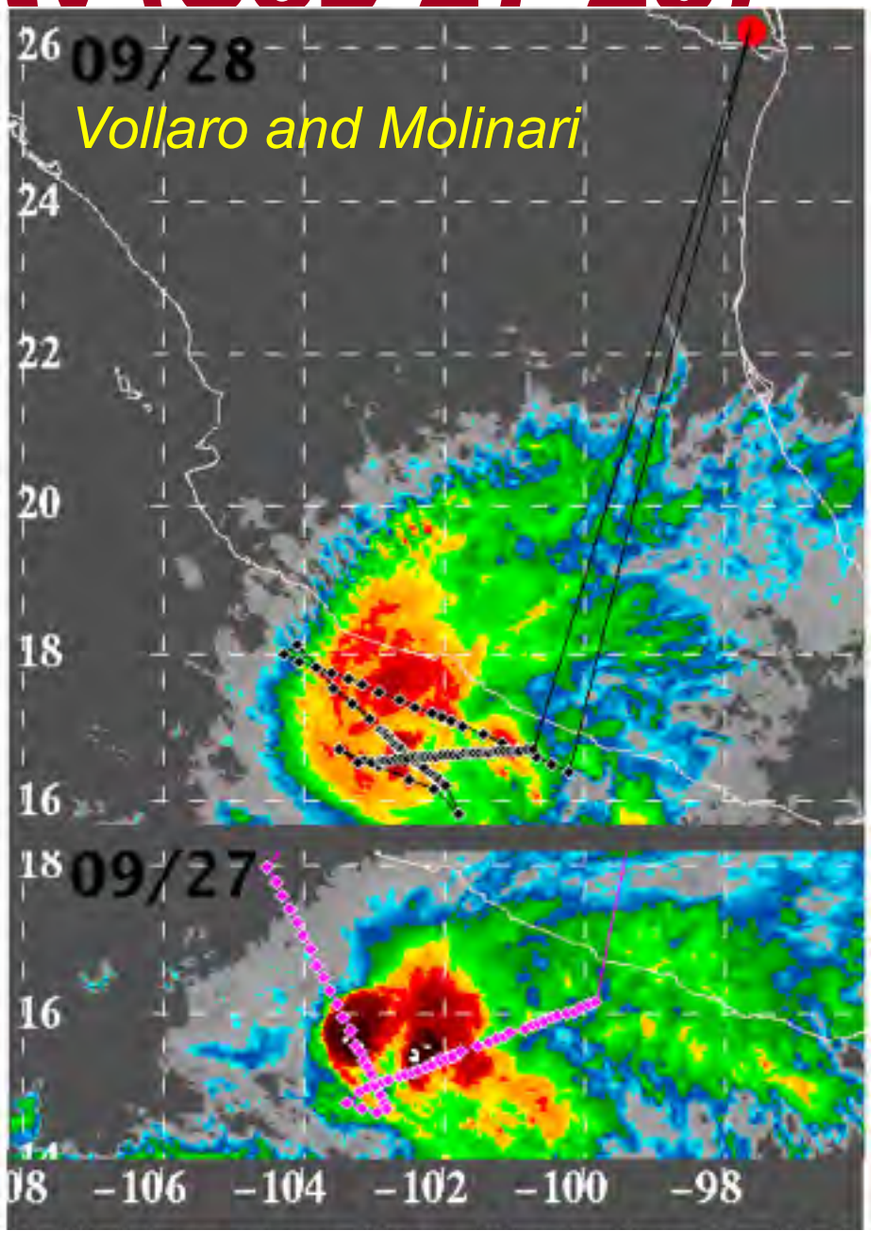

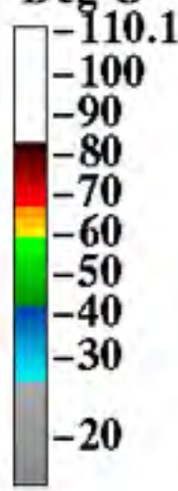

- **Hurricane Marty (Cat 1) intensified in the presence of moderate shear**
- **TCI performed 2 missions with transects across eye and outflow**

Tropical Cyclone Intensity (TCI)

Hurricane Joaquin (Oct 2-5)

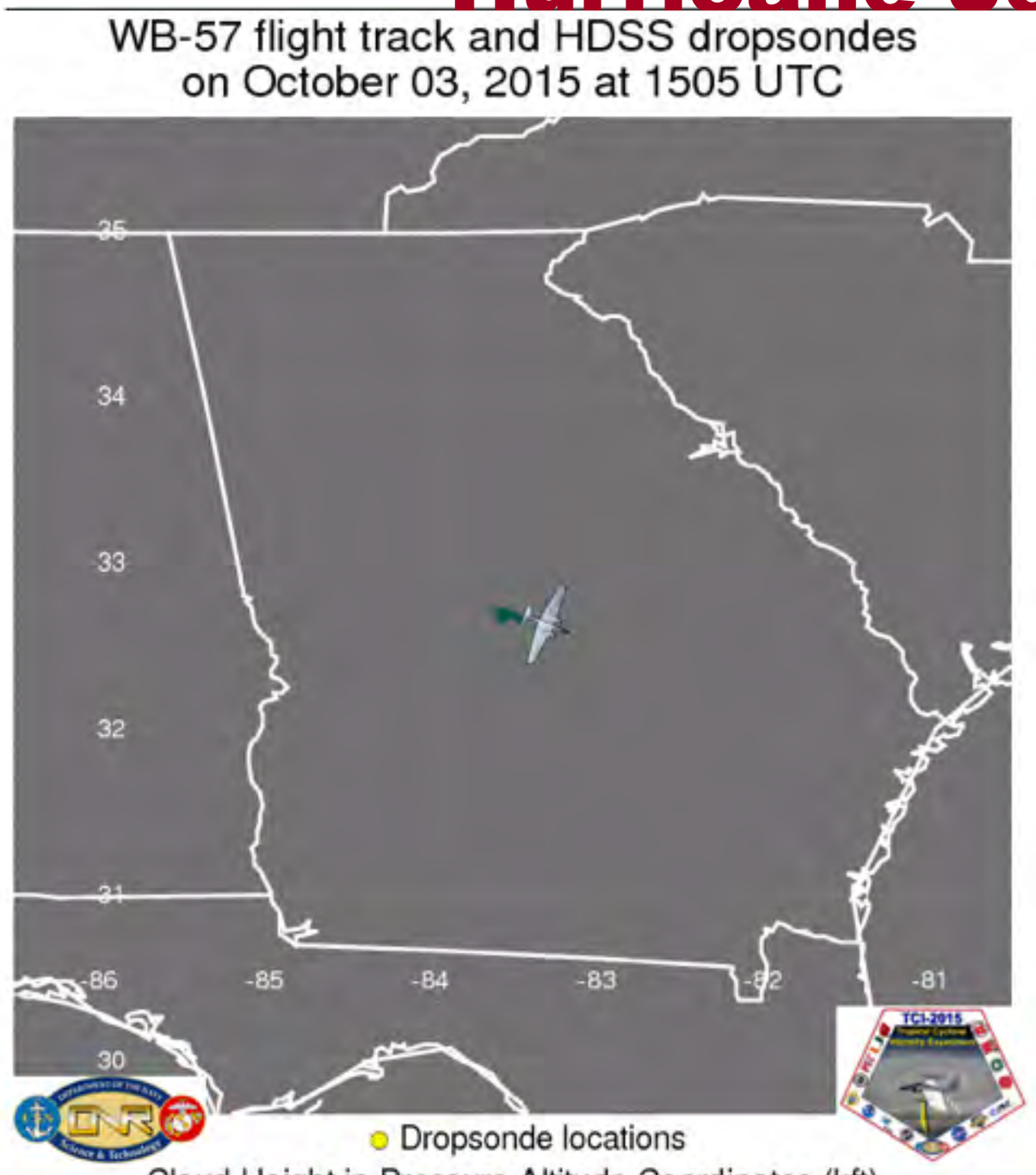

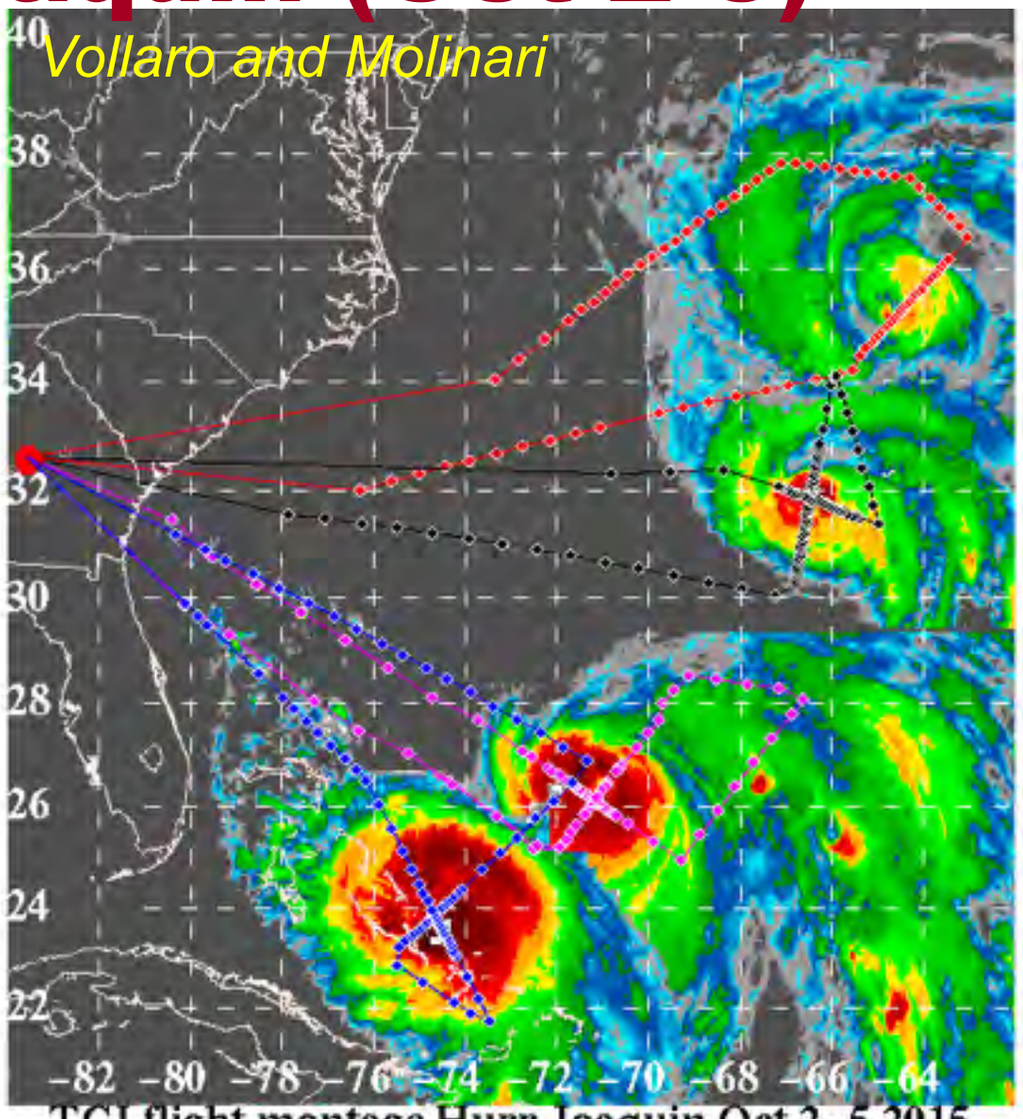

TCI flight montage Hurr Joaquin Oct 2–5 2015

Hurricane Joaquin (Cat 4) was the strongest W. Atlantic Hurricane in 5 years. (poorly forecasted)
TCI performed 4 missions with transects across eye and outflow

Tropical Cyclone Intensity (TCI)

Hurricane Patricia (Oct 20-24)

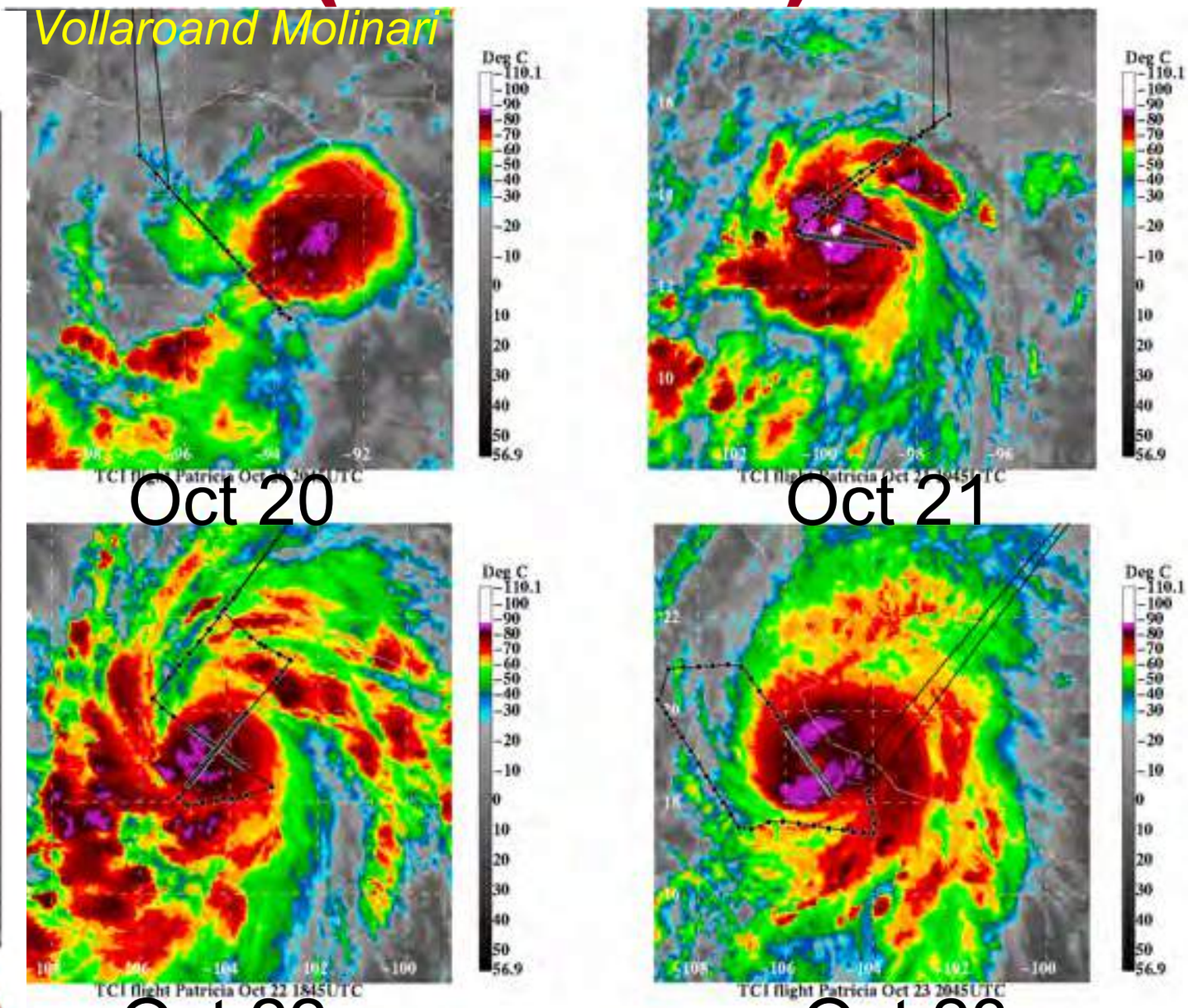

Hurricane Patricia was most intense TC on record (max wind ~185 kts) and was poorly forecasted
Intensified from a TS to Cat 5 in 24 h
46 dropsondes across Patricia at 2 nmi on 23 Oct

Datasets

- Quality controlled HDSS dropsondes
- Airborne Doppler radar from NOAA P3
- Hourly Atmospheric Motion Vectors

Date	# of Sondes
20-Oct	13
21-Oct	77
22-Oct	83
23-Oct	84

Analysis Methodology

- SAMURAI 3DVAR analysis (Bell et al. 2012)
- Combine observations in both Cartesian and cylindrical (axisymmetric) geometry
- No background field, and no balance or physical constraints other than mass continuity

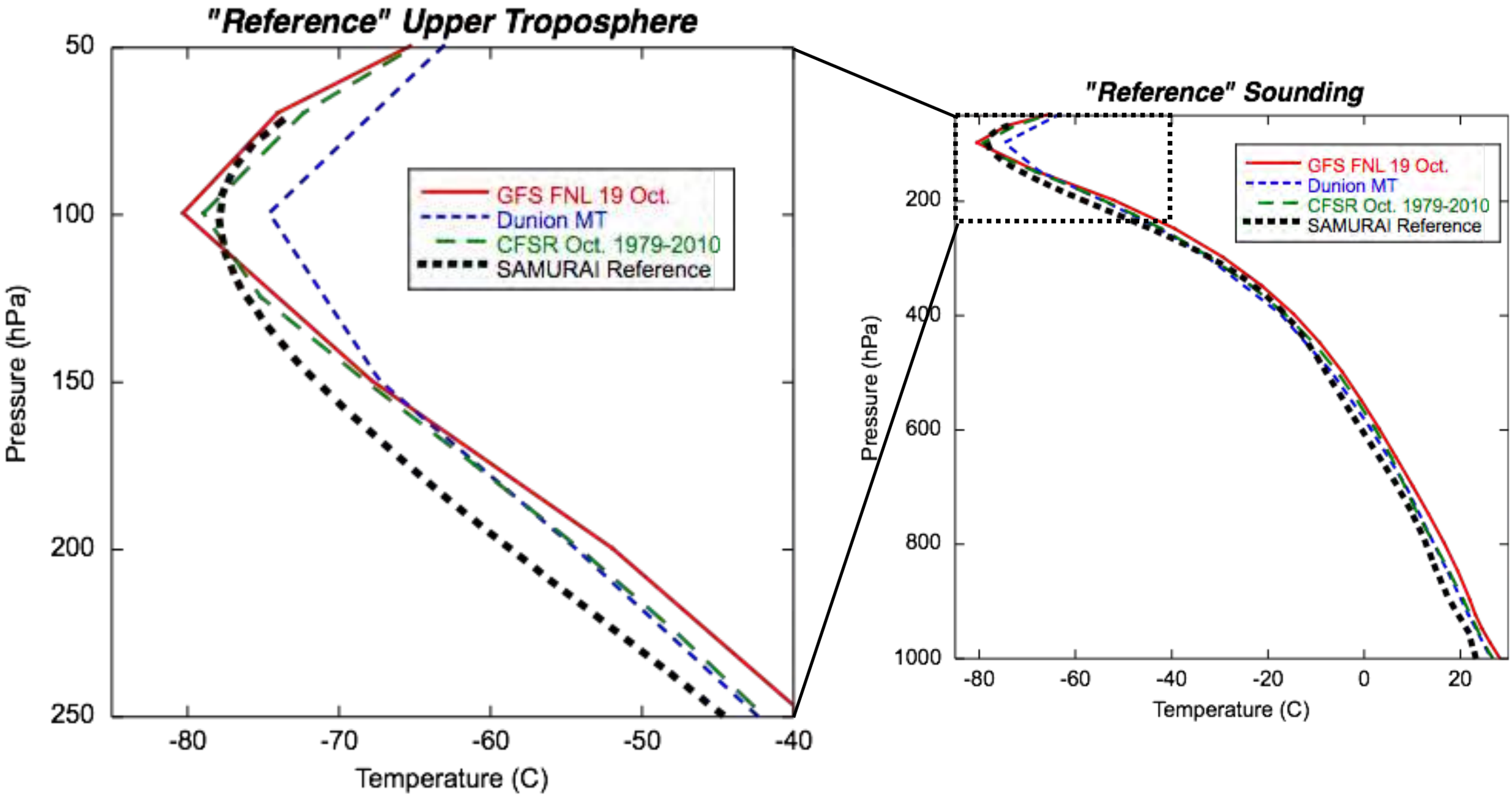

See Stern and Zhang (2016) for more on warm core reference state

18 UTC October 22 at 2 and 6 km altitude

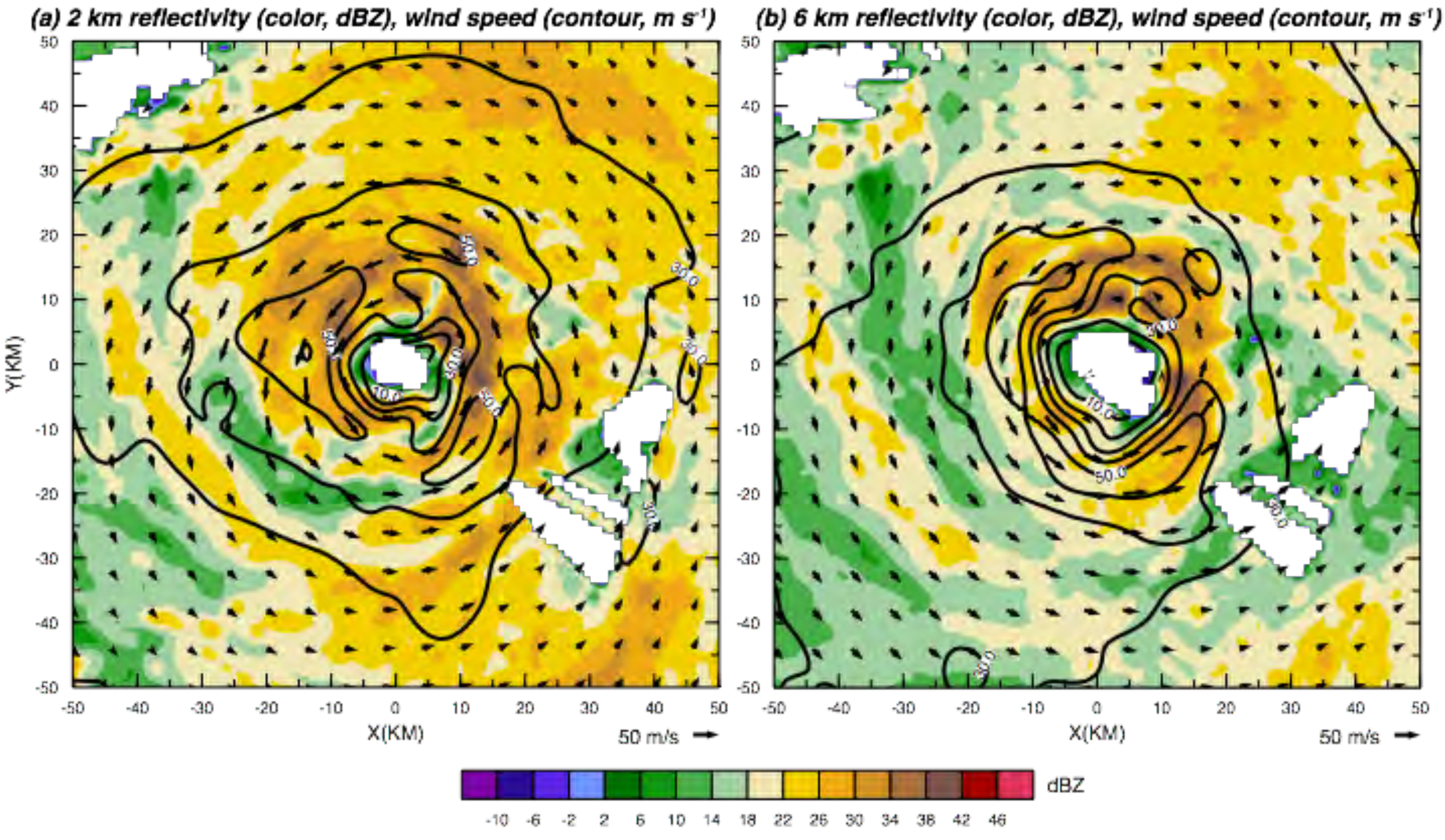

Preliminary analysis

18 UTC October 22 at 2 and 6 km altitude

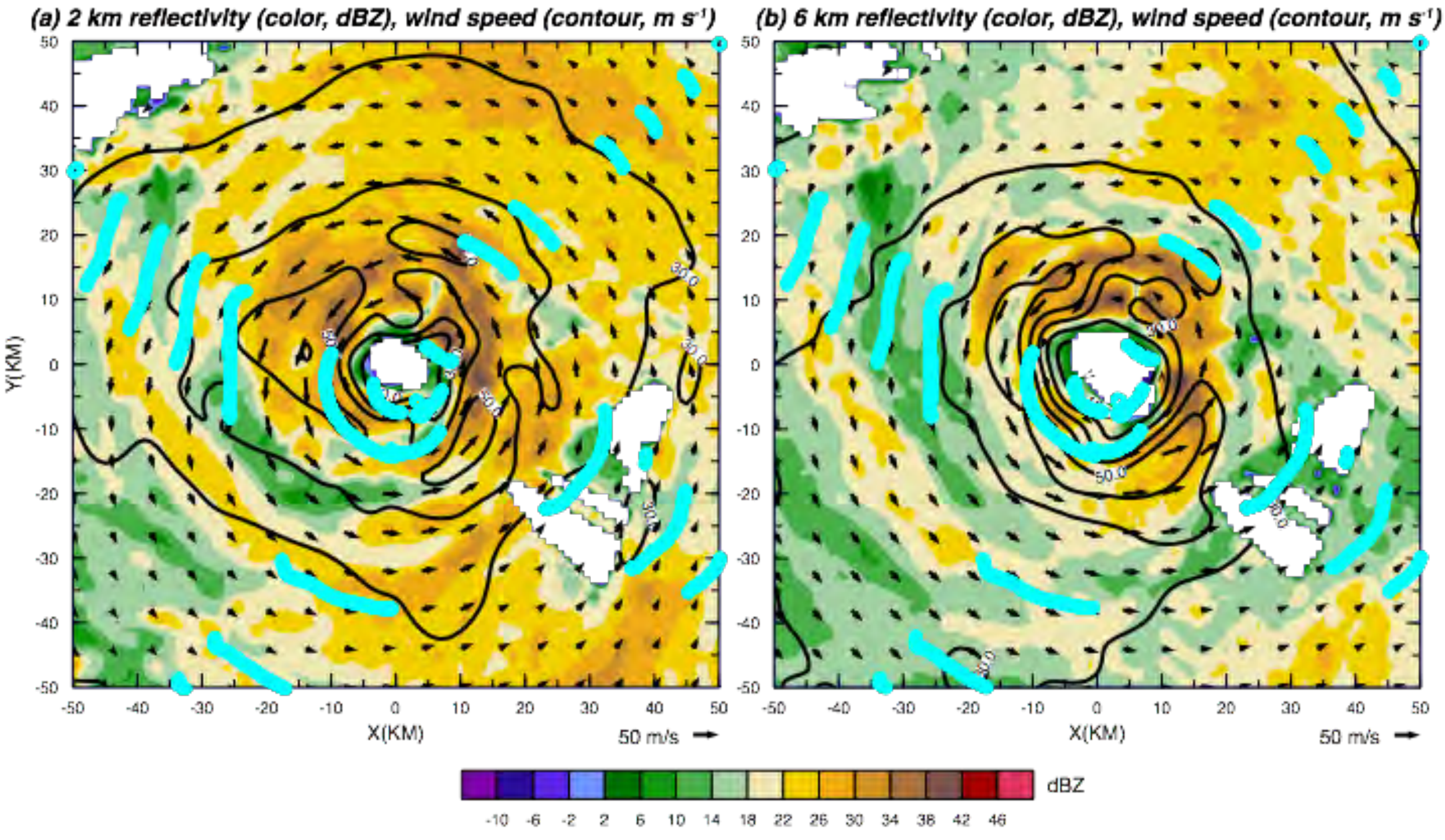

Preliminary analysis

18 UTC October 22 Axisymmetric Structure

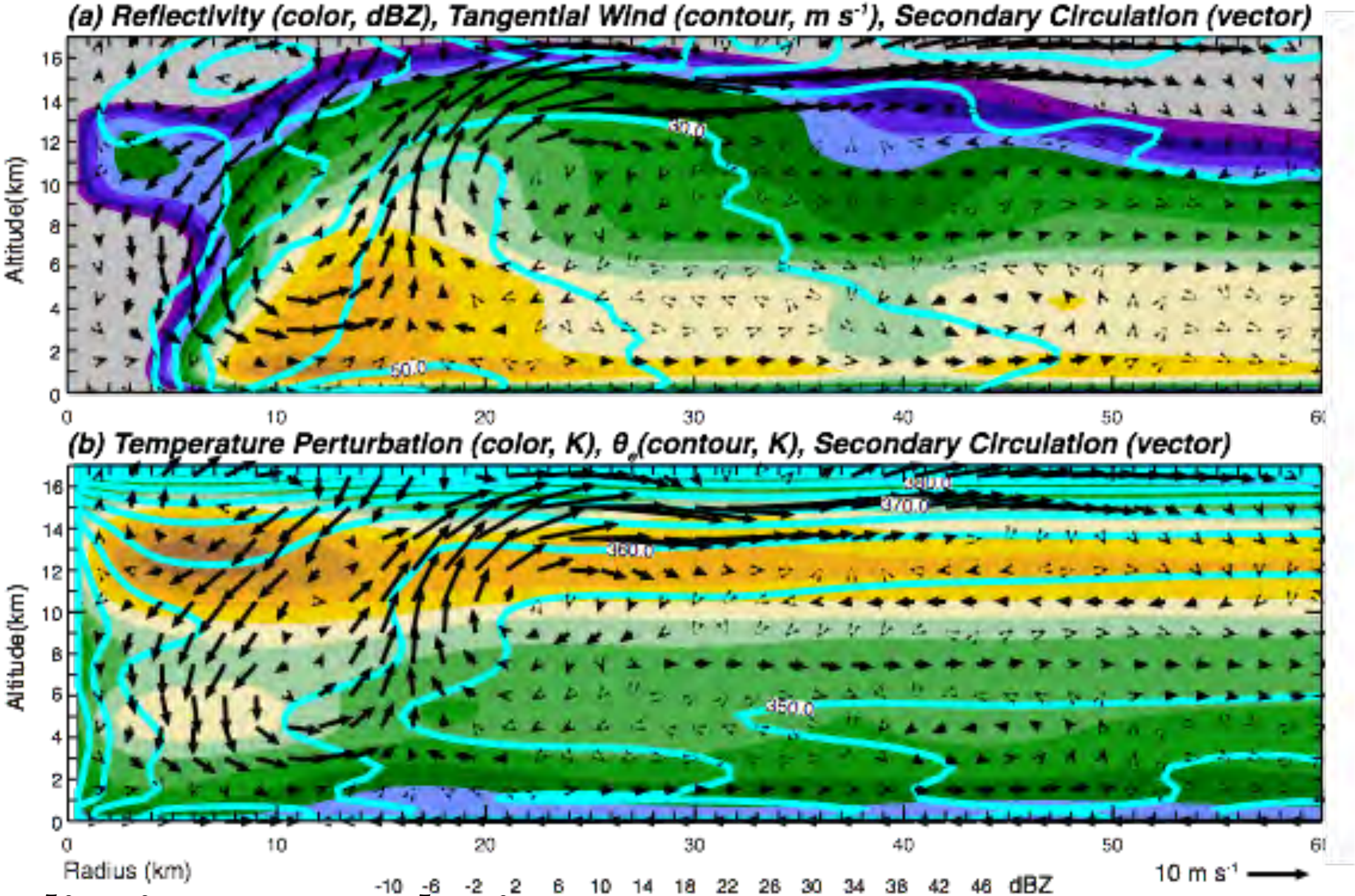

Preliminary analysis

18 UTC October 22 Axisymmetric Structure

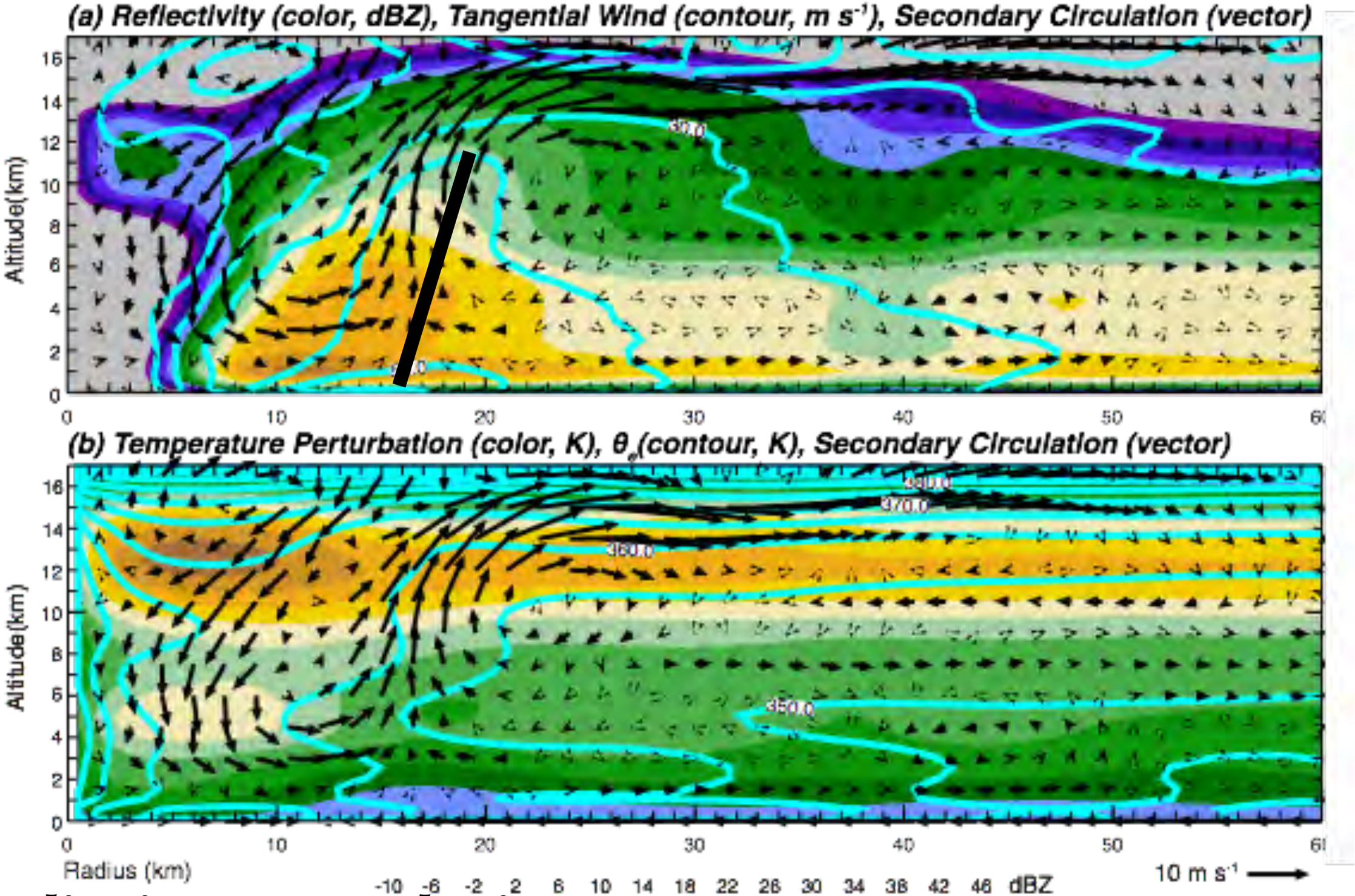

Preliminary analysis

20 UTC October 23 at 2 and 6 km altitude

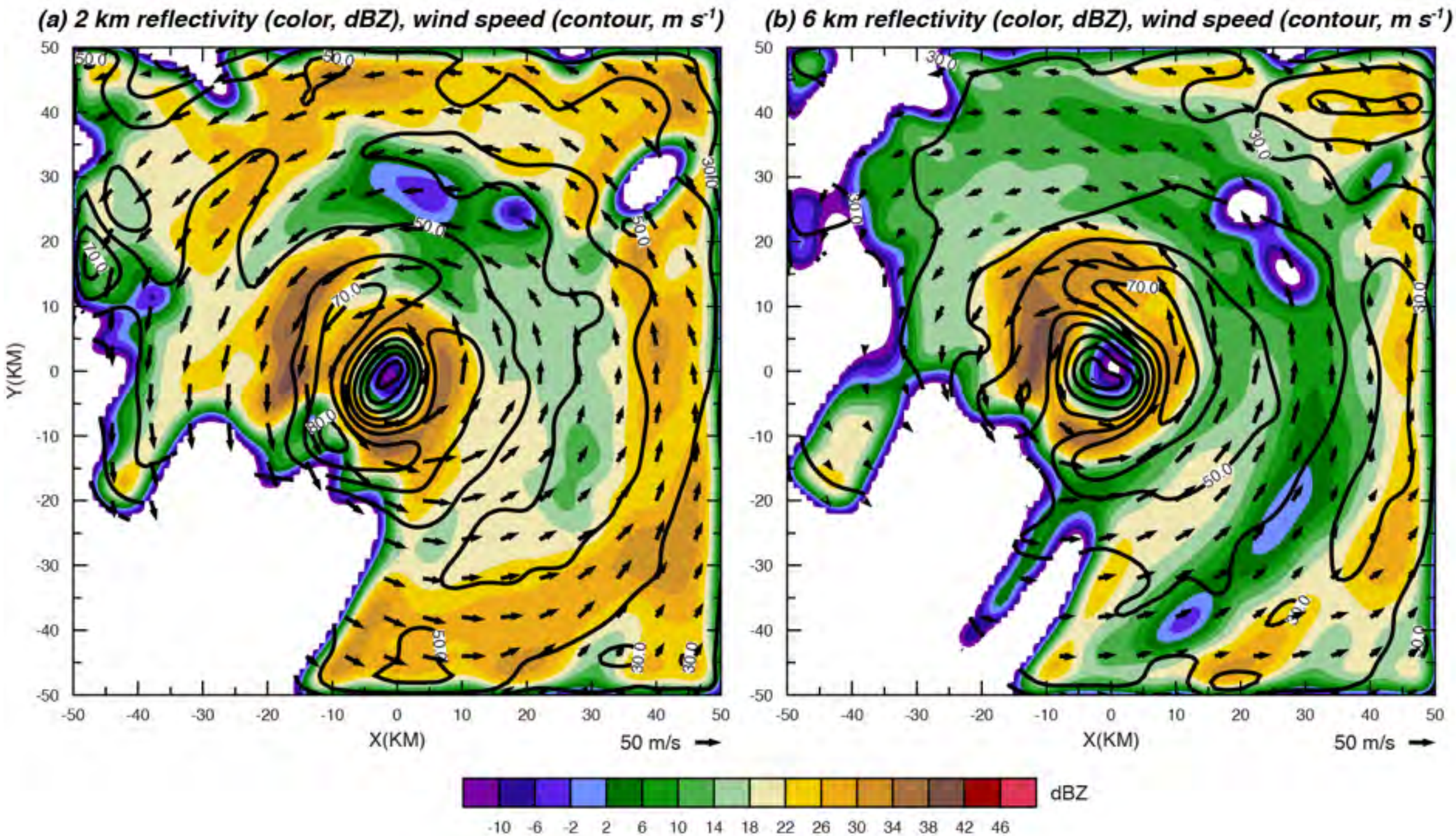

Preliminary analysis

(a) 2 km reflectivity (color, dBZ), wind speed (contour, m s^{-1})

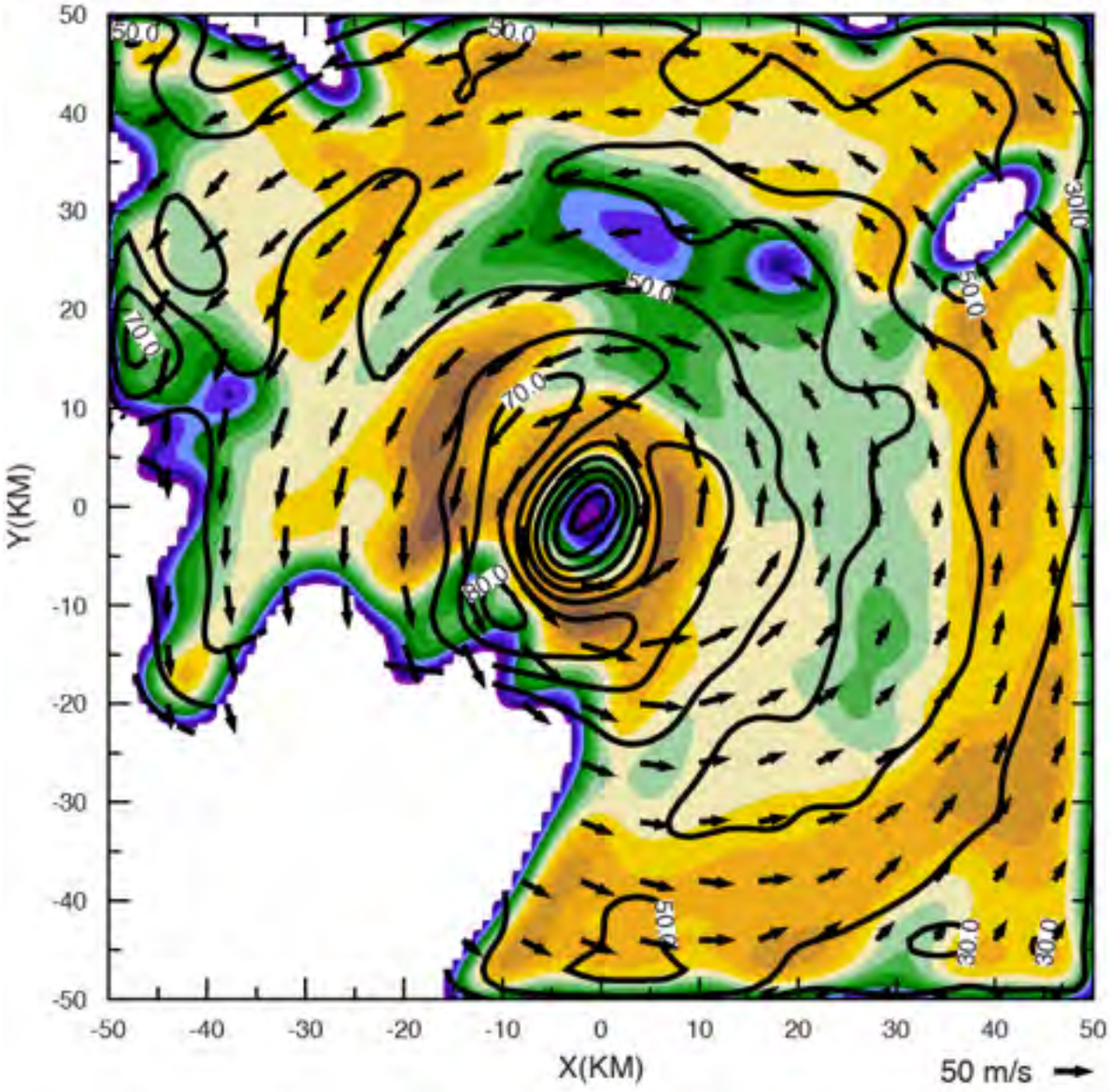

(b) 6 km reflectivity (color, dBZ), wind speed (contour, m s^{-1})

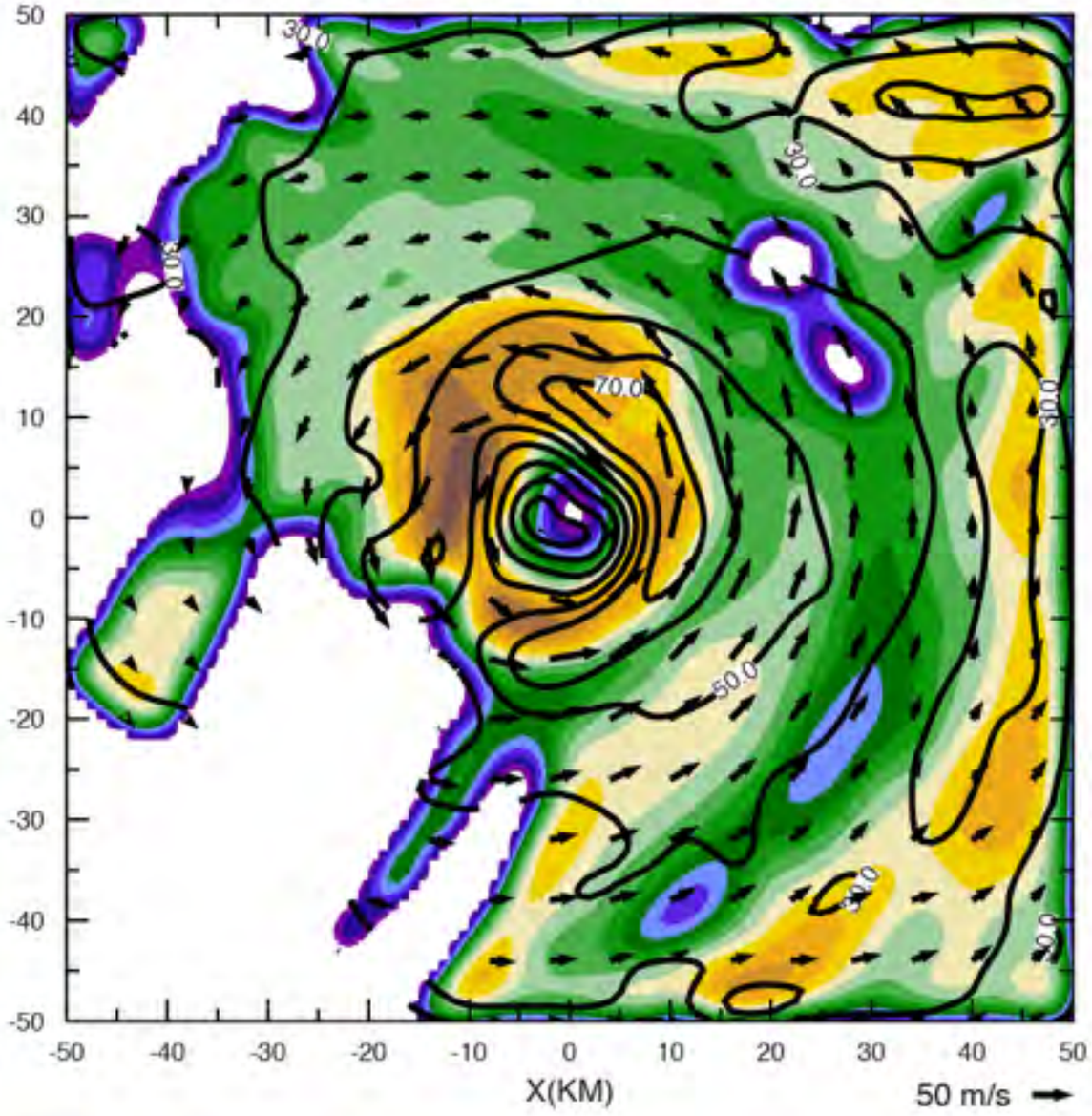

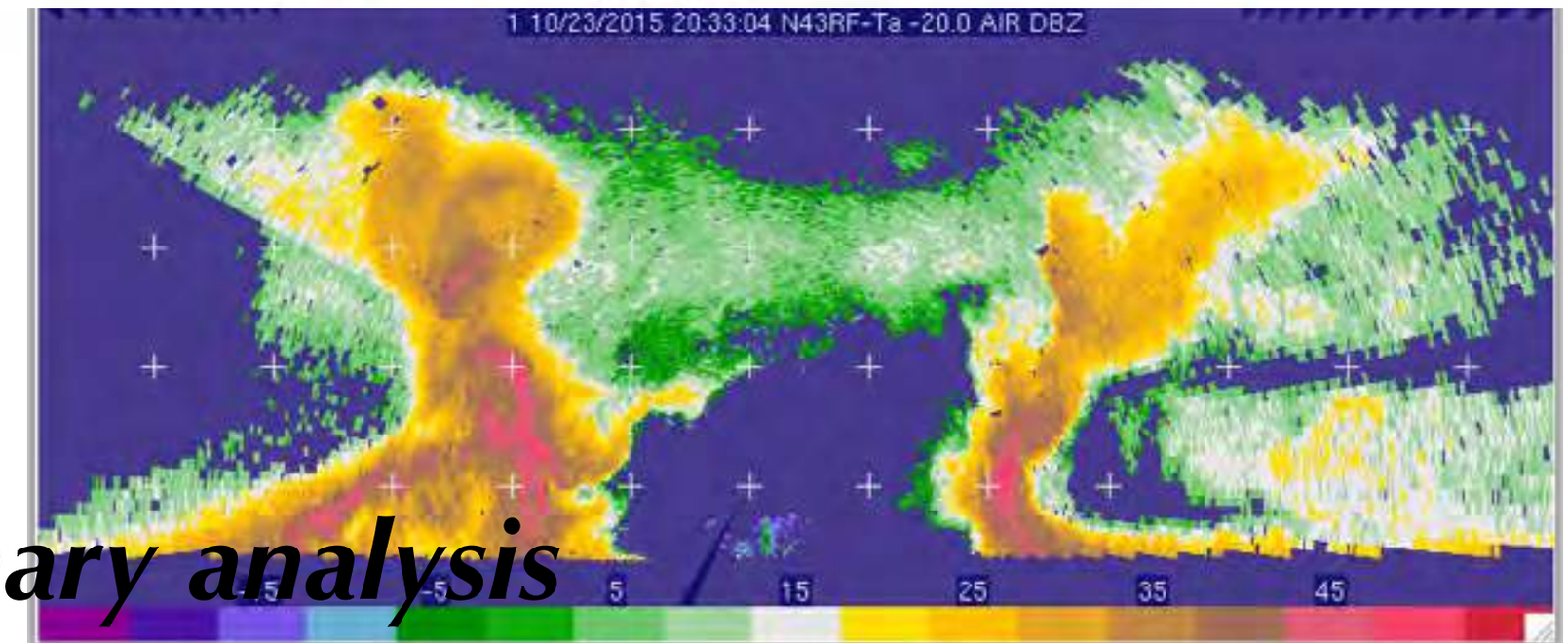

Preliminary analysis

(a) 2 km reflectivity (color, dBZ), wind speed (contour, m s^{-1})

(b) 6 km reflectivity (color, dBZ), wind speed (contour, m s^{-1})

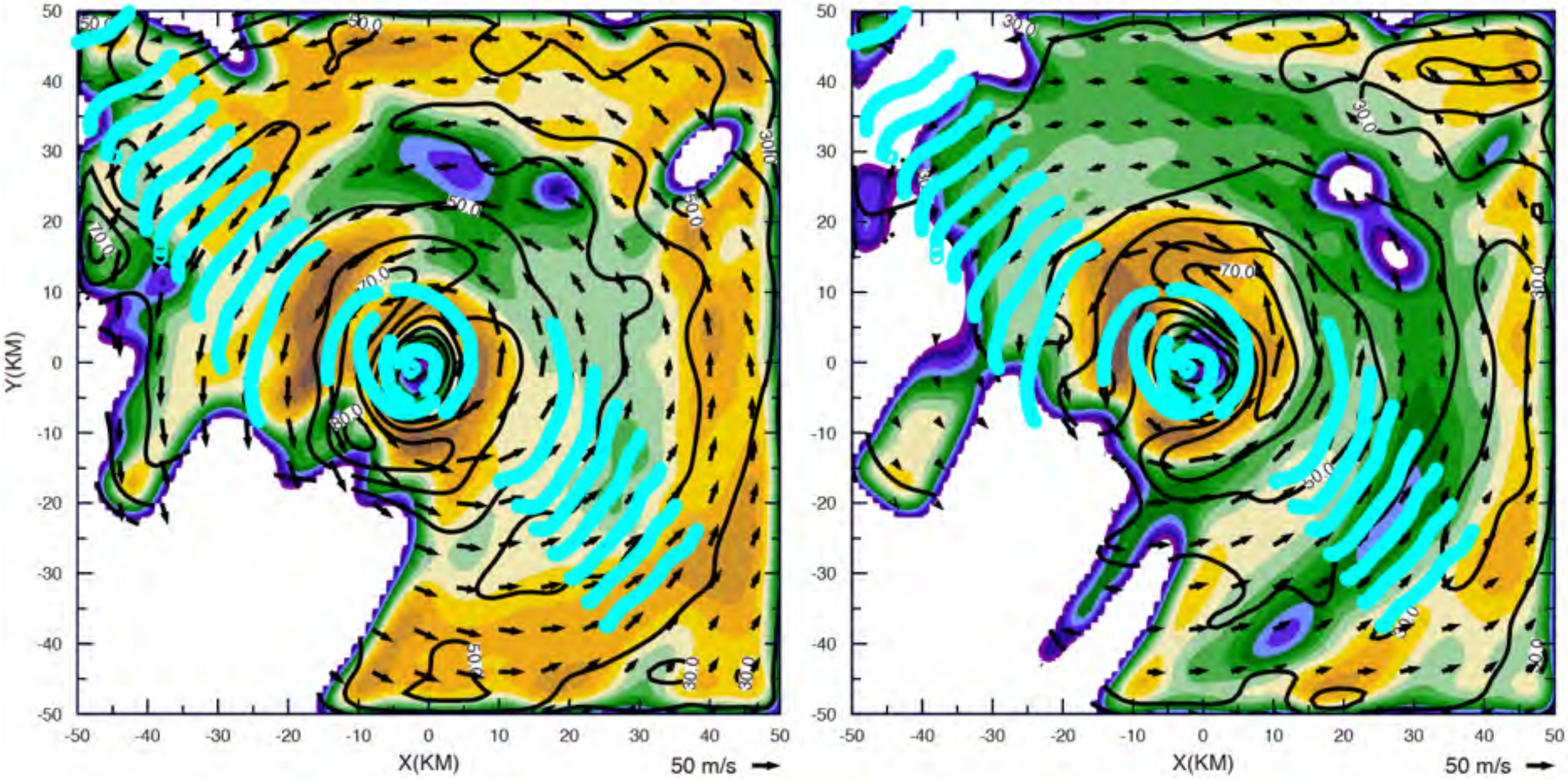

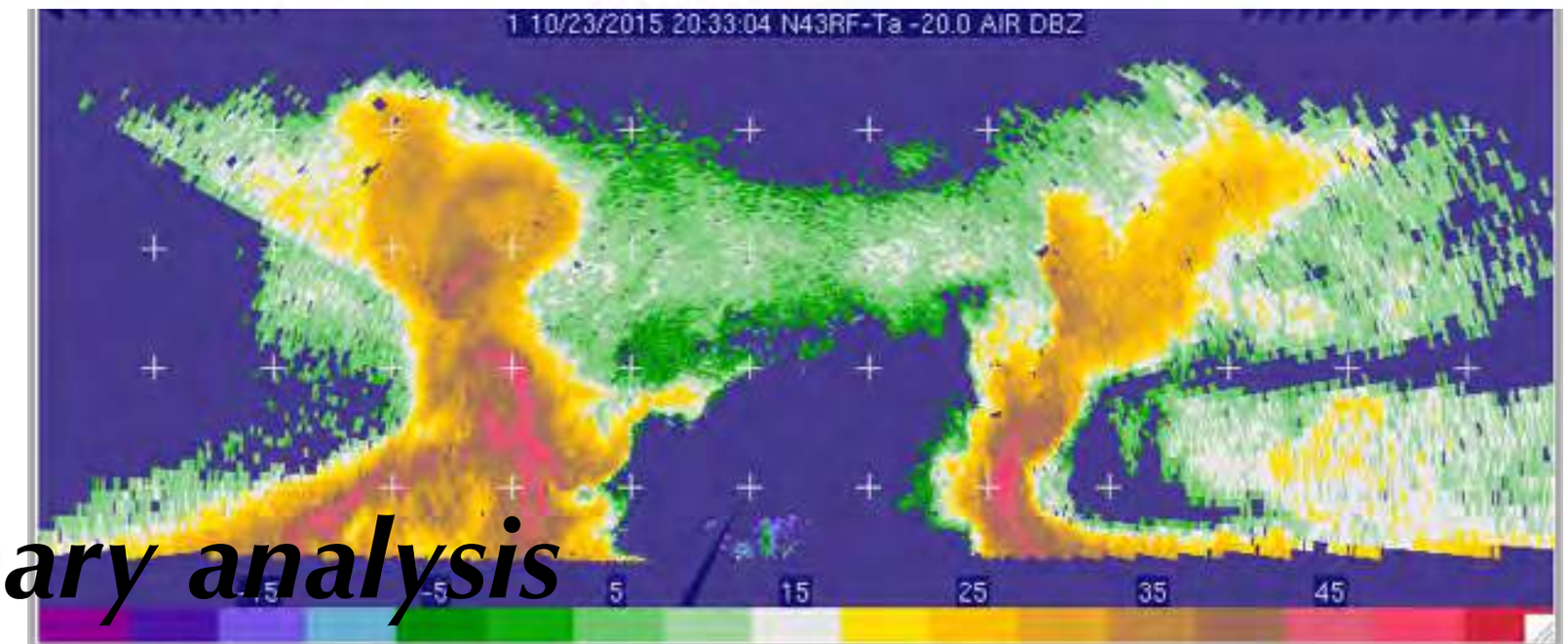

Preliminary analysis

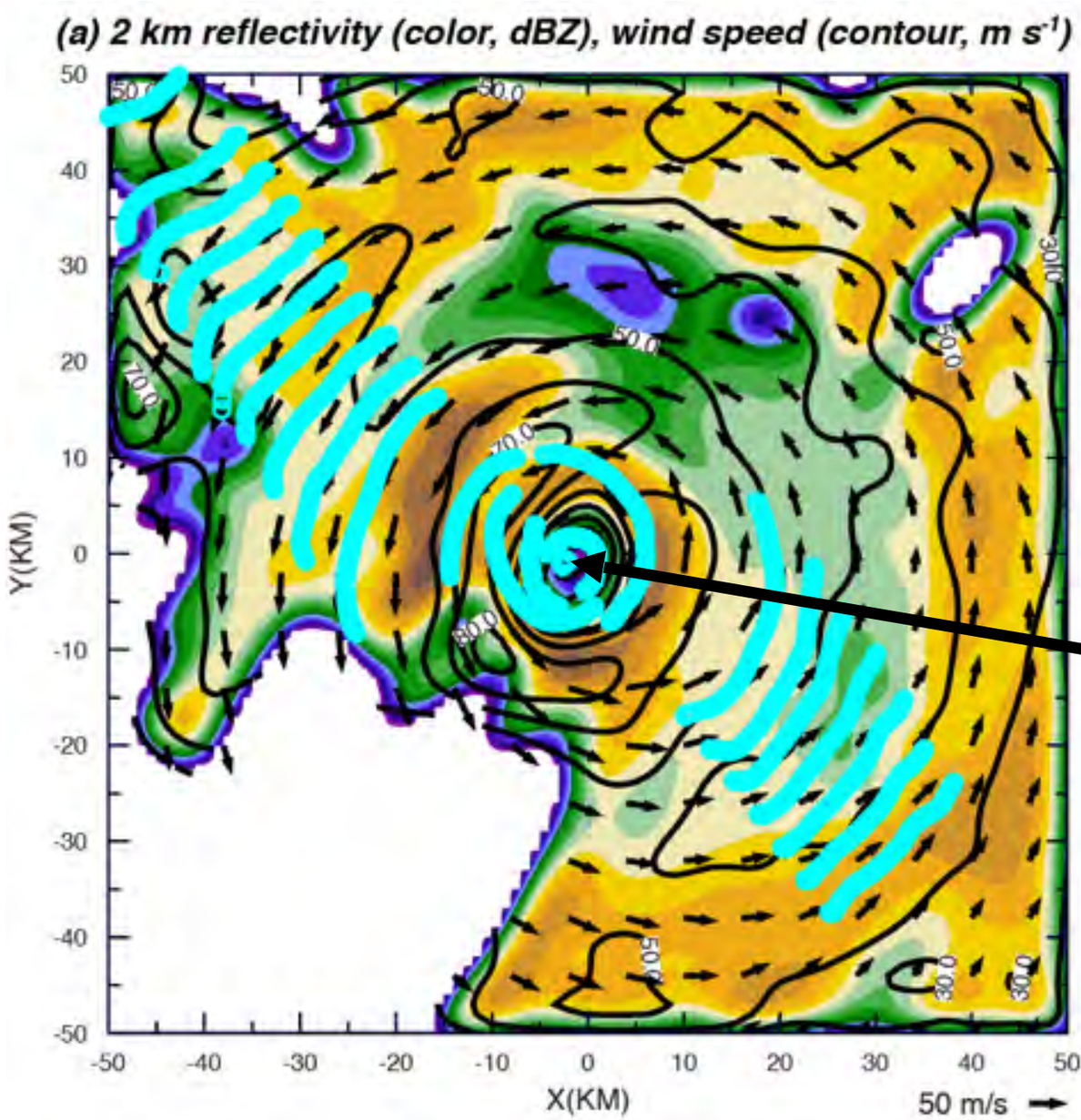

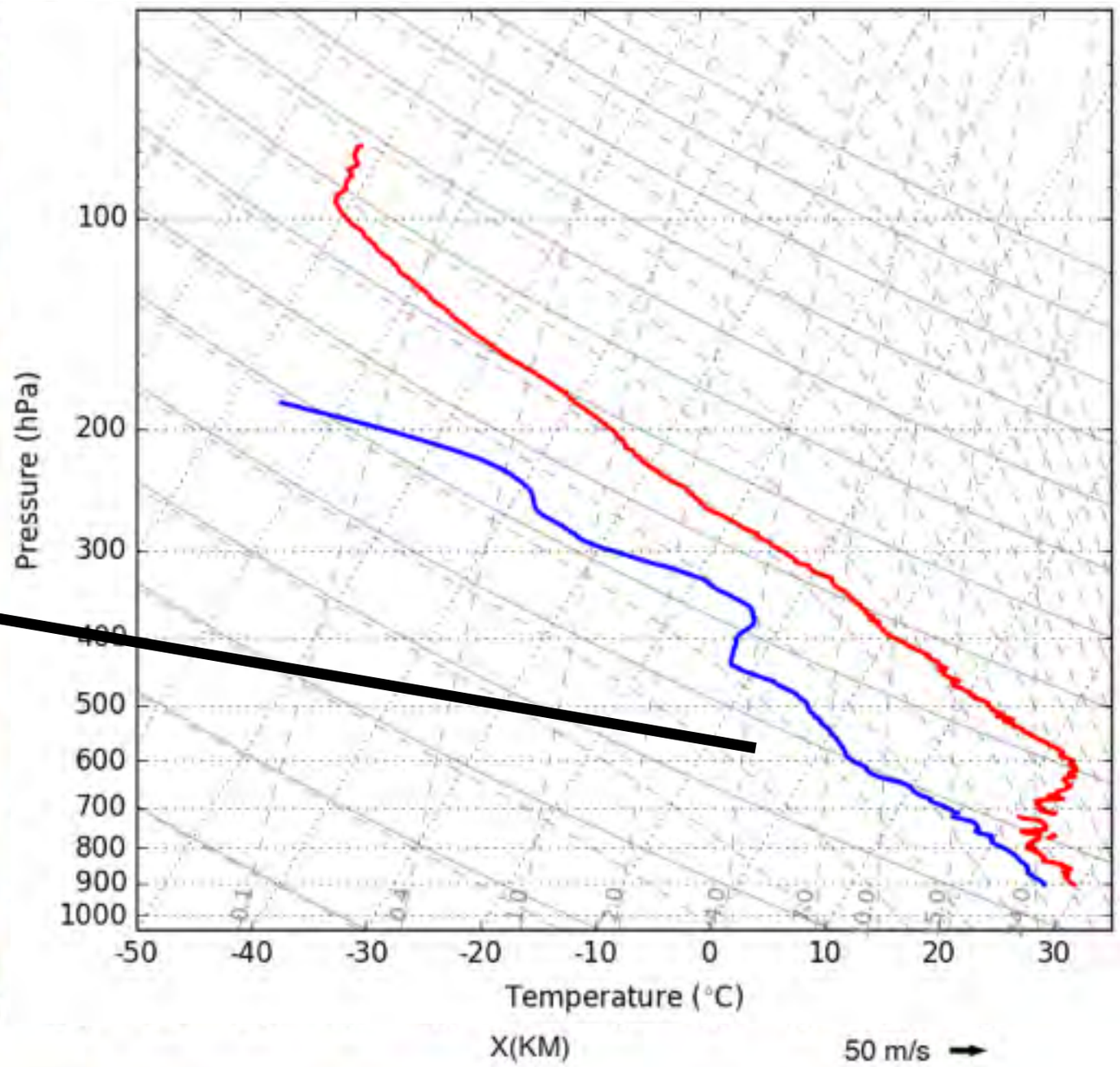

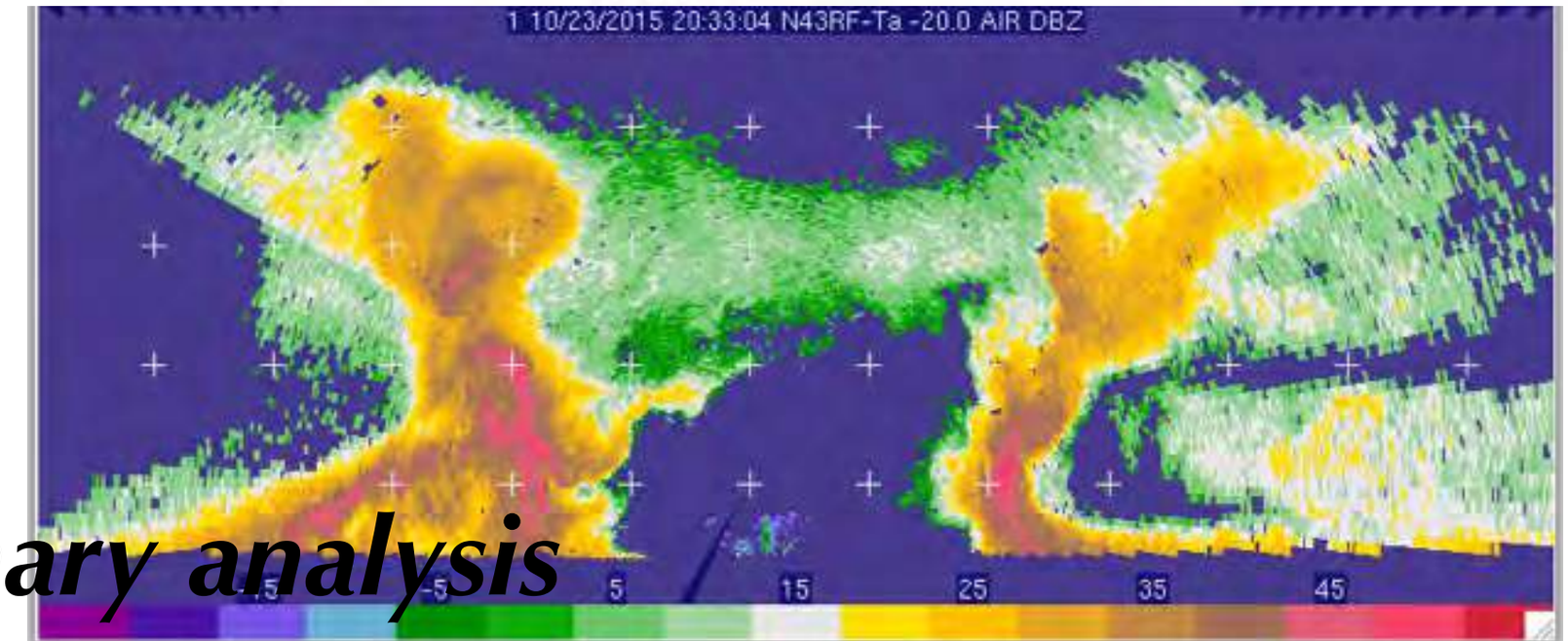

Preliminary analysis

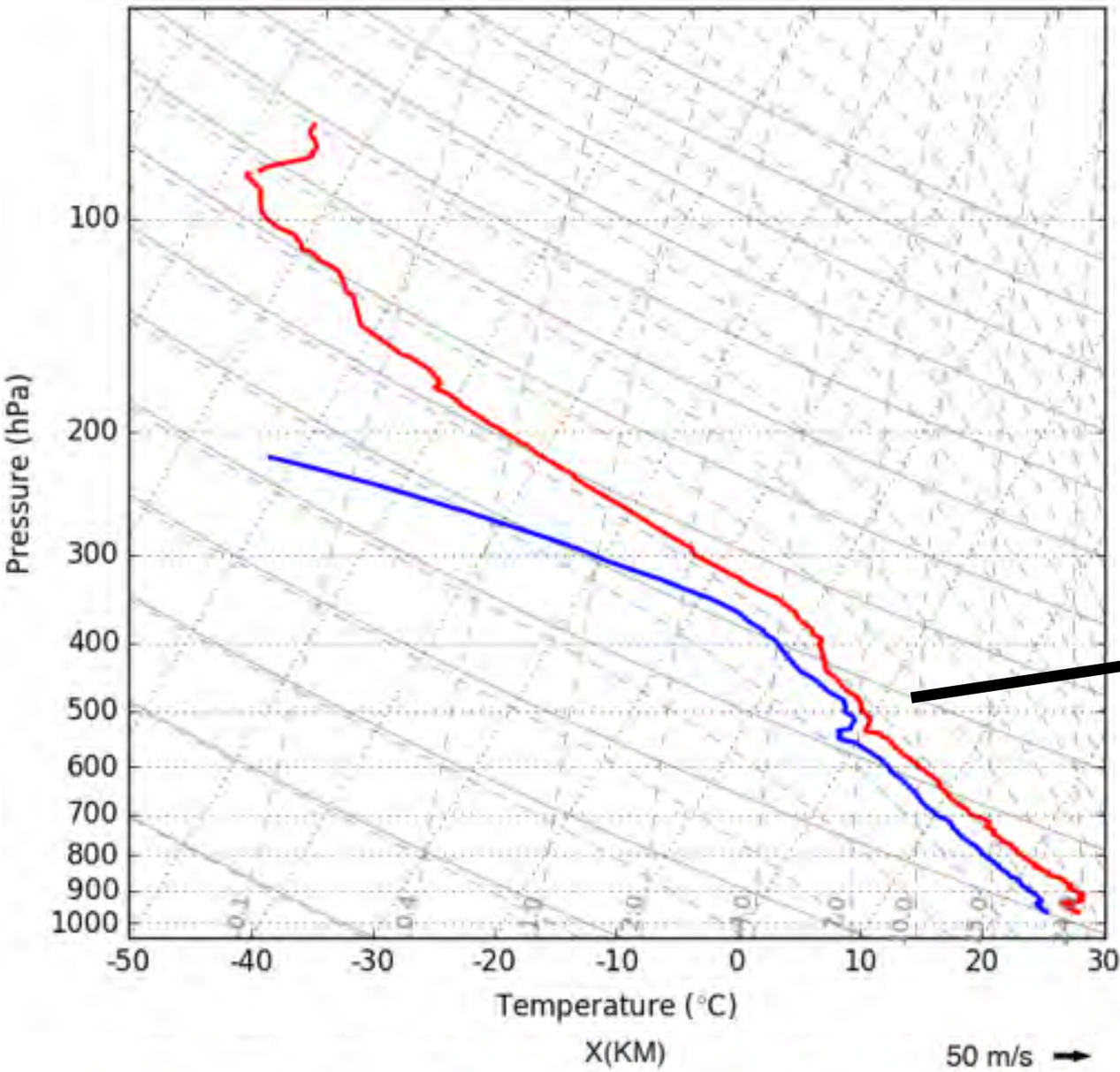

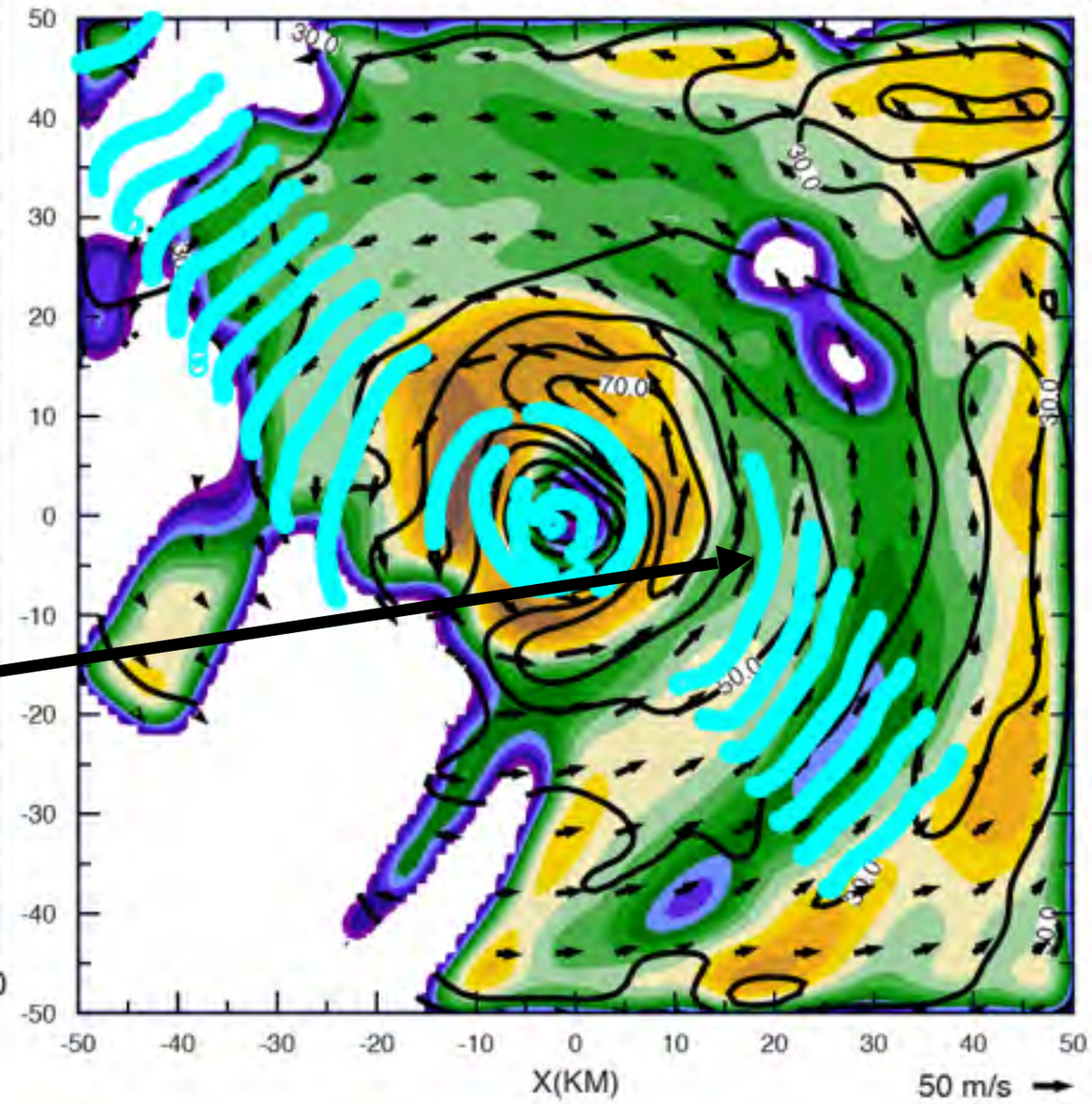

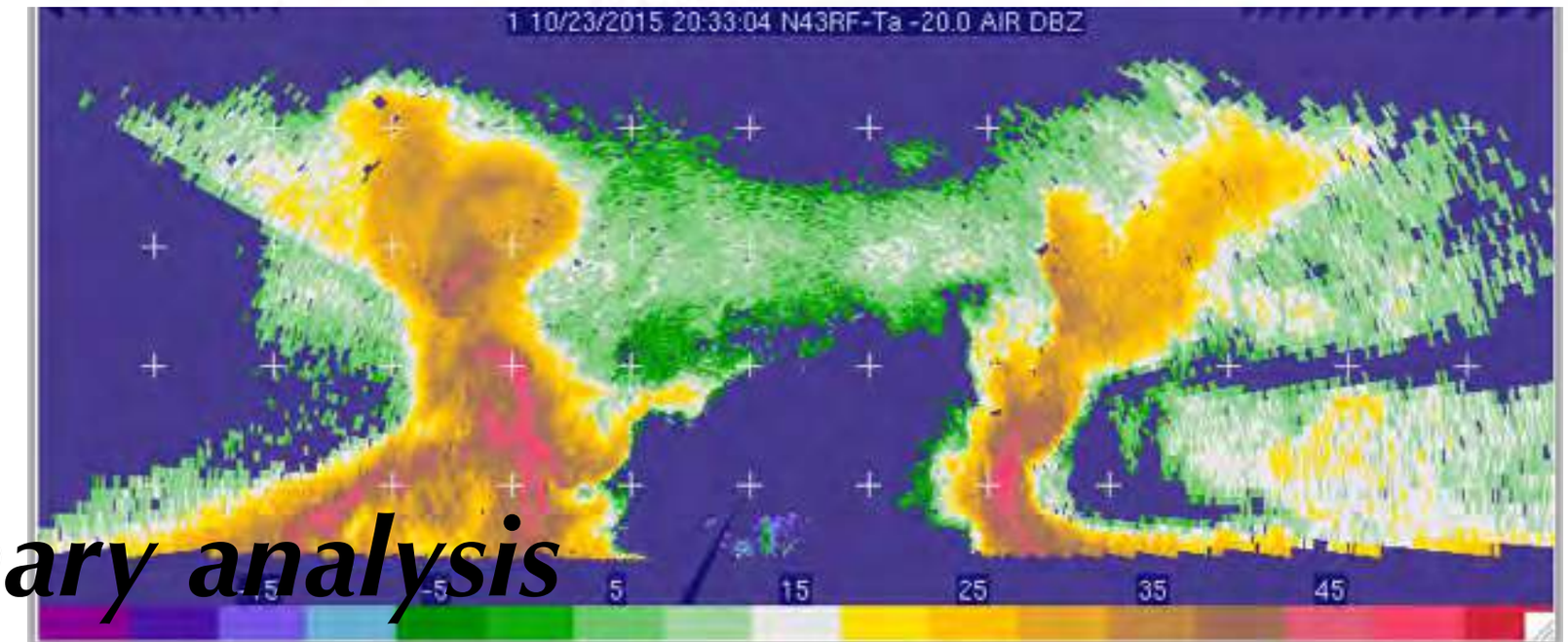

Preliminary analysis

20 UTC October 23 Axisymmetric Structure

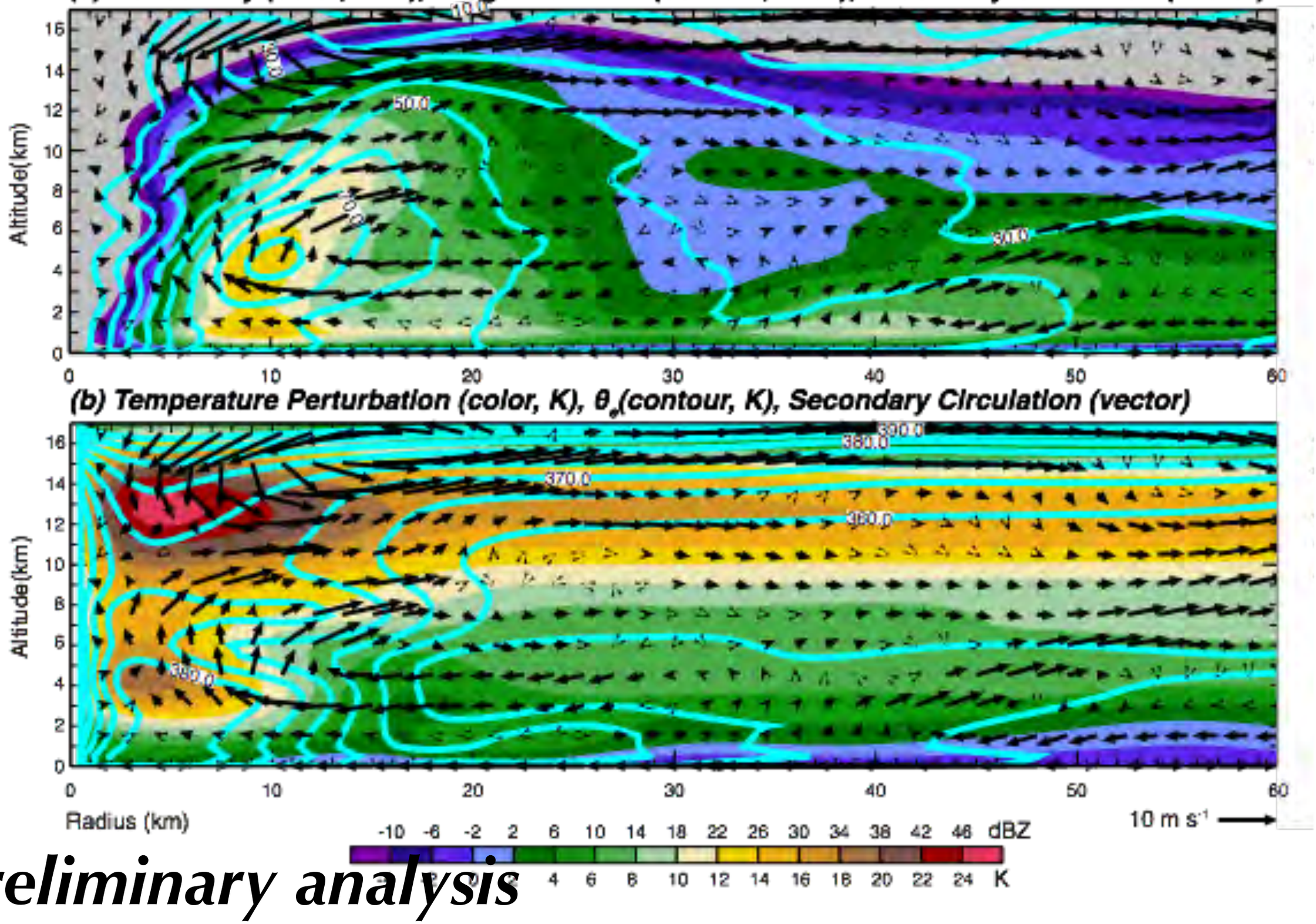

Preliminary analysis

20 UTC October 23 Axisymmetric Structure

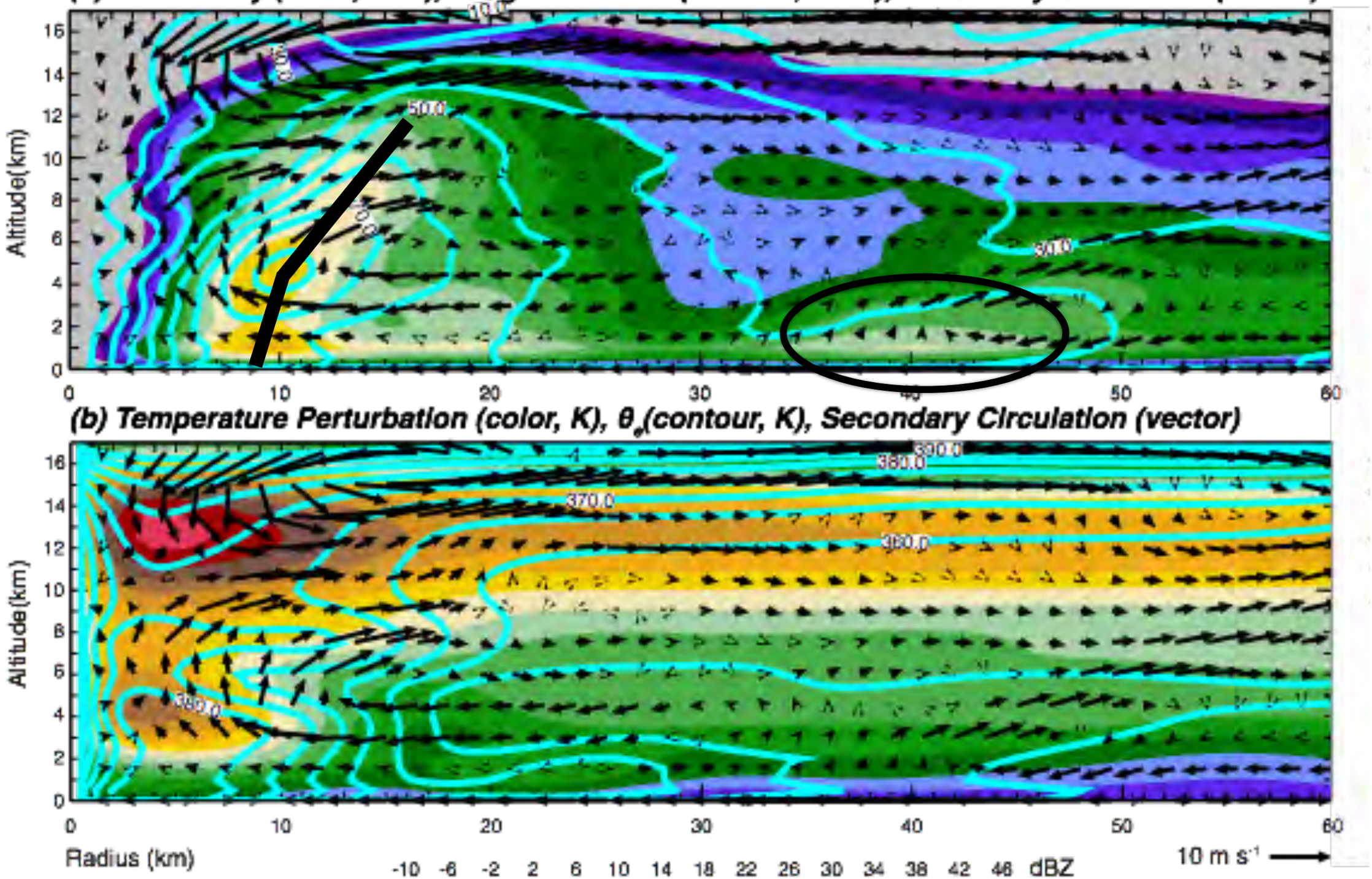

Preliminary analysis

Summary of Preliminary Results from TCI-2015

- An excellent full-tropospheric and lower-stratospheric dataset was collected during TCI-15, including 4 days during Hurricane Patricia's rapid intensification
  - Data is restricted for 1-year, but open to collaborators

- Preliminary SAMURAI analyses combining AMVs, HDSS dropsondes, and P-3 Doppler radar show consistent kinematic and thermodynamic structures

- Further analysis should provide interesting insights into rapid intensification, extreme intensity, and the outflow structure of tropical cyclones

Newly Developed and Future Airborne Technologies

National Center for Atmospheric Research
Earth Observing Laboratory

HIAPER Cloud Radar

The HIAPER Cloud Radar (HCR) is a research-grade airborne millimeter wavelength radar that serves the atmospheric science community by providing remote sensing capabilities to the NSF/NCAR HIAPER aircraft. The combination of the high sensitivity and high resolution HCR measurements and the high-altitude, long-range capabilities of HIAPER provides the ability to study a wide range of clouds in remote regions. The HCR makes dual-polarization and Doppler measurements that are useful for estimating microphysical and dynamical cloud characteristics. Thus, the HCR can be used to study cloud microphysics and document cloud properties in remote locations such as over the oceans and in arctic regions, benefitting research ranging in scale from cloud scale processes to determining how cloud systems impact regional and global climate.

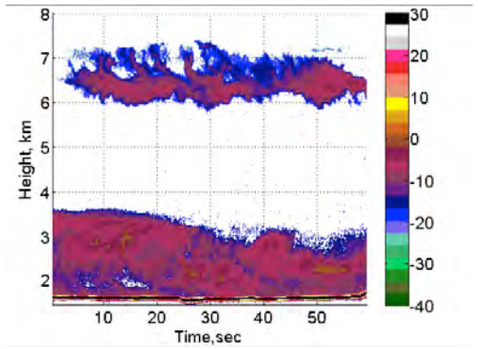

Time-height plot of reflectivity (dBZ) looking in the nadir direction for 1 minute of NSF/NCAR HIAPER flight.

Requestable Facility

About APAR

The proposed APAR system consists of four removable, C-band active electronically scanned array antennas (AESA) strategically mounted on the fuselage of the NSF/NCAR C-130 turboprop aircraft, using aerodynamic fairings. Two AESAs will be mounted on either side of the fuselage behind the rear doors; the third will be mounted on the top of the fuselage and the fourth on the upper portion of the tail ramp. Each AESA measures approximately 1.5 m x 1.9 m and is composed of 3584 active, radiating elements, arranged in a rectangular array of 7 x 8 line replaceable units (LRU). Each LRU is composed of 64 radiating elements.

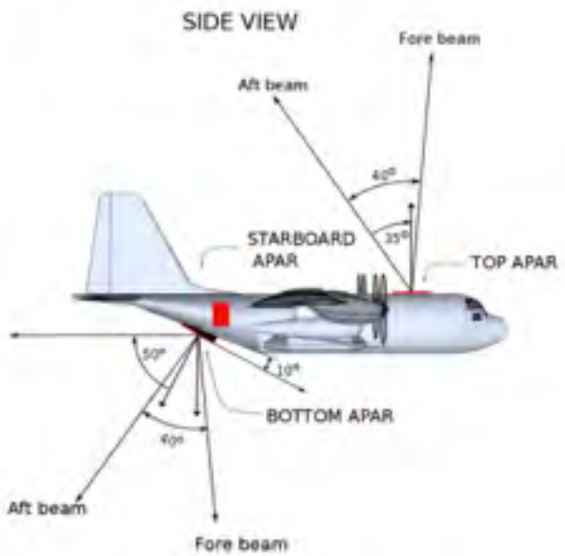

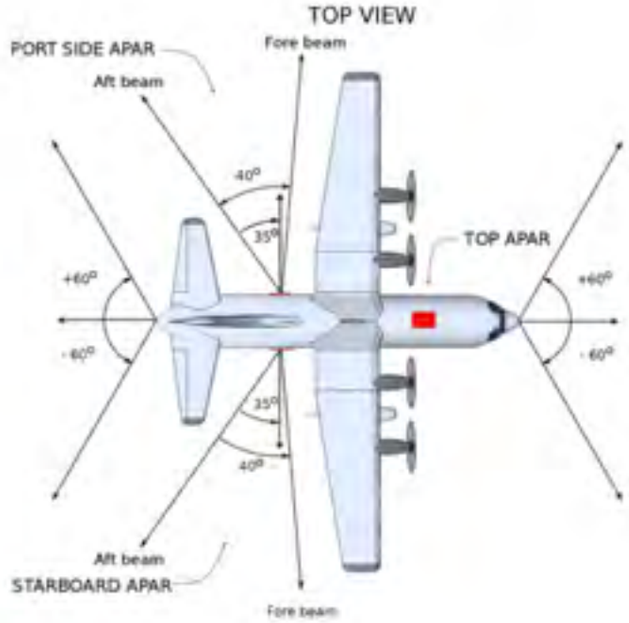

Technical Specifications

- Frequency: 5.35 GHz – 5.45 GHz
- Elements (El/Az): 64/56
- Total Elements per Panel: 3584
- Beamwidth (El/Az): 1v.6°/1.8°
- Antenna Gain: 41 dB
- MDR @ 10 km: -15 dBZ
- Peak Transmit Power: 14.3 kW
- Polarization: Dual Linear
- Spatial Resolution @ 10 km: 314 m
- Along Track spacing: 130 m
- Pulse width: 0.5 μs to 30 μs

Advantages of APAR

APAR will be a state-of-the-art airborne radar, with unique capabilities and auxiliary instruments aboard the C-130 aircraft. It will significantly improve our understanding of processes involving raindrops and ice crystals, leading to better estimates of heavy precipitation and potential impacts. The design will be adaptable to other C-130 aircraft operated by many agencies in the United States and other nations, including the U.S. Air Force for hurricane reconnaissance and research.

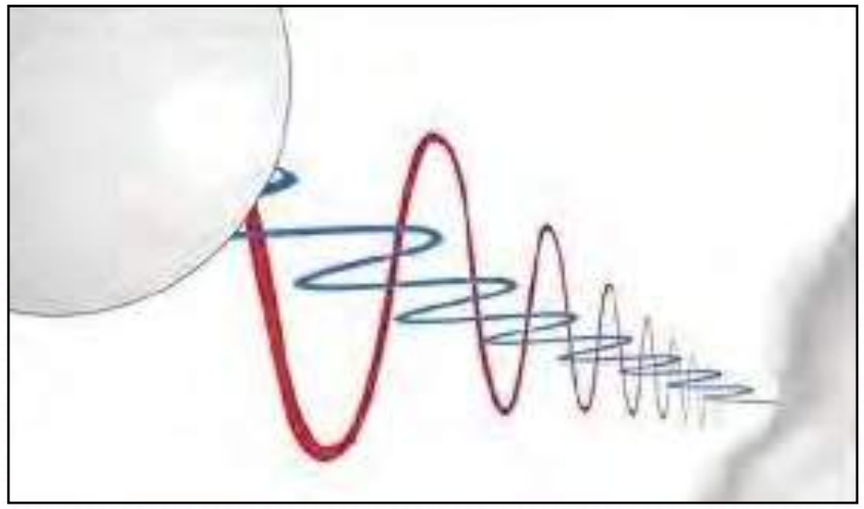

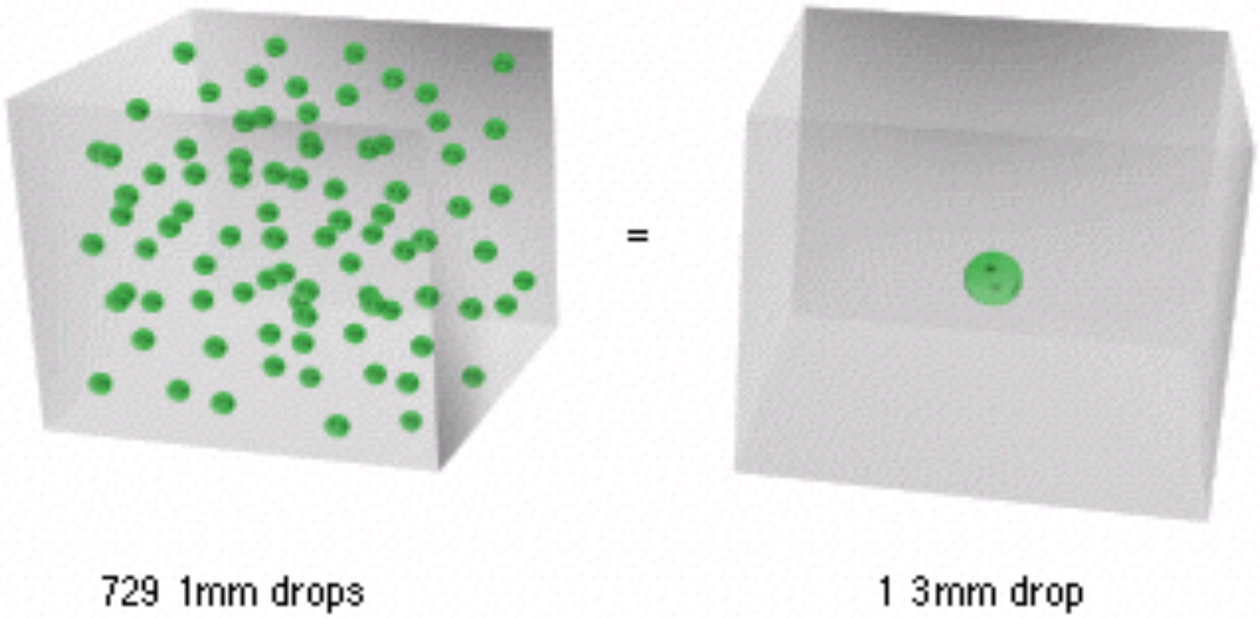

Major Axis Diameter (mm)	Image	ZDR (dB)
< 0.3 mm		~ 0.0 dB
1.35 mm		~ 1.3 dB
1.75 mm		~1.9 dB
2.65 mm		~2.8 dB
2.90 mm		~3.3 dB
3.68 mm	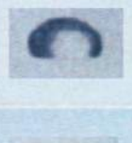	~4.1 dB
4.00 mm		~4.5 dB

$$Z = 10\log_{10}\left(\int_0^\infty N(D)D^6\,dD\right)$$

$$Z_{DR} = Z_H - Z_V$$

Radar Reflectivity (Z_H) proportional to drop size and concentration

Differential Reflectivity (Z_{DR}) proportional to shape and orientation

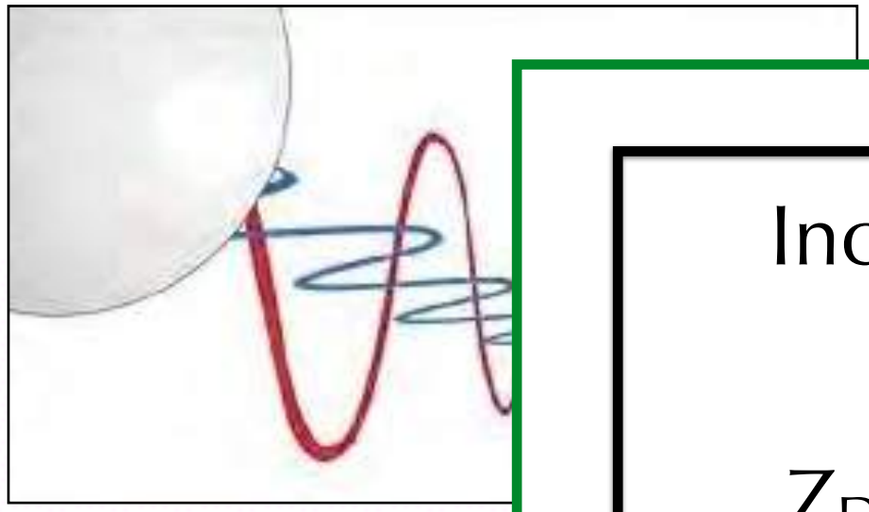

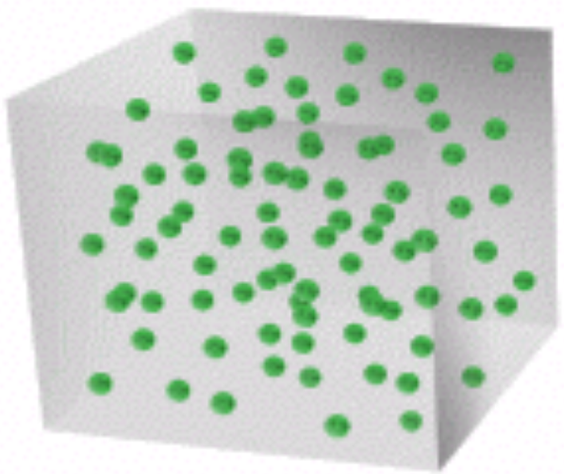

729 1mm drops

=

Increased dB

Z_{DR} ↑

Increased Raindrop Size

Increased dBZ

Z_H →

Increased Rainfall

Image	ZDR (dB)
	~ 0.0 dB
	~ 1.3 dB
	~1.9 dB
	~2.8 dB
	~3.3 dB
	~4.1 dB
	~4.5 dB

Hurricanes Ana and Arthur (2014)

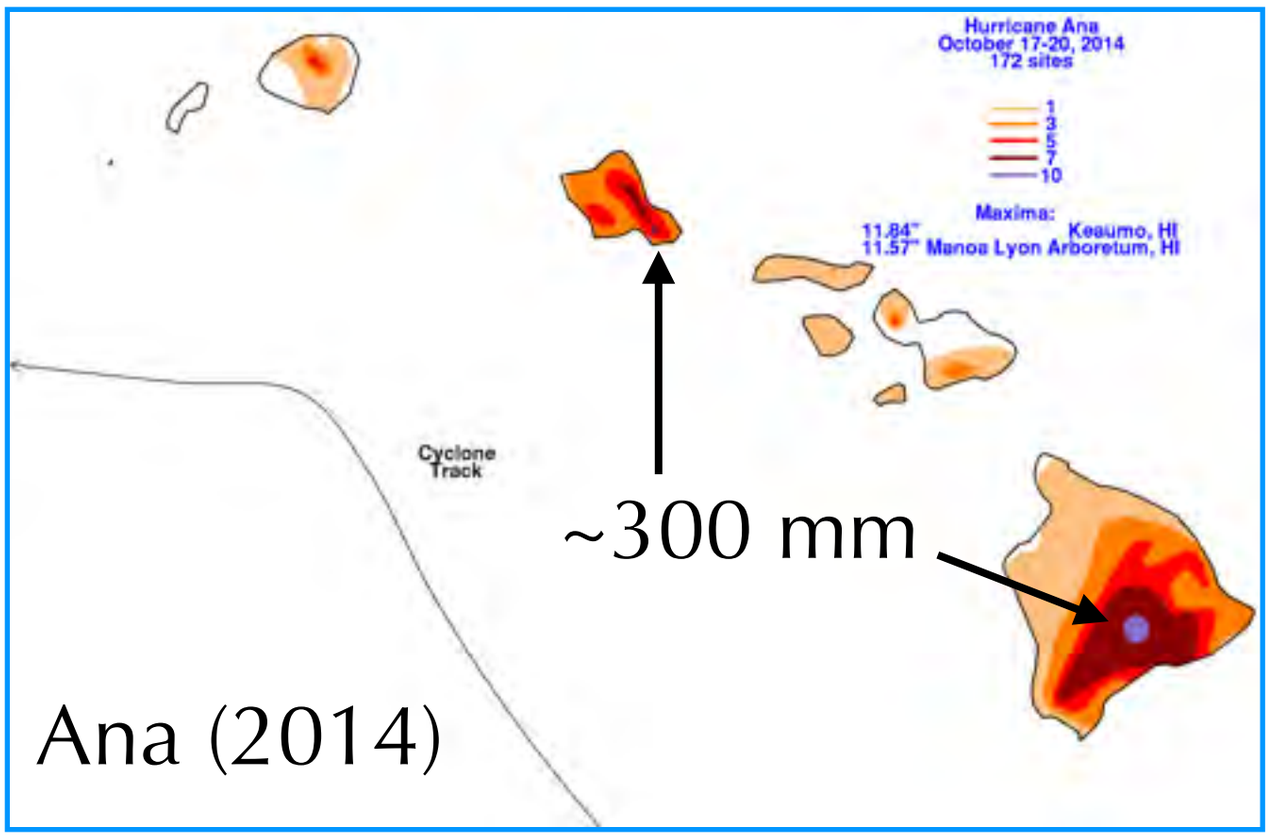

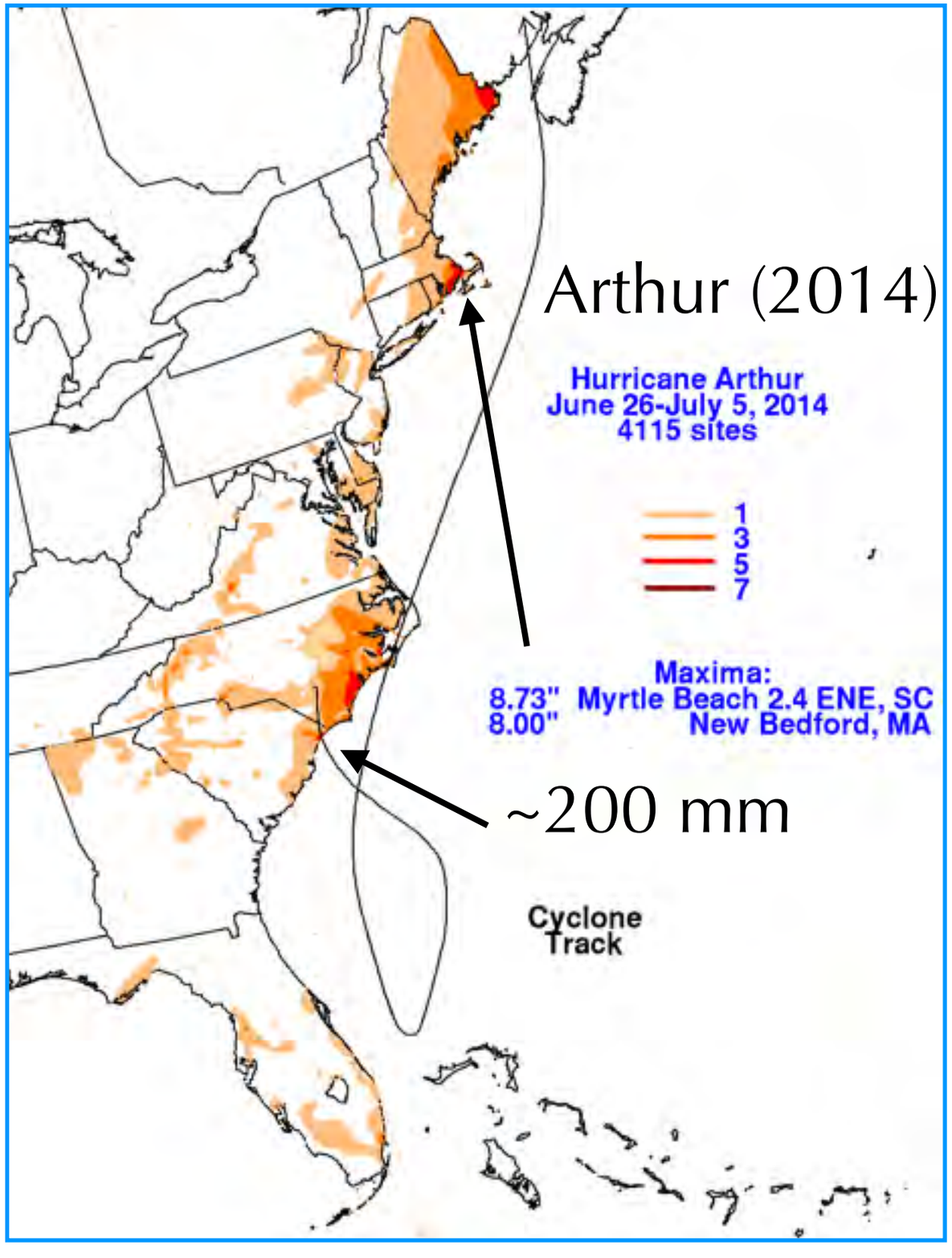

Geophysical Research Letters

AN AGU JOURNAL

Explore this journal >

Open Access

Research Letter

Validation of Simulated Hurricane Drop Size Distributions using Polarimetric Radar

Bonnie R. Brown, Michael M. Bell, Andrew J. Frambach

Experimental Design

- 12/18 Hour WRF ARW v3.6.1 Simulations
- 4 nests down to 2/3 km with TC surface layer
- GFS FNL analysis 1.0 degree cold start
- 2 single-moment (Lin and WSM6), 3 double-moment, 1 bin

	CCN	Cloud	Rain	Ice	Snow	Graupel
WDM6	✓	✓	✓			
Morrison			✓	✓	✓	✓
Thompson	IN ✓ CCN✓	✓	✓	✓		
SBM	✓	✓	✓	✓	✓	✓

- Initial investigation into liquid raindrops only
- Scattering amplitudes used to calculate H & V radar backscatter (Mishchenko 2000, Jung et al. 2010)
- Numerically integrate over drop size distribution from WRF output of N_T and q_r (except SBM)
- Idealized radar with no attenuation, beam broadening, clutter, or noise

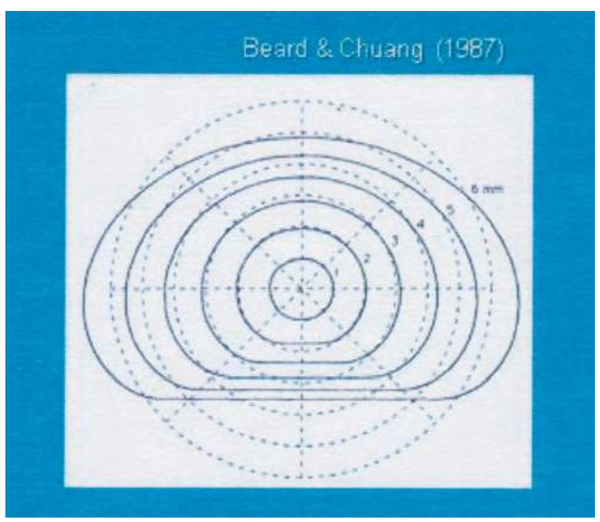

Hurricane Ana (2014)

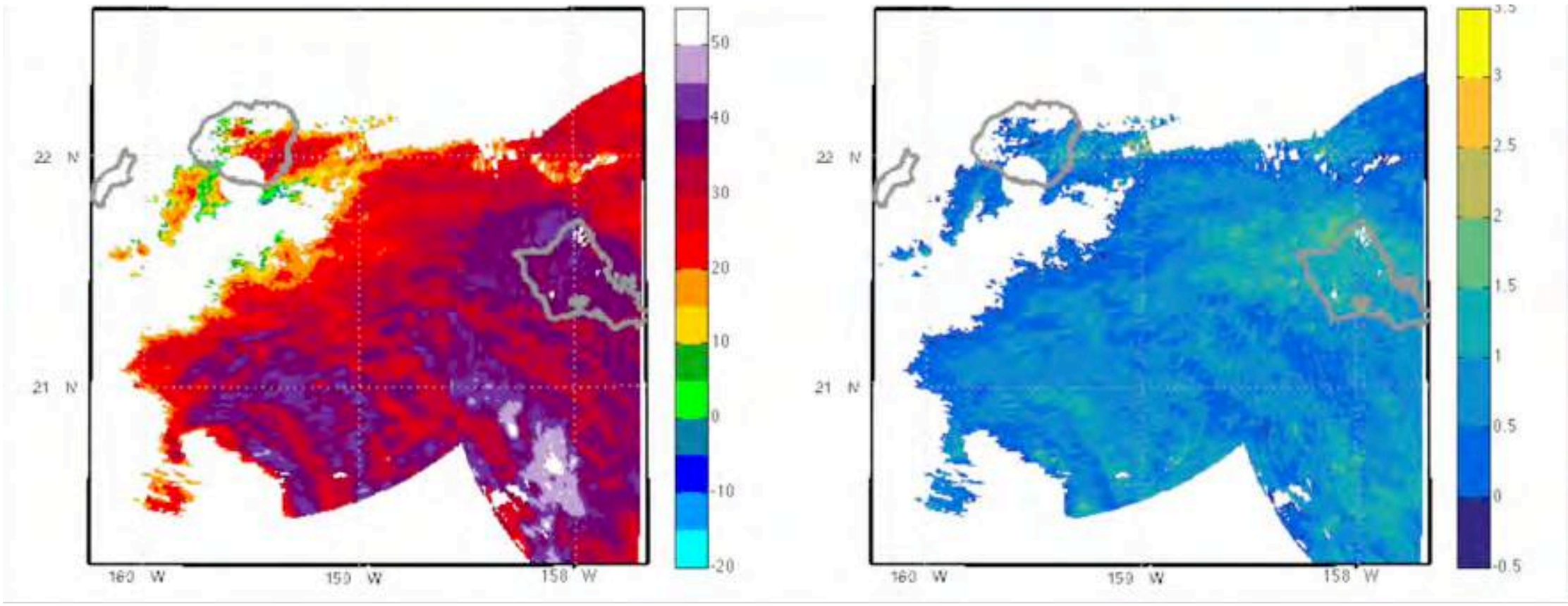

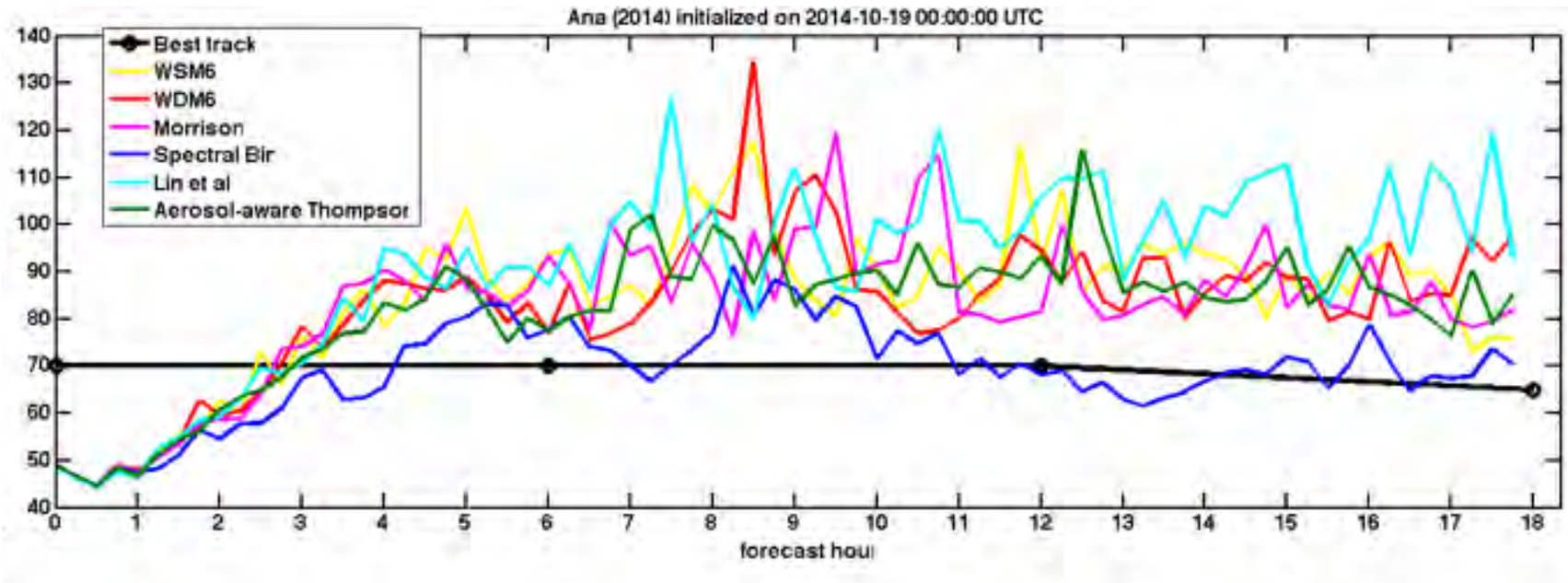

1630 UTC on 19 October 2014

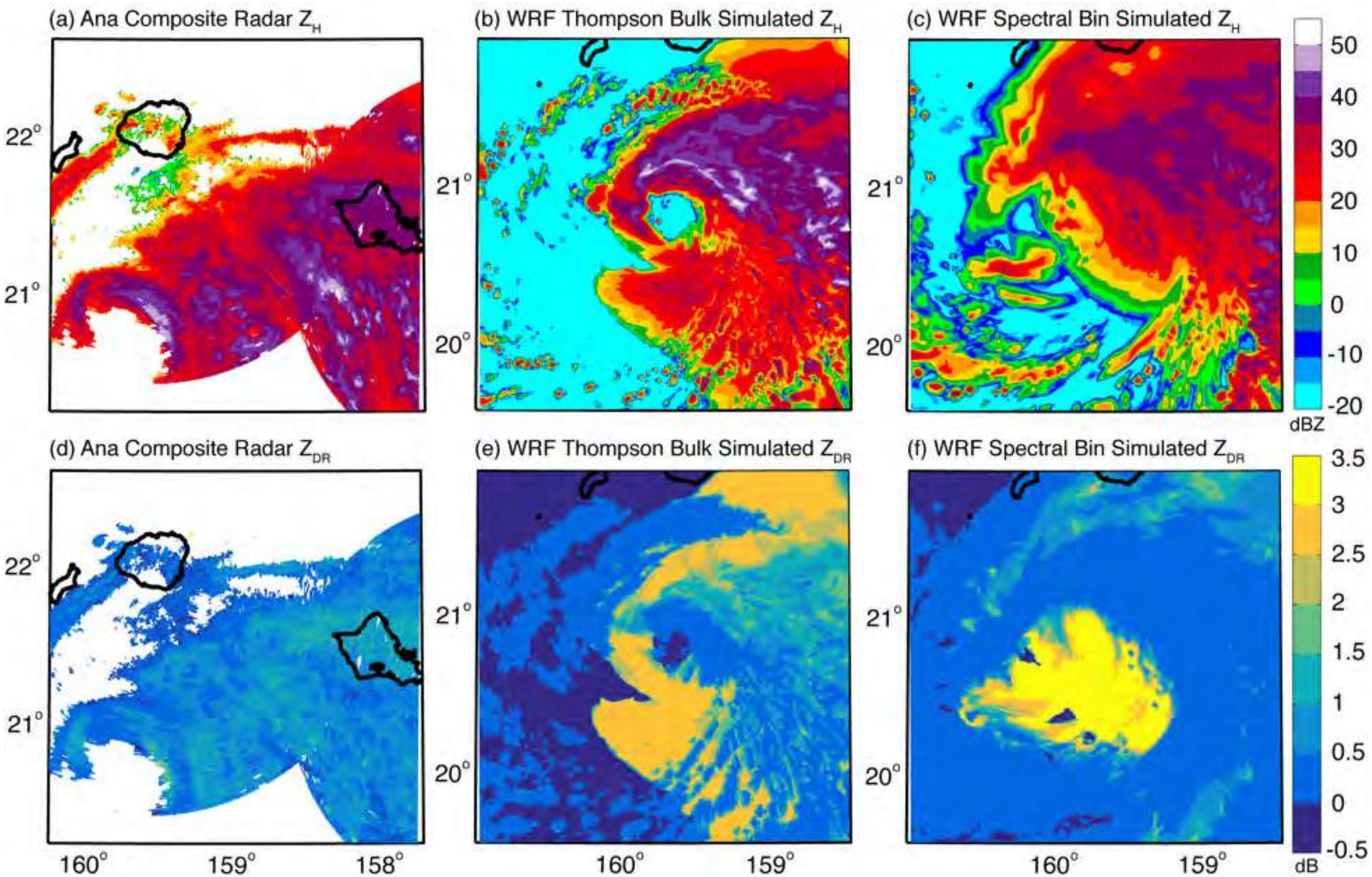

From Brown et al. (2016)

Increased dB

Z_{DR} ↑

Increased Raindrop Size

Increased dBZ

Z_H →

Increased Rainfall

From Brown et al. (2016)

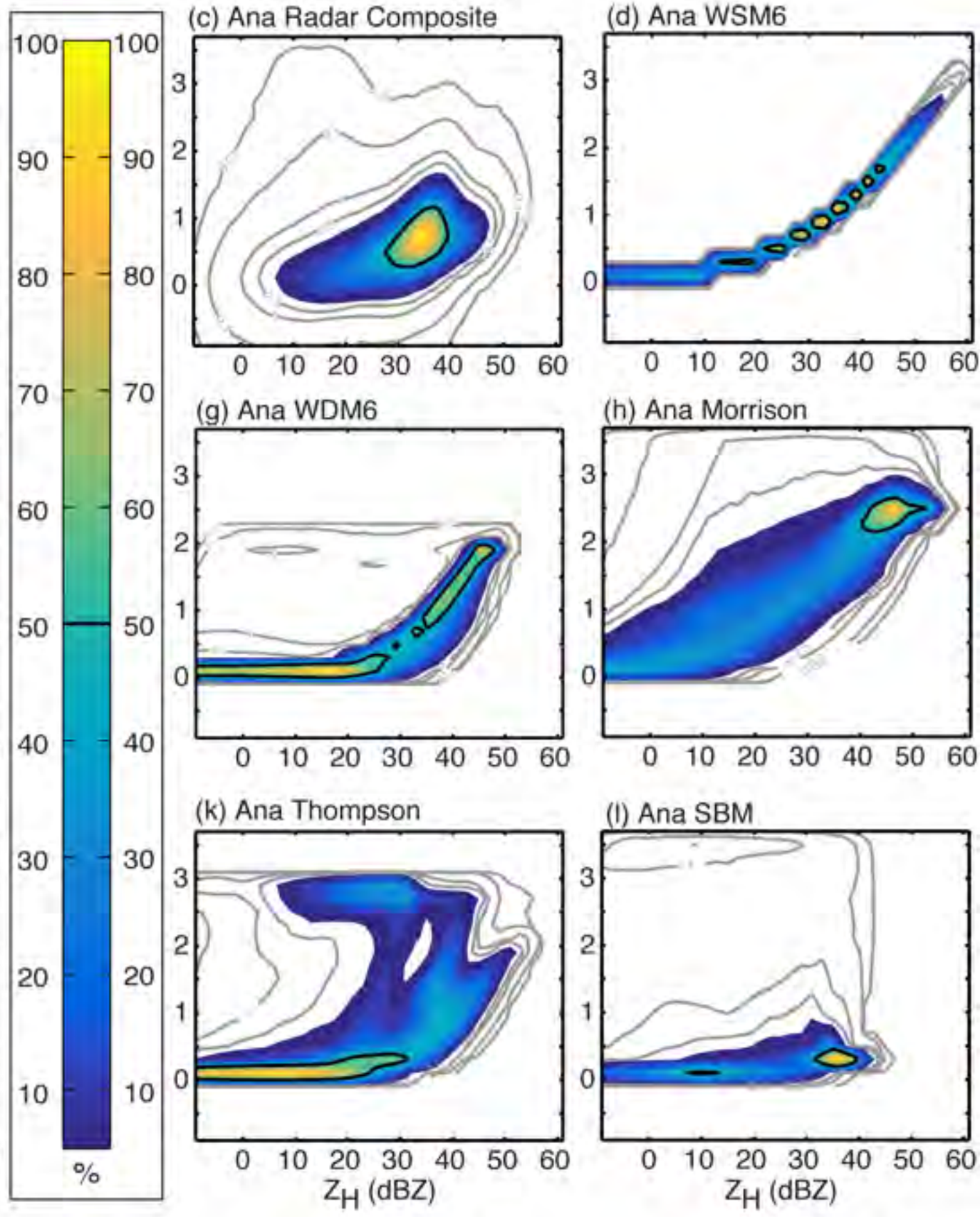

Accumulated Rainfall

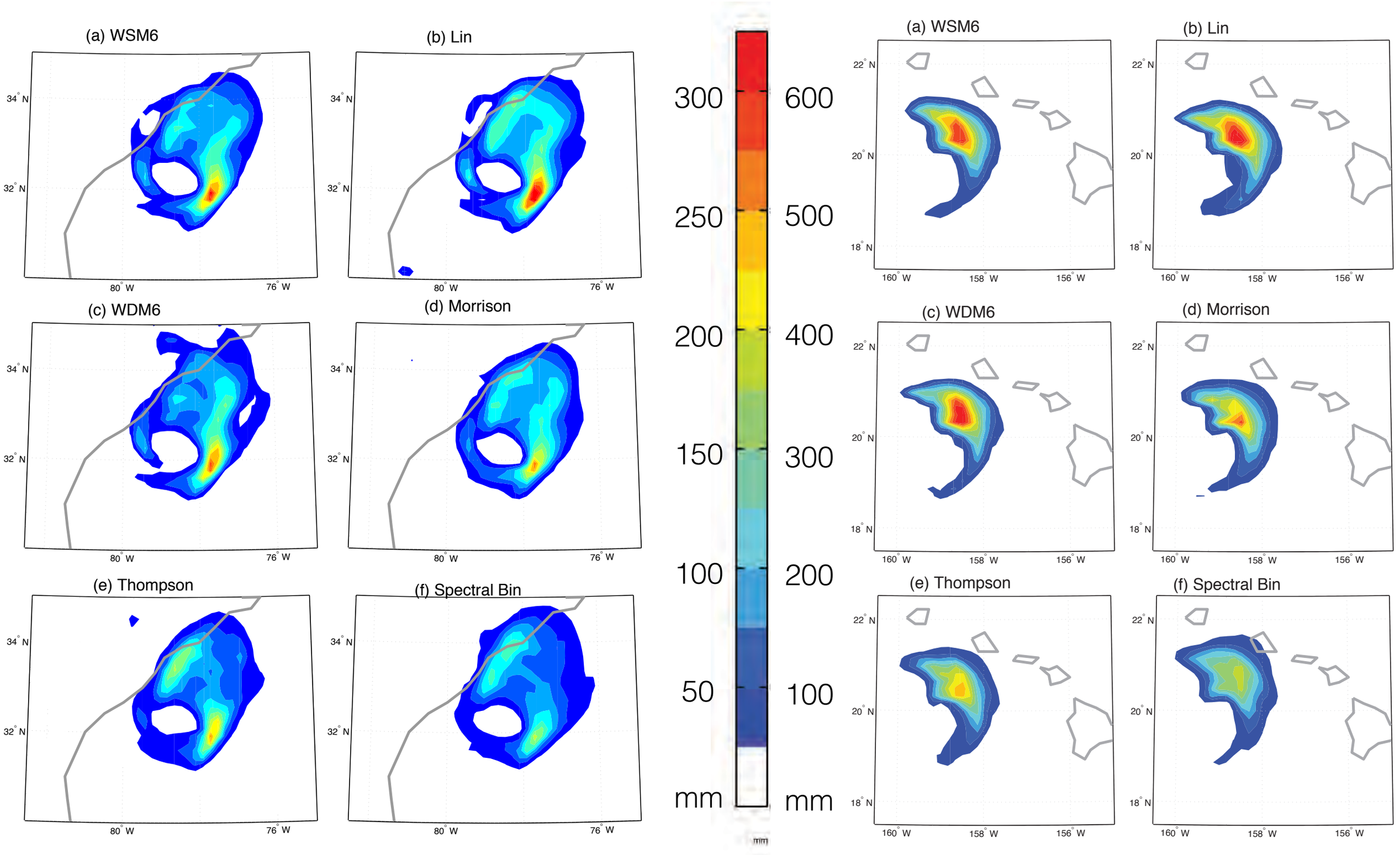

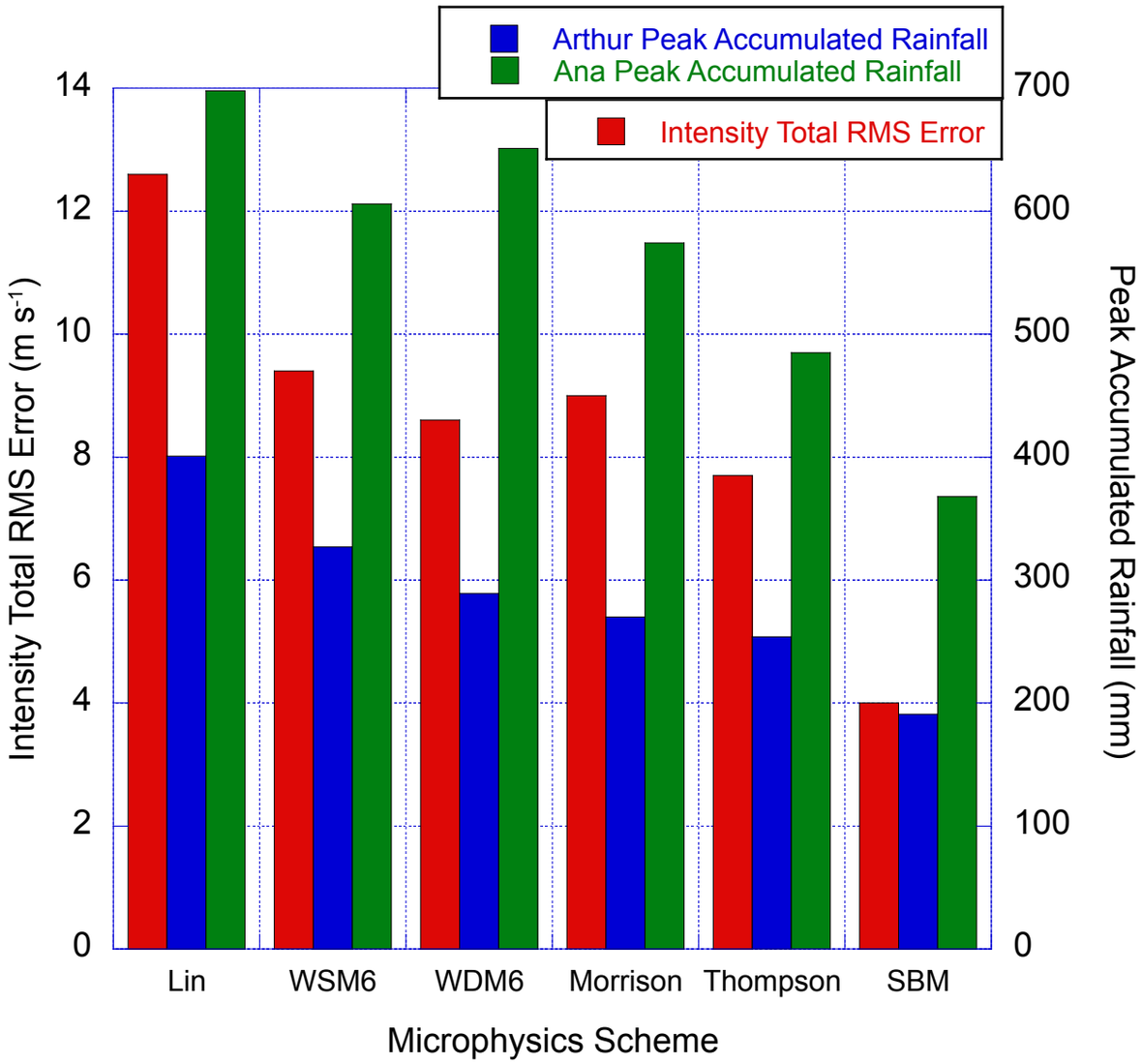

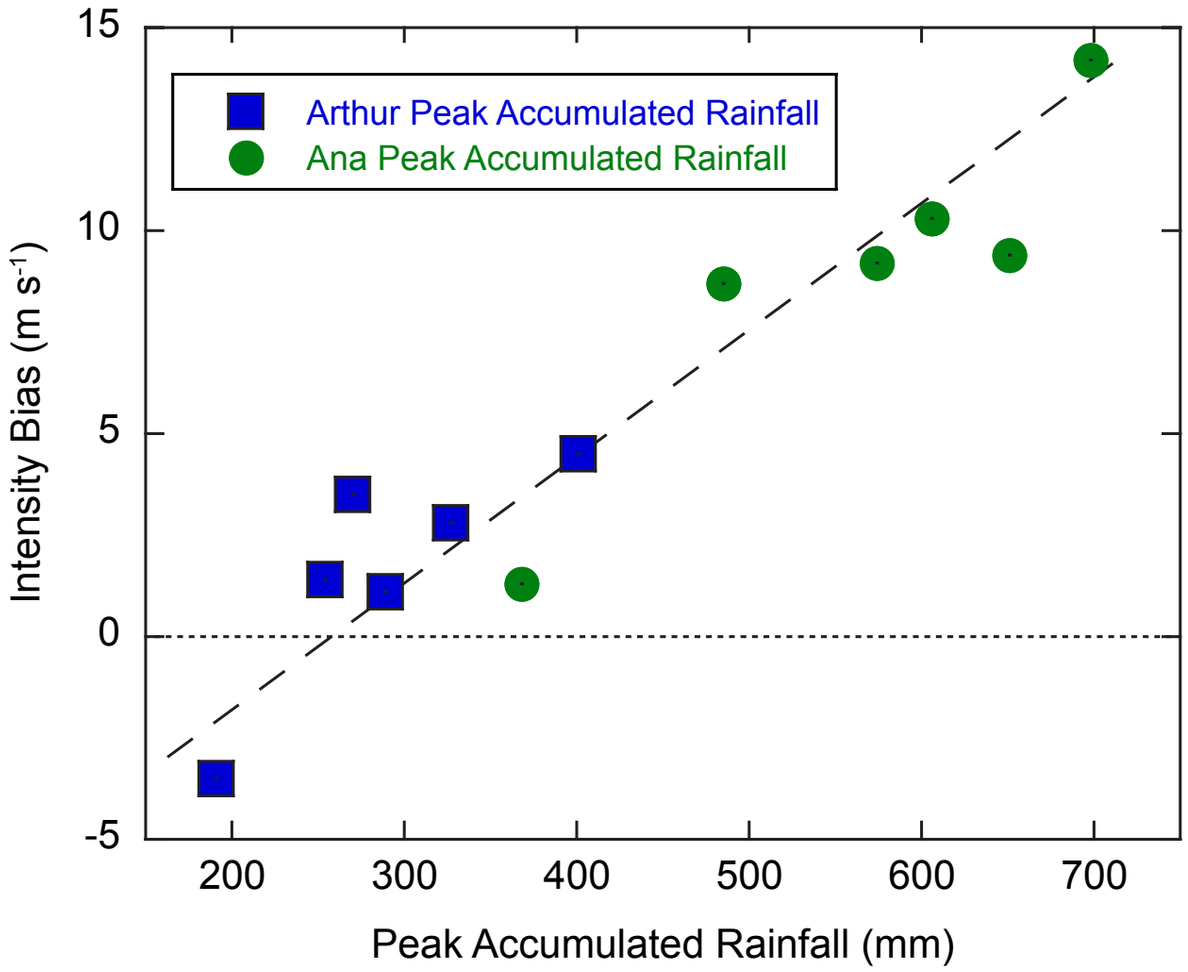

	WDM6	Thompson	'Fast' SBM
Cost over WSM6	11%	33%	1471%

using 480 processors on NCAR Yellowstone supercomputer

Working with airborne radar data can be intimidating compared to other datasets

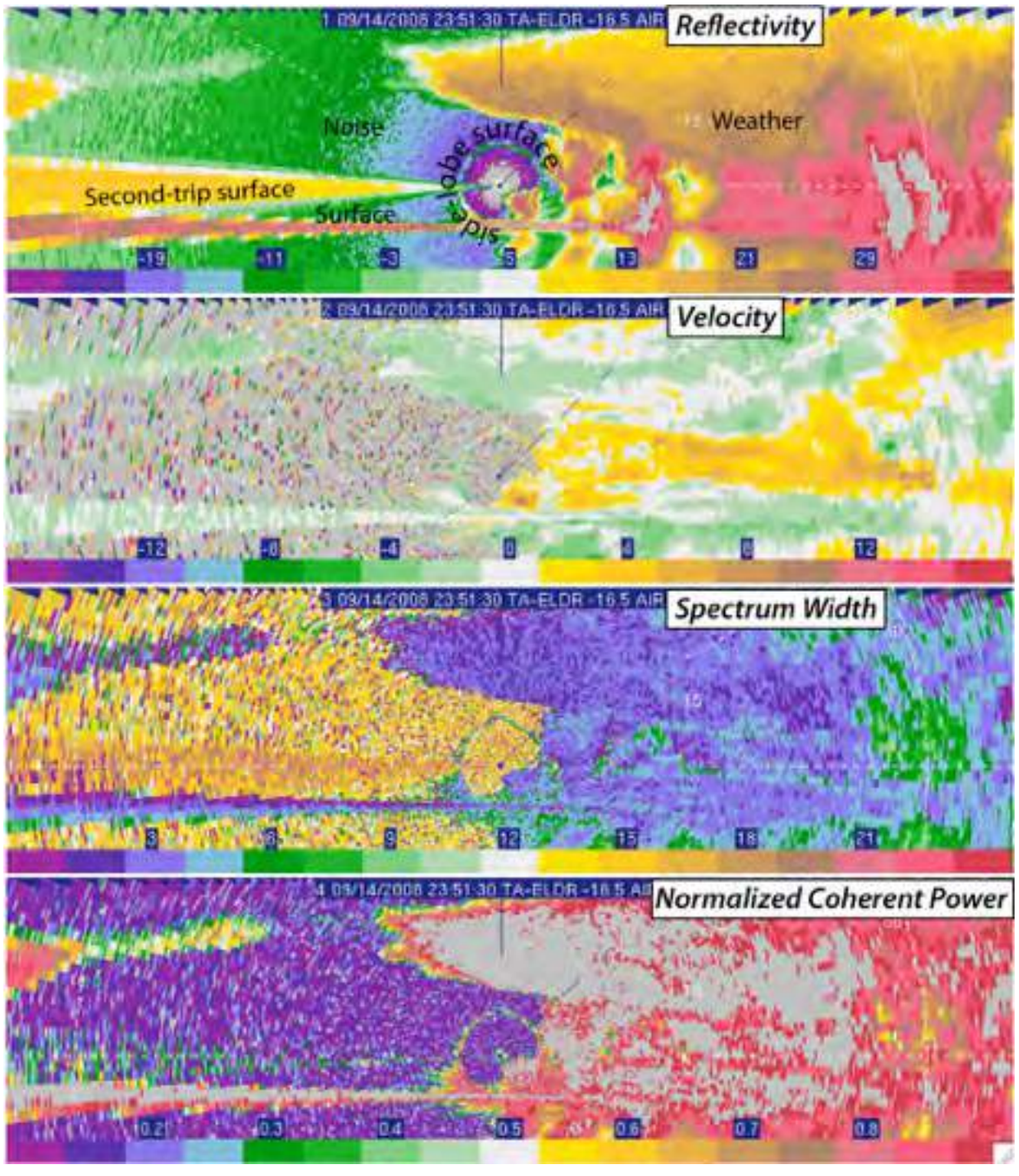

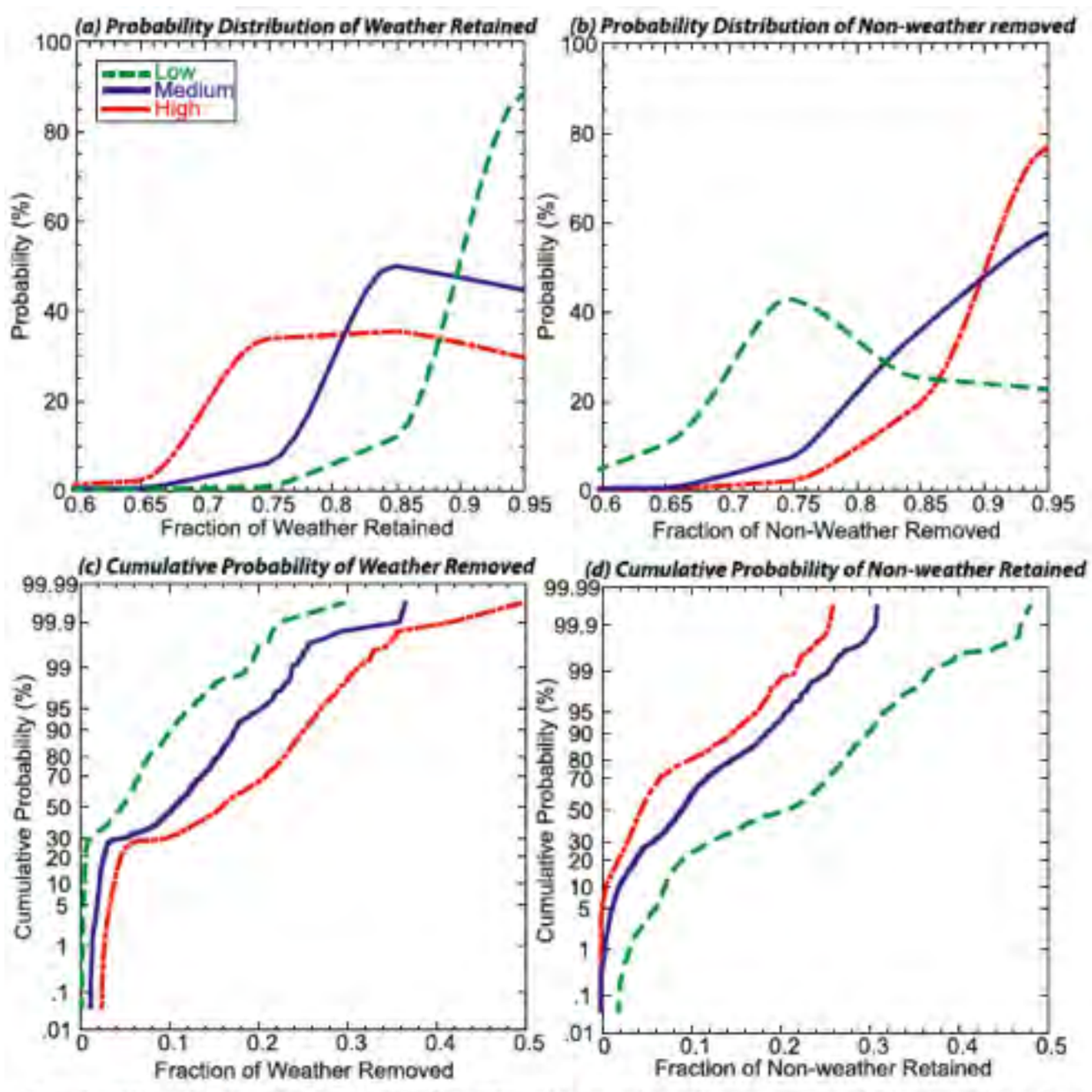

FIG. 7. PDFs and CDFs for the QC algorithm. PDFs of (a) weather echoes retained and (b) nonweather echoes removed from the test dataset. CDFs of (c) weather echoes removed and (d) nonweather echoes retained. Dashed green, solid blue, and dash–dotted red lines represent the low-, medium-, and high-threshold levels, respectively.

From Bell et al. (2013)

New algorithms and software for airborne radar are being developed

- Cai et al. (2016) describes new airborne navigation correction algorithm
- Lidar/Radar Open Software Environment (LROSE) was recently recommended for funding by NSF
  - Collaborative effort between CSU (Bell PI) and NCAR (Wen-Chau Lee & Mike Dixon Co-PIs)
  - Airborne and ground based radar software improvements for international community

Future Field Experiments

- ONR-sponsored PISTON in conjunction with Year of Maritime Continent (YMC) in Aug./Sep. 2018
  - CSU SEA-POL ship will deploy in South China Sea to study MJO with tropical cyclogenesis component

- Potential Western Pacific field experiment to study heavy rainfall from typhoons in planning stage
  - Details TBD, potential overlap with Tokyo 2020?

Conclusions and Future Directions

- **Aircraft observations have greatly advanced our knowledge of TC structure and intensity change**
  - RAINEX (2005), TPARC/TCS08, and PREDICT (2010) revealed many new insights about TCs

  - Composite TC structures from the new FLIGHT+ dataset indicate statistically significant differences depending on both intensity and intensity change

  - Recently completed Tropical Cyclone Intensity (TCI-2015) project just finished QC stage and preliminary analyses are promising

Conclusions and Future Directions

- **Newly Developed and Future Technologies will enable further improvements in TC aircraft observations**
  - HDSS system shows great promise
  - New pod-mounted cloud and phased array, polarimetric precipitation radars can probe TC structure
  - New LROSE radar software tools are being developed
  - International efforts to increase TC observations (Japanese synoptic aircraft surveillance)
  - Future field programs (YMC 2018, Tokyo 2020?)

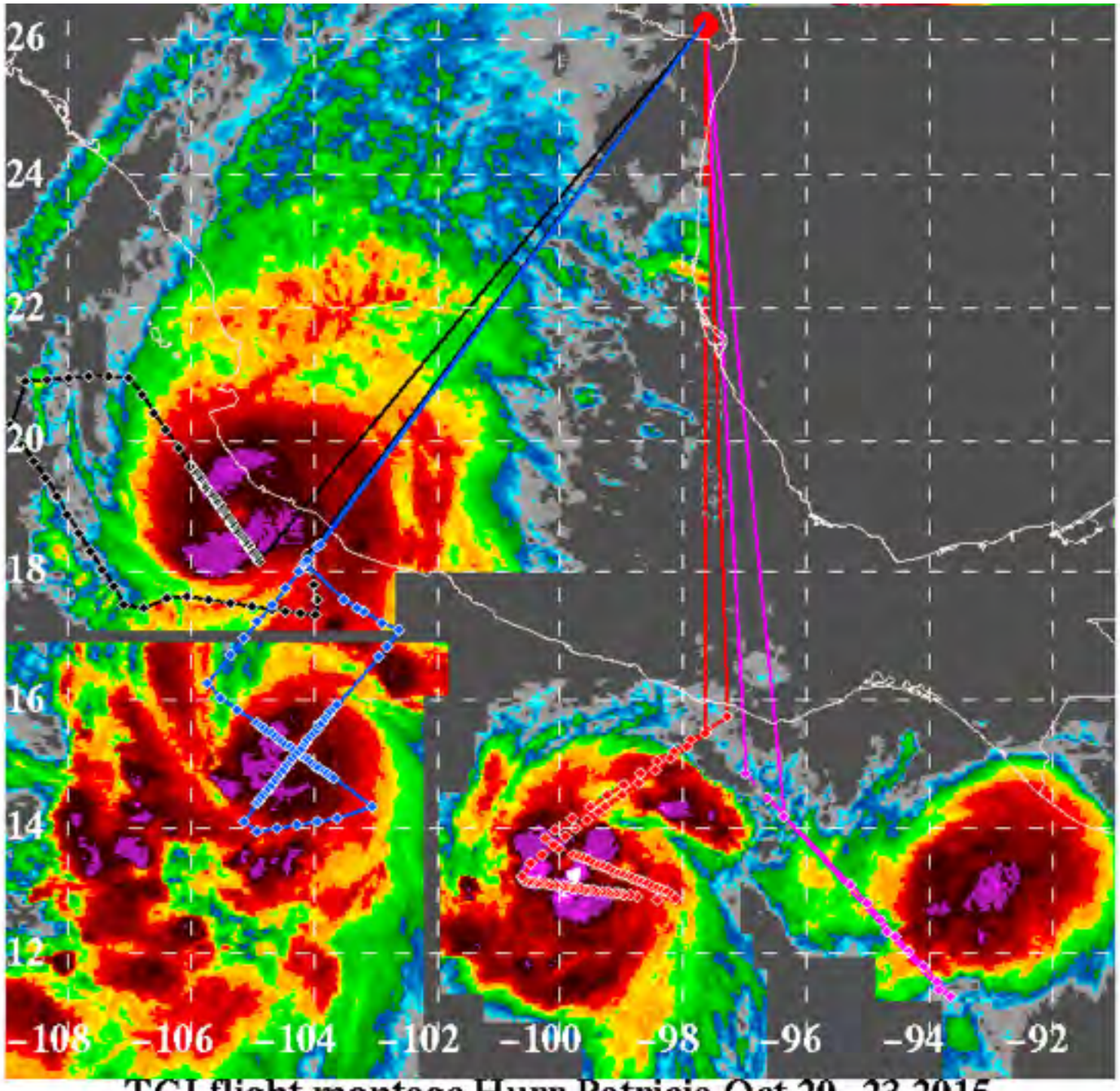

TCI flight montage Hurr Patricia Oct 20–23 2015

ありがとうございました

mmbell@colostate.edu